



# **Semi-Passive Control Strategy using Piezoceramic Patches in Non Linear Commutation Architecture for Structural-Acoustic Smart Systems**

**Ph.D. Thesis**  
of  
**Monica Ciminello**

submitted to

**University of Naples “Federico II”**  
Department of Aerospace Engineering, Naples, Italy  
*Ingegneria Aerospaziale, Navale e della Qualità*

and

**Conservatoire National des Arts et Métiers**  
Structural Mechanics and Coupled System Laboratory, Paris, France  
*Conservatoire National des Arts et Métiers / spécialité : Mécanique*

Italian Supervisors  
**Prof. Leonardo Lecce**  
**Dr. Salvatore Ameduri**

French Supervisors  
**Prof. Roger Ohayon**  
**Prof. Jean-François Deü**

## **Members of the jury**

Prof. Paolo Gaudenzi, Aerospace Dept.- University of Rome “La Sapienza”, Italy  
Prof. Mohamed Ichchou, Ecole Centrale de Lyon, Lab. LTDS, France  
Prof. Leonardo Lecce, Aerospace Engineering Dept.- University of Naples “Federico II”, Italy  
Prof. Roger Ohayon, Structural Mechanics and Coupled System Lab., CNAM, France

**Presented at “Federico II” University of Naples, 28 January 2010**



*Dedicated to all those who have wished me well*



# Preface

The work presented in this thesis has been carried out at the Department Division of Aerospace Engineering (DIAS) at Federico II University of Naples under the direction of Prof. Leonardo Lecce.

An important part of the research activity has been conducted within the position of Early Stage Researcher, in the framework of the European Marie Curie Research Training Network project “Smart Structures” MRTN-CT-2006-035559, focusing on Computer Aided Engineering Approaches to Smart Structures Design. The research activities of one year, has been performed in the Structural Mechanics and Coupled System Laboratory (LMSSC) of the Conservatoire National des Arts et Metiers (Cnam), in Paris, under the direction of Prof. Roger Ohayon. The researchers at LMSSC/Cnam having a deep experience in structural-acoustics and piezoelectric finite element modelling.

The experimental activity were conducted at the Italian Aerospace Research Centre (CIRA). The laboratory of Smart Structures (SMAS) under the direction of Dr. Antonio Concilio has been the centre where the finite element modelling, structural vibration, as well as definition and development of smart systems concepts, have been introduced to me.

The Italian-French doctoral convention has been approved between the University of Naples "Federico II" and the Conservatoire National des Arts et Métiers (CNAM) under the protocol signed by the Ministries of Foreign Affairs and the University of France and Italy.

Federico II, in fulfilment of the requirements, will assign the degree of Ph.D. in Aerospace Engineering.

CNAM, in fulfilment of the requirements, will assign the degree of Ph.D. in Mechanical Engineering.

Naples, January 2010.

Monica Ciminello



# Acknowledgements

Few lines, for not dispersing in streams of words my gratitude, to those who have been my support, my reference for knowledge, experience, leadership, comprehension, to those who have made this dream possible and those to whom I humbly dedicated this work.

Prof. Leonardo Lecce who, after our first meeting, said me “...welcome on board...”

Prof. Roger Ohayon who, the last day in Paris, promised me “...we will still take care of you...”

Prof. Jean-François Deü who considered me “...to be efficient...”

Dr. Antonio Concilio who has always thought of myself as “...a volcano of energies...”

Dr. Salvatore Ameduri who keep thinking that “...working with me is fun...”

My “Ph.D. friend”, Silvestro Barbarino who always encouraged me, since the first exam, “...to take a deep breath and go...”

Prof. Antonio Moccia, who has guided the class of the XXII Ph.D. cycle, every single day with his constant and reliable presence.

My colleagues and co-authors, Antonio Calabrò, Walid Larbi, Jean-Sebastien Schotté, Daniele Ghiglione, with whom it was a pleasure to work.

To Sandro Santangelo of whom I have always trusted.

To those who wanted to hinder me, thanks for making me understand what is the perseverance and the strength of a teamwork!

and .....to myself!

**...is for you that I never gave up;  
...is for you that all this has a reason;  
...is for you that I am happy today.**

*"Of all the things that wisdom attorney for a good  
life, the greatest asset is the purchase of friendship".  
(Epicurus)*



# Contents

<b>Preface</b>	<b>pag.5</b>
<b>Acknowledgements</b>	<b>pag.7</b>
<b>Contents</b>	<b>pag.9</b>
<b>Motivation of the work</b>	<b>pag.11</b>
<b>Overview of the thesis</b>	<b>pag.15</b>
<b>Part I : State of Art</b>	
Piezoelectric ceramics for structural applications	<b>pag.23</b>
Modelling of Piezoelectric Smart Structures	<b>pag.29</b>
Shunted Architectures for Smart Systems and Applications	<b>pag.35</b>
<b>Part II : Included Papers and Abstract Proceedings</b>	
Accepted for Publication on International Peer Reviewed Journals	<b>pag.43</b>
Submitted to International Peer Reviewed Journals	<b>pag.121</b>
International Conferences Abstract Proceedings	<b>pag.159</b>
<b>Appendix: Complementary Ongoing Activities</b>	
Sound Power Radiation in Elasto-Acoustic System	<b>pag.175</b>
Computational Modal Analysis for FSI Problems	<b>pag.181</b>
<b>Conclusions and Prospects</b>	<b>pag.183</b>
<b>Riassunto (extended abstract in Italian language)</b>	<b>pag.187</b>
<b>Résumé (extended abstract in French language)</b>	<b>pag.189</b>
<b>References</b>	<b>pag.191</b>
<b>Career Development Plan</b>	<b>pag.201</b>



# Motivation of the work

Smart materials have one or more properties that can be significantly changed in a controlled fashion by external stimuli, such as stress, temperature, moisture, pH, electric or magnetic fields. Smart materials that can damp mechanical vibration in an intelligent way (i.e. adaptability to environmental conditions changing), have long been heralded as the dawn of a new era in the construction of automotive vehicles, airplanes and other structures that have to meet ever more demanding performance requirements. The dynamic performance of a structure may represent the main target of the design, as undesirable large-amplitude vibrations often impede the effective operation of various types of mechanical systems, including antennae, spacecrafts, rotorcrafts, automobiles, and sensitive instruments. It is therefore desirable to introduce structural damping into a system to achieve a more satisfactory response and to delay fatigue damages. Many types of smart materials are currently available or are at various stages of development. Applications are largely focused on spacecraft, aircraft and military industries. However, space structures have to minimize their weight extremely, with consequent increase of the flexibility level of some components. For this reason space structures are more prone to vibrations compared with structures on earth with less weight restriction. Moreover, vibrations are more difficult to suppress or control effectively for space structures than for structures on earth. Figure 1 illustrates one of the concepts of future space stations. We can easily see that the flexible truss structure is used for its construction. The structures connecting the several modules are flexible and light-weight trusses.

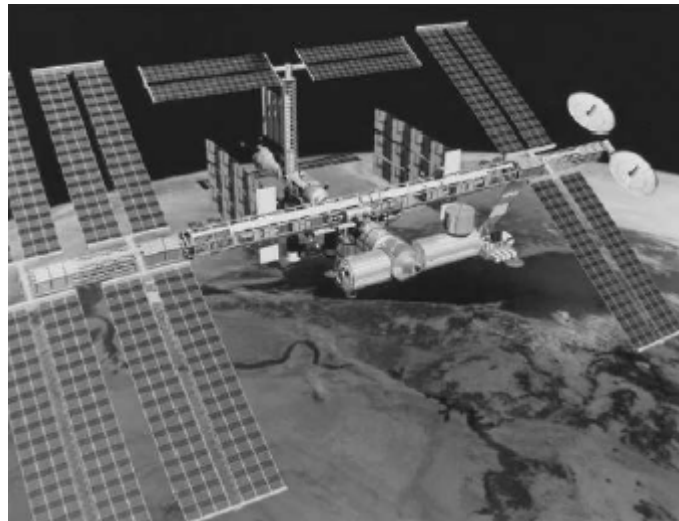


**Figure 1: International space station currently under construction**

There is currently a large effort underway to effectively suppress the vibration of structures. Researches for vibration control are roughly categorized into two groups; active vibration control and passive vibration control. Active vibration control that supplies energy to the system for suppressing the vibration is expected to have high performance in vibration suppression. In general, accurate mathematical models and fine-tuning for parameters are indispensable for making active vibration control feasible, however, it is usually quite difficult to construct precise mathematical models and to perform the fine-tuning for active vibration control, especially in space, because these structures have to be supported to cancel the influence of its own weight, which results in different environment for the structures. Secondly because, space structures are reassembled in space and therefore their construction is not expected to be accurate, etc. In conclusion, errors of mathematical models may damage the robustness for active vibration control. Controllers to damp vibration were implemented mostly in a purely

active arrangement, i.e. an electrical field is applied to the piezoelectric materials based on sensor feedback and control commands [FEN96, PKPM99, SC98]. This is shown in Figure 2, where the active controller produces an actuator-signal based on a sensor-signal from an accelerometer, velocity or strain sensor. Normally, active controllers are implemented in microprocessors that are connected to the sensors and actuators by special amplifiers as illustrated in Figure 2 a).

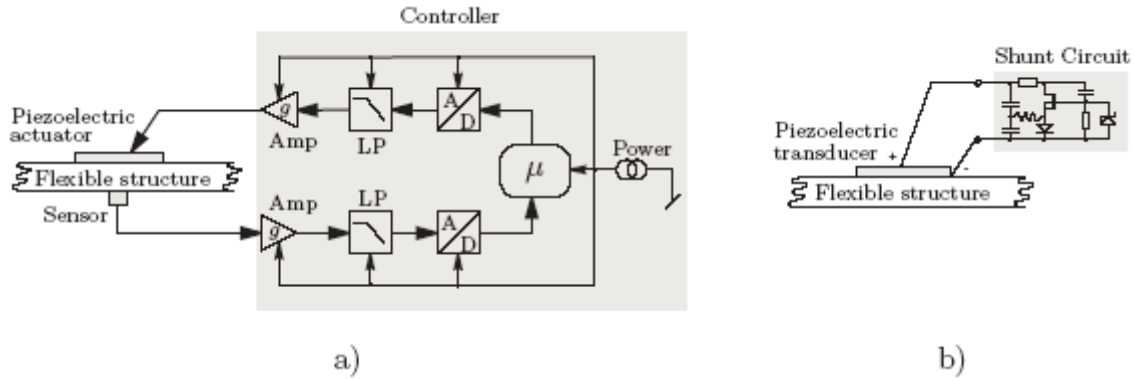


**Figure 2 (courtesy of [NIE05]) : a) Conventional vibration control and b) the piezoelectric shunting technique. The latter approach is described in the present thesis.**

These approaches have several disadvantages. First, every sensor and actuator needs bulky amplifiers (*Amps*) and the implementation with a digital microprocessor implies the use of anti-aliasing and reconstructing filters (*LP*) and *A/D*, *D/A*-converters. This hinders the integration of the controller into the structure, which exactly would be required for smart damping materials. Additionally, the large instrumentation overhead raises the costs and extra power-supplies for amplifiers, filters, converters and the microprocessor are needed. This makes the system more sensitive to failures and the wiring of the power supply also becomes difficult.

On the other hand, passive vibration control uses energy-dissipative mechanism with dampers, frictional devices, electric resistors and so on. Since passive method does not supply energy to the system, the system with passive method is always stable. A passive vibration control is easier to be implemented in actual systems than active vibration control system, because it does not need controllers, sensors, or filters. However, in most cases, it does not provide satisfactory performance in vibration suppression.

The vast majority of research in smart damping materials has concentrated on the control of structures made from composite materials with embedded or bonded piezoelectric transducers because damping with passive materials (e.g. mufflers, damping plates, etc.) is not very effective at low frequencies and requires more space and weight (Figure 3).

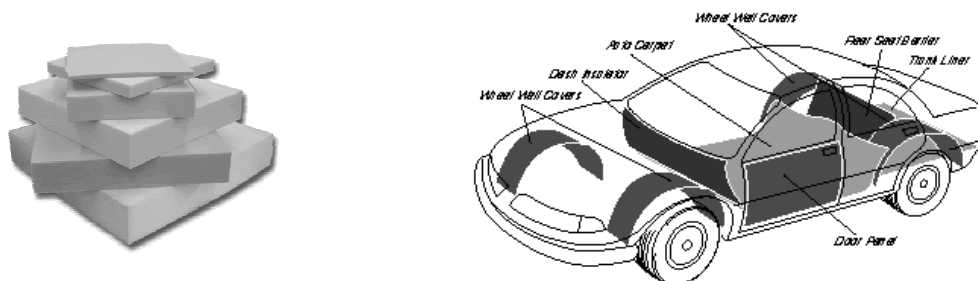


**Figure 3: One idea of a car structural element to be interested by damping layer**

To account for the drawbacks of the just described common vibration control techniques, a different approach for smart damping materials is investigated based on the following demands here summarized as proposed in [KPVG97]:

- External power source is not required for operation

- Device does not need to be tuned to a specific frequency
- Device operation is not affected by changes in modal frequency
- Device suppresses vibration over a number of modes, i.e. it is broadband
- Weight and size of the device should be minimized
- Device is to be a self-contained unit

**The thesis focus on the previous points and it shows how the approach based on the semi-passive technique can solve the dilemma between active and passive vibration control in terms of robustness and performance, simply connecting a resonant circuit to a piezoelectric transducer. This leads to a simple and low cost device for vibrations reduction in such a way to fulfil these demands.**

**The semi-passive synchronised switch shunt architecture is modelled and investigated. The idea of using piezo transducers to convert mechanical into electrical energy and elaborating related signal within an external time variant electrical circuit, represents the inspiring principle of this type of control.**



# Overview of the thesis

The thesis consists of two parts. The first is an overview of the state of art in the field of interest: piezoelectrics smart materials for structural applications, piezo modelling and shunt circuits architectures and their applications.

The second part includes papers accepted and submitted to international peer reviewed journals, the abstract of papers presented at international conferences proceedings as well, and the complementary ongoing activities, focusing on our investigation and our approach to model and simulate the semi-passive non linear commutation control for structural-acoustic smart systems.

Part I and Part II are briefly summarised in what follows.

## Part I: State of Art

The way to solve the dilemma between active and passive vibration control in robustness and performance of vibration suppression can be represented by a semi-passive shunt circuit architecture as alternative approach based on piezoelectric elements shunted on simple electrical components. With the advancement of smart material technology, smaller, flexible piezoelectric materials are attractive because of their ability to withstand large amounts of strain and because they can be successfully incorporated into structures. Larger strains provide more mechanical energy available for conversion into electrical energy. This is the starting point of a shunt control architecture involving the energy conversion ability of the piezo to reduce amplitude of structural vibration. The state of art review focusing on these studies presents a wide variety of configurations to improve the efficiency of piezoceramics in structural applications in order to maximize the energy extracted from the ambient source. Another focal point is the approach for the piezoelectric effects modelling. The structure including the piezoelectric components is commonly described with classical finite elements formulation but inverse and direct electromechanical coupling effects can be modelled in original, non standard way. A number of researchers have demonstrated promising results in the use of the thermal analogy to model the static and dynamic behaviour of a piezoelectric shell structures. The purpose of developing such computational tool is first to provide a simplified but enough accurate description of the dynamic response of structures incorporating active piezoelectric elements and to allow the description of an entire structure of moderate complexity, where some regions of the structure will incorporate piezoelectric sensors or actuators as active multilayered regions. Finally, the shunt circuits for structural acoustic applications are reviewed. In the last decade, many different electrical shunt topologies have been proposed. These shunts circuits can be divided into passive and active. Basically, if a shunt is passive, stability of the whole system is guaranteed, because no energy is added to the system. If a shunt is active, stability is not automatically guaranteed, moreover, additional power to drive the shunt circuit is required. Passive shunts can also be categorized into linear and non-linear.

A non linear commutation architecture is investigated in this thesis. The state of art addressed to this kind of control refers to: classical finite element formulation based on local equations of the fully coupled system; numerical and experimental validation for sdof models; analytical and experimental validation of the vibrations reduction efficiency based on the electromechanical coupling coefficient for isotropic structures.

Moreover interesting solutions have been formulated, even being still an open problem, about the optimal switching control law for multimodal excitations. Finally different type of “autonomous” circuits basically based on transistors and synthetic inductors have been proposed.

## Part II: Included Papers and Abstract Proceedings

In the included papers the following original aspects have been dealt:

### International Peer Reviewed Journals

A multi-dofs electro-mechanical coupled system has been numerically modelled by means of a finite element formulation [1.J].

1.J M. Ciminello, S. Ameduri, A. Concilio, **“FE Modelling of an Innovative Vibration Control Shunt Technique”**. *Journal of Intelligent Material Systems and Structures* Vol.19, N°8, August 2008 pp.875-887.

The single mode and multi mode synchronised switch control have been experimentally validated for both aluminium cantilevered beam [2.J] and a fiber-glass 10-ply laminate plate [3.J]. The piezo sensor-actuator collocated couples have been used in both bonded and embedded configurations and placed according to an optimization process based on the max stored electrical energy. Piezo strain actuation has been modelled with a 3D finite element description of the structural laminate using the analogy between thermal strain and piezoelectric strain. The effects exerted on the structure have been applied as concentrated moments at the piezo nodes interface. The piezo moments have been compared and validated using well-established strain actuation analytical model. The sensing has instead been modelled with a 2D piezoelectric constitutive equation and experimentally validated. A finite element tool integrating Nastran features with Matlab routines has been developed [3.J].

Moreover an original circuit, based on a tachometer and CMOS devices (needing a very weak supply 12V and -12V to allow the signal passing during both the semi positive and semi negative wave), has been realised to implement the synchronized shunt control. The tachometer device can generate a pulse train signal activating the CMOS perfectly synchronized with the zero crossing of the input. Moreover the amplitude of the logical signal can be opportunely set according to a voltage threshold fail-safe criterion [2.J]. A 4-independent channel electric card of 10×10cm in-plane dimensions and 80gr in weight with a plug and play philosophy have been built up, in order to friendly manage a set of piezo transducers network for multimode control test [3.J].

2.J M. Ciminello, S. Ameduri, A. Calabrò, A. Concilio, **“Synchronised Switched Shunt Control Technique Applied on a Cantilevered Beam: Numerical and Experimental Investigations”**. *Journal of Intelligent Material Systems and Structures* Vol.19, N°9, September 2008 pp.1089-1100.

3.J M. Ciminello, L. Lecce, S. Ameduri, A. Calabrò, A. Concilio, **“Switched Shunt Control implemented through a PZT network embedded within a composite panel: design, manufacture and test”**. Accepted for publication to – *Journal of Intelligent Material Systems and Structures* JIM-09-188.

Numerical results concerning the dynamic response reduction of structural-acoustic systems, attained by using a synchronized switch control technique, are also investigated. The considered coupled system is an elastic plate with a surface-mounted piezoelectric patches, coupled with an acoustic cavity filled with an inviscid, compressible and barotropic fluid, gravity effect being neglected. The piezo actuator has been located in a random position in order to avoid the effect just for odd modes (mainly the first) if placed at centered position.

A full home-made finite element procedure, according to local equation describing the fully coupled system has been implemented in Matlab environment. The effect of a passive inductive shunt and the semi-passive switched shunt have been compared in order to highlight the broad band features of the second technique [4.J].

4.J W. Larbi, J.-F. Deu, M. Ciminello, R. Ohayon, “**Structural-acoustic vibration reduction using switched shunt piezoelectric patches. A finite element analysis**”. Submitted revised version to the - *Journal of Vibration and Acoustics* VIB-09-1143.

In order to validate a general-purpose procedure simulating the SSC also for electro-elasto-acoustic systems, the results obtained from the finite element code discussed in the previous paper, have been compared with a non standard procedure integrating Nastran/Matlab routines. The matrices are extracted from Nastran and reassembled in Matlab where the electro-mechanical coupling terms have been added. Moreover taking advantage of the eigenvectors that Nastran can compute, a modal reduction has been approached. Correlations in the results demonstrate the coherence of the non standard method [5.J].

5.J M. Ciminello, L. Lecce, A. Concilio, “**Structure borne sound for acoustic cavity through pzt patch in switched shunt configuration: a non standard finite element analysis**”. Submitted to: *Aerotecnica missili e spazio*.

An attempt to face with a semi analytic solution exclusively for a simple 1D test case of a fluid duct, has also been taken into account [6.J].

6.J S. Ameduri, M. Ciminello, “**Fourier Expansion Solution for a Switched Shunt Control Applied to a Duct**”. Accepted for publication to : *Journal of Theoretical and Applied Mechanics (JTAM)*, No. 2 or No. 4, Vol. 48, 2010.

### International Conferences Proceedings

The possibility of jointly implementing both a switched and an inductive shunt architectures may guarantee a more efficient multi mode control. As a matter of fact, it is possible to simultaneously control a low and a high frequency mode through a switch and an inductive architecture [1.C].

1.C Monica Ciminello, Salvatore Ameduri, Antonio Concilio, **Simulation of a Combined Switched and Inductive Shunt Control Acting on a 2D Structure** – *The 14th International Congress on Sound and Vibration*, 9 – 12 July 2007, Cairns, Australia. *Proceedings of the ICSV*, Vol. 5952, pp. 314-323, 2007.

The necessity of extending benefits due to this technique to more realistic applications has led to numeric solving schemes, prevalently based on a FE approach. However, due to the complexity of real applications, despite the efficient reduction techniques employed, numerical computations result heavy and, consequently, time consuming. On the contrary, a semi-analytical solution would allow eliminating the time consuming due to the integration [2.C].

2.C Monica Ciminello, Salvatore Ameduri, Antonio Concilio, **Semi-analytical Solution of a Structural System Controlled by a Switched Shunt Architecture** – *Proceeding of the 36th International Congress and Exhibition on Noise Control Engineering - Session ANVC "Active Noise and Vibration Control*, Paper N° IN07-032. August 28 – 31, 2007 Istanbul - Turkey.

The simulation control scheme focusing attention on the FE model integration within the logic of control is fully described [3.C].

3.C Monica Ciminello, Salvatore Ameduri, Antonio Concilio, Leonardo Lecce, **Flow-chart design of a pzt network based on a Switched Shunt Control** - *Proceeding of the International Conference and Exhibition on new Actuators and Drive Systems (Actuator 2008)*, Session "Aerospace applications" P143. June 9–11, Bremen, Germany.

Numerical results concerning vibration reduction of structural-acoustic systems using the synchronized switch control technique has also taken into consideration. In order to develop a general procedure to model the coupled system (composed by the fluid domain, the structure and the piezoelectric elements), the idea is to use the performances of a standard commercial code such as Nastran [4.C].

4.C Monica Ciminello, Jean-François Deü, Roger Ohayon, Salvatore Ameduri, **Vibration reduction of structural-acoustic systems using synchronized switch damping techniques** - *Proceeding of 2008 ASME International Conference on Smart Materials, Adaptive Structures & Intelligent Systems*, Paper - SMASIS08-320. October 28-30, 2008, Ellicott City, MD, USA.

The wide band performances of the switched shunt control in the low frequency domain (low modal density) and the low inductor and resistor values needed were the main peculiarities of this approach. The tested system showed a good independence on environmental drifts and a high thermal stability [5.C].

5.C Daniele Ghiglione, Wim Desmet, Monica Ciminello, Salvatore Ameduri, Antonio Concilio, **Noise Reduction in coupled vibro-acoustic systems using synchronized switch control** - *Proceeding of AC2009 Adaptronic Congress*, Paper AC2009-pp. 159-167. May 19-20, 2009, Berlin - Germany.

An attempt to critically summarise the most remarkable points of the author's work in the last period, corresponding to her PhD studies is finally presented [6.C].

6.C Monica Ciminello, Leonardo Lecce, **Experiences on Switched Shunt Control on Radiating Elastic Plate Structures** - *Proceeding of ICSV16 The sixteenth International Congress on Sound and Vibration*, paper ICSV16-476-S09. July 5-9 2009, Kraków, Poland.

### **Complementary Ongoing Activities**

Since Nastran doesn't implement fluid structure interactions model well suited for specific acoustic situation where an added mass operator is needed, i.e. as incompressible fluid, further complementary investigation involves the FSI finite element modelling. In order to implement some direct and reduction procedures for more general fluid-structure interactions problems, a specific formulation in terms of  $(u, p, \phi)$  has been implemented by means of DMIG code [1.O].

The preliminary investigations have been conducted without any passive or active treatment and it has been the occasion to interact with researchers of ONERA.

1.O J.-S. Schotté, M. Ciminello, R. Ohayon, **"Reduced Order Models for Modal Analysis of Structural-Acoustic Interior Vibrations"**. Under preparation.

Finally, a numerical and experimental validation test has been planned to compare the sound power radiation of an elastic plate partly windowing an acoustic room with the acoustic energy level with and without control [2.O]. A shaker excite the plate with tonal, sweep and random signals as well. In order to save CPU time a modal reduction procedures will be implemented.

2.O M.Ciminello, S.Ameduri, I.Dimino, A.Concilio, **"SSC effect on the sound power radiation of an elastic plate coupled to an acoustic room"**. Under preparation.

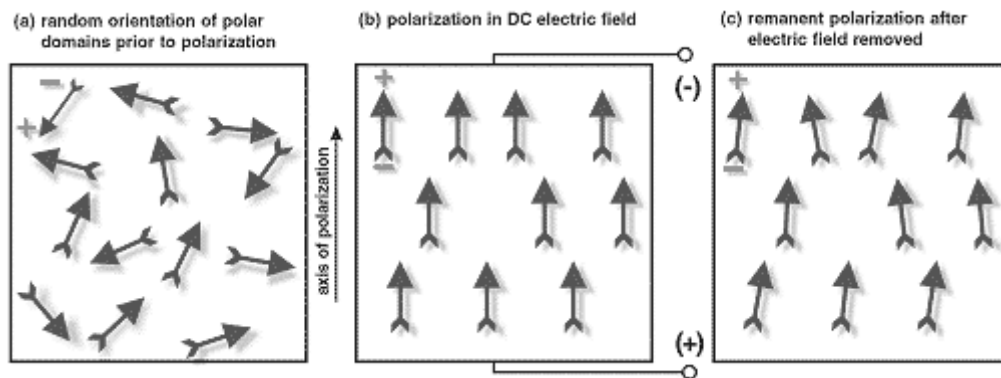
# **Part I**

## **State of Art**



## Piezoelectric ceramics for structural applications

Piezoelectric ceramics belong to the group of ferroelectric materials. Ferroelectric materials are crystals which are polar without an electric field being applied. This state is also called spontaneous polarization. Ferroelectric components may be made piezoelectric in any chosen polar direction by the poling treatment (Figure 1.1) which involves exposing the material to a high electric field at a temperature not far below the Curie point.



1.1: Polarizing (poling) a piezoelectric ceramic

Because of the random orientation of the domains and the fact that only certain dipole directions are allowed within the crystal, it is not possible to get the perfect dipole alignment with the field. However, there are several allowed directions within every domain and so a reasonable degree of alignment with the field is possible. After cooling of the product and removal of the poling field, the dipoles cannot easily return to their original positions, and we have now what is known as permanent polarization of the material. The body has become permanently piezoelectric and can convert mechanical energy into electrical energy, and vice versa (Figure 1.2).

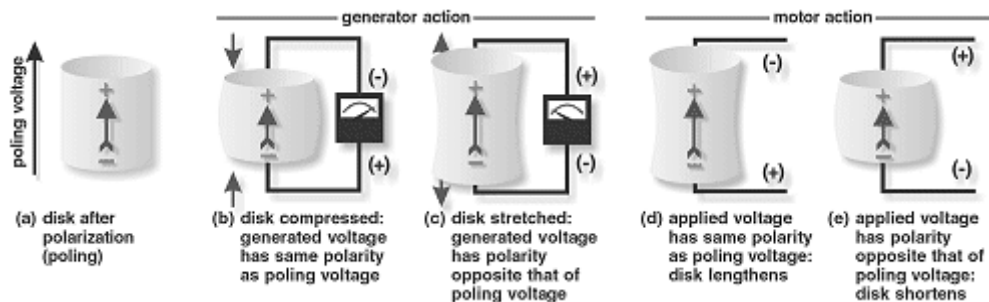
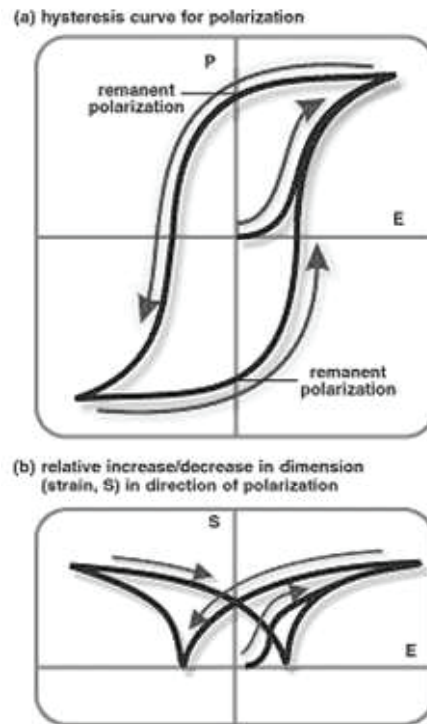


Figure 1.2: Generator and motor actions of a piezoelectric element

As each of the allowed direction has the same probability to appear, the net electric dipole summed over the whole crystal is zero. Nevertheless, when the crystal is cooled down in the presence of an electric field, the domains tend to align in the allowed direction nearest to the electric field. The crystal as a whole presents an electric dipole. If this crystal is subjected to stress, the lattice will be distorted and the stress will also cause some domains to grow at the expense of others. This results in a change in the total dipole moment of the crystal. Within a certain range of stress, this variation of dipole moment with the stress is approximately linear and reversible (Figure 1.3).



**Figure 1.3: PZT: electric field / strains**

The reversibility of the polarization, and the coupling between mechanical and electrical effects are of crucial significance for the wide technological utilization of piezoceramics. In particular piezoelectric materials can be configured in many different ways that prove useful in structural applications. The configuration of the device can be changed through modification of piezoelectric materials, altering the electrode pattern, changing the poling and stress direction, layering the material to maximize the active volume, adding pre-stress to maximize the coupling and applied strain of the material, and tuning the resonant frequency of the device.

The following articles have all investigated ways to improve the efficiency of piezoceramic in structural applications by altering the configuration of the device in order to maximize the energy extracted from the ambient source. A review of these studies presents a wide variety of configurations, each of which proves to be advantageous under certain circumstances.

A number of different piezoelectric materials have been developed. The main piezoceramics in use today,  $\text{PbTiO}_3$  -  $\text{PbZrO}_3$  are synthesized from the oxides of lead, titanium and zirconium.  $\text{BaTiO}_3$  is also used. Special doping of these lead zirconate titanate ceramics (PZT) with, for example, Ni, Bi, Sb, Nb ions etc., make it possible to adjust individual piezoelectric and dielectric parameters as required.

Although PZT is widely used, its extremely brittle nature causes limitations in the strain that it can safely absorb without being damaged. [LEE05] note that piezoceramics are susceptible to fatigue crack growth when subjected to high frequency cyclic loading. In order to eliminate the disadvantages of piezoceramic materials and improve upon their efficiency, researchers have developed and tested other, more flexible, piezoelectric materials.

Another common piezoelectric material is poly (vinylidene fluoride) (PVDF). PVDF is a piezoelectric polymer that exhibits considerable flexibility when compared to PZT. [LEE04,LEE05] developed a PVDF film that was coated with poly (3, 4-ethylenedioxythiophene)/poly(4 styrenesulfonate) [PEDOT/PSS] electrodes.

They compared the PEDOT/PSS coated films to films coated with the inorganic electrode materials, indium tin oxide (ITO) and platinum (Pt). When subjected to vibrations of the same magnitude over varying frequencies, it was found that the films with Pt electrodes began to show fatigue crack damage of the electrode surface at a frequency of 33 kHz. The ITO electrodes became damaged when operating at a frequency of 213 Hz. The PEDOT/PSS film, however, ran for 10 h at 1 MHz without electrode damage. One can conclude that, by utilizing a more durable electrode layer, a piezoelectric device can operate under more strenuous conditions. This may give the device the ability to convert electro-mechanical energy throughout its lifespan; however, the exact effect of a stronger electrode layer may vary depending on the specific application.

[MOH03] developed a fiber-based piezoelectric (piezo fiber) material consisting of PZT fibers of various diameters (15, 45, 120, and 250  $\mu\text{m}$ ) that were aligned, laminated, and molded in an epoxy [BEN95]. This resulted in flexible composites with 40% of the volume consisting of aligned piezoelectric fibers and the remaining 60% made up of epoxy. Several samples were made in which several 34 mm  $\times$  11 mm rectangular plates of various thicknesses (1.2–5.8 mm) were diced from the composite such that the fibers were oriented in the plate thickness direction. The voltage output of the samples was tested by dropping a 33.5 g, 20 mm diameter stainless steel ball on them from a height of 10 cm. A maximum voltage and power output of 350 V was obtained for the thickest transducer, 5.85 mm thick, with the smallest fiber diameter, 15  $\mu\text{m}$ . Upon studying the relationship between voltage output and its physical geometry, it was determined that thicker plates have the capability of larger fiber displacements, and that samples with smaller diameter fibers have the highest piezoelectric coefficient, and lowest dielectric constant, both of which contribute towards higher power outputs and more efficient systems.

[SOD04a] presented a comparison of several piezoelectric composite devices. The harvesting ability of the macro-fiber composite (MFC), quick pack IDE (model QP10ni), and the quick pack model (QP10n) actuators was tested. The MFC contains piezo fibers embedded in an epoxy matrix which affords it extreme flexibility, and it utilizes interdigitated electrodes, which allow the electric field to be applied along the length of the fiber and act in the higher coupling mode. A detailed explanation of the operation and of various applications of MFC devices is presented by [SCH06]. The quick pack IDE contains interdigitated electrodes but conventional monolithic piezoceramic material, and the quick pack simply uses a traditional electrode pattern and a monolithic piezoceramic. To experimentally compare the efficiencies of these materials, all three were mounted to the same cantilever beam and thus subjected to the same vibration input. Tests were run at the first 12 vibration modes of the beam and the power output, which was normalized to volume because of the varying sizes of the specimens, was recorded for each device. It was found that at all vibration modes the quick pack proved to be the most efficient by harvesting the most energy, and that the MFC and quick pack IDE, while comparable, harvested considerably lower amounts of energy. The conclusion was made that the interdigitated electrode pattern of the MFC and the quick pack IDE results in low-capacitance devices which limit the amount of power that can be harvested. In a later study, [SOD05a] once again compared the efficiencies of three piezoelectric materials. The materials used in this study included a traditional PZT, a quick pack (QP) actuator, and the macro-fiber composite (MFC). Each specimen was excited at resonance, subjected to a 0–500 Hz chirp, and lastly exposed to random vibrations recorded from an air compressor of a passenger vehicle. The random vibrations recorded exhibited frequencies between 0 and 500 Hz. Both the power into the system and the power harvested by the piezoelectrics were measured in order to directly compute the efficiencies of each specimen. It was found that **the efficiency of the PZT for each vibration scheme was fairly consistent (4.5% at resonance, 3.0% for a chirp, and 6.8% for random vibrations) and was higher than the other two devices.** It was noted that the experimental configuration along with other factors varied between experiments so the efficiencies reported do not represent those of the actuators themselves, but simply present a comparison between the three actuators tested. The QP had efficiencies of 0.6% at resonance, 1.4% for a chirp, and 3% under random vibrations. The MFC had efficiencies of 1.75% at resonance, 0.3% for a chirp, and 1.3% for random vibrations. Again, these results suggest that

the QP actuator is more efficient than the MFC, however, it is also concluded that the PZT is the most efficient of all three materials.

A second method of increasing the amount of energy harvested from a piezoelectric is to utilize a more efficient coupling mode. Two practical coupling modes exist; the  $-31$  mode and the  $-33$  mode. In the  $-31$  mode, a force is applied in the direction perpendicular to the poling direction, an example of which is a bending beam that is poled on its top and bottom surfaces. In the  $-33$  mode, a force is applied in the same direction as the poling direction, such as the compression of a piezoelectric block that is poled on its top and bottom surfaces. Conventionally, the  $-31$  mode has been the most commonly used coupling mode, however, [BAK05] have shown that, for three different types of piezoelectric materials, the  $-31$  mode has a lower coupling coefficient,  $k$ , than the  $-33$  mode. Upon comparing a piezoelectric stack operating in the  $-33$  mode to a cantilever beam operating in the  $-31$  mode of equal volumes, it was observed that, although the stack was more robust and had a higher coupling coefficient, the cantilever produced two orders of magnitude more power when subjected to the same force. This result is due to the high mechanical stiffness in the stack configuration which makes straining of the material difficult. It was concluded that in a small force, **low vibration level environment, the  $-31$  configuration cantilever proved most efficient**, but in a high force environment, such as a heavy manufacturing facility or in large operating machinery, a stack configuration would be more durable and generate useful energy. This result was also presented by [ROU05] who concluded that the resonant frequency of a system operating in the  $-31$  mode is much lower, making the system more likely to be driven at resonance in a natural environment, thus providing more power. Analytically, [YAN05] have shown that, for a piezoelectric plate operating in the  $-33$  mode, the output power of the device is proportional to the coupling coefficient,  $k$ , and the dielectric constant,  $\epsilon$ . This confirms that **devices with higher coupling coefficients will produce more energy and behave more efficiently**. Also, through their analytical calculations it was shown that, **when the driving frequency is near a resonant frequency of the system, the output power is significantly increased. This is because when a system operates at resonance, much higher displacements and strains are observed** than when operating slightly above or below resonance.

[RIC04] present a similar study in which a general approach to establishing the relationship between the coupling coefficient, quality factor,  $Q$ , and the efficiency is presented. The quality factor,  $Q$ , is inversely proportional to the damping in an oscillating system caused by energy loss via heat transfer. **A system with a high  $Q$  value, therefore, does not lose much energy to heat, thus more energy is available for energy conversion through a piezoelectric device**. Richards found that **generally, high efficiencies can be achieved with moderate coupling coefficients but large quality factors** are necessary for the reasons described above. It can be concluded that the quality factor of systems deployed in field applications is an important design issue in order to optimize the efficiency of the control system.

[CHO05a] continued the work presented by Richards et al (2004) by analytically optimizing the coupling coefficient in a piezoelectric energy harvesting system and then testing the optimization scheme experimentally. First, an analytical model was created for a rectangular thin-film PZT membrane consisting of two layers, a passive elastic material and a piezoelectric material with a variable sized electrode on either side. Their model predicted that **the coupling coefficient increases with electrode size and reaches a maximum when the electrode covers at least 42% of the membrane area**. It was also found that the coupling coefficient can be increased by increasing the stiffness of the passive elastic layer and that an optimal piezoelectric layer thickness exists for each substrate layer thickness. Lastly, of all the process and design parameters, the residual stress was found to have the greatest effect on the coupling coefficient. Decreasing the residual stress in the device leads to significant gains in the coupling coefficient.

Another method of changing the configuration of a system in order **to improve its energy capabilities is to add multiple pieces of piezoelectric material to the system**. Many conventional systems consist of a single piezoceramic in bending mode, referred to as a

unimorph. The design of such a unimorph cantilever beam is described by [LOH06]. Another common configuration is a bimorph, which consists of two bonded piezoelectrics in bending. [SOD04c] developed a mathematical model to predict the energy generated from a piezoelectric bimorph cantilever beam. Upon experimentally validating the model, a maximum error of 4.61% was found.

[NG04, NG05] presented two types of bimorphs along with a unimorph piezoelectric. The unimorph consisted of a single piezoelectric patch mounted to a metallic cantilever beam. The first bimorph, referred to as the series triple layer, consisted of two piezoelectrics with a metallic layer sandwiched between them. The piezoelectric patches were connected electrically in series. The second bimorph, called the parallel triple layer, was the same as the series triple layer except that the piezoelectrics were connected electrically in parallel. Findings showed that under low load resistances and excitation frequencies the unimorph generated the highest power, under medium load resistances and frequencies the parallel triple layer had the highest power output, and under high load resistances and frequencies the series triple layer produced the greatest power. This result is due to the concept that **maximum power transfer from the piezoelectric device occurs when the load resistance is matched to the impedance of the piezoelectric device. A series connection increases the device impedance, leading to more efficient operation at higher loads**, as was found.

[JI05] also investigated methods of increasing the efficiency of a piezoelectric bimorph. Their study involved modelling a cantilever bimorph with a proof mass attached to its end and using the model to determine the relationship between performance and physical and geometrical parameters. Results showed that, by both reducing the thickness of the bimorph's elastic layer and by increasing the proof mass attached to the end of the cantilever, the resonant frequency of the system was substantially decreased. The **maximum power harvested was shown to be greater for lower resonant frequencies**.

Another effective way to improve the energy output is to stack a large number of thin piezoceramic wafers together, called the stack configuration, with the electric field applied along the length of the stack. [PL05b] investigated a 145 PZT wafers stacked mechanically in series, but electrically in parallel, to form a 1.0 cm square stack with a height of 1.8 cm. A solid monolithic cylinder of PZT with a diameter of 1.0 cm and a height of 2.0 cm was tested for comparison. The monolithic cylinder had a low capacitance of about 47 pF and a very high open circuit voltage of around 10 000 V. The PZT stack, however, had an increased capacitance in the range of 1–10  $\mu$ F and a decreased open circuit voltage of around 30 V. Through experimentation it was found that stacked and monolithic PZTs of the same geometry produce the same energy if the load resistance is matched to the physical system, but that the matching load is in the k $\Omega$  range for stacked configurations and in the G $\Omega$  range for monolithic elements. It was concluded that both **the voltage output and the matching resistive load are much more manageable in a PZT stack than in a monolithic configuration**, thus making the stack a more useful option.

Various geometries, have been studied. [MAT05] presented a brief analytical comparison between a rectangular cantilever and a triangular shaped cantilever with the large end clamped and the small end free. It was proven mathematically that a triangular cantilever with base and height dimensions equal to the base and length dimensions of a rectangular beam will have a higher strain and maximum deflection for a given load. **Higher strains and deflections in piezoelectric materials translate to higher power outputs**.

Rather than altering the profile of the conventional rectangular cantilever, [MOS05] changed the end constraints on the beam and created a so-called 'unimorph pre-stressed bender'. This is an initially curved, arc shaped, rectangular piezoelectric device that elongates when a force is applied to the top of the arc. The elongation causes strain in the active material which produces a voltage. The device is simply supported and allows for movement only in the lateral direction. Typically, these devices are used as actuators. The effects of varying different physical parameters of the pre-stressed bender mentioned in this study are presented. The conductivity of

the adhesive layer between the piezoelectric material and the passive metal layer, the thickness of the PZT layer, the thickness and type of the metal layer, and the width of the device were investigated. **Varying the metal thickness and type had a significant effect on the amount of curvature of the beam**, also known as dome height. **Larger dome heights correspond to larger strains and energy generation when compressed**. The most notable **increase in energy occurred, when the conductivity of the adhesive layer was increased by adding nickel particles**. This resulted in a 15.2% increase in the energy produced.

One final method of improving **the efficiency of piezoelectric energy conversion involves tuning the device so that its resonant frequency matches the frequency of ambient vibrations**. [COR05] investigated the concept of attaching a tuned auxiliary structure, similar to a vibration absorber, to a host structure to maximize the mechanical energy available. Analytically, it was shown that the auxiliary structure should be tuned to the frequency of the most dominant vibration mode of the host structure and placed at the location of maximum displacement for that mode. Also, it was found that the length of the auxiliary structure should be maximized and that a lower elastic modulus helps to increase the deflection in the beam, thus improving power output. Experimentally, a conventional piezoelectric harvester was attached to a host structure. A mistuned auxiliary structure was then used and a voltage output of 0.133 V was measured. Lastly, a tuned auxiliary structure was used and 0.335 V was measured.

[ROU05] further developed the idea of tuning the resonant frequency of a piezoelectric device to match the frequency of ambient vibrations. The concept of active self-tuning was explored. Active self-tuning is defined as a process in which power must be continually applied to the system to achieve resonant frequency matching. Passive self-tuning, on the other hand, only requires power to be supplied initially in order to tune the structure and then power is turned off while maintaining the new resonant frequency. Through mathematical modelling, it was shown that an active actuator that tunes the natural frequency of the system by either altering the stiffness or mass of the system will never result in a net increase in electrical power output. This discovery assumes that the system is well represented by the second order model developed by [WIL95]. In order to validate this conclusion, a PZT generator with an active tuning electrode was created in which the stiffness of the device could be altered by varying the voltage applied to the tuning electrode. When testing the device, it was found that, although the tuning circuit was able to alter the resonant frequency of the device, the power required to tune the frequency far outweighed the increase in power output. These results validated the conclusion that **an active self-tuning device will never result in an increase in energy generation**. It was suggested that passive self-tuning actuators be investigated for improving the efficiency of piezoelectric.

In order to create a completely passive system, [SHA06a, SHA06b] designed a device capable of resonating at various frequencies without the need for adjustment. The device consisted of multiple cantilever beams with various lengths and end masses attached to a common base. Each cantilever had a unique resonant frequency, the combination of which into a single device created a so-called ‘mechanical bandpass filter.’ By properly selecting the length and end mass of each beam, some of which had no end mass, the overall device was designed to have a wide band of resonant frequencies. An analytical model was developed to assess both the performance and limitations of the device. It was found that **a limited frequency band exists in which the device optimally converts ambient vibrations into electrical energy**.

## Modelling of Piezoelectric Smart Structures

The best known smart materials are certainly the piezoceramics. However, several others are available, Table 1.1 summarizes the different effects and couplings existing in materials considering the different conjugated physical fields classically involved. Couplings that are off-diagonal in Table 1.1 are typically responsible for the so called smart behaviour of materials. A material can be said smart if one of its smart coupling is (or can be made) sufficiently important to be used in active or semi-active devices.

Output Input field	Strain	Charge Current	Magnetic field	Temperature	Light
Stress	<i>Elasticity</i>	Piezo- electricity	Inverse magnetostriction		Photo- elasticity
Electrical field	Inverse Piezo- electricity	<i>Permittivity</i> <i>Conductivity</i>	Electro- magnetic effect	Electro- caloric effect	Electro- optic effect
Induction	Magneto- striction	Magneto- electric effect	<i>Permeability</i>	Magneto- caloric effect	Magneto- optic effect
Heat	Thermal expansion Shape memory	Pyro- electricity		<i>Specific heat</i>	
Light	Photo- striction	Photovoltaic effect			<i>Refractive index</i>
<i>Actuation</i>		<i>Sensing</i>			

**Table 1.1: Some effects in materials (off-diagonal coupling -> smart materials)**

An important characteristic of piezoelectric materials compared to other smart materials is its linear behaviour within a certain range. In linear piezoelectricity, the equations of linear elasticity are coupled to the charge equation of electrostatics by the means of the piezoelectric constants [IEEE]. **The quasi-electrostatic approach is adequate because the phase velocities of acoustic waves are several order of magnitude less than the velocities of electromagnetic waves.** Taking advantage of the symmetries of the mechanical tensors, a compressed matrix notation is introduced in place of the tensor notation. The constitutive equations read:

$$\{S\} = [s^E]\{T\} + [d]^T \{E\} \quad (1)$$

$$\{D\} = [d]\{T\} + [\epsilon^T] \{E\} \quad (2)$$

or (alternate forms using alternative choices of independent variables)

$$\{T\} = [c^E]\{S\} - [e]^T \{E\} \quad (3)$$

$$\{D\} = [e]\{S\} + [\epsilon^S]\{E\} \quad (4)$$

$$\{S\} = [s^D]\{T\} + [g]^T \{D\} \quad (5)$$

$$\{E\} = -[g]\{T\} + [\beta^T] \{D\} \quad (6)$$

$$\{T\} = [c^D]\{S\} - [h]^T \{D\} \quad (7)$$

$$\{E\} = -[h]\{S\} + [\beta^S]\{D\} \quad (8)$$

with

$$\{T\} = \{T_{11} \ T_{22} \ T_{33} \ T_{23} \ T_{13} \ T_{12}\}^T \text{ the stress vector}$$

$\{S\}$ , the deformation vector

$\{E\}$ , the electric field vector

$\{D\}$ , the electric displacement vector

$[c]$  and  $[s]$ , the elasticity constants matrices

$[\epsilon]$  and  $[\beta]$ , the dielectric constants matrix

$[d]$ ,  $[e]$ ,  $[g]$  and  $[h]$ , the piezoelectric constants matrix

The following relations between dielectric, elastic, and piezoelectric constants are verified; superscripts D, E, S and T indicate values at D, E, S and T constant respectively:

$$[c^E][s^E] = [c^D][s^D] = I_6 \quad (9)$$

$$[\beta^S][\epsilon^S] = [\beta^T][\epsilon^T] = I_3 \quad (10)$$

$$[c^D] = [c^E] + [e]^T [h] \quad (11)$$

$$[s^D] = [c^D] - [d]^T [g] \quad (12)$$

$$[\epsilon^T] = [\epsilon^S] + [d]^T [e] \quad (13)$$

$$[\beta^S] = [\beta^T] - [g]^T [h] \quad (14)$$

$$[e] = [d][c^E] \quad (15)$$

$$[d] = [\epsilon^T][g] \quad (16)$$

$$[g] = [h][s^D] \quad (17)$$

$$[h] = [\beta^S][e] \quad (18)$$

Due to crystal symmetries, the piezoelectric coupling matrices may have only few non zero elements [TZOU]. Referring to the equations (1), and (2), the element  $d_{ij}$  of  $[d]$  represents the coupling between the electric field in the direction  $i$  (if a poling occurred, its direction is taken as direction 3) and the strain in the  $j$  direction. Typical constitutive equations, for sensing (direct effect) and actuation (reverse effect) are written below.

$$\text{Sensing : } \begin{Bmatrix} D_1 \\ D_2 \\ D_3 \end{Bmatrix} = \underbrace{\begin{bmatrix} 0 & 0 & 0 & 0 & d_{15} & 0 \\ 0 & 0 & 0 & d_{24} & 0 & 0 \\ d_{31} & d_{32} & d_{33} & 0 & 0 & 0 \end{bmatrix}}_{\text{Coupling}} \underbrace{\begin{Bmatrix} T_{11} \\ T_{22} \\ T_{33} \\ T_{23} \\ T_{13} \\ T_{12} \end{Bmatrix}}_{\text{Permittivity}} + \underbrace{\begin{bmatrix} \epsilon_{11} & 0 & 0 \\ 0 & \epsilon_{22} & 0 \\ 0 & 0 & \epsilon_{33} \end{bmatrix}}_{\text{Permittivity}} \begin{Bmatrix} E_1 \\ E_2 \\ E_3 \end{Bmatrix} \quad (19)$$

$$\text{Actuation: } \left\{ \begin{matrix} S_{11} \\ S_{22} \\ S_{33} \\ 2S_{23} \\ 2S_{13} \\ 2S_{12} \end{matrix} \right\} = \underbrace{\begin{bmatrix} s_{11} & s_{12} & s_{13} & 0 & 0 & 0 \\ s_{12} & s_{22} & s_{23} & 0 & 0 & 0 \\ s_{13} & s_{23} & s_{33} & 0 & 0 & 0 \\ 0 & 0 & 0 & s_{44} & 0 & 0 \\ 0 & 0 & 0 & 0 & s_{55} & 0 \\ 0 & 0 & 0 & 0 & 0 & s_{66} \end{bmatrix}}_{\text{Compliance}} \left\{ \begin{matrix} T_{11} \\ T_{22} \\ T_{33} \\ T_{23} \\ T_{13} \\ T_{12} \end{matrix} \right\} + \underbrace{\begin{bmatrix} 0 & 0 & d_{31} \\ 0 & 0 & d_{32} \\ 0 & 0 & d_{33} \\ 0 & d_{24} & 0 \\ d_{15} & 0 & 0 \\ 0 & 0 & 0 \end{bmatrix}}_{\text{Coupling}} \left\{ \begin{matrix} E_1 \\ E_2 \\ E_3 \end{matrix} \right\} \quad (20)$$

The design of actuation and sensing devices is dictated by the available coupling modes (non-zero elements) in the piezoelectric coupling matrix. The modelling of piezoelectric material used has been addressed by many authors.

[CRA87] and [CRA89] proposed an analytical model for segmented piezoelectric actuators. The model consists in a Bernoulli-Euler beam with piezoelectric actuators bonded to the surface or embedded in a laminate. **A piezoelectric actuator can be replaced by an equivalent localized tensile force and bending moment.** The equivalent piezoelectric force and moment equations, so called equivalent actuator equations, are developed. An experimental validation with a cantilever beam actuated with a given voltage across the piezo actuator is presented. [CRA91] extended that model to the induced strain actuation **of both isotropic and anisotropic plates.** Equivalent normal forces and bending moments for piezo actuation of plates are derived **using the Kirchhoff-Love plate** assumptions. A Ritz formulation for approximate solutions is developed and applied to sandwich experimental models; aluminium and composite cantilever plates are presented.

[DIM91] did a similar work to model bidimensional patches bonded to the surface of a structure, deriving the equivalent actuator equations and applied them to the vibration of a rectangular plate for various actuator configurations. Similarly to the equivalent actuator equations, **an equivalent sensor equation can be written taking into account the contributions from extension and curvature of the sensor to the electrical charge** appearing on the piezoelectric media. [LEE96] established the general formulation for an **anisotropic piezoelectric laminate using the Kirchhoff-Love hypothesis.** Sensor and actuator equivalent equations are derived, boundary conditions are discussed and **the reciprocity between actuation and sensing is pointed out.**

[PAR96] modelled the piezo actuation of beams in torsion. **A one-dimensional beam model is used to determine the coupled extension/bending/torsion response to an applied voltage** across the piezo actuator. It uses the principle of virtual work and takes into account the cross sectional warping. Detailed results are derived **for a thin isotropic beam (Bernoulli-Euler)** with a surface bonded piezoceramic actuator and compared to experiments.

[CON92] extended Crawley's **theoretical model for a piezo-structure sandwich including the assumption of linear strain along the piezo thickness.** The developing and validation of a multilayered finite element for piezoelectric actuators elements bonded (or embedded) onto a homogeneous (or composite) structure. **Using an approach based on the analogy between thermal strains and piezoelectric strains,** the 1D, 2D and 3D models are investigated showing good agreements.

**The in-plane deformations become relatively more important when the thickness of the structure becomes comparable to that of the strips** [PRE97, LOI98]. Moreover it is worth insisting that for both the actuator and the sensor, **it is not the shape of the piezoelectric patch that matters, but rather the shape of the electrodes.**

[PIE00, LPP98] compared a **simplified approach of a pure bending beam model for surface bonded piezoelectric actuator/sensor**, with a shell model of embedded piezo actuation/sensing taking the membrane strains into account. **The strong reciprocity existing between actuation and sensing relationships has been demonstrated.** The beam theory accounts only for the component of the bending moment normal to the beam axis and neglects totally the in-plane force (Figure 1.4). Conversely, the sensor signal given by the beam theory accounts only for the component of the rotation along the contour normal to the beam axis.

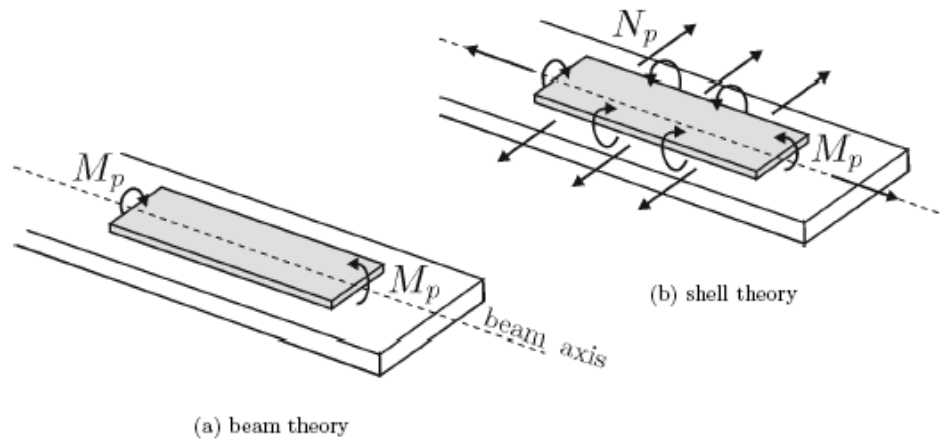


**Figure 1.4 (courtesy of [PIE00]): Equivalent piezoelectric loads for a rectangular piezoelectric patch**

Different approach for modelling thin and thick shells have been proposed in literature.

[TZ90, TZ91] derived a thin brick element for distributed dynamic measurement and active vibration control of a rectangular plate; the element consists in a **thin solid piezo electric brick having 8 structural nodes with 4 degrees of freedom per node** (3 translations and the electric potential). A classic configuration for an intelligent structure is composed of a master structure sandwiched between 2 piezoelectric thin layers acting as the distributed sensor and actuator. **Both bonded and embedded piezoelectric sensors and actuators result in a laminate; the multilayer structure is modelled by stacking the thin brick elements together and connecting the corresponding nodes.** The model is applied to the vibration control of a simply supported square plate. Mode shape and modal voltage distribution are obtained thanks to the model.

[HA92] used a **similar brick element** where the multilayer structure is taken into account. That element is used **to model the cantilever plate** described in [CRA91] (static case), to determine the step-response of a cantilever beam and to design the active damping of the first mode of sensor/actuator composite cantilever plate. The results are compared to the results found in [CRA91] and shown good agreement with experiments.

[RA93] established a **finite element formulation of thermo piezoelectric problems** starting from the linear thermo piezoelectric constitutive equations established by Mindlin and the Hamilton's principle. In their paper, they used the quasi-static equations of thermo piezoelectricity to develop sensor and actuator equations; a finite element formulation is presented. A distributed control system consisting in a **cantilever beam sandwiched between a piezoelectric sensor/actuator pair** is used to evaluate the proposed finite element approach on the static and dynamic behaviour.

[TZ96] derived a **12-nodes triangular thin solid plane element with 4 degrees of freedom per node**; it uses shape functions quadratic in the two in-plane directions and linear in the transverse direction **with the assumption of a layer wise constant shear angle (Mindlin hypothesis)**. A laminated structure is obtained by stacking elements together and connecting the corresponding nodes; this element is validated by modelling the actuation of a bimorph pointer. To stress the influence of the piezoelectric coupling on the vibration characteristics, a semicircular ring shell has been modelled using 60 triangular shell elements (20 for each layer and 10 element meshes along the length); the evolution of its eigenfrequencies with a growing number of short-circuited electrodes is examined.

This element has been extended later by [KO98] to **isoparametric curved triangular and quadrangular elements** with shape functions of different polynomial degree for each layer; the model is applied to a rectangular plate of composite material with surface bonded piezo patches under static voltage load, simply supported on two edges. **The modelling of shells using solid elements results in an excessive shear strain energy in the thickness direction.** A commonly used solution to overcome this difficulty consists in adding internal degrees of freedom resulting in large problem size requiring techniques such as the Guoyan's reduction.

When the thickness becomes small, the behaviour of the elements accounting for the transverse shear strain is driven by transverse shear stiffness while the transverse shear strain should be negligible. This also leads to the shear locking phenomenon. Solutions to overcome this problem can be to use a reduced integration scheme for the transverse shear stiffness or to use different interpolation functions for the transverse shear strain. The latter is the solution adopted by the element used by [PIE00]: Mindlin shell element from the commercial finite element package Samcef (Samtech s.a.).

[LEE96] derived a **thermo piezoelectric multilayer beam element**; it uses shape functions linear along the beam and linear through the thickness of each layer. **A reduced integration scheme for the transverse shear stiffness is used**; the element takes into account the effect of constant thermal load (constant gradient of temperature). A cantilever beam under thermal load is modelled.

Later, [SAR97] presented a multilayer **piezoelectric thin plate using the Kirchhoff-Love assumption** (linear displacement field through the thickness) and bilinear shape functions; it has **1 electrical degree of freedom per piezoelectric layer per node, assuming a constant electric field through the thickness for each layer** (layer wise linear transverse shape function for the electric potential). That shell element has been applied to the modelling of a simply supported plate and shown good agreement with exact solutions for moderately thin plates, an actuated cylindrical panel to study the effect of the actuator placement through the thickness which exactly matches a Ritz solution and a cantilever cylindrical shell to show the effect on actuation and sensing of the difference between continuous and discontinuous transducers and the effect of the curvature on the tip displacement and sensing. It was later used to evaluate the passive damping of piezoelectric shells with integrated electrical network and compared with experiments.

A **pure bending (Kirchhoff assumption) plane rectangular plate element** is proposed in [HW93], the main idea is the use of a multilayered plate element with a single electrical degree of freedom per piezoelectric layer, the voltage across the thickness of the layer, uniform on the element surface. This **multilayer element has 4 nodes with 3 degrees of freedom per node (1 translation and 2 rotations) and 1 electrical degree of freedom for each piezoelectric layer (voltage across the layer)**. This element **neglects the transverse shear and is therefore not suitable to model thick shells**; it does not account for the extension, modelling only the bending behaviour. The bimorph pointer is modelled numerically and the results were compared to an analytical solution and shown a good agreement.

[SUL95] proposed a **4 node plate element using** bilinear shape functions and the **Mindlin assumption (constant shear angle) to accommodate thick as well as thin shells; each node has 5 degrees of freedom (3 translations and 2 rotations), the element has one additional electrical degree of freedom per piezoelectric layer (voltage across the thickness).** This element is demonstrated using the plate described by [CRA91], a bimorph pointer and panel flutter control is made.

[SAM96] used a **cubic displacement field with a 8 node quadratic rectangular multilayer plate with 2 electrical degrees of freedom (constant voltage over the element across the only two piezoelectric outer layer) and 11 mechanical degrees of freedom per node (3 translations, 3 slopes and 5 higher order rotations).** A simply supported plate is modelled; the fundamental natural frequencies and forced response were computed and shown good agreement with exact solutions.

As a first step towards the development of simplified integrated computational tools for the dynamic and static modelling of smart structures, [COT04] validates both theoretically and experimentally the implementation of a **multilayered three-dimensional model based on the analogy between thermal strains and piezoelectric strains under MSC/NASTRAN.** To assess the piezoelectric–thermal analogy for different loading conditions, the numerical results obtained from this model are first compared to the results obtained from a finite element reference model based on a three-dimensional piezoelectric formulation. An experimental assessment is also conducted on a clamped AS4/3501-6 carbon/epoxy composite beam structure excited in the vicinity of the clamped end using an embedded piezoelectric actuator. Results obtained from the dynamic response of the structure show that the properties of the insulating layer appear to have an important effect and thus demonstrate the need for their modelling. In the last part of the paper, as a tool for further development of the computational tools for smart structures, the piezoelectric–thermal analogy model is used with a large number of three-dimensional elements to describe the complexity of the strain and stress fields in the vicinity of the active region.

## Shunted Architectures for Smart Systems and Applications

Many different electrical circuit using shunted piezoceramics have been proposed to damp structural vibrations and to reduce sound pressure level as well. In Figure 1.5 some shunt circuit are proposed. The reason of the big interest and demands of designing a shunt circuit for smart damping materials can be summarized as follows: the shunt circuit should minimize structural vibration efficiently. This efficiency should be robust against system parameter variations, and stability should also be guaranteed. Furthermore, the shunt circuit should not require power for operation and the weight and cost of the implemented circuit should be kept to a minimum. Since it is intended to integrate the shunt circuit into the structure, its size should be as small as possible.

### Shunt architectures review

#### • *Resistive Shunts*

Hagood and von Flotow [HA91] suggested an R shunt, i.e. the connection of a piezoelectric transducer to a resistor dissipating structural energy by heat. This shunt is very easy to implement, very cheap and does not require any power for operation. However, its damping performance is very poor and in some applications even not measurable.

#### • *Capacitive Shunts*

Networks of capacitors which can be shunted on piezoelectric transducers have been suggested by [DDL01, DLD97]. This technique changes the stiffness of the transducer and therefore the natural frequency and modal damping ratio of a piezoelectric actuator is altered. In this method, the shunt circuit is only used to change the stiffness of the piezoelectric transducer and thus changing natural frequency of the piezoelectric mechanical damper. This means that unlike resonant shunts, no electrical resonance is created.

#### • *Resonant Shunts*

More efficient are resonant shunts [For79, HA91, TW99, Moh03, NFMM04], like single mode R–L or resonant multi-mode shunts. These types of shunts generate an electrical resonance with the piezoelectric capacitance. If this electrical resonance is tuned to one of the structural modal frequencies, a considerable effective damping of the corresponding mode is achieved. In literature, this is often compared with a mechanical damper. However it can be shown that it is not exactly the same but similar. Resonant shunts can be divided into resonant single mode shunts and resonant multi mode shunts. To implement resonant single mode shunts, parallel [Wu96] or serial [HA91] resistor-inductor (R–L) networks were proposed. While single mode shunts can only damp one structural mode, multi-mode shunts are able to damp several structural modes with one single piezoelectric patch. [Wu01] proposed blocking circuits whereas [BM02] suggested current flowing circuits for multi mode shunts. The performance of blocking circuits is slightly better for 2 or 3 modes than with current flowing circuits, but for more modes, the blocking circuit gets very complex whereas the complexity of the current flowing circuit increases linearly. Generally, all resonant shunts suffer from the drawback that their damping performance is very sensitive to variations in the system's parameters. In this case, the resonant shunts get mistuned and do not damp anymore. Therefore, online tuned resonant shunts have been proposed [KC01, FM03a]. However, the suggested tuning algorithms have not shown satisfying results, as they are very slow, difficult to implement and do not converge well. Moreover, the implementation of these adaptive resonant shunts is very bulky, e.g. Hollkamp and Starchville [HT94] used a motorized potentiometer to change the inductance. In some publications, adaptive shunts are referred to as semi-active, because they are actively online-tuned. According to the definition of passive shunts in equation, adaptive resonant shunts are still passive if the inductor and resistor value remain positive. However, these online-tuned shunts are no longer linear. Since very large inductance values are required for resonant shunts, they have to be synthesized with virtual inductors using operational amplifiers.

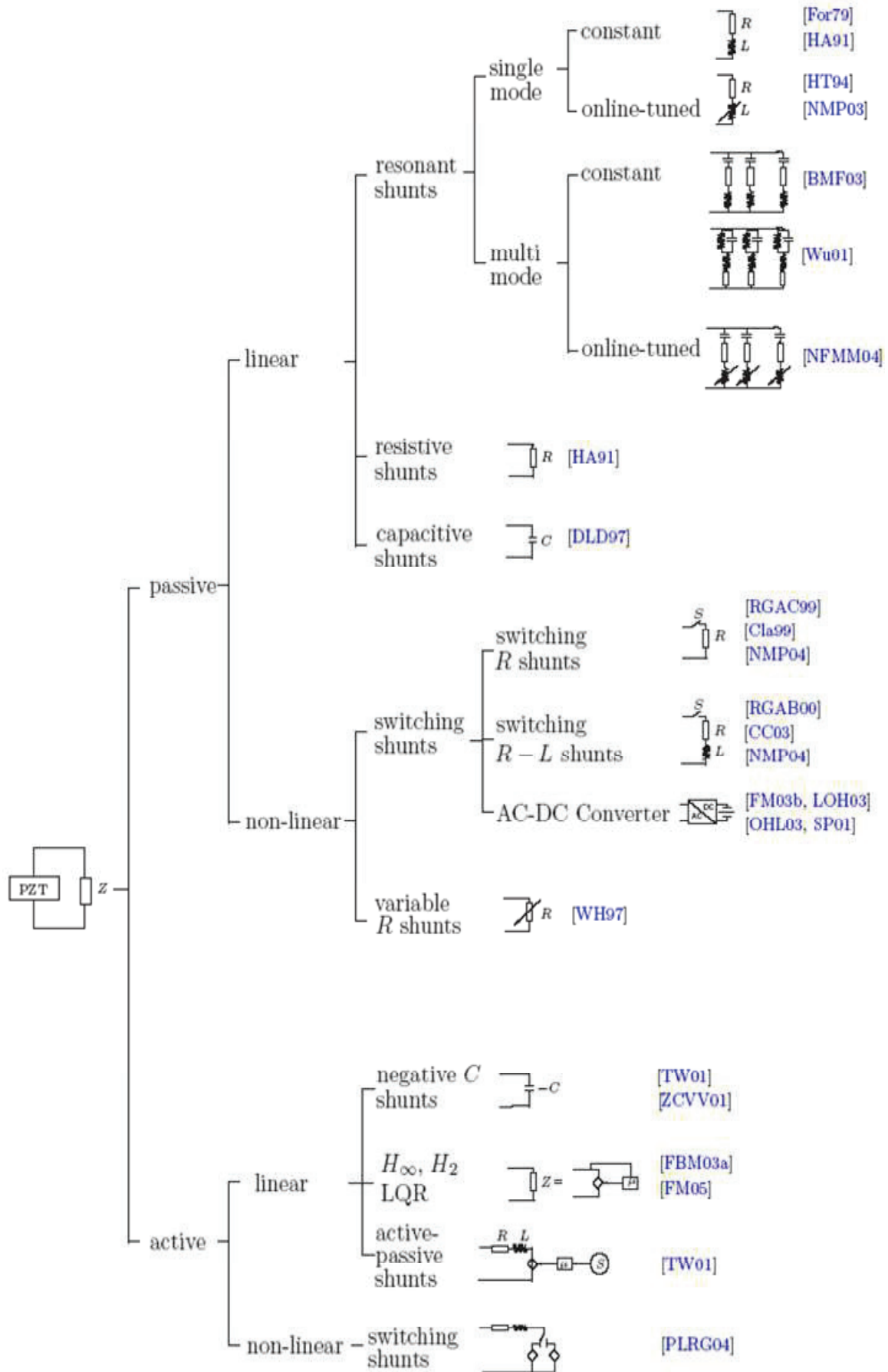


Figure 1.5 (courtesy of [NIE05]) : Different topologies of shunt architectures for shunt damping

The main achievements of [NIE05] are the development and implementation of novel online-tuned multi-mode resonant shunts for piezoelectric shunt damping. An online-tuned resonant shunt is introduced that automatically adapts itself for the optimal vibration suppression of one or several modes using a novel adaptation technique. It turns out that this new adaptation methodology tunes much faster than traditional methodologies and shows less miss-adjustment. Furthermore, implementation of the adaptation law is shown to be straight forward and realizable with a simple analogical circuit.

#### • *Switching Shunts*

These circuits implement switches to change the dynamics of the shunt in such a way that the vibration damping can be improved. Switching shunts seem to be promising for an implementation that does not require power, because the switches can be realized with MOSFETs that require meaningless power to be switched and the small amount of power required to switch the MOSFETs that could be supplied by an additional piezoelectric patch. However, all switching shunts proposed in the scientific literature have been implemented with complex digital processors and signal conditioners requiring more power for operation. The switching shunt proposed by [Cla00] is based on the switching of the active piezo element from an open circuit to a short circuit state at specific times synchronously with the structure's vibration. This method referred to as "State Switching", for adjusting the stiffness of the piezoelectric structure to the motion phase. The piezoelectric element is short-circuited at each maximum of the strain and held in short circuit until mechanical energy in the piezo disappears. The effect of the switching action is to remove the electrical potential energy converted from the mechanical strain through the piezoelectric effect. Experimental and anecdotal evidences have shown that state-switched control strategies for piezoelectric actuators can be advantageous. However most discussions of the stability of these systems has relied on heuristic, or physically motivated arguments. This paper shows that open-circuit-short-circuit state switching control laws can be viewed as hybrid dynamical systems of [WIT96] type. Roughly speaking, hybrid systems are a class of dynamical system containing both discrete and continuous states. Within this framework, the closed-loop stability of this kind of switching is rigorously established using the method of multiple Lyapunov functions [CLA00, KUR03]. Later, switching R-L shunts have been proposed by [RGAB00, CC03]. These switching shunts achieved more promising results, but the optimal switching law still remains unclear. This second method is the Synchronised Switching Damping (SSD). It consists also in modifying the voltage on a piezoelectric element bonded on the structure with a simple switch driven during short periods. The switch connects the piezoelectric element to a circuit which can be either a simple short circuit (SSDS), a small inductor (SSDI) or voltage source (SSDV). This methods, again offers several advantages: it is insensitive to environmental changes due to its self-adaptive broadband behaviour. It doesn't require a very large tuning inductor for low and very low frequencies, multi-modal damping is achievable without complex circuits and only a very low power supply is required to operate the switch. [LE04] improved the switching shunts by adding a negative capacitor. Nevertheless, only simulations have been done and the problem of the optimal switching law has not been solved. Moreover, negative capacitors are difficult to implement, tend to instability and require an active implementation, exactly what is tried to be avoided with switching shunts. In the past, it was unclear how to switch these kinds of circuits in order to achieve optimal damping, because the system of interest is hybrid in nature. [NIE05] shows how to apply a hybrid system framework using a control methodology in order to obtain the optimal switching sequence. Additionally, a multi parametric programming approach is presented that leads to the optimal switching law. Afterwards, the derived switching law is approximated and implemented with a simple analogical circuit that does not need power for operation. Experiments demonstrate that this circuit achieves better vibration suppression than all other shunt circuits that do not need power for operation and have been proposed so far. [FA06, RIC07] proposed an analytical model for multimode switch signal. They showed that the detection of a local maximum is not optimal for the case of multimodal control. The authors proposed a probabilistic criteria (detection of the maxima significantly exceeding the average level) giving a good result. The control was applied also to the acoustic comfort field. In [KAN03] an innovative method of semi-active vibration suppression

with energy-recycling approach has been proposed and investigated to improve the performance of semi-active vibration control with piezoelectric transducers attached to a vibrating structure. Vibration of the structure are suppressed semi-actively by controlling a switch of a passive electric circuit, so as to change the state of the passive system, instead of actively supplying electric charge or voltage to the piezoelectric transducer. Therefore, since no external energy can flow into the system, the system is stable even if it is controlled improperly. [DUC09] deals with mechanical vibrations reduction by means of passive and semi-passive shunt circuits. Two electromechanical reduced order models (based on analytical and finite element formulations) are proposed, allowing the accurate study of the dynamics of the whole structure-piezo-circuit system. The electromechanical coupling factor is shown to be the decisive factor for the performance of the system. In order to obtain good performance without having to tune the system, one can use a switching passive circuit which opens and closes at a precise timing. This system, which is the main object of this study, uses the electrical charge stored on the piezoelectric elements to counter the vibrations, with an effect similar to dry damping. As the switch timing is synchronized on the vibrations, no precise tuning is required, the system is self-adaptive and can be self-powered. For each system, a theoretical analysis of the performance is made, with either one or several degrees of freedom models. Experimental results are found to be in good agreement with the theory; however the strong non linearity in time domain create a high frequency excitation of the structure which can disturb the synchronization and the difficulty of correct switch timing is also observed.

#### • *AC/DC converter*

Power harvesting from piezoelectric transducers can either be used to damp vibration [LOH03] or to supply power to other electronic circuits. [OHL03] proposed an AC-DC rectifier circuit with a switch-mode DC-DC converter to control the maximal power flow, which was then used to charge a battery with an efficiency of around 74% to 88%. A half-bridge AC-DC converter was proposed in [FM03b] to synthesize an impedance, i.e. to shunt damp the system, and to harvest power. However due to the highly reactive nature of piezoelectric shunt damping circuits, such operation has been avoided to date. In shoes, power harvesting was used to supply wearable computer systems with power [SP01], e.g. an active radio frequency tag that transmits a short-range 12-bit wireless identification code while the bearer walks. For this application, an AC-DC diode-bridge rectifier with a DC-DC step-down converter was used. However, the well-developed power harvesting circuits require almost as much power as they harvest, especially in cases where low vibration are found.

#### • *Variable Resistive Shunts*

[WH97] suggested a variable resistive shunt. They tried to find the “ideal” periodic resistance time history by assuming that the resistance varies linearly with time between the values at the endpoints of each vibration interval. The varying resistance was determined by maximizing the loss factor of the shunted composite system. This was done by dividing each half-cycle into a number of equal intervals and using a simplex optimization routine. However, no experimental results were presented and it remains unclear whether this shunt is able to significantly damp the structure since resistor shunts or switched resistors have not shown promising results. Additionally, the implementation of the variable resistor with controller is not straightforward.

#### • *Negative Capacitors*

As the resistive  $R$  shunt cannot dissipate much energy because of the reactive power components of the piezoelectric capacitor, negative capacitor shunts have been proposed [Wu01, WB96, Wu00, Par03]. The negative capacitor eliminates the piezoelectric capacitance such that the resulting resistor can optimally dissipate energy. This means that the power factor is corrected by the negative capacitor in the shunt. In experiments, it was shown that this shunt circuit is highly sensitive to variations within the piezoelectric capacitance. If the absolute value of the negative capacitor is larger than the piezoelectric capacitance, then the system becomes unstable. Moreover, the implementation of a negative capacitor requires active circuit components.

#### • *Active Shunt Controller via Control Oriented Synthesis*

Generally, any shunt circuit can be regarded as a controller that regulates the current as a function of voltage or vice versa. This means that the shunt circuit can be designed using a standard control technique like the LQG, H2 or  $H_\infty$  design [FM05]. However, it turned out that a very well identified model of the system is needed and the control design is not straightforward due to the highly reactive impedance of the piezoelectric transducer. Additionally, the resulting shunt circuits are active and it is very difficult to implement them with analogical circuitry. Therefore, they have been implemented with a synthetic impedance that is introduced later in this chapter. Nevertheless, Fleming and Moheimani [FM05] implemented an active impedance with considerable damping that is robust against small variations in the mechanical structure. It could be shown that the resulting controller is similar to a resonant shunt with additional negative capacitance.

#### • *Active Switching Shunts*

[PLRG04, RIC07] proposed a switching shunt (SSDV), where a switch connects two different voltage sources through a resonant network to the piezoelectric transducer. This technique is similar to the Synchronized Switch Damping Inductor (SSDI), but in the case of a weak coupling coefficient, this new configuration can enhance the damping performance. However, it requires an additional energy source.

Other shunt circuit solutions with less impact on the research scene have also been described for sake of completeness:

#### • *Distributed Electrical Networks*

Distributed electrical shunts were proposed by [PdFM04, MdV04]. In this technique, several piezoelectric transducers are interconnected via shunt circuits. However, their solution resulted in very complex networks with gyrators and transformers that are hard to build and require active filters. Their latest results with simple distributed networks [dMP04] are comparable with the damping performance of a resonant shunt for one piezoelectric transducer.

#### • *Discrete time piezoelectric damper*

In [KPVG97, KPVG00], a method of vibration control using a discrete time controller is presented. This controller is called Strain Amplitude Minimisation Patch (STAMP) damper. Experiments with four piezoelectric patches as both actuators and power sources and one piezoelectric patch as a sensor showed that at resonance frequency the vibration was reduced by 39.5 %, while for a resistor or a parallel  $R - L$  shunt the vibration was reduced by 17.3 % and 62.7 %, respectively. Furthermore, it is self-powered and therefore does not need any external power. Unfortunately, over the last few years there has been a lack of publications using this method, and a reduction of 39.5 % (4.4dB) for five piezoelectric patches is rather poor.

#### • *Self-Sensing Technique*

The self-sensing or sensor-actuation technique estimates the strain of the piezoelectric transducer by subtracting the piezoelectric capacitive voltage drop from the applied voltage at the terminals of the transducer [AHG92, DIG92, LLH03]. This strain information is feedback through a controller to the terminal voltage of the piezoelectric transducer. The self-sensing technique is similar to active shunts, but suffer from the drawback that the estimation of the strain is highly sensitive to the piezoelectric capacitance. This uncertainty may decrease significantly the performance and could cause instability.

## Shunt techniques applications

Shunt damping has been applied for high-end products in the aerospace industry and also for low-cost products like sports equipments. In aerospace, vibration suppression is challenging because the weight of the damping devices should be kept as light as possible. Shunted piezoelectric materials can be an alternative.

An interesting industrial application in the field of aeronautics and automotive in general, is the interior sound level reduction. The acoustic comfort is a very important problem in everyday life. In order to control sound waves propagation and related resonances, active control techniques have been used for several years and implemented in noise control [HO00]. The most usual practice is the use of antinoise, which consists in controlling the interference of the incident unwanted sound waves with a properly controlled wave generated by a secondary source. This methods has been successfully applied to reduce the noise level experienced by passengers in the compartment of a motorcar [PF05]. A piezoelectric actuator is driven by a voltage generator controlled by a proper feedback law based on a model of the structure [MATA06]. The main negative aspect is a complexity of the system and a large required operative energy. Another approach has been suggested, namely a combination of active and passive noise reduction techniques [LEE02], but it requires an increased panel's mass. Many studies reported the reduction of noise transmission by proper control of the transmitting structure vibration damping [HO01]. [Lie01] proposed shunted piezoelectric transducers to damp blades of helicopters. In [MK01], the nonlinear, supersonic panel flutter was reduced using shunted piezoelectric patches and [AHvFV93] implemented a shunted piezoelectric patch configuration for damping space structures. [MPS+99] proposed to damp the solar array of the Hubble Space Telescope with shunted piezoelectric materials and [NGDH93] suggested to suppress vibrations in spacecrafts with the same approach. [CF02] used shunted piezoelectric patches to suppress turbo machine blading-flow induced vibrations. As shown in [AJI01] and suggested in a patent [Mat03], shunt damping can be applied for reducing the noise transmission through structures. [ZCVV01] used R–L or negative C shunts for echo cancellation of a submarine. In the patents [BH01, QSWH02], R–L shunts are used to damp the head of a disc drive and patent [Tre01] suggests an R–L shunt to damp breaks. [PLC+04] proposed an R–L shunt to reduce vibration of a CD-ROM case. Most of the low-cost applications using shunt damping have been presented for sport equipments. For example, the ski company K2 proposes shunts for skis and snowboards [Van98]. They use a passive (resistor) or an active damper, with the latter requiring a battery. The former Active Control Experts ACX, published many patents of shunt damping for sport equipments. For example [LMJA99, LGR+01, BSP99] proposed R shunts and shunting LED lights for skis, tennis racquets, baseball bats and golf clubs. They claimed to achieve 30% additional damping. In particular, [LMA+02] describes smart snowboards where vibration is unwanted because they can lead to instability of the boarder. Thus the vibration was suppressed using resistive shunted piezoelectric patches, like R shunts. Patent [LRM+00] proposes resonant shunt circuits for skis. However, a bulky inductor of 22 H is required, that was wound on a core which was mounted mid-plane in the circuit board. As the temperature on skis can vary by more than 30C°, it is doubtful, whether this resonant shunt can damp the structure well over such temperature ranges, as we will show in Section 4.1. Head's patent [KL01] also proposes R or R–L shunts for tennis rackets. In a recent patent of the Head Company, Lammer [Lam03] proposed switching shunts for skis and tennis rackets. These shunt circuits are self-powered, i.e. no external energy source like a battery is necessary. The proposed circuit is claimed to reduce the oscillation amplitude by a factor of at least 1.5, preferably at least 2.0. The circuit comprises 4 transistors, 6 resistors, 4 diodes, 4 capacitors and one piezoelectric actuator. The piezoelectric transducers are laminated to the ski body. A similar approach is also described in Heads patent [Lam04].

## **Part II**

### **Included Papers and Abstract Proceedings**



# Accepted for Publication on International Peer Reviewed Journals

M. Ciminello, S. Ameduri, A. Concilio, “**FE Modelling of an Innovative Vibration Control Shunt Technique**”. *Journal of Intelligent Material Systems and Structures* Vol.19, N°8, August 2008 pp.875-887.

M. Ciminello, S. Ameduri, A. Calabrò, A. Concilio, “**Synchronised Switched Shunt Control Technique Applied on a Cantilevered Beam: Numerical and Experimental Investigations**”. *Journal of Intelligent Material Systems and Structures* Vol.19, N°9, September 2008 pp.1089-1100.

M. Ciminello, L. Lecce, S. Ameduri, A. Calabrò, A. Concilio, “**Switched Shunt Control implemented through a PZT network embedded within a composite panel: design, manufacture and test**”. Accepted for publication to – *Journal of Intelligent Material Systems and Structures JIM-09-188*.

*A multi-dofs electro-mechanical coupled system has been numerically modelled by means of a finite element formulation. A finite element tool integrating Nastran features with Matlab routines has been developed. Piezo strain actuation has been modelled with a 3D finite element description of the structural laminate using the analogy between thermal strain and piezoelectric strain. The effects exerted on the structure have been applied as concentrated moments at the piezo nodes interface. The piezo moments have been compared and validated using well-established strain actuation analytical model. The sensing has instead been modelled with a 2D piezoelectric constitutive equation and experimentally validated. The single mode and multi mode synchronised switch control have been experimentally validated for both aluminium cantilevered beam and a fiber-glass 10-ply laminate plate. The piezo sensor-actuator collocated couples have been used in both bonded and embedded configurations and placed according to an optimization process based on the max stored electrical energy.*

*Moreover an original circuit, based on a tachometer and CMOS devices has been realised to implement the synchronized shunt control. The tachometer device can generate a pulse train signal activating the CMOS, perfectly synchronized with the zero crossing of the input. Moreover the amplitude of the logical signal can be opportunely set according to a voltage threshold fail-safe philosophy. A 4-independent channel electric card of 10×10cm in-plane dimensions and 80gr in weight with a plug and play philosophy have been built up, in order to friendly manage a set of piezo transducers network for multimode control test. Numerical results concerning the dynamic response reduction of structural-acoustic systems, attained by using a synchronized switch control technique, are also investigated.*

---

S. Ameduri, M. Ciminello, “**Fourier Expansion Solution for a Switched Shunt Control Applied to a Duct**”. Accepted for publication to : *Journal of Theoretical and Applied Mechanics (JTAM)*, No. 2 or No. 4, Vol. 48, 2010.

*An attempt to face with a semi analytic solution exclusively for a simple 1D test case of a fluid duct, has also been taken into account.*



# FE Modeling of an Innovative Vibration Control Shunt Technique

MONICA CIMINELLO,<sup>1,\*</sup> SALVATORE AMEDURI<sup>2</sup> AND ANTONIO CONCILIO<sup>2</sup>

<sup>1</sup>*Università degli Studi di Napoli "Federico II", Via San Donato 25, zip 80126, Napoli, Italy*

<sup>2</sup>*Centro Italiano di Ricerche Aerospaziali, CIRA, Via Maiorise, zip 81043, Capua (CE), Italy*

**ABSTRACT:** The possibility of simulating and predicting the dynamic behavior of controlled structural systems is a challenging goal because of the complexity of the related architectures. As a matter of fact, obtaining accurate information on system response in pre-design and design phases may reduce both computational and experimental efforts. In this study, the numerical simulation of a specific family of semi-active vibration control devices is taken into account: piezoelectric acting in the synchronized switched shunt architecture (SSSA). Different from the classic shunt inductive architecture, the SSSA is characterized by a switch component adaptively synchronized with the structural response to be controlled, whatever it is. The ability of controlling low range frequencies without large limitations in terms of inductive components represents, together with the adaptive skill, the main advantage of this technique.

The reference structure is represented by an isotropic plate, clamped on the edges; the active system is made of an isolated PZT patch, located at the center. A dedicated simulation tool has been realized and implemented to predict piezo effectiveness for the considered configuration. Related matrices have been suitably integrated within the complete model. The switching state of the electrical circuit causes the matrices elements to be time-variant; the related problems have been dealt with in a Newmark-Beta-based integration solver. The integrated structural system has been fully and simultaneously simulated, considering at the same time the structural dynamics, the nonlinear behavior of the electrical device, and the piezoelectric electromechanical response. Results have been presented in terms of time response. The innovative contribution reported in this study concerns the application of the FE approach to the design of a SSSA integrated within MDOF structural systems. A characteristic of the approach is the ability of interacting with commercial FE codes, like MSC-Nastran, in designing and simulating the SSSA control action. References reported in this study face the SSSA control problem applied to single DOF systems (not directly applicable to complex systems, but through modal analysis reduction operations) or deal with FE simulation of classical inductive shunt (not switched). The details of this statement are fully reported in the Introduction.

*Key Words:* switched shunt control, piezoelectric, semi-active control.

## INTRODUCTION

STRUCTURAL vibrations control can be considered as a real technological challenge because of the large amount of related problems. As a consequence, many efforts have been made on defining, realizing, and characterizing different typologies of control techniques, according to the specific problem.

Passive typology (Ciminello and Ameduri, 2005) is one among the most commonly adopted techniques: they never provide the structure with artificial energy and their functionality is essentially based on

appropriate modifications of the structural mass, damping, and stiffness matrices.

Despite their easy implementation and low cost, their performance is generally inadequate to meet all the necessities (Bisegna and Caruso, 1999).

A specific passive typology is represented by the shunt resonator family: vibrations are reduced by using electric circuits and electromechanical devices, suitably positioned on the element.

Four typologies of shunted circuits (Figure 1), inductive, resistive, capacitive, and switched, were presented by Lesieutre (1998) for the first time in literature.

Lesieutre emphasized that the inductive circuits which include an inductor and a resistance in parallel with the PZT (Figure 2) are the most widely used in damping as

\*Author to whom correspondence should be addressed.

E-mail: monicacimm@libero.it

Figures 3, 5, 6, 10, 11 and 13–15 appear in color online: <http://jim.sagepub.com>

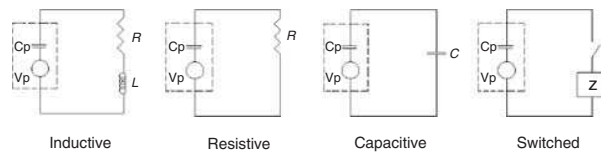


**Figure 1.** Configuration of the four different shunted circuits.

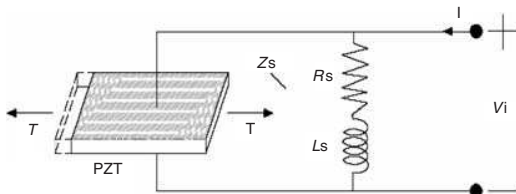


**Figure 2.** Mechanical model of the PZT patch with shunted circuit.

they are analogous to the mechanical vibration absorbers.

Hagood and von Flotow (1991) presented the first quantitative analysis on the mechanical energy dissipation with PZT shunted with passive electrical circuits. They introduced a nondimensional model that indicates that the damping effect of shunted circuit resembles that of viscoelastic materials. Shunting with a resistor and an inductor introduces an electrical resonance, which can be optimally tuned to structural resonances in a manner analogous to a mechanical vibration absorber. They applied their model to a cantilever beam and verified the accuracy of the model experimentally.

Law et al. (1996) presented a method for analyzing the damping behavior of resistor shunted PZT materials, based on energy conversion principle rather than mechanical analogies. A two degree of freedom (DOF) experiment was set up to test the accuracy of the model, and the experimental results were in good agreement with the model predictions. Park and Inman (1999) compared the results of shunting the PZT elements with an RL circuit connected either in parallel or in series. They developed an analytical model to predict the behavior of a beam with a shunted circuit. The predictions of the model were verified experimentally.

McGowan (1999) pointed out how passively controlled shunt circuits were a viable alternative to the active control. In her research she pointed out that there were two important issues that needed to be considered in using PZT as actuators for active control systems: the large amount of power for operation, and the complexity of the hardware involved with active control (added hardware, control law design, and implementation). McGowan showed how passive damping with shunted PZT required simple electrical circuitry and very small power.

Although either passive or active control techniques are highly recommended for a wide range of applications, (Agneni et al., 2003) there are some instances

when hybrid systems provide the best solution for vibration suppression.

Kahn and Wang (2001) presented for the first time the results of a hybrid technique in the structural vibration control field. The advantage of such a system is the overall stability increase. More recently, Corr and Clark (2001) compared two novel hybrid shunt techniques to the traditional passive tuned resonant shunt circuit. The first technique, the 'state switching', is a semi-active variable stiffness technique in which bonded PZT actuators are switched from short to open circuit states. This technique changes the stiffness of the structure for two quarters of its vibration period, thus dissipating energy. The second technique, the 'synchronized switching', is a semi-active continuous switching architecture in which a resistor-inductor shunt circuit is periodically connected to the bonded PZT actuators. The equations of motion are derived for a single DOF system with a parallel wired stack actuator attached on a clamped-clamped aluminum beam. Numerical and preliminary experimental results showed good accordance for 12 dB reduction. The advantages of the novel over the resonant shunt technique are: smaller shunt inductance needed, lower sensitivity to environmental changes, and easy tuning.

The synchronized switch damping was proposed by Richard et al. (2000) for vibration damping. Inverting the voltage on a PZT transducer through the inductive element when the switch is on causes the structural response to be distorted, shifted in time domain from the beam deflection, and magnified. The proposed approach is inherently a broadband technique. The equations of motion are derived for a single DOF system. Experimental results on cantilever beam showed 6 dB of reduction for a viscoelastic epoxy beam and 10 dB for an aluminum beam at the first resonant frequency.

Ameduri et al. (2005) proposed an energetic approach for a beam vibration control system through the synchronized switched shunt resonator architecture (Moheimani and Behrens, 2004 and Wu 2001). Both theoretical and numerical models were implemented to estimate the effects due to this kind of control. By taking advantage of PZT energy transmission model, an optimization process was carried out; in this way, the proposed system is able to maximize the energy transmission from the structure to the PZT elements and vice versa. The assessed system, comprehensive of the electrical components, was simulated by using a FE approach. Mechanical and electrical components interaction key-point was represented by assembling the coupling matrices. After a preliminary validation by means of the MSC-Nastran code, the aforementioned model was used to estimate SSSA control ability at the first three structural modes for an aluminum beam clamped on one edge. The estimated vibration reduction level resulted equal to 12 dB. The aforementioned

literature works illustrate a wide variety of methods to control structures with bonded PZT elements, but the related simulation methods appeared to be applicable for the special cases and lacked generality. This is the reason why the authors addressed some efforts in the definition of a more general and flexible theoretical and numerical model describing electromechanical nature of PZT elements.

Tzou and Tseng (1990) developed a FE model for sensors and actuators bonded on structures. A specific FE model was built for a thin PZT solid. Hamilton's principle was used to formulate the dynamic problem in the FE form, and Guyan reduction was applied to condense the DOFs associated with electrical potential. The system time response was calculated using the Wilson method.

Hwang and Park (1993) introduced a model for plate elements with bonded PZT sensors and actuators. They introduced a four-node non-conforming quadrilateral element. In their study, they investigated the effect of different PZT sensor and actuator configurations on the vibration control. Kim and Moon (2001) presented for the first time a FE formulation for PZT plate elements with passively shunted circuit elements that incorporated the electric circuit dynamics. They used the Hamilton's principle to derive the nonlinear FE model. The electrical DOFs of a single element were presented both as one per node and one per element, showing good accordance.

Galucio et al. (2005) presented a FE formulation for the dynamic transient analysis of a damped adaptive sandwich beam composed of a viscoelastic core and elastic PZT laminated faces. No electrical DOF was introduced in the formulation. The electromechanical coupling was taken into account by means of an augmentation of the stiffness of the PZT layers for a sensor configuration. The equation of motion was using a direct time integration method based on the Newmark-Beta scheme.

In the present work, the FE modeling of a synchronized switched shunt control technique is described.

The mechanical system is a rectangular isotropic plate, clamped at the edges with a PZT patch bonded at the center, as shown in Figure 3.

The control system is an RLC electrical circuit with a switch component added in serial configuration (Figure 9).

A specific multi DOFs FE model of the PZT element has been defined and implemented, based on the constitutive law and the virtual work principle. The integration with the structural system has been obtained by adding the PZT structure to the corresponding matrices of the structure, computed by the MSC/Nastran code.

The Newmark-Beta integration method has been taken advantage of, to compute the system behavior in the time domain.

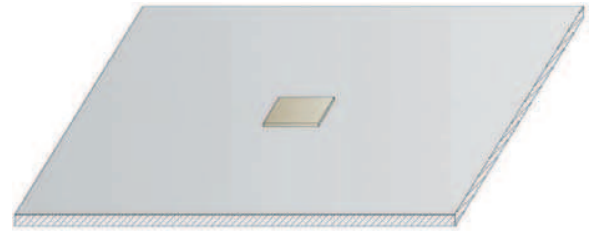


Figure 3. Mechanical model.

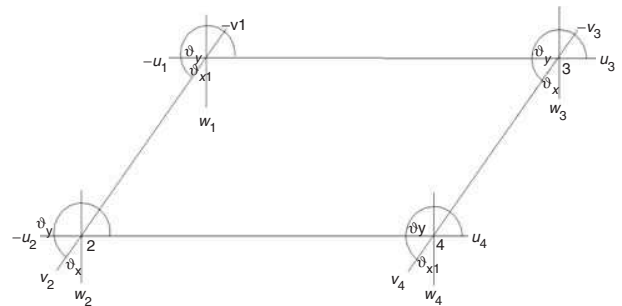


Figure 4. Piezo finite element model's DOFs.

A description of the theoretical methodology adopted to define the PZT FE and to integrate this within the plate structure, is provided; then, the integration method, adopted to predict the dynamic response of the system with and without control is illustrated; finally, related results are expressed in terms of time response (Heylen et al. 2003 and Srinivasan and McFarland, 2005).

## NUMERICAL APPROACH

The working modality of the piezo bonded on the plate determines both bending and in-plane actions on the structure.

For the sake of completeness, both the in-plane,  $x_{M,in-plane}$  and the bending,  $x_{M,bending}$  DOFs have been taken into account in the implementation of the FE model. In this section, the FE model of the PZT patch is derived.

### The PZT FE Implementation: Mechanical DOFs

The FE sketched in Figure 4 representing an elementary rectangular plate has been taken into account to derive the PZT FE model. Each node has three translational and three rotational DOFs, for a total of six.

The nodal displacement vector may be expressed as:

$$x_M = \{u, v, w, \vartheta_x, \vartheta_y, \vartheta_z\} \quad (1)$$

and the corresponding force vector is:

$$f = \{F_x, F_y, F_z, M_x, M_y, M_z\}. \quad (2)$$

In the hypothesis of small displacements the in-plane and out-of-plane DOFs are uncoupled; then, the aforementioned vectors can be simply reordered by placing at first the in-plane followed by the out-of-plane DOFs. The piezo stiffness matrix can be subsequently written as:

$$\begin{bmatrix} F_{\text{in-plane}} \\ F_{\text{bending}} \\ M_z \end{bmatrix} = \begin{bmatrix} [K]_{\text{in-plane}} & 0 & 0 \\ 0 & [K]_{\text{bending}} & 0 \\ 0 & 0 & 0 \end{bmatrix} \begin{bmatrix} x_{M, \text{in-plane}} \\ x_{M, \text{bending}} \\ \vartheta_z \end{bmatrix}. \quad (3)$$

The zero rows and columns introduced corresponding to  $\vartheta_z$  rise from the choice to make the element unable to react to the out-of-plane moment. As these zeroes lead to ill-conditioning problems of the structural stiffness matrix, according to Zienkiewicz, the last four elements of the principal diagonal have been assumed to be equal to one thousandth of the smallest diagonal one (Zienkiewicz, 1979).

Since the adopted FE should represent a PZT lamina, an additional electrical DOF is required, given by the piezo electrodes charge,  $q$ .

### Piezo Stiffness Matrix

From the structural point of view, Expression (3) can be derived by taking into account the PZT constitutive relation. Their general form is written as:

$$\begin{Bmatrix} \sigma_x \\ \sigma_y \\ \sigma_{xy} \\ D \end{Bmatrix} = \begin{bmatrix} [Y]^E & -[e] \\ [e]^T & \epsilon \end{bmatrix} \begin{Bmatrix} \varepsilon_x \\ \varepsilon_y \\ \varepsilon_{xy} \\ E \end{Bmatrix} \quad (4)$$

where  $[Y]^E$  is the mechanical stress-strain constitutive matrix at constant electric field given by:

$$[Y]^E = \begin{bmatrix} \frac{E_p}{1-\nu^2} & \frac{\nu E_p}{1-\nu^2} & 0 \\ \frac{\nu E_p}{1-\nu^2} & \frac{E_p}{1-\nu^2} & 0 \\ 0 & 0 & \frac{E_p}{2(1+\nu)} \end{bmatrix}. \quad (5)$$

Relation (4) can be rearranged as (Tawfik and Baz, 2004):

$$\begin{bmatrix} [\sigma] \\ E \end{bmatrix} = \begin{bmatrix} [Y]^E + [e][e]^T \beta & -[e]\beta \\ -[e]^T \beta & \beta \end{bmatrix} \begin{bmatrix} [\varepsilon] \\ D \end{bmatrix}. \quad (6)$$

From the virtual work principle:

$$\delta \Pi = \delta(U - T - W) = 0 \quad (7)$$

the variation of the mechanical potential energy can be computed:

$$\delta U = \int_V [\delta \varepsilon]^T [\sigma] dV + \int_V \delta D E dV. \quad (8)$$

The substitution of Expression (6) in (8) gives:

$$\begin{aligned} \delta U &= \int_V [\delta \varepsilon]^T [(Y)^E + [e][e]^T \beta] [\varepsilon] - [e]\beta D dV \\ &+ \int_V \delta D [-[e]^T \beta [\varepsilon] + \beta D] dV \\ &= \int_V [\delta \varepsilon]^T [Y]^E [\varepsilon] dV \\ &+ \int_V [\delta \varepsilon]^T [e][e]^T \beta [\varepsilon] dV \\ &- \int_V [\delta \varepsilon]^T [e]\beta D dV - \int_V \delta D [e]^T \beta [\varepsilon] dV \\ &+ \int_V \delta D \beta D dV. \end{aligned} \quad (9)$$

By taking into consideration the relation occurring between nodal displacement,  $x_M$ , and strain,  $\varepsilon$  (Anderson and Crawley, 2007), that is:

$$[\varepsilon] = [B][x_M] \Rightarrow [\varepsilon]^T = [x_M]^T [B]^T \quad (10)$$

the potential energy may be expressed as:

$$\begin{aligned} \delta U &= [\delta \varepsilon]^T \left[ \int_V [B]^T [Y]^E [B] dV + \int_V [B]^T [e][e]^T \beta [B] dV \right] [x_M] \\ &- [\delta x_M]^T \left[ \int_V [B]^T [e]\beta dV \right] D - \delta D \left[ \int_V [e]^T \beta [B] dV \right] [x_M] \\ &+ \delta D \left[ \int_V \beta dV \right] D \end{aligned} \quad (11)$$

being

$$\begin{aligned} \int_V [B]^T [Y]^E [B] dV + \int_V [B]^T [e][e]^T \beta [B] dV &= [K_S]_{Pzt} \\ \int_V [B]^T [e]\beta dV &= [K_{SE}]_{Pzt} \\ \int_V [e]^T \beta [B] dV &= [K_{ES}]_{Pzt} \\ \int_V \beta dV &= [K_E]_{Pzt}. \end{aligned} \quad (12)$$

Finally, by using the following relation:

$$D = \frac{q}{A} \quad (13)$$

the above matrices (12) may be arranged in order to point out mechanical and electrical DOFs:

$$\begin{bmatrix} [K_S] & [K_{SE}] \\ [K_{ES}] & [K_E] \end{bmatrix} \begin{bmatrix} x_M \\ q \end{bmatrix} = \begin{bmatrix} F_{exc} \\ 0 \end{bmatrix}. \quad (14)$$

### Piezo Mass and Damping Matrices

From the virtual work principle (7), the variation of the external work  $W$ , performed by the shunt circuit in the absence of applied forces, can be now computed:

$$\delta W = \int_A \delta D(-L\ddot{q} - R\dot{q}) dA. \quad (15)$$

By considering (13), Expression (15) becomes:

$$\delta W = -\delta q \int_A \frac{L}{A} dA \ddot{q} - \delta q \int_A \frac{R}{A} dA \dot{q} \quad (16)$$

where

$$\begin{aligned} \int_A \frac{L}{A} dA &= L = [M_E]_{Pzt} \\ \int_A \frac{R}{A} dA &= R = [C_E]_{Pzt} \end{aligned} \quad (17)$$

are, respectively the mass and damping PZT matrices due to the electrical nature of the element.

The piezo mass,  $[M_S]_{Pzt}$ , and damping,  $[C_S]_{Pzt}$ , structural matrices have been taken by the Przemieniecki description (Przemieniecki, 1985).

Some tests have been carried out to validate the model (see Tables 1–3).

These results are in good accordance with the theoretical ones predicting the PZT behavior in terms of free deformations and voltage load produced for in-plane actions.

## DYNAMICS

### Piezo Dynamic Equation

In order to integrate the PZT FE within the structure to be controlled, the aforementioned matrices have to undergo a reference system changing. Both nodal and forces DOFs expressed in the local (PZT) reference system, have to be ‘transposed’ in the global one (plate).

According to Figure 5, by assuming a distance  $h$  between the PZT middle plane axes  $O'X'$  and the plate middle plane one  $OX$ , Relations (18) and (19) about DOFs and nodal forces, respectively, may be found out as:

$$\begin{bmatrix} u \\ v \\ w \\ \vartheta_x \\ \vartheta_y \\ \vartheta_z \\ q \end{bmatrix}'_{Pzt} = \begin{bmatrix} 1 & 0 & 0 & 0 & -h & 0 & 0 \\ 0 & 1 & 0 & -h & 0 & 0 & 0 \\ 0 & 0 & 1 & 0 & 0 & 0 & 0 \\ 0 & -\frac{1}{h} & 0 & 1 & 0 & 0 & 0 \\ -\frac{1}{h} & 0 & 0 & 0 & 1 & 0 & 0 \\ 0 & 0 & 0 & 0 & 0 & 1 & 0 \\ 0 & 0 & 0 & 0 & 0 & 0 & 1 \end{bmatrix} \begin{bmatrix} u \\ v \\ w \\ \vartheta_x \\ \vartheta_y \\ \vartheta_z \\ q \end{bmatrix}_{Str} \quad (18)$$

**Table 1. In-plane displacements of Nodes 3 and 4 (with reference to the piezo model sketch in Figure 4) for a unitary applied voltage, by considering fixed the first and the second nodes.**

Nodes	Voltage (V)	Displacements (m)
First	1	Fixed
Second	1	Fixed
Third	1	$u_3 = -2.315E-008, v_3 = -9.218E-009$
Fourth	1	$u_4 = -2.315E-008, v_4 = 9.218E-009$

**Table 2. In-plane displacements of Nodes 2 and 3 (with reference to the piezo model sketch in Figure 4) for a unitary applied voltage, by considering fixed nodes 1 and 4.**

Nodes	Voltage (V)	Displacements (m)
First	1	Fixed
Second	1	$u_2 = 1.199E-008, v_2 = -1.580E-008$
Third	1	$u_3 = -1.199E-008, v_3 = -1.580E-008$
Fourth	1	Fixed

**Table 3. Voltage induced by in-plane forces applied on Nodes 3 and 4 along x-direction, Nodes 1 and 2 being fixed (with reference to the piezo model sketch in Figure 4).**

Nodes	Force (N)	Voltage (V)
First	–	Fixed
Second	–	Fixed
Third	1	–0.871
Fourth	1	–0.871

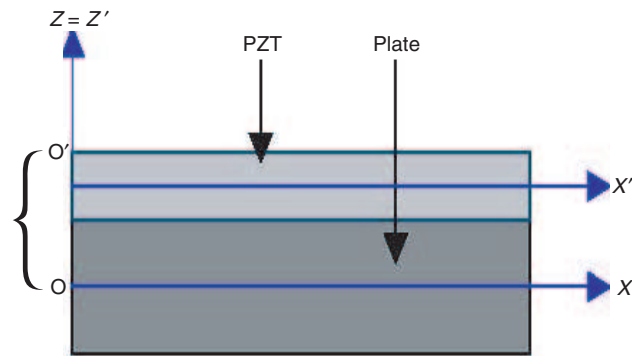


**Figure 5. Reference systems coinciding to the middle planes.**

$$\begin{bmatrix} F_x \\ F_y \\ F_z \\ M_x \\ M_y \\ M_z \\ q \end{bmatrix}'_{Pzt} = \begin{bmatrix} 1 & 0 & 0 & 0 & -\frac{1}{h} & 0 & 0 \\ 0 & 1 & 0 & -\frac{1}{h} & 0 & 0 & 0 \\ 0 & 0 & 1 & 0 & 0 & 0 & 0 \\ 0 & h & 0 & 1 & 0 & 0 & 0 \\ h & 0 & 0 & 0 & 1 & 0 & 0 \\ 0 & 0 & 0 & 0 & 0 & 1 & 0 \\ 0 & 0 & 0 & 0 & 0 & 0 & 1 \end{bmatrix} \begin{bmatrix} F_x \\ F_y \\ F_z \\ M_x \\ M_y \\ M_z \\ q \end{bmatrix}_{Str} \quad (19)$$

in a compact form:

$$[X]'_{Pzt} = [S_1][X]_{Str} \quad (20)$$

and

$$[F]'_{Pzt} = [S_2][F]_{Str} \quad (21)$$

where  $S_1$  and  $S_2$  are the 'transposing' matrices (Ciminello and Ameduri).

Setting:

$$\begin{aligned} \begin{bmatrix} [M_S]_{Pzt} & 0 \\ 0 & [M_E]_{Pzt} \end{bmatrix}' &= [M]'_{Pzt} \\ \begin{bmatrix} [C_S]_{Pzt} & 0 \\ 0 & [C_E]_{Pzt} \end{bmatrix}' &= [C]'_{Pzt} \\ \begin{bmatrix} [K_S]_{Pzt} & [K_{SE}]_{Pzt} \\ [K_{ES}]_{Pzt} & [K_E]_{Pzt} \end{bmatrix}' &= [K]'_{Pzt} \end{aligned} \quad (22)$$

the PZT equations of motion in the local reference system results:

$$[M]'_{Pzt}\{\ddot{X}\}' + [C]'_{Pzt}\{\dot{X}\}' + [K]'_{Pzt}\{X\}' = [F]'_{Pzt}. \quad (23)$$

Substituting relations (20) and (21) in (23) it comes out:

$$\begin{aligned} [S_1][M]'_{Pzt}[S_2] &= [M]_{Pzt} \\ [S_1][C]'_{Pzt}[S_2] &= [C]_{Pzt} \\ [S_1][K]'_{Pzt}[S_2] &= [K]_{Pzt}. \end{aligned} \quad (24)$$

Expressions (24) represent the corresponding piezo matrices in the global reference system.

### The System Dynamic Equation

The equation of motion (25) for the entire structure (PZT + plate) has been now derived.

$$[M]\{\ddot{X}\} + [C]\{\dot{X}\} + [K]\{X\} = [F]. \quad (25)$$

The mass, stiffness, and damping matrices of the plate have been extracted by the MSC-NASTRAN code; the partitions of the plate matrices corresponding to the coincident PZT-structure DOFs are summed to the PZT ones (24), results of the reference system changing.

The PZT matrices elements summed to the corresponding ones at coincident plate DOFs, leads to:

$$\begin{aligned} [M]_{pztUstr} &= [M]_{Pzt} + [M]_{Str} \\ [C]_{pztUstr} &= [C]_{Pzt} + [C]_{Str} \\ [K]_{pztUstr} &= [K]_{Pzt} + [K]_{Str}. \end{aligned} \quad (26)$$

The main features of the structure and PZT patch are provided in Tables 4–6.

**Table 4. Structural material properties.**

Material	Aluminum alloy 7075-T6
In-plane dimensions	330 × 220 mm <sup>2</sup>
Thickness	1 mm
Young's modulus	72 GPa
Poisson's modulus	0.3
Density	2700 kg/m <sup>3</sup>
Structural damp.	0.008–0.01

**Table 5. PZT structural characteristics.**

PZT model	PPK-11
In-plane dimensions	30 × 20 mm
Thickness	0.5 mm
Modulus of elasticity	62 GPa
Poisson's ratio	0.3
Density	8000 Kg/m <sup>3</sup>

**Table 6. PZT main electric and electromechanical characteristics.**

PZT coefficient $g_{31}$	−8.0e−3 V/m
PZT coefficient $d_{31}$	−350E−12 m/V
PZT coefficient $d_{33}$	680E−12 m/V
Dielectric constant	5000

FEMAP pre-processing software has been used to realize the plate FE model (Figure 6), whose main characteristics are summarized in Table 7. Each element has the same in-plane dimensions as the selected PZT patch in order to make easier the model integration.

According to Relations (26), the PZT has been integrated within the central plate element. In Figure 7, the single piezo non-zero stiffness, mass, and damping matrix elements are sketched; the bottom right corner element represents the pure electric term; the last row and column represent the mechanic-electric coupling terms; and finally the remaining part of these matrices constitute the pure mechanical components.

In Figure 8, the PZT matrices assembled within the plate ones, according to relations (26), are sketched. For the sake of simplicity, without losing generality, the contact DOFs have been concentrated in the bottom right corner of the matrices.

The coupling terms describing the PZT behavior have been estimated only for the stiffness matrix, assuming the corresponding mass and damping terms negligible.

Moreover, the migration period of the electrons on the two leads being remarkably shorter than the typical time mechanic period, it is reasonable to assume a constant charge distribution, according to Kim and Moon (2001).

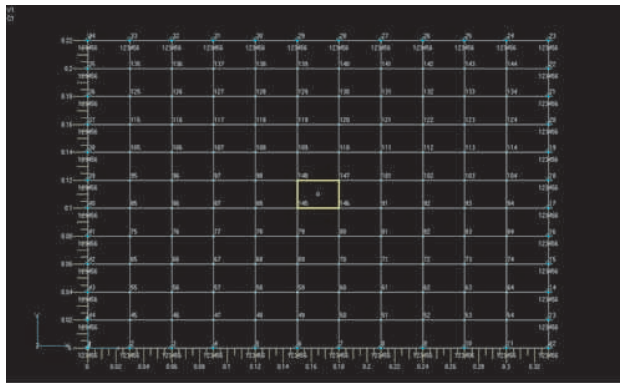


Figure 6. Plate FE model: the red dot is the position of the applied force, the yellow rectangle is the PZT element.

Table 7. FE model main features.

Element type	CQUAD
Mesh discretization	$11 \times 11$
Number of total nodes	144
Number of constrained nodes	44
Mechanical DOF per node	6
Total mechanical DOFs	600
Electrical DOF	1
Total (electromechanical) DOFs	601

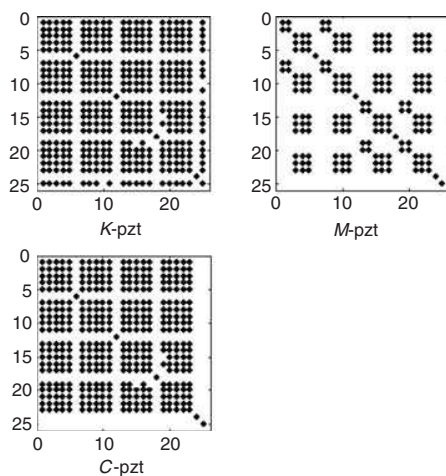


Figure 7. Piezo matrices assembly.

## SSSA CONTROL SYSTEM AND INTEGRATION

### The Switched Shunt Resonator Control System

The adopted electrical network is an RLC resonant circuit having the PZT as capacitance. The circuit is sketched in Figure 9.

The switch element, generally in off state (open) during structural vibrations, corresponding to maxima deformations, assumes the on state (close) for 1/10 of the highest excitation signal period to be controlled

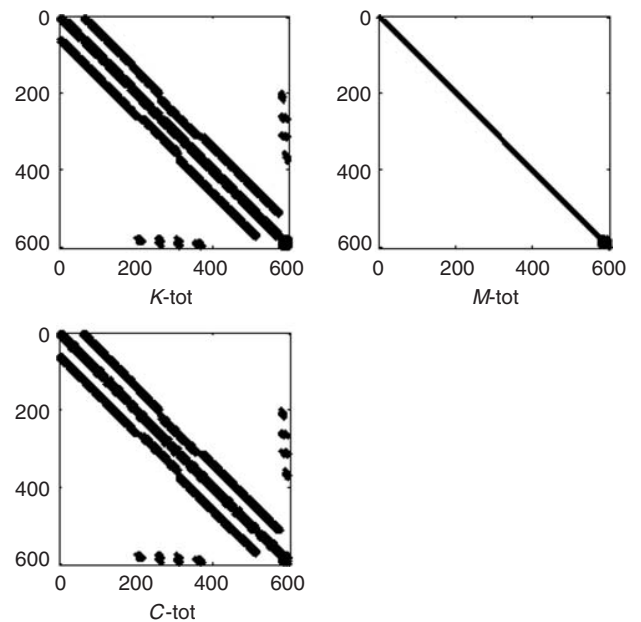


Figure 8. Global matrices assembly.

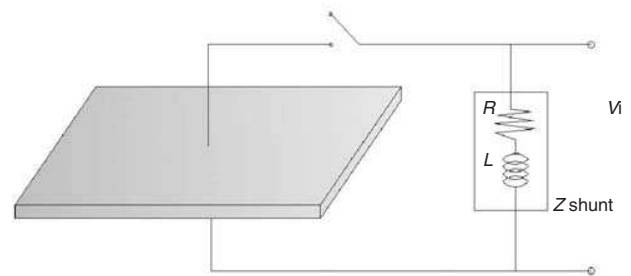


Figure 9. Synchronized switched shunt circuit.

(Figure 10), allowing current to flow in the RL branch, with a resulting charge inversion on the PZT leads. This value ensures the charge, stored on the PZT, to remain approximately constant while the switch is on, that is to say, the voltage reversing is as instantaneous as possible without commutation losses (Figure 11).

Due to PZT electromechanical nature, the transmitted electrical energy is reversed into a mechanical strain actuation pulse train, opposed to the maxima structure deflections generating it. In other words, the piezo charge flows in the inductor which sends it back reversed on piezo electrodes and producing, in this way, a local strain in phase opposition with respect to the vibration that generated it.

The pulsation  $\omega_{el}$  of the electrical switching is simply related to  $C$  and  $L$  through the well known equation:

$$\omega_{el} = \frac{1}{\sqrt{CL}}. \quad (27)$$

The pulsation of the electrical oscillation, in the SSSA, is designed to be independent of the structure so it has to

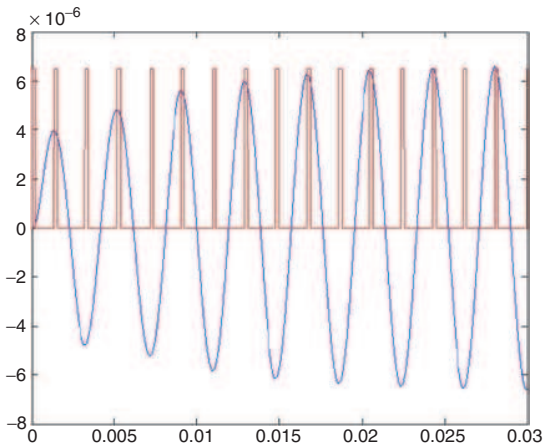


Figure 10. Switch signal simulation.

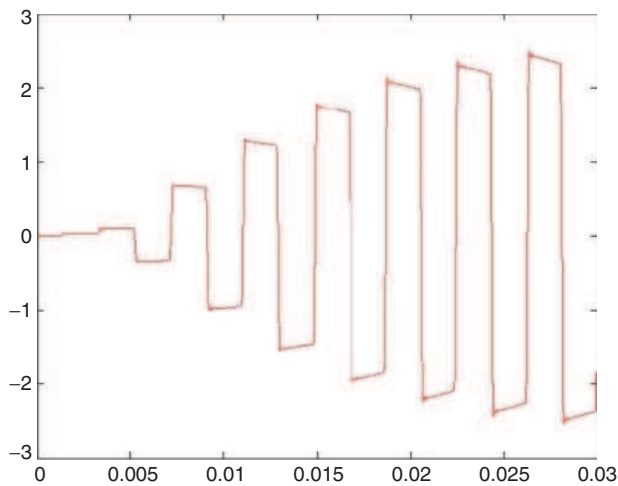


Figure 11. Switch control on harmonic signal.

be high enough if compared with the highest mechanical resonance frequency to be controlled. Anyway an optimal range must be defined to optimize synchronized switching performance (Corr and Clark, 2001), a lower and upper limit has to be guaranteed:

$$10f_{\text{mec}} \leq f_{\text{el}} \leq 50f_{\text{mec}} \quad (28)$$

The lower one must be set to ensure that the electrical frequency is at least 10 times of the highest mechanical mode of interest, in agreement with the aforementioned observations about the electrical period.

The upper one is quite arbitrary; however it is showed (Richard et al., 2000; Corr and Clark, 2001) that in order to avoid the frequency switching induce non-controlled electrical self-inductions in the circuit, it should be set no more than 50 times the mechanical one.

According to Expressions (27) and (28), as  $C$  is fixed by the piezo element, a suitable value should be set for  $L$ .

### Integration Strategy

Since the working principle of the SSSA control system is characterized by fast state variations, due to the electric circuit quick commutation times, the system behavior will suffer a continuous transient regime. According to the MSC-NASTRAN code, a specific version of the Newmark-Beta numerical integration method has been adopted. The transient structural output is computed using a set of coupled equations through direct numerical integration. The coupled system matrices are time dependent and, in particular, assume an on/off state. In short, the integration method may be schematized as shown in Figure 12.

As illustrated in the diagram, after the time integration performed by the Newmark-Beta block, a suitable algorithm detects eventual maxima. If the actual system configuration  $x(t_i)$  results in a maximum, the circuit state becomes on and the structural matrices are assigned with the corresponding on state values. The circuit remains in this state for a specific time interval, according to what is defined in the following paragraph. After this short interval or if no maxima are detected, the off state values are assigned to the structural matrices.

The electrical parameter adopted in the numerical simulation integration of the control systems are summarized in Tables 8 and 9.

### RESULTS

The SSSA dynamic numerical simulation is presented here. First of all, after the realization of a FE model of the plate, a normal modes/eigenvalues analysis type has been performed, in the MSC/NASTRAN environment, to get the natural frequencies of the structure. In addition, a frequency response function has been computed to have a wide view of the dynamic behavior in the frequency domain.

The reason is that the switched shunt resonator control design needs to know the highest mechanical frequency to be controlled, as the frequency switch signal must be set at 10 times the mechanical one.

The next simulation step, on the basis of the data just gained, is the integration of the control system dynamic equation, through the Newmark-Beta numerical solver. The simulation has been performed by adopting sinusoidal signals. The excitation frequencies have been chosen in order to excite normal modes controlled by the PZT patch located on the center of the structure, i.e., the first and third modes, among the ones in the range of 0–800 Hz.

Moreover, two different structural damping coefficients have been adopted, to appreciate the effect of the

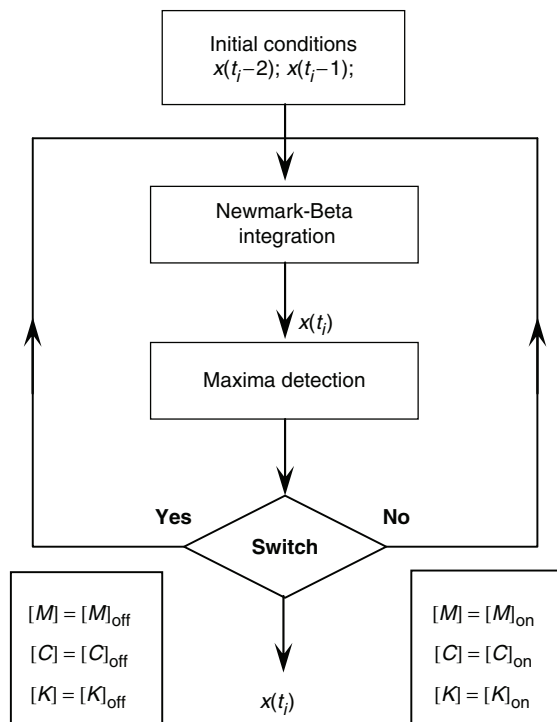


Figure 12. Flow chart.

Table 8. Open circuit properties.

Frequency: $f_{\text{mech}}$	See Table 10
Resistance: $R$	1E10 $\Omega$
Inductance: $L$	2E6 H
PZT free capacitance: $C$	49E-9 Farad

Table 9. Closed loop circuit properties.

Frequency: $f_{\text{el}}$	$10 * f_{\text{mech}}$
Resistance: $R$	100 $\Omega$
Inductance: $L$	$1/((2 * \pi * f_{\text{el}})^2 * C)$
PZT free capacitance: $C$	49E-9 Farad

semi-active control with respect to the self-damping features of the structure.

### FRF and Eigenvalues

In the modal analysis, the modal shapes and their frequencies in the range 1–800 Hz have been taken into account. In Figures 13 the model FRF is sketched.

Related normal frequencies are illustrated in Table 10.

As evident from the first and the third modal shapes shown in Figures 14 and 15, the PZT patch is located on a high transmission zone (max curvature).

Table 10. First nine modal frequencies of the system.

Modes	Frequencies (Hz)
1	135
2	206
3	330
4	331
5	390
6	497
7	505
8	629
9	746

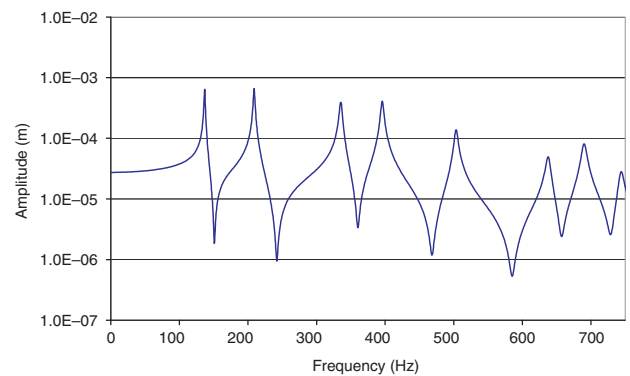


Figure 13. Structure FRF obtained for a normal force applied as shown in Figure 6; nonstructural damping has been considered.

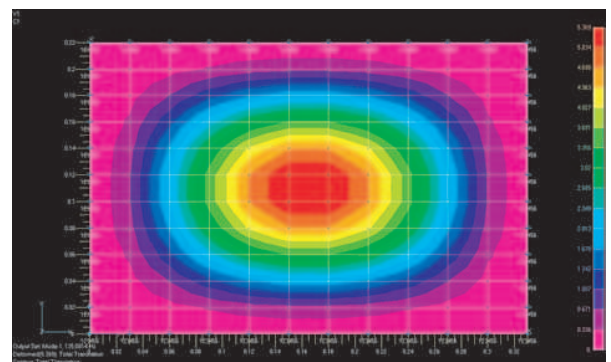


Figure 14. Structure first modal shape.

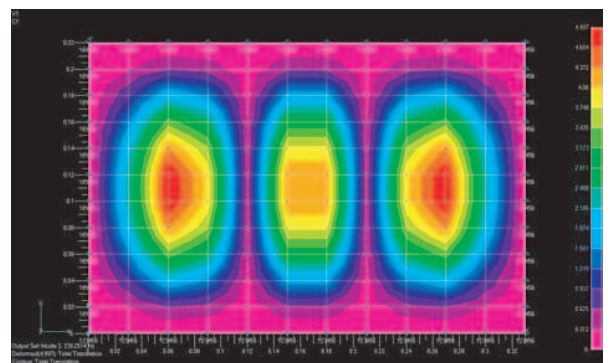


Figure 15. Structure third modal shape.

### SSSA Harmonic Response

According to the previous results, sinusoidal signals have been used to induce first and third system resonance.

In Figures 16–19 the first mode response of the system has been traced with and without control, for 0.8 and 1.0% damping coefficients, respectively.

In Figures 20 and 22, the third mode response of the system has been traced with and without control, for 0.8 and 1.0% damping coefficients, respectively. Figures 21 and 23 are structure vibration third mode damping at 0.8% and 1% details respectively.

The displacement reduction in dB is summarized in Table 11.

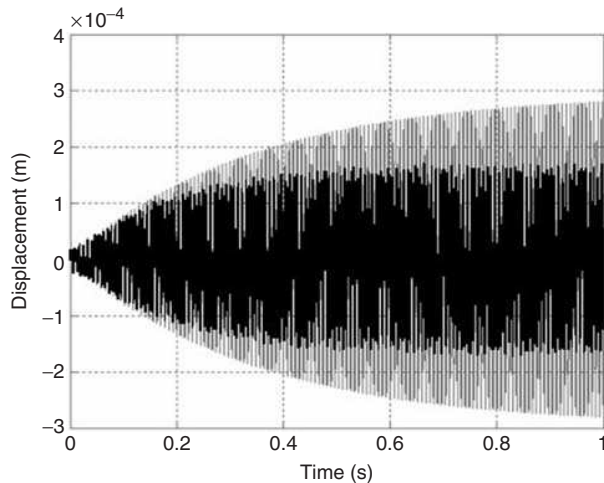


**Figure 16.** Structure vibration first mode damping at 0.8%.

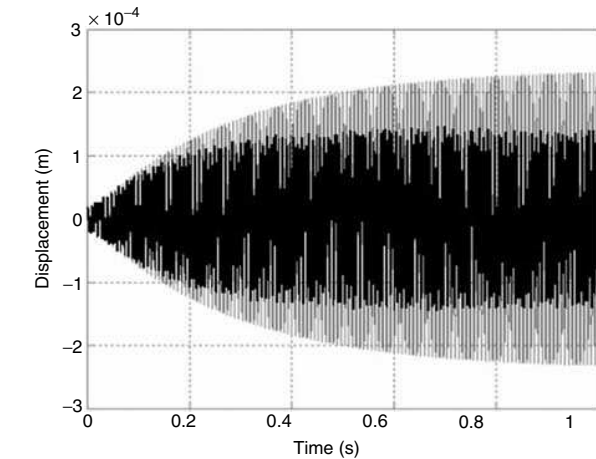


**Figure 18.** Structure vibration first mode damping at 1.0%.

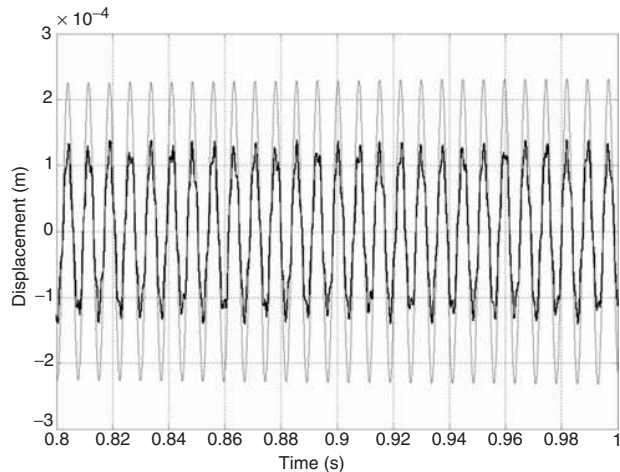


**Figure 19.** Structure vibration first mode damping at 1.0%, details.

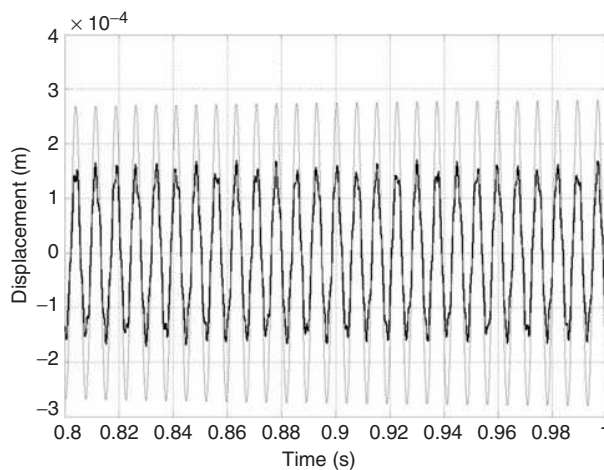


**Figure 17.** Structure vibration first mode damping at 0.8%, details.

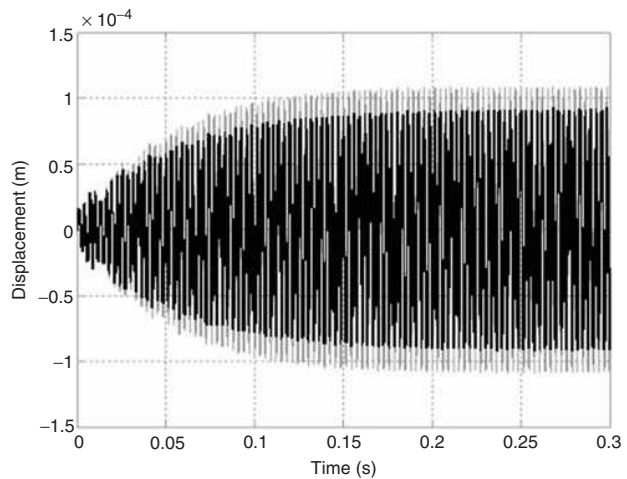


**Figure 20.** Structure vibration third mode damping at 0.8%.

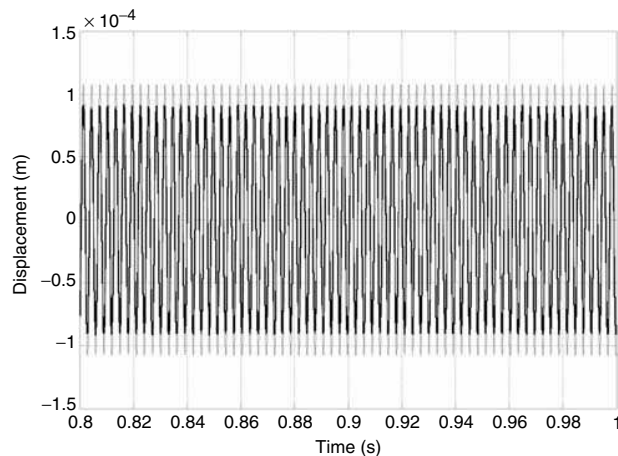


**Figure 21.** Structure vibration third mode damping at 0.8%, details.

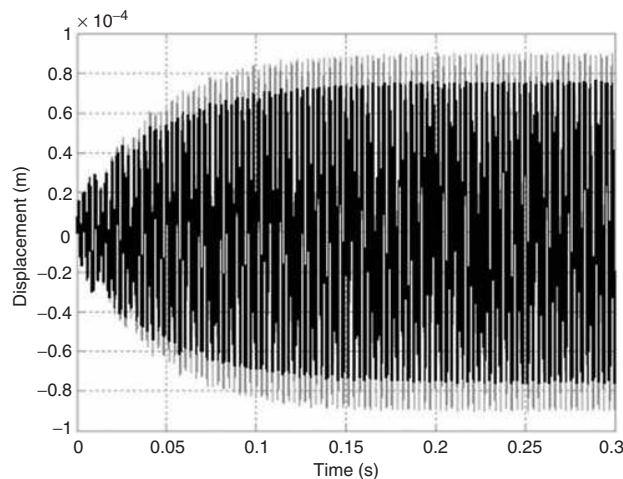


**Figure 22.** Structure vibration third mode damping at 1.0%.

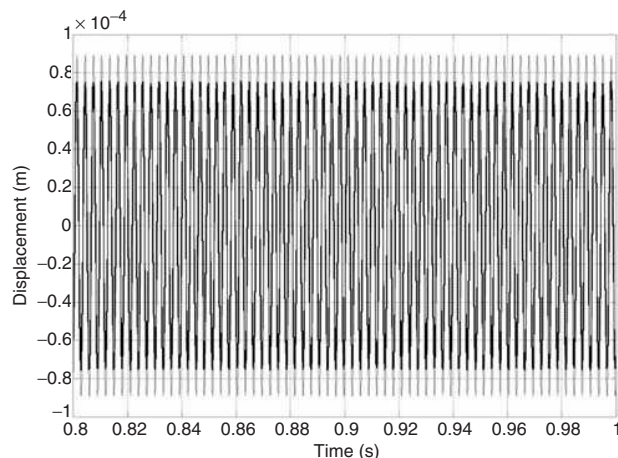


**Figure 23.** Structure vibration third mode damping at 1.0%, details.

**Table 11.** Displacement reduction versus damping coefficient versus mode id.

Mode id.	Damping coefficient (%)	Displacement reduction (dB)
1	0.8	4.87
1	1	4.44
3	0.8	1.53
3	1	1.52

## CONCLUSIONS

The PZT patch FE model derived by an energy criterion combined with the numerical multi DOFs simulator, based on a FE able to predict the structural response under the action of a SSSA, represent the novelties of this research.

In the present work, the modeling of a synchronized switched shunt control technique by adopting a FE approach is described. The structural reference system is constituted by a rectangular plate, with a PZT patch bonded in the center of one side where the strain is maximum for the first and third flexural modes.

The structure has been excited on a single node by sine signals at the first and third resonance frequencies.

The integration with the structural system has been obtained by adding the PZT matrices to the corresponding structural ones. The Newmark-Beta integration method has been taken advantage of, to compute the system behavior in time domain, with and without control. Different from the classical shunt resonator techniques, the SSSA does not require any tuning between the circuit resonance and the specific structural mode to be controlled: generally speaking it is a broadband control system. As another consequence, no high inductive elements are necessary to control low frequencies modes; moreover, a higher stability degree with respect to environmental changes may be achieved. A maximum reduction of 4.87 dB on the displacement has been estimated for the first mode, starting from an intrinsic damping coefficient of 0.8%. Moreover, ability of the system of controlling further modes (third) has been validated.

Further investigations will be carried out on more complex systems, constituted by a PZT network. An experimental campaign will be devoted to validate the attained numerical results.

## ACKNOWLEDGMENTS

The activities described in this study have been developed under the ‘SMART’ Government frame. The authors would like to express their deep gratitude to the Project management team, and especially to Dr. C. Camerlingo. The precious scientific supports of Mr. A. Calabrò are much appreciated.

## NOMENCLATURE

SSSA = synchronized switched shunt architecture  
 $x_M$  = vector of mechanical degrees of freedom  
 $u$  = in-plane translation along  $x$ -direction  
 $v$  = in-plane translation along  $y$ -direction  
 $w$  = transversal translation  
 $\theta_x$  = rotation around  $x$ -axis  
 $\theta_y$  = rotation around  $y$ -axis  
 $\theta_z$  = rotation around  $z$ -axis  
 $f$  = nodal forces vector  
 $F_x$  = force  $x$ -component  
 $F_y$  = force  $y$ -component  
 $F_z$  = force  $z$ -component  
 $M_x$  = moment  $x$ -component  
 $M_y$  = moment  $y$ -component  
 $M_z$  = moment  $z$ -component  
 $x_{M,\text{in-plane}}$  = vector of in-plane degrees of freedom  
 $x_{M,\text{bending}}$  = vector of bending degrees of freedom  
 $q$  = piezo surface electric charge  
 $F_{\text{in-plane}}$  = in-plane nodal forces  
 $F_{\text{bending}}$  = bending nodal forces  
 $[K]_{\text{in-plane}}$  = in-plane DOF's stiffness matrix  
 $[K]_{\text{bending}}$  = bending DOF's stiffness matrix  
 $\sigma_x$  = stress  $x$ -component  
 $\sigma_y$  = stress  $y$ -component  
 $\sigma_{xy}$  = shear stress component  
 $\varepsilon_x$  = strain  $x$ -component  
 $\varepsilon_y$  = strain  $y$ -component  
 $\varepsilon_{xy}$  = strain  $xy$ -component  
 $D$  = electric displacement  
 $E$  = electric field  
 $[e]$  = piezoelectric material constant  
 $\epsilon$  = material dielectric constant at constant stress  
 $[Y]^E$  = mechanical stress-strain constitutive matrix at constant electric field  
 $\nu$  = Poisson's modulus  
 $E_p$  = Young's modulus of elasticity at constant electric field  
 $\beta = 1/\epsilon$   
 $\pi$  = system total energy  
 $U$  = system potential energy  
 $T$  = system kinetic energy  
 $W$  = system external work  
 $V$  = piezo volume  
 $A$  = piezo face area  
 $B$  = shape function matrix  
 $[K_S]_{\text{Pzt}}$  = piezo stiffness structural matrix  
 $[K_{SE}]_{\text{Pzt}}$  = piezo stiffness coupling matrix  
 $[K_E]_{\text{Pzt}}$  = piezo stiffness electrical matrix  
 $F_{\text{exc}}$  = external excitation  
 $[M_E]_{\text{Pzt}}$  = piezo mass electrical matrix  
 $[C_E]_{\text{Pzt}}$  = piezo damping electrical matrix  
 $[M_S]_{\text{Pzt}}$  = piezo mass structural matrix  
 $[C_S]_{\text{Pzt}}$  = piezo damping structural matrix

$[M]_{\text{Str}}$  = plate mass structural matrix  
 $[C]_{\text{Str}}$  = plate damping structural matrix  
 $[K]_{\text{Str}}$  = plate stiffness structural matrix  
 $[M]_{\text{pztUstr}}$  = PZT-plate mass structural matrix  
 $[C]_{\text{pztUstr}}$  = PZT-plate damping structural matrix  
 $[K]_{\text{pztUstr}}$  = PZT-plate stiffness structural matrix  
 $X$  = electromechanical DOF vector  
 $F$  = electromechanical forces vector  
 $S_1$  = system reference changing matrix for the electromechanical DOF  
 $S_2$  = system reference changing matrix for the electromechanical forces  
 $Z_{\text{shunt}}$  = shunt impedance  
 $T_{\text{el}}$  = capacitance oscillating discharge time period  
 $C$  = shunt circuit capacitance  
 $L$  = shunt circuit inductance  
 $R$  = shunt circuit resistance  
 $f_{\text{el}}$  = switching frequency  
 $f_{\text{mech}}$  = structural resonance frequency

## REFERENCES

- Agneni, A., Mastroddi, F. and Polli, G.M. 2003. "Shunted Piezoelectric Patch in Elastic and Aeroelastic Vibrations," *Computer and Structures*, 81:91–105.
- Ameduri, S., Ciminello, M., Sorrentino, R. and Concilio, A. 2005. (CIRA) "Beam Vibrations Control Through a Synchronised Switched Shunt Resonator (SSSR) System," *AIDAA XVIII National Congress*, 19–22 September.
- Anderson, E.H. and Crawley, E.F. "Piezoceramic Actuation of One and Two Dimensional Structures," *Space Systems Laboratory*, Rep. N.5-89, MIT, Cambridge, (Ma, USA), 6 July 2007.
- Bisegna, P. and Caruso, G. "A Critical Analysis of Electric Shunt Circuit Employed in Piezoelectric Passive Vibration Damping," *Smart Materials and Structures*, 10:1059–1068, 8–11 September 1999.
- Ciminello, M. and Ameduri, S. "Beam Vibrations Control Through a Synchronised Switched Shunt Resonator (SSSR) System," *'SMART' Project*, 1st Deliverable, CIRA Contract CIRA TR 05 0015, 27 May 2005.
- Corr, L.R. and Clark, W.W. 2001. "Comparison of Low Frequency Piezoceramic Shunt Techniques for Structural Damping," *Smart Structures and Materials 2001: Damping and Isolation, Proceedings of SPIE*, Vol. 4331, pp. 262–272.
- Crawley, E.F. and de Luis, J. 1998. "Use of Piezoelectric Actuators as Elements of Intelligent Structures," *AIAA Journal*, 25(10):1373–1385.
- Galucio, Deu and Ohayon. 2005. "A Fractional Derivative Viscoelastic Model for Hybrid Active-Passive Damping Treatments in Time Domain - Application to Sandwich Beams," *Journal of Intelligent Materials Systems and Structures*, 16.
- Hagood, N.W. and von Flotow, A. 1991. "Damping of Structural Vibrations with Piezoelectric Materials and Passive Electrical Networks," *MIT Journal of Sound and Vibration*, 146(2):243–268.
- Heylen, W., Lammens, S. and Sas, P. 2003. *Modal Analysis Theory and Testing*, KU Leuven, ISBN 90-73802-61-X.
- Hwang and Park. 1993. "Finite Element Modeling of Piezoelectric Sensors and Actuators," *AIAA Journal*, 31(5):930–937.

- Kahn and Wang. 2001. "Active-passive Hybrid Piezoelectric Network for Vibration Control. Comparison and Improvement," *Smart Material and Structure*, 10:794–806.
- Kim and Moon. 2001. "Active and Passive Suppression of Nonlinear Panel Flutter Using Finite Element Method," *AIAA Journal*, 39(11):2042–2050.
- Law, Rossiter, Simon and Koss. 1996. "Characterization of Mechanical Vibration Damping by Piezoelectric Material," *Journal of Sound and Vibration*, 197(4):489–513.
- Lesieutre, G.A. 1998. "Vibration Damping and Control Using Shunted Piezoelectric Materials," *The Shock and Vibration Digest*, 30(3):187–195.
- McGowan. 1999. "An Examination of Applying Shunted Piezoelectrics to Reduce Aeroelastic Response," *CEAS/AIAA/ICASE/NASA Langley International Forum on Aeroelasticity and Structural Dynamics*, Williamsburg –Virginia.
- Moheimani, S.O.R. and Behrens, S. 2004. "Multimode Piezoelectric Shunt Damping With Highly Resonant Impedance," *IEEE Transactions on Control Systems Technology*, 12(3):484–491.
- Park and Inman. 1999. "A Uniform Model for Series RL and Parallel RL Shunt Circuits and Power Consumption," In: *SPIE Conference Proceedings on Smart Structure and Integrated Systems*, Newport Beach, CA, 3668, pp. 797–804.
- Przemieniecki, J.S. *Theory of Matrix Structural Analysis*, Dover (ed.), ISBN-0-486-64948-2; 1985.
- Richard, C., Guyomar, D., Audigier, D. and Bassaler, H. 2000. "Enhanced Semi Passive Damping using Continuous Switching of a Piezoelectric Device on an Inductor," In: *Proceedings of SPIE*, Vol. 3989, *Damping and Isolation*, pp. 288–299.
- Srinivasan, A.V. and McFarland, D.M. 2005. *Smart Structures*, Cambridge University Press.
- Tawfik, M. and Baz, A. 2004. Experimental and Spectral Finite Element Study of Plates with Shunted Piezoelectric Patches, *International Journal of Acoustics and Vibration*, 9(2):87–97.
- Tzou and Tseng. 1990. "Distributed Piezoelectric Sensor/Actuator Design for Dynamic Measurement/Control of Distributed Parameter System: A Piezoelectric Finite Approach," *Journal of Sound and Vibration*, 138(1):17–34.
- Wu, S. 2001. "Broadband Piezoelectric Shunts for Passive Structural Vibration Control," *Proceeding of SPIE*, 4331:251–261.
- Zienkiewicz, O.C. 1979. *The Finite Element Method*, McGraw Hill (ed.), 3rd edn.



# Synchronized Switched Shunt Control Technique Applied on a Cantilevered Beam: Numerical and Experimental Investigations

MONICA CIMINELLO,<sup>1,\*</sup> ANTONIO CALABRÒ,<sup>2</sup> SALVATORE AMEDURI<sup>2</sup> AND ANTONIO CONCILIO<sup>2</sup>

<sup>1</sup>*Department of Aerospace Engineering (DIAS), University of Naples "Federico II" Naples, Italy*

<sup>2</sup>*The Smart Structures Laboratory – CIRA, The Italian Aerospace Research Centre, Capua, Italy*

**ABSTRACT:** During the last decades, some research interest in noise and vibration suppression has been focused on a specific control typology, based on semi-active architectures. Related advantages, like low or absent external power supply and intrinsic adaptive capacities, constitute an acceptable compromise between passive and active systems. Among the proposed ones, the so-called Synchronized Switched Shunt Architecture (SSSA) has shown good potential. Theoretical and numerical models able to describe simple systems (concentrated DOFs), controlled by an SSSA were already implemented. Anyway, these models are not immediately applicable to continuous structures (beams, plates, etc.). For this reason, and taking advantage of the previous works, a dedicated simulation code was ideated and implemented. In this article, the cited code was used to predict the benefits due to an SSSA device, applied on a beam element; later on, an experimental campaign was carried out on a dedicated prototype; finally, numerical and experimental results were compared in order to point out eventual discrepancies and assess the modeling capabilities. Sine signals were used to excite the beam resonance frequencies. Both numerical and experimental outcomes were expressed in time domain because of the unsteady nature (and consequent nonlinearity) of the examined semi-active control system.

*Key Words:* control, actuator, piezoelectric, sensor.

## INTRODUCTION

WITH the recent advances in smart structural systems, an increased interest in the applications of piezoelectric materials (PZTs) arose, primarily devoted to the development of feedback systems aimed, for instance, at implementing additive sources of (active) structural damping.

Passive techniques are widely used for reducing structural noise and vibration levels, but some physical limitations prevent their use at low frequencies; in detail, these treatments are ineffective at frequencies below 200 Hz and add a significant amount of weight to the structure (Caruso, 2001; Corr and Clark, 2001; Hagood and von Flotow, 1991).

With the possibility of attaining good performance in the low frequency range, active controls have been widely studied; McGowan (1999) was the first to point out how passively controlled circuits are a viable alternative to the active ones (Agneni, 2003). In her research she identified two important issues that needed to be considered in using active control systems:

the large amount of power for operation, and the complexity of the hardware involved with active control (added hardware, control law design and implementation). In particular, McGowan showed how passive damping with shunted PZT required simple electrical circuitry and very small power.

Although either passive or active control techniques are highly recommended for a wide range of applications, there are some instances when hybrid systems provide the best solution for vibration suppression (Kim and Moon, 2001; Law et al., 1996; Tzou and Tseng, 1990; Wu, 2001).

Kahn and Wang (2001) presented for the first time the results of a hybrid technique in the structural vibration control field. The advantage of such a system is the overall stability increase.

The research conducted in this study focuses on a specific hybrid vibration damping technique, based on a Synchronized Switched Shunt Architecture (SSSA), (Amedari, 2005, Ciminello et al., 2007) where piezoelectric materials are used to control structural vibrations with low weight penalties and simple operative systems, particularly targeting the low frequencies band. The SSSA allows good reduction of vibrations in broadband cases, and is self-adaptive with environmental variations.

\*Author to whom correspondence should be addressed.  
E-mail: monicacimm@libero.it

It consists of a RLC electrical circuit with a switch component added in serial configuration (Figure 1).

In shunted circuit-based dissipation techniques, piezoelectric materials are called to transform energy (Lesieutre, 1998; Park and Inman 1999; Moheimani and Behrens, 2004). Mechanical is converted into electric energy. In a vibrating structure, a shunting network can be configured to dissipate vibration energy by tuning the electrical system dynamics. A switched semi-active electrical network, connected to piezoelectric patches, could be then powered simply, thanks to this kind of conversion. When the circuit switch is on, the piezo charge flows in the inductor, which almost instantaneously sends it back, reversed, to the piezo electrodes producing in turn local strain in phase opposition with respect to the vibration that generated it. In this article, both numerical and experimental results of an SSSA-based semi-active control system are presented.

An efficient numerical simulation tool, previously developed (Ciminello et al., 2007), was used to predict the vibration control performance of this kind of architecture when applied onto a beam element; a laboratory test campaign was then carried out on a dedicated prototype, allowing a successive comparison between numerical and experimental data, carried out in order to point out possible discrepancies. Sine signals were used to excite beam resonance frequencies.

Results are presented both in terms of vibration levels reduction and overall controller efficiency. Both numerical and experimental outcomes were expressed in time domain because of the characteristic nonlinearity of the faced problem. As a last step, the further research objectives of this study are discussed.

## NUMERICAL APPROACH

### Structural Characterization

The structure is a 250 mm long aluminium cantilever beam (Figure 2).

The piezoelectric ceramic patch is bonded on the beam, close to the clamp, where the strain is expected to be large for the flexural modes of interest. The PZT material and the structure characteristics are reported in Tables 1 and 2, respectively.

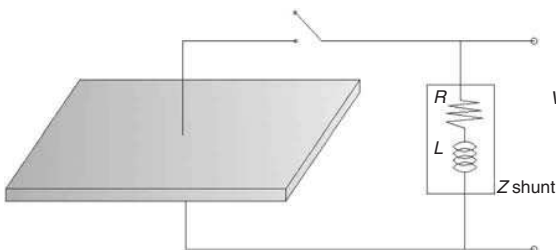


Figure 1. Synchronised switched shunt circuit.

Modal shapes and frequencies in the range between 1 and 500 Hz are taken into account, considering only the flexural modes the PZT is able to detect and control (Table 3). Numerical modal analysis was performed through MSC-Nastran for the beam without PZT patches and the first, second, and fifth modes are sketched in Figures 3–5, respectively.

### Electrical Characterization

The working principle consists of synchronizing the switch component 'on state' with the piezo displacement maxima. When this event occurs, the switch device is turned on for about 1/10 the highest excitation signal period to be controlled (Figure 6).

During the on state, the piezo charge flows through the inductor which sends it back, reversed, to piezo leads, producing an impulsive strain, opposite to the vibration that generated it. Because  $C$  is fixed by the piezo element, a suitable value should be set for  $L$ , to optimize the device performance. An upper limit for the inductance should be also considered, to ensure that the stored charge (inside the piezo element) remains approximately constant while the switch is on.



Figure 2. Cantilever beam with PZT patches bonded.

Table 1. Main beam properties.

Beam material	Al 7075 T6
In-plane dimensions (mm)	250 × 25
Total thickness (mm)	2
Young mod. E (GPa)	72
Poisson's ratio	0.32
Density (Kg/m <sup>3</sup> )	2700
Structural damping $\zeta$	0.01

Table 2. Main PZT properties.

PZT model (Stettner Co.)	PPK-11
N° of PZT	1
In-plane dimensions (mm)	30 × 25
Thickness (mm)	0.5
Young mod. (GPa)	62
Poisson's ratio	0.3
Density (kg/m <sup>3</sup> )	8000

Table 3. Selected reference beam eigenfrequencies.

Modes	Frequency(Hz)
1	26,56
2	154,67
5	417,22

This also implies that the voltage conversion should occur over a very short period (Figure 7), avoiding commutation losses.

The lower limit for the inductance is quite arbitrary, apart the necessity to prevent the excitation of structural resonance modes by the switch action. Since the resistance is chosen to be very small, the switching electrical frequency may be computed as:

$$f_{el} = \frac{1}{2\pi\sqrt{CL}} = 10f_{mec}. \quad (1)$$

Numerical simulations were then carried out, based on the electrical characteristics, summarized in Tables 4 and 5.

### FE Characterization

PZT patches are able to react both to bending and to in-plane stresses. The numerical simulation had to take into account this characteristic. Each node of a PZT finite element had six mechanical DOFs, three translational and three rotational; moreover, an additional electrical DOF, represented by the unknown PZT leads charge  $q$  (Ciminello et al., 2007), was considered for each element. The presence of only one electrical DOF per element implies that the charge is uniform on the surface, coherent with the physical observation that the electrons migration velocity on the conductive surface is remarkably lower than the highest mechanic period considered in this work. As a consequence, the charge

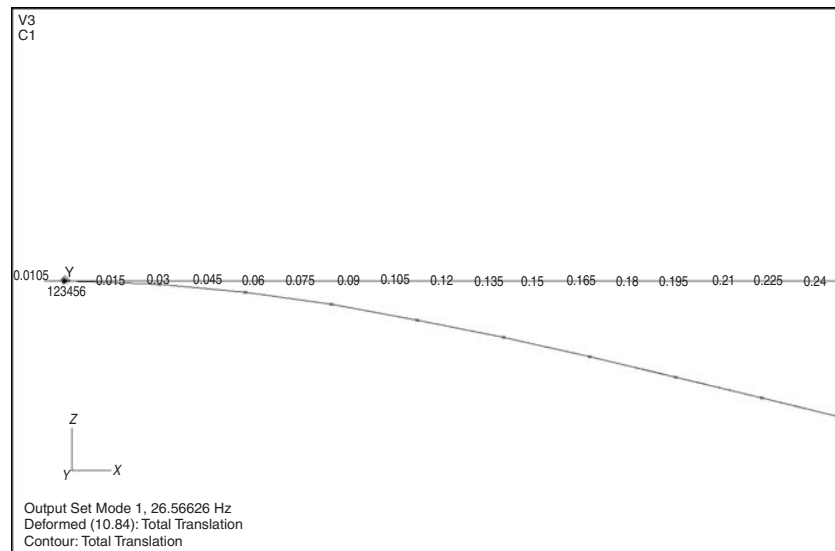


Figure 3. First mode shape: 26.56 Hz.

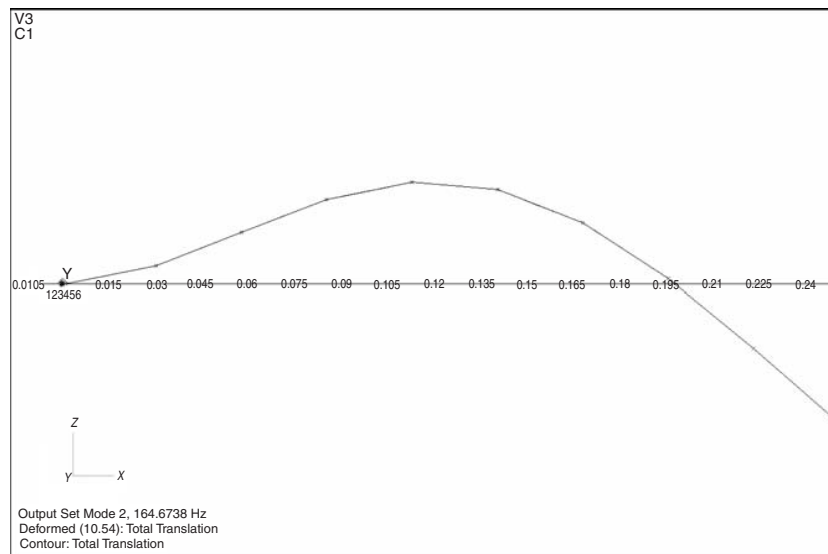
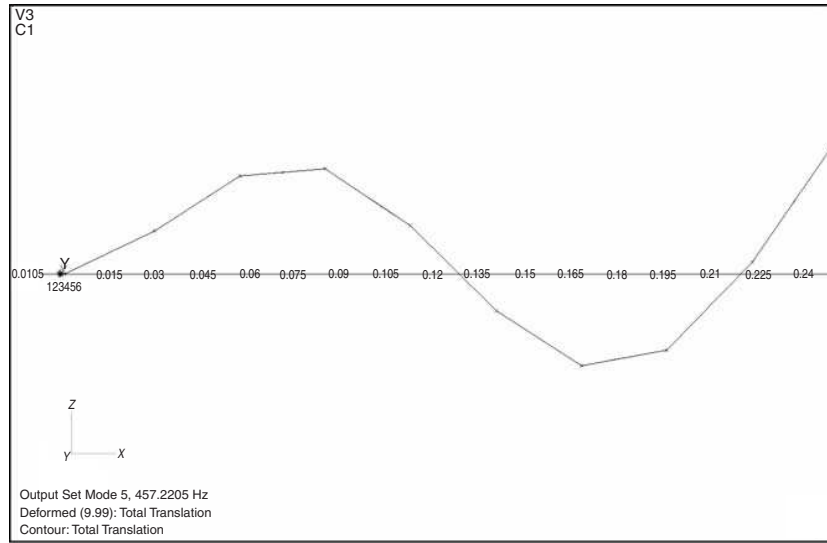
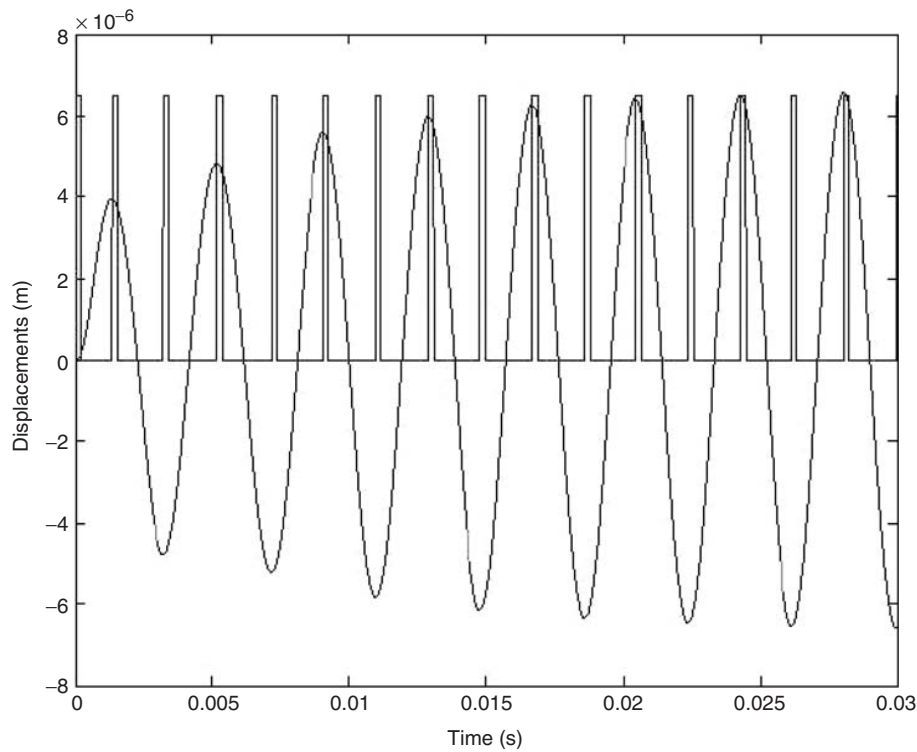


Figure 4. Second mode shape: 164.67 Hz.



**Figure 5.** Fifth mode shape: 457.22 Hz.



**Figure 6.** Example: switch pulse signal, synchronized to an harmonic excitation.

has enough time to uniformly distribute during the deformation.

From the virtual work principle, the relation (2) among the different terms, contributing to the total energy, is found:

$$\delta\Pi = \delta(U - T - W) = 0. \quad (2)$$

Expressing the potential energy variation  $\delta U$ , the kinetic energy  $\delta T$  and the external work  $\delta W$ , considering

the PZT constitutive law, PZT stiffness, damping and mass matrices are found, as shown in detail in Ciminello et al., 2007

Both PZT and beam matrices were suitably combined, by taking into account the common DOFs (Ciminello et al., 2007), in order to achieve a system in the form of:

$$[M]\{\ddot{x}\} + [C]\{\dot{x}\} + [K]\{x\} = \{F_{\text{exc}}\}. \quad (3)$$

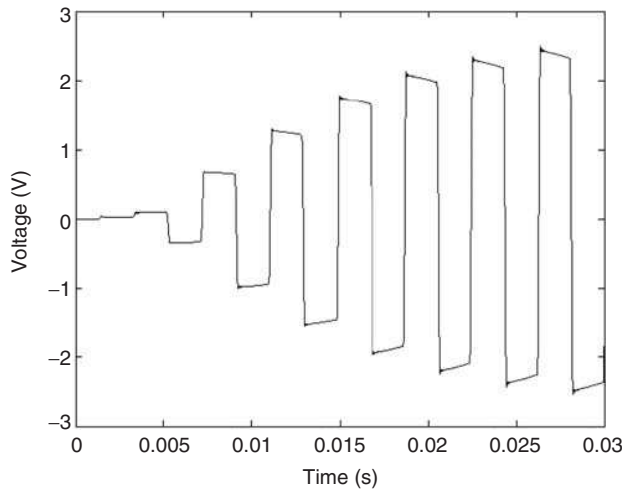


Figure 7. PZT voltage reversing in time domain.

Table 4. Switch off circuit numerical characteristics.

Quantity	Value
$f_{mec}$ (Hz)	See Table 3
$C$ (F)	49E-9
$R_{off}(\omega)$	1E10
$L_{off}$ (H)	2E6

Table 5. Switch on circuit numerical characteristics.

Quantity	Value
$f_{el}$ (Hz)	$10 * f_{mec}$
$C$ (F)	49E-9
$R_{on}(\omega)$	100
$L_{on}$ (H)	$1/((2 * \pi * f_{el})^2 * C)$

Damping matrix was assumed as a linear combination of the mass and stiffness ones; proportional coefficients were determined by imposing a constant value of damping  $\zeta$  (0.01) for the normal frequencies of interest. Corresponding structural matrices were integrated for the aluminium beam (Ciminello et al., 2007; Anderson and Crawley, 2007; Srinivasan and McFarland, 2005; Zienkiewicz, 1979; Heylen et al., 2003; Crawley and de Lius, 1998). FEMAP pre- and post-processing software was used to build a plate FE model (Figure 8), whose main characteristics are summarized in Table 6.

Each element had the same in-plane dimensions as the selected PZT patch in order to make the model integration easier.

### Integration Logical Scheme

Since the working principle of the SSSA control system is characterized by fast state variations, related to electric circuit quick commutation times, the system behavior will undergo a continuous transient regime.



Figure 8. FE Model of the referred cantilever beam.

Table 6. FE model main features.

Element type	CQUAD
Mesh discretization	$9 \times 1$
Number of total nodes	22
Number of constrained nodes	2
Mechanical DOFs per node	6
Total mechanical DOFs	132
Electrical DOFs	1
Total (electromechanical) DOFs	133

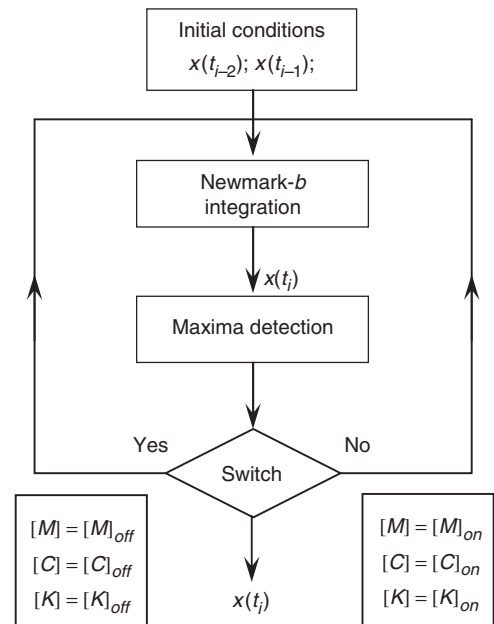
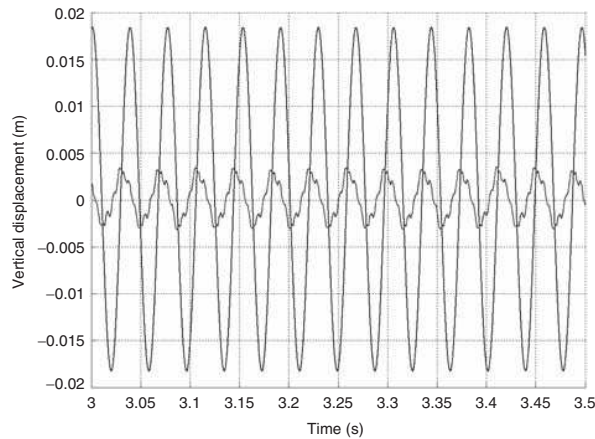
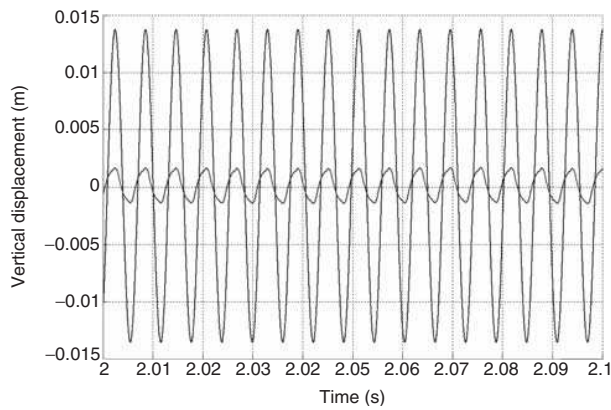


Figure 9. Flow chart.

A specific version (one step, implicit) of the Newmark-Beta numerical integration method was adopted, compatible with the MSC/Nastran solver (Richard et al., 2000). The transient structural output is computed through direct numerical integration of a set of coupled equations (Hwang and Park, 1993). Related matrices are time-dependent and, in particular, assume two forms, depending on the on/off state. The schematic of the integration method is illustrated in Figure 9 (Galucio et al., 2005; Tawfik and Baz, 2004; Zienkiewicz, 1979).



**Figure 10.** Time evolution of the beam with and without control for a sine excitation (damp. coeff  $\zeta = 0.01$ ).



**Figure 11.** Time evolution of the beam with and without control for a sine excitation (damping coeff  $\zeta = 0.01$ ).

Following the above diagram, after the time integration, a suitable algorithm detects eventual maxima. If the current system configuration  $x(t_i)$  results in a maximum, the circuit state is set to *on* and the structural matrices are consequently assigned. The circuit remains in this state for a specific time interval, according to what is defined in the next paragraph. After this short interval or if no maxima are detected, the system is switched to *off* and the structural matrices accordingly change.

## NUMERICAL RESULTS

A sinusoidal excitation signal has been used to excite the structure and to investigate SSSA suppression ability. The frequency of the excitation has been set to 26.56 Hz, 154.56 Hz, and 417.22 Hz for the three tests, respectively.

The first three bending modes have been controlled. Due to the time dependence of the global system, the results, in terms of free edge beam displacements, have been estimated in time domain (Figures 10–12).

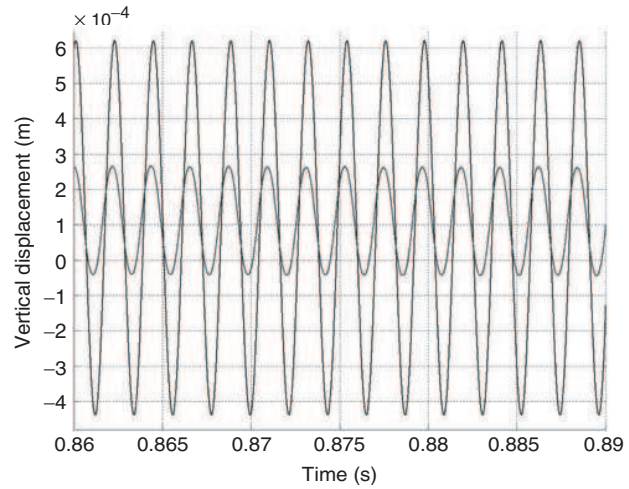


**Figure 12.** Time evolution of the beam with and without control for a sine excitation (damping coeff  $\zeta = 0.01$ ).

**Table 7. Off circuit experimental characteristics.**

Quantity	Value
$f_{\text{mech}}$ (Hz)	See Table 3
$C$ (F)	49E-9
$R_{\text{off}} (\omega)$	–
$L_{\text{off}}$ (H)	–

**Table 8. On circuit experimental characteristic.**

Quantity	Value
$f_{\text{el}}$ (Hz)	$10 * f_{\text{mec}}$
$C$ (F)	49E-9
$R_{\text{on}} (\Omega)$	100
$L_{\text{on}}$ (H)	10E-3

**Table 9. Control system electrical characteristics.**

Quantity	Value
Band width (Hz)	500
Switch freq. (Hz)	5000
Max switch freq. (kHz)	20
Pzt $d_{31}$ (m/V)	–350E-12

The numerical simulations were carried out through the adoption of the electrical characteristics that are summarized in Tables 7–9.

## SSSA ARCHITECTURE

The complete SSSA control system is represented schematically in Figure 13. It consists of a switching control unit connected to the shunt branch RL and a PZT transducer device.

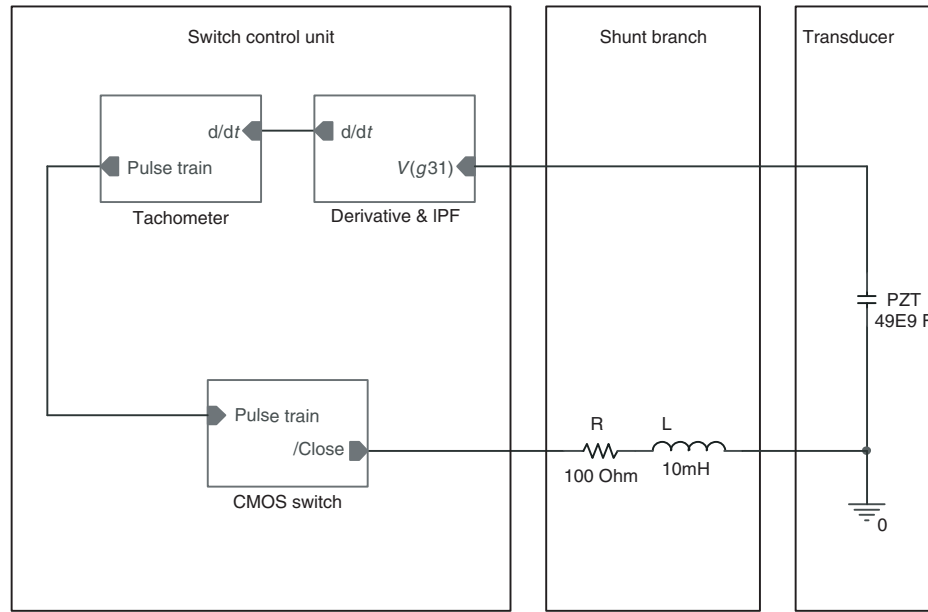


Figure 13. SSSA control system scheme.

The PZT transducer is connected to the shunt branch through the switch control unit, which drives the CMOS switch device. The switch control unit is described in detail as being made of a:

- Derivative & LPF (Low Pass Filter) unit;
- Tachometer;
- CMOS switch.

#### Derivative & LPF Unit

The input to the Derivative & LPF Unit is the PZT transducer voltage, converting the structural strain through the  $g_{31}$  (direct) piezoelectric constant. In fact, since the tachometer is sensitive to a zero crossing signal while the switch activation must be synchronized to the maximum strain, the input was opportunely derived.

The operational amplifier used to set-up the D & LPF unit belongs to the LM324 low power quad series, (Figure 14) (National Semiconductor Corporation, 2000). In detail, it consists of four independent, high gain, internally frequency compensated operational amplifiers, specifically designed to operate for a single or even dual power supply over a wide range of voltages. In Table 10 the main features of the component are summarized.

#### Tachometer

The tachometer input is the derived excitation signal. The tachometer output is a pulse train signal. The circuitry is able to produce the signal synchronized with the maxima deformations and with the width of 1/10 of the input signal period. The component used

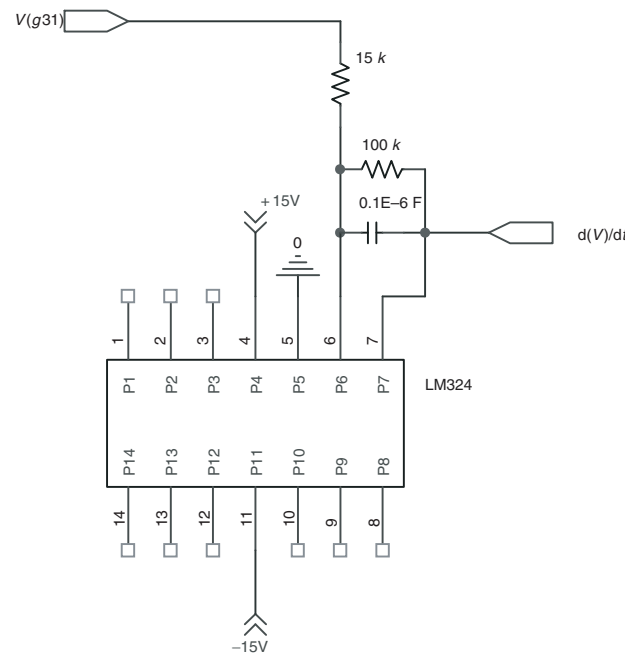


Figure 14. Derivative & LPF unit – schematic.

Table 10. LM324 main features.

Single power supply	3 V to 32 V
Dual power supply	+/-1.5 V to +/-16 V

belongs to the LM2907 series. In keeping with the system building block concept, this device provides an output voltage which is proportional to input frequency and provide zero output at zero frequency.

The device is designed to operate from a single supply voltage, which makes it particularly suitable for battery operation. Referring to National Semiconductor Corporation (2000) the device includes three basic components: an input amplifier with built-in hysteresis; a charge pump frequency to voltage converter; and an op amp/comparator with an output transistor.

The LM2907 can be used to provide zero crossing datum to a digital system using the circuits illustrated in Figure 15. At each zero crossing of the input signal the charge pump changes the state of capacitor  $C_2$  and provides a one-shot pulse into the zener diode  $D_1$  at pin 3. The width of this pulse is controlled by the internal current of pin 2 and the size of capacitor  $C_2$  as well as by the supply voltage. Since a pulse is generated by each zero crossing of the input signal, we call this a 'two-shot' and this can be used for doubling the frequency that is presented to the control system.

In Table 11 the output signal features are summarized:

$V_{cc}$ ,  $i_2$ , and  $C_2$  being the DC supply voltage, the current, and the capacitance in the branch afferent to pin 2 of the tachometer component, respectively (Figure 15); finally,  $V_{Zener}$  represents the voltage on the leads of the Zener diode of branch 3 sketched in the same figure.

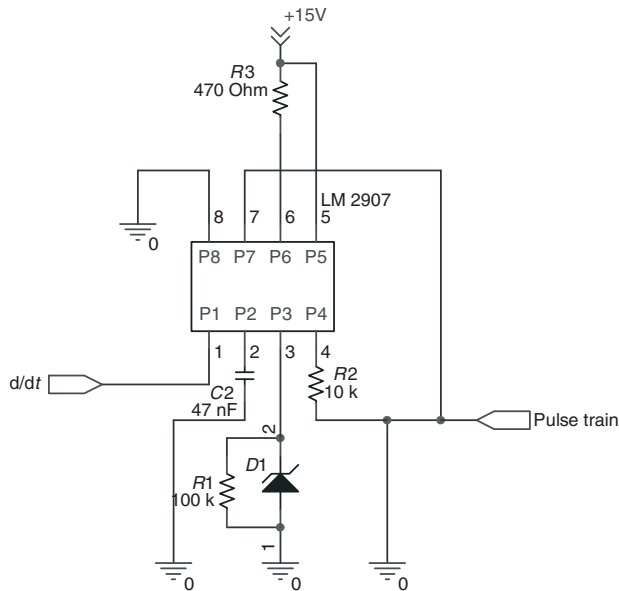


Figure 15. Tachometer – schematic.

Table 11. LM2907 output signal main features.

Pulse width	$(V_{cc}/2) * (C_2/i_2)$
Pulse height	$V_{Zener}$

## CMOS Switch

The switch component is a solid state device, typically a CMOS transistor, in order to face the high frequencies and the high number of commutations. The component used is an ADG452 monolithic CMOS (Analog Device, 2004) (Figure 16) device comprising of four independently selectable switches (Zienkiewicz, 1979).

They are designed using an enhanced LC2MOS process that provides low power dissipation yet gives high switching speed and low resistance. CMOS construction ensures ultra-low power dissipation, making the parts ideally suited for portable and battery-powered instruments. The CMOS switch driving input signal is a pulse train. The output is an *off/on* state. In Table 12 the ADG452 features are summarized.

## EXPERIMENTAL SET-UP

The experimental test structure is a 250 mm long aluminium cantilever beam, clamped at one end (Figure 17). The structure is excited through a PZT bonded at 1/3 span, towards the clamped edge.

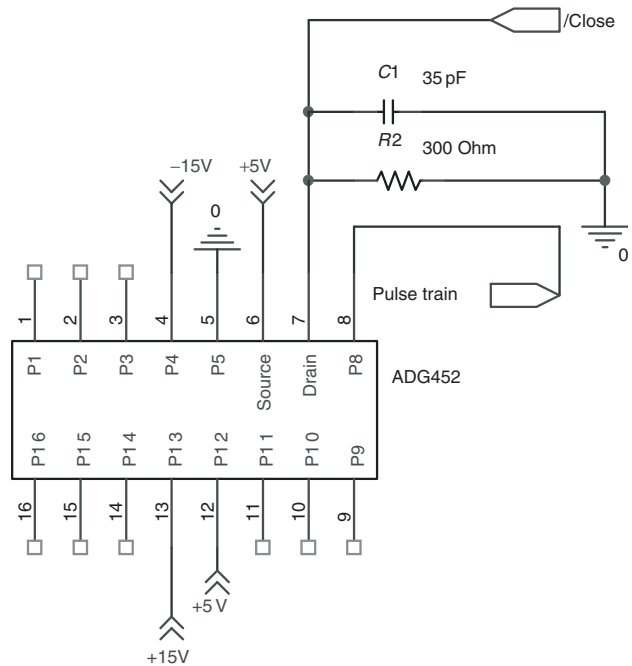


Figure 16. CMOS switch – schematic.

Table 12. ADG452 main features.

Logic power supply	5V
Analog signal range	$\pm 15V$
Fast switching time	$t_{on}$ 70 ns to $t_{off}$ 60 ns

A peak-to-peak amplified harmonic signal  $V_{pp}$  was used to drive the actuator, at each of the first three structural resonances (Table 3).

The following Figure 18 shows the SSSA electrical circuit, as realized for lab experiments.

The following instrumentation was used to perform the test campaign:

- Oscilloscope – Lecroy 9304AD 200 MHz
- Signal generator – Hp 33120A
- PZT power amplifier – CIRA HVA
- Dual power supply – EL 302 D
- Logic power supply – Lascar
- Fiber vibrometer laser – Polytec OFV-552
- Vibrometer controller – Polytec OFV-5000
- LMS modal analysis software

The input signal to the exciter (Figure 19) was provided by a signal generator, then amplified by the CIRA HVA (High Voltage Amplifier) (Figure 20). This signal was compared with the logical signal produced by the circuit.

The uncontrolled and controlled beam responses are detected through an optical laser vibrometer (Figure 21).

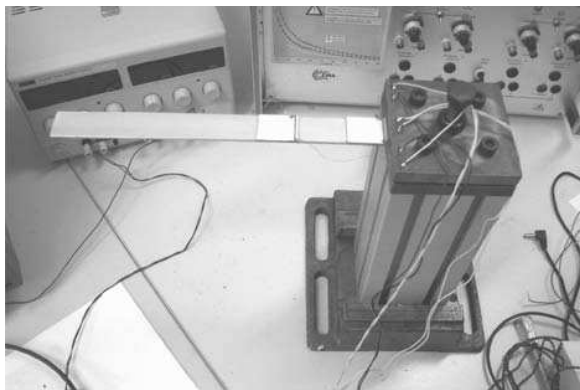


Figure 17. Experimental cantilever beam.

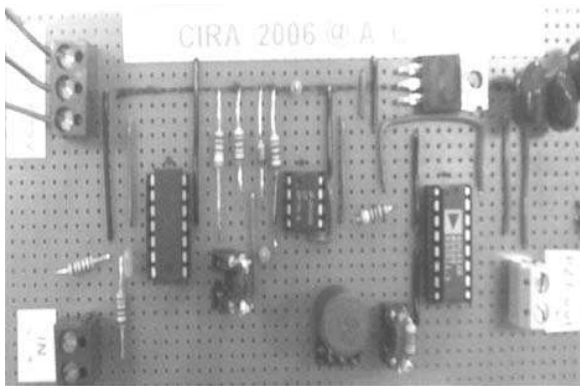


Figure 18. The SSSA control system realization.

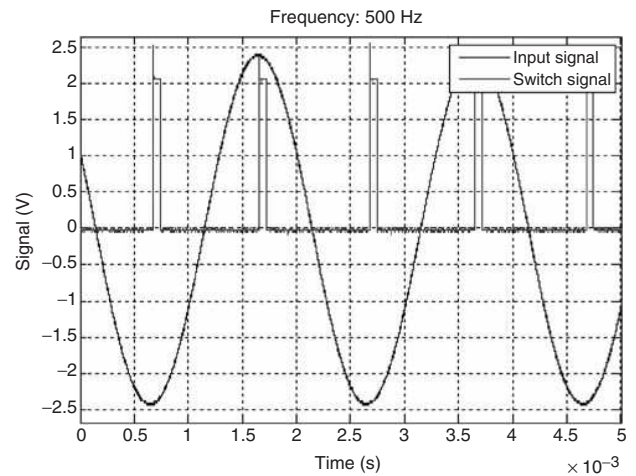


Figure 19. Input signal and logical switch produced by the circuit.

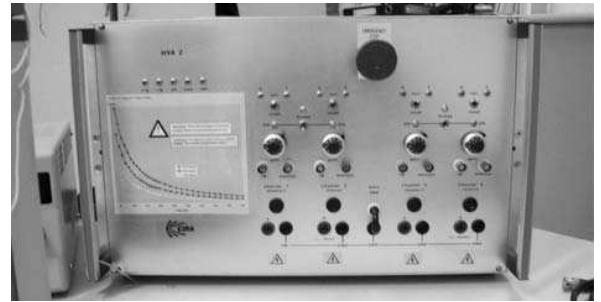


Figure 20. PZT high voltage amplifier (HVA).

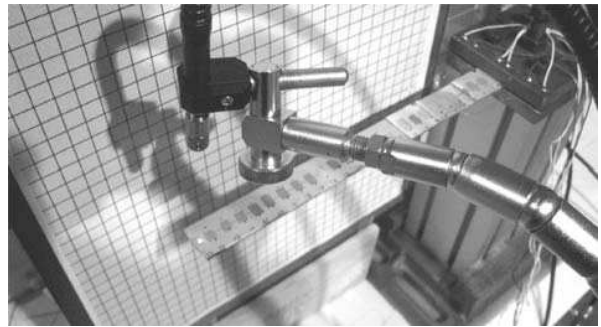


Figure 21. Optical laser vibrometer pointed at the free edge.

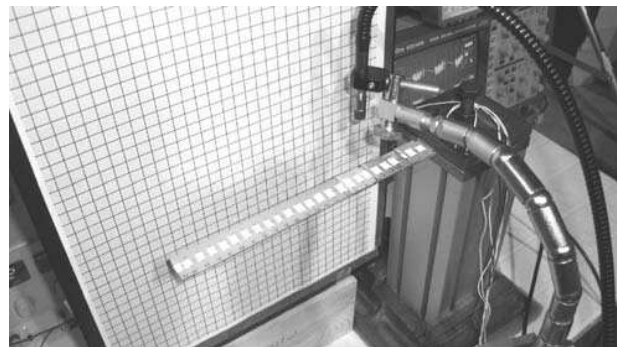
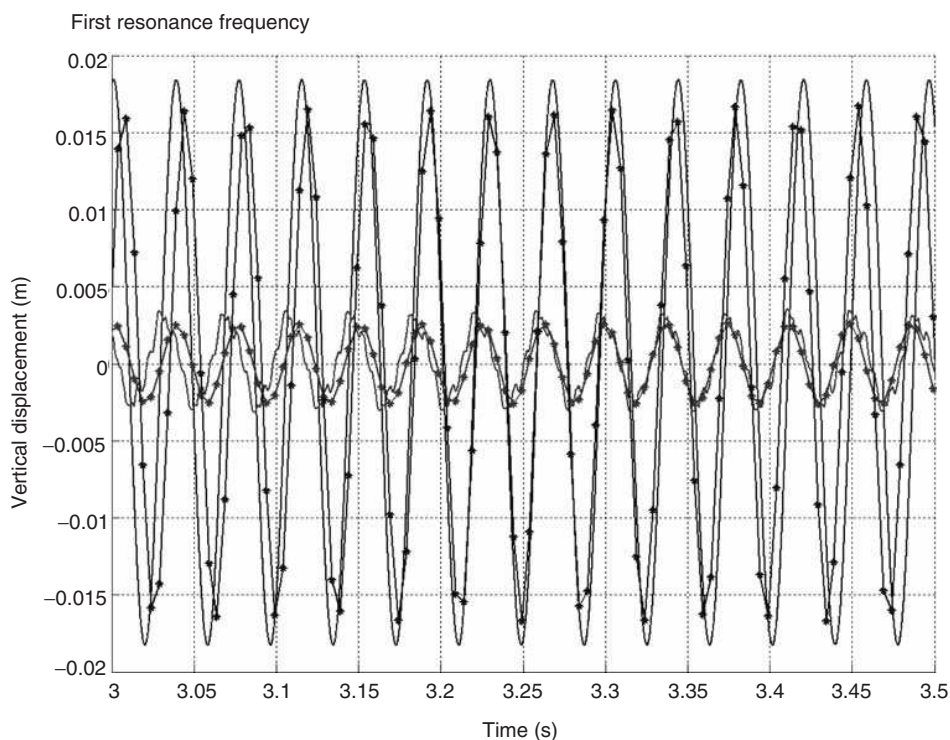
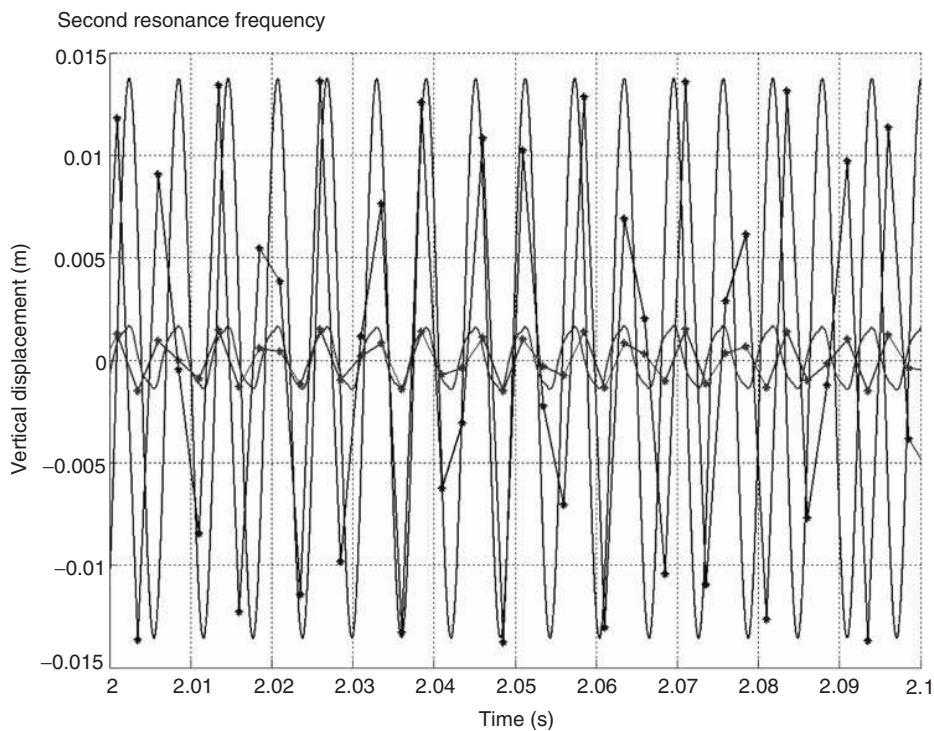


Figure 22. Cantilever beam 25 dot trace.



**Figure 23.** System time response to a sine excitation of 26.56 Hz: numerical (—) and experimental (-\*) comparison of the system response with and without control.



**Figure 24.** System time response to a sine excitation of 154.67 Hz: numerical (—) and experimental (-\*) comparison of the system response with and without control (second resonance frequency).

## NUMERICAL AND EXPERIMENTAL RESULTS

The measurements are conducted tracing a 25 dot line on the cantilever beam surface and detecting through an optical laser vibrometer the velocity of each point (Figures 21 and 22). Although the results presented concern the tip point, the acquisitions performed on the remaining points have been used to trace the experimental modal shapes. The recorded numerical values are processed through the LMS modal analysis software to get the corresponding displacements, in time domain, in order to compare the first, second, and fifth experimental displacement reduction with the numerical ones with and without control. In Figures 23 and 24, experimental and numerical results for the first two modes, with and without control, have been compared; in more detail, the higher amplitude curves refer to the non controlled response, while the lower amplitude ones refer to the controlled behavior. Experimental data have been highlighted by means of dotted lines. According to related numerical predictions, the displacement reduction expressed in dB is equal to 15.5 and 16.2, for the first and the second mode, respectively.

## CONCLUSIONS AND FURTHER STEPS

The control system presented here was tested to compare experimental and numerical results. The damping ability of the techniques has been estimated for the first bending modes; a max reduction of the displacements of 16.2 has been found. The experienced test campaign showed to be in good accordance, confirming the goodness of the adopted numerical model.

The vibrations damping gained here is the result of a single PZT device, without power amplification for its actuation. This strongly encourages testing systems with multiple active elements.

Concerning the switch control signal processing unit, a powerful improvement is expected by adopting a noise filtering and a voltage threshold fail-safe control device. Moreover, an electronic tachometer can be adopted to control impulse signals, as well. The optimized circuitry will be integrated on a chip to achieve better performance in terms of management and space saving.

Future experimental test campaigns will be carried on isotropic and anisotropic plates, to validate multimode control approaches (Ciminello et al., 2006; Przemieniecki, 1985).

## ACKNOWLEDGMENTS

The activities described in this article have been endorsed by the Italian Ministry of Scientific Research

that granted this activity inside the PON (Operative National Plan) SMART Project. The authors would like to express their gratitude to the project management team, and especially to Dr Carlo Camerlingo. Moreover, fervid appreciates go to Ing. Barbara Tiseo because of her scientific support.

## NOMENCLATURE

SSSA = Synchronized Switched Shunt Architecture

$C$  = Shunt circuit capacitance

$L$  = Shunt circuit inductance

$R$  = Shunt circuit resistance

$F_{exc}$  = External excitation

$f$  = Frequency

el = Referred to the switch circuit

mech = Referred to the structure

$\Pi$  = PZT total energy

$U$  = PZT potential energy

$T$  = PZT kinetic energy

$W$  = Electric circuit external work

$\nu$  = Poisson modulus

$\zeta$  = Structural damping coefficient

$[M]$  = Mass matrix

$[C]$  = Damping matrix

$[K]$  = Stiffness matrix

PZT = Referred to the PZT

str = Referred to the structure

$PZT \cup str$  = Referred to the PZT-structure coincident nodal points

$\{x\}$  = Vector of the mechanical and electrical unknowns

$q$  = Unknown electric charge

$Z_{shunt}$  = Shunt impedance

$V_{pp}$  = Peak-to-peak supply voltage signal for the PZT used to excite the structure

$V_{cc}$  = DC voltage supply of the tachometer

$i_2$  = Current of the branch 2 of the tachometer

$C_2$  = Capacitor of the branch 2 of the tachometer

$V_{Zener}$  = Zener diode voltage of the tachometer

## REFERENCES

- Agneni, A., Mastroddi, F. and Polli, G.M. 2003. "Shunted Piezoelectric Patch in Elastic and Aeroelastic Vibrations," *Computer and Structures*, 81:91–105.
- Ameduri, S., Ciminello, S., Sorrentino, R. and Concilio, A. (CIRA) 2005. "Beam Vibrations Control Through a Synchronised Switched Shunt Resonator (SSSR) System," AIDAA XVIII National Congress, September 19–22.
- Analog Device, LC2MOS 5W Ron SPST Switches, ADG452. 2004. Datasheets Downloading from ChipDocs, pp. 1–20.

- Anderson, E.H. and Crawley, E.F. 2007. "Piezoceramic Actuation of One and Two Dimensional Structures," *Journal of Materials Processing Technology*, 231–236.
- Caruso, G. 2001. "A Critical Analysis of Electric Shunt Circuit Employed in Piezoelectric Passive Vibration Damping," *Smart Materials and Structures*, 10:1059–1068.
- Ciminello, M., Ameduri, M. and Concilio, A. 2006. "Semiactive Vibration Control using Piezoelectrics in Shunt Configuration," The Second International Conference on Dynamics, Vibration and Control (ICDVC 2006) Beijing, China, August 23–26, No. ICDVC2006-W72.
- Ciminello, M., Ameduri, S. and Concilio, A. 2007. "FE Modelling of an Innovative Vibration Control Shunt Technique," The Smart Structures Laboratory – The Italian Aerospace Research Center, CIRA. Online ahead of print publication, 11.6.2007 10.1177/1045389X07082379.
- Corr, L.R. and Clark, W.W. 2001. "Comparison of Low Frequency Piezoceramic Shunt Techniques for Structural Damping," *Smart Structures and Materials 2001: Damping and Isolation, Proceedings of SPIE*, 4331:262–272.
- Crawley, E.F. and de Luis, J. 1998. "Use of Piezoelectric Actuators as Elements of Intelligent Structures," *AIAA Journal*, 25(10):1373–1385.
- Galucio, A.C., Deü, J.F. and Ohayon, R. 2005. "A Fractional Derivative Viscoelastic Model for Hybrid Active-Passive Damping Treatments in Time Domain - Application to Sandwich Beams," *Journal of Intelligent Materials Systems and Structures*, 16:33–45.
- Hagood, N.W. and von Flotow, A. 1991. "Damping of Structural Vibrations With Piezoelectric Materials and Passive Electrical Networks," *Journal of Sound and Vibration*, 146(2):243–268.
- Heylen, W., Lammens, S. and Sas, P. 2003. *Modal Analysis Theory and Testing*, KU Leuven. ISBN 90-73802-61-X; 2003
- Hwang, S.M. and Park, B.H. 1993. "Finite Element Modeling of Piezoelectric Sensors and Actuators," *AIAA Journal*, 31(5): 930–937.
- Kahn, B.K., Wang, R.Y. 2001. "Active-Passive Hybrid Piezoelectric Network for Vibration Control, Comparison and Improvement," *Smart Materials and Structures*, 10:794–806.
- Kim, S.J. and Moon, S.H. 2001. "Active and Passive Suppression of Nonlinear Panel Flutter Using Finite Element Method," *AIAA Journal*, 39(11):2042–2050.
- Law, H.H., Rossiter, P.L., Simon, G.P. and Koss, L.L. 1996. "Characterization of Mechanical Vibration Damping by Piezoelectric Material," *Journal of Sound and Vibration*, 197(4):489–513.
- Lesieutre, G.A. 1998. "Vibration Damping and Control Using Shunted Piezoelectric Materials," *The Shock and Vibration Digest*, 30(3):187–195.
- McGowan, A.R. 1999. "An Examination of Applying Shunted Piezoelectrics to Reduce Aeroelastic Response," CEAS/AIAA/ICASE/NASA Langley International Forum on Aeroelasticity and Structural Dynamics 1999, Williamsburg, Virginia, June 22–25, pp. 553–571.
- Moheimani, S.O.R. and Behrens, S. 2004. "Multimode Piezoelectric Shunt Damping With Highly Resonant Impedance," *IEEE Transactions on Control Systems Technology*, 12(3):484–491.
- National Semiconductor Application Note 162, LM2907 Tachometer/Speed Switch Building Block Applications, June 1976, pp. 1–18.
- National Semiconductor Corporation, LM324 Low Power Quad Operational Amplifiers, August 2000, pp. 17–20.
- Park, C.H. and Inman, D.J. 1999. "A Uniform Model for Series RL and Parallel RL Shunt Circuits and Power Consumption," *SPIE Conference Proceedings on Smart Structure and Integrated Systems*, Newport Beach, CA, 3668, pp. 797–804.
- Przemieniecki, J.S. 1985. *Theory of Matrix Structural Analysis*, Ed. Dover. ISBN-0-486-64948-2.
- Richard, C., Guyomar, D., Audigier, D. and Bassaler, H. 2000. "Enhanced Semi Passive Damping Using Continuous Switching of a Piezoelectric Device on an Inductor," *Proceedings of SPIE*, Vol. 3989, *Damping and Isolation*, pp. 288–299.
- Srinivasan, A.V. and McFarland, D.M. 2005. *Smart Structures*, Cambridge University Press.
- Tawfik, M. and Baz, A. 2004. "Experimental and Spectral Finite Study of Plates with Shunted Piezoelectric Patches," *International Journal of Acoustics and Vibration*, 9(2):87–97.
- Tzou, H.S. and Tseng, C.I. 1990. "Distributed Piezoelectric Sensor/Actuator Design for Dynamic Measurement/Control of Distributed Parameter System: A Piezoelectric Finite Approach," *Journal of Sound and Vibration*, 138(1):17–34.
- Wu, S. 2001. "Broadband Piezoelectric Shunts for Passive Structural Vibration Control," *Proceedings of SPIE 2001*, 4331, pp. 251–261.
- Zienkiewicz, O.C. 1979. *The Finite Element Method*, 3rd edn, McGraw Hill.

Salvatore Ameduri

---

**Da:** onbehalfof+dinman+vt.edu@manuscriptcentral.com per conto di dinman@vt.edu  
**Inviato:** mercoledì 4 novembre 2009 4.24  
**A:** s.ameduri@cira.it  
**Cc:** dinman@vt.edu; journals@vt.edu; dinman@vt.edu  
**Oggetto:** Journal of Intelligent Material Systems and Structures - Decision on Manuscript ID JIM-09-188

03-Nov-2009

Dear Dr. Ameduri:

It is a pleasure to accept your manuscript entitled "Multi-tone Switching Shunt Control by a PZT Network Embedded into a Fibreglass Panel: Design, Manufacture and Test" in its current form for publication in the Journal of Intelligent Material Systems and Structures . The comments of the reviewer(s) who reviewed your manuscript are included at the foot of this letter.

If you wish your article to be freely available online immediately upon publication (as some funding bodies now require) you can opt for it to be included in SAGE Open on payment of a publication fee. Manuscript submission and refereeing procedure is unchanged, but on acceptance of your article you will be asked to let SAGE know directly if you are choosing SAGE Open. For further information, please visit <http://www.sagepub.com/sageopen>. Authors wishing to publish their papers under the SAGE Open scheme should contact [SAGE Production Editor].

PLEASE NOTE THAT YOUR DIGITAL FILES MUST BE IN AN EXECUTABLE FORMAT SUCH AS WORD OR LATEX. PDF FILES CANNOT BE USED IN THE PRODUCTION PROCESS. Artwork should be supplied as EPS files or .tif files, at a minimum resolution of 300 dpi for superior reproduction.

Line Drawings. Originals should always be submitted. Wherever possible, graphs should be boxed in, and scale divisions should be marked on the inside of the boxes. Grids should not be shown. Insofar as possible, explanations should be placed in the legend. Original drawings should not be larger than 20\_25 cm (8\_10 in.); if this is impossible, they must be accompanied by two sets of small photoprints. Measurements should be indicated in SI units.

Lettering should be planned for 50% reduction; text should be readable after reduction.

Illustrations should be referred to as Figure 1, Figure 2 etc.

IF YOUR PAPER HAS BEEN ACCEPTED AND IT IS NOT IN THIS FORMAT PLEASE EMAIL THE PROPER FILES TO journals@vt.edu IMMEDIATELY.

Thank you for your fine contribution. On behalf of the Editors of the Journal of Intelligent Material Systems and Structures , we look forward to your continued contributions to the Journal.

Sincerely,

Dr. Daniel J. Inman

Editor-in-Chief, Journal of Intelligent Material Systems and Structures dinman@vt.edu

Reviewer(s)' Comments to Author:



**Journal of Intelligent Material Systems and Structures**

Journal of Intelligent Material Systems &amp; Structures

**Multi-tone Switching Shunt Control by a PZT Network  
Embedded into a Fibreglass Panel: Design, Manufacture and  
Test**

Journal:	<i>Journal of Intelligent Material Systems and Structures</i>
Manuscript ID:	JIM-09-188
Manuscript Types:	Original Article
Date Submitted by the Author:	02-Nov-2009
Complete List of Authors:	Ameduri, Salvatore; Centro Italiano Ricerche Aerospaziali, CIRA, Smart Structures and Materials Laboratory, SMAS Ciminello, Monica; University of Naples "Federico II", Aerospace Engineering Lecce, Leonardo; University of Naples, Aerospace Engineering Calabrò, Antonio; CIRA Italian Aerospace Research Center, SMAS/OSALAB Smart Structures Optic Sensors Laboratory Concilio, Antonio; Italian Aerospace research center, Smart Structures

<http://mc.manuscriptcentral.com/jimss>

## Abstract:

Research in noise and vibration control has partially focused on semi-active attenuation techniques such as Switching Shunt Control (SSC) systems. Among the various methods, SSC architectures exhibit several interesting advantages such as low power absorption and intrinsic adaptive capabilities. This approach may represent an acceptable compromise between passive and active solutions. In previous work the authors implemented and validated 1D and 2D numerical models, addressed to describe continuous simple isotropic structures under tonal excitations controlled by single-element SSC system. Further efforts were then directed to extend the applicability of those models to non-isotropic structures and to multi-tone control devices. In this paper, a 6-PZT network multi-tone SSC system is presented, and embedded into a balanced fibreglass laminate. The network geometry is defined according to an optimisation process following modal information. The former 1-channel control circuit was extended to drive up to 4 independent channels. The complete system dynamics was simulated by assembling the structural matrices into a Matlab code, where both the electromechanical coupling and the control circuit behaviour were taken into account. The structure was excited by broadband sweep signals in a selected range. Numerical and experimental results were compared and discussed.



# Multi-tone Switching Shunt Control by a PZT Network Embedded into a Fibreglass Panel: Design, Manufacture and Test

\*Monica Ciminello,\*Leonardo Lecce

\*\*Salvatore Ameduri,\*\*Antonio Calabrò,\*\*Antonio Concilio

\*Department of Aerospace Engineering (DIAS) University of Naples "Federico II", Italy

\*\*Lab of Smart Structures, the Italian Aerospace Research Centre (CIRA), Capua, Italy

Research in noise and vibration control has partially focused on semi-active attenuation techniques such as Switching Shunt Control (SSC) systems. Among the various methods, SSC architectures exhibit several interesting advantages such as low power absorption and intrinsic adaptive capabilities. This approach may represent an acceptable compromise between passive and active solutions. In previous work the authors implemented and validated 1D and 2D numerical models, addressed to describe continuous simple isotropic structures under tonal excitations controlled by single-element SSC system. Further efforts were then directed to extend the applicability of those models to non-isotropic structures and to multi-tone control devices. In this paper, a 6-PZT network multi-tone SSC system is presented, and embedded into a balanced fibreglass laminate. The network geometry is defined according to an optimisation process following modal information. The former 1-channel control circuit was extended to drive up to 4 independent channels. The complete system dynamics was simulated by assembling the structural matrices into a Matlab code, where both the electromechanical coupling and the control circuit behaviour were taken into account. The structure was excited by broadband sweep signals in a selected range. Numerical and experimental results were compared and discussed.

## Keywords

Switch shunt control, semi-active control, embedded piezoceramic

## Nomenclature

SC	Shunt Control
SSC	Synchronised Shunt Control
PZT	Piezoceramic (Lead Zirconate Titanate)
$\sigma_{ii}$	mechanical in-plane stress
$\tau_{ii}$	mechanical angular stress
$\varepsilon_{ii}$	mechanical in-plane strain
$\gamma_{ii}$	mechanical angular strain
$D_j$	dielectric displacement
$E_j$	electric field
$\nu$	Poisson ratio
$d_{ij}$	the piezoceramic inverse dielectric constant
$s_{ij}$	compliance constants
$\epsilon_{ij}$	dielectric constants
$Y$	Young modulus
$\theta$	rotation
$u$	displacement along x axes
$v$	displacement along y axes
$w$	displacement along z axes
$q$	electrical charge
$C_p$	pzt blocked capacitance
$q$	electrical charge
$G$	direct electromechanical coupling matrix

$D$	inverse electromechanical coupling matrix
$t$	thickness
$\psi$	flexural stiffness ratio
$\Lambda$	pzt free strain
$\alpha_{eq}$	equivalent thermal coefficient
$V_{pzt}$	sensor voltage
$\omega$	angular frequency
$a$	pzt length
$b$	pzt width
$[M]$	mass structural matrix
$[C]$	damping structural matrix
$[K]$	stiffness structural matrix
$F_{ext}$	external excitation
$M_{pzt}$	piezoceramic actuation moment
$\zeta$	damping coefficient
$\phi$	electromechanical eigenvectors matrix
$L$	shunt circuit inductance
$R$	shunt circuit resistance
$E_c$	kinetic energy
$T$	referred to a transpose vector
$x$	referred to the in plane mechanical dof
$y$	referred to the in plane mechanical dof
$z$	referred to the transversal mechanical dof
$i$	referred to the electrical field direction
$j$	referred to the mechanical field direction
$s$	referred to the structure
$p$	referred to the piezoceramic
$int$	referred to the pzt/structure interface

### Introduction.

A first example of PZT-based commutation *State Shunted Circuits* was proposed in [1, 2]. Therein the author studied a resistive SC with comparable open and closed circuit periods. This kind of device can be compared to a variable stiffness mechanical system. In [3, 4], the authors proposed to close the circuit for a very short period and to add an inductor to boost the electric charge produced on the PZT elements. This technique was called *Synchronized Switch Damping*. The switching approach can be further modified to produce:

- *Synchronized Switch Damping on Short*, a purely resistive shunt;
- *Synchronized Switch Damping on Inductance*, including an inductive component;
- *Synchronized Switch Damping on Voltage Source*, implementing a voltage input, function of the vibration amplitude [5].

This last option changes the system into one of active control requiring an external power supply. It also involves instability risks, eventually mitigated by forcing slow input voltage variations, [6]. In [1-6], the damping effects were estimated by simple 1D simulations and MDOF models were considered in [7-9] where state and Synchronized Switching techniques were compared. The latter resulted in a more effective approach. Further improvements were presented in [10], where different modal filters were implemented. Good performance was achieved but complex electronics was required. Guyomar et al. refined the Inductive Switching Shunt structure and proposed an autonomous guidance circuit [11-12]. In particular, they showed how the detection of local maxima was not optimal for multimode control. They proposed instead the use of probabilistic criteria, getting good results [13] by filtering the detected signal maxima using a threshold (averaged vibration level) value.

Numerical procedures were developed in order to apply these methods to real structural systems, as in [14-15]. In [14], an isotropic, simply supported rectangular plate is referred to, controlled by a single PZT patch. Coupled electromechanical system matrices were assembled into a dedicated Matlab routine, while the structural matrices were computed by the MSC/Nastran code. Control logic was then implemented and system time response was finally computed. The proposed approach was experimentally validated in [15], on a cantilever beam resulting in a 5-dB displacement reduction around the 1<sup>st</sup> and 3<sup>rd</sup> mode band, following the action of a single PZT patch, with no power amplification. The goal of this paper is to extend the abovementioned results to multi-tone control systems, implemented on 2D isotropic structures (fibreglass laminate).

A 6-couple actuator-sensor PZT network is considered. The active devices were embedded within a 10-ply plate. A proprietary *plug-and-play* electronic circuit was realised, an evolution of earlier releases [15]. Classical PZT strain

actuation analytical models were implemented [16-19]. PZT sensor response was computed by relations directly derived by the constitutive equations. A multi-parameter genetic optimisation process, taking advantage of the complete numerical model, was carried out to determine the PZT devices layout and number. The control system authority and its bandwidth were elements of the cost function considered. Laboratory tests were finally performed and the attained results compared with the numerical predictions.

### 1. PZT coupling modelling

The complete system is modelled, made of the structural part, the active devices, the electrical elements and the control logic. MSC/Nastran is used to derive the structural matrices. In this paragraph, equations regulating PZT behaviour as actuator (produced moment,  $M_{pzt}$ ) and sensor (derived voltage,  $V_{pzt}$ ), are recalled; converse and direct piezoelectric effects are then considered.

#### 1.1 Constitutive equation

PZT constitutive matrix, linking resulting deformation to imposed stress and electric field, may be assembled according to the following assumptions (non-zero terms):

1. *PZT material is elastic and transversally isotropic.* These relations then hold, for the elastic:

$$\begin{aligned} c_{11} &= c_{22} \\ c_{13} &= c_{23} \\ c_{44} &= c_{55} = \frac{1}{2}(c_{33} - c_{13}) \end{aligned} \quad (1)$$

and the electromechanical and electric constants:

$$\begin{aligned} d_{31} &= d_{32} \\ d_{24} &= d_{15} \\ \epsilon_{11} &= \epsilon_{22} \end{aligned} \quad (2)$$

The other non-zero constants, independent from the above terms, are (mechanical):

$$\begin{aligned} c_{33} \\ c_{12} \\ c_{66} &= \frac{1}{2}(c_{11} - c_{12}) \end{aligned} \quad (3)$$

and (electromechanical and electric):

$$\begin{aligned} d_{33} \\ d_{36} &= 0 \\ \epsilon_{33} \end{aligned} \quad (4)$$

The PZT electromechanical constitutive equation is, then:

$$\begin{Bmatrix} \varepsilon_x \\ \varepsilon_y \\ \varepsilon_z \\ \varepsilon_{xz} \\ \varepsilon_{yz} \\ \varepsilon_{xy} \\ D_x \\ D_y \\ D_z \end{Bmatrix} = \begin{bmatrix} c_{11} & c_{12} & c_{13} & 0 & 0 & 0 & 0 & 0 & d_{13} \\ c_{12} & c_{11} & c_{13} & 0 & 0 & 0 & 0 & 0 & d_{13} \\ c_{13} & c_{13} & c_{33} & 0 & 0 & 0 & 0 & 0 & d_{33} \\ 0 & 0 & 0 & c_{44} & 0 & 0 & 0 & d_{15} & 0 \\ 0 & 0 & 0 & 0 & c_{44} & 0 & d_{15} & 0 & 0 \\ 0 & 0 & 0 & 0 & 0 & c_{66} & 0 & 0 & 0 \\ 0 & 0 & 0 & 0 & d_{15} & 0 & \epsilon_{11} & 0 & 0 \\ 0 & 0 & 0 & d_{15} & 0 & 0 & 0 & \epsilon_{11} & 0 \\ d_{13} & d_{13} & d_{33} & 0 & 0 & 0 & 0 & 0 & \epsilon_{33} \end{bmatrix} \begin{Bmatrix} \sigma_x \\ \sigma_y \\ \sigma_z \\ \sigma_{xz} \\ \sigma_{yz} \\ \sigma_{xy} \\ E_x \\ E_y \\ E_z \end{Bmatrix} \quad (5)$$

2. The PZT is unloaded along the vertical direction, so that:

$$\sigma_{zz} = 0 \quad (6)$$

3. Electric field is zero in the patch plane; then:

$$E_x = E_y = 0 \quad (7)$$

Since the thickness is very small with respect to the other dimensions, no contribution derives from the action of  $V_z$ ; the potential may be considered linear along the vertical dimension. It follows, from (5):

$$\begin{aligned} \varepsilon_{xz} &= c_{44} \sigma_{xz} \\ \varepsilon_{yz} &= c_{44} \sigma_{yz} \\ \varepsilon_{xy} &= c_{66} \sigma_{xy} \\ \varepsilon_z &= f(\varepsilon_x, \varepsilon_y) \\ D_x &= d_{15} \sigma_{yz} \\ D_y &= d_{15} \sigma_{xz} \end{aligned} \quad (8)$$

These variables may be therefore considered a linear combination of others. The constitutive relationship reduces into:

$$\begin{Bmatrix} \varepsilon_x \\ \varepsilon_y \\ D_z \end{Bmatrix} = \begin{bmatrix} c_{11} & c_{12} & d_{31} \\ c_{12} & c_{11} & d_{31} \\ d_{31} & d_{31} & \epsilon_{33} \end{bmatrix} \begin{Bmatrix} \sigma_x \\ \sigma_y \\ E_z \end{Bmatrix} \quad (9)$$

The elastic constants  $c_{11}$  and  $c_{12}$  may be expressed as function of the Young's modulus ( $Y_p$ ) and Poisson ratio ( $\nu$ ) as:

$$\begin{aligned} c_{11} &= 1/Y_p \\ c_{12} &= -\nu/Y_p \end{aligned} \quad (10)$$

This matrix may be inverted and assumes the form:

$$\begin{Bmatrix} \sigma_x \\ \sigma_y \\ E_z \end{Bmatrix} = \begin{bmatrix} Y_p \\ \epsilon_{33}(\nu-1)+2Y_p d_{31}^2 \end{bmatrix} \begin{bmatrix} \frac{-\epsilon_{33}+d_{31}^2 Y_p}{(1+\nu)} & \frac{\nu\epsilon_{33}+d_{31}^2 Y_p}{(1+\nu)} & d_{31} \\ \frac{\nu\epsilon_{33}+d_{31}^2 Y_p}{(1+\nu)} & \frac{-\epsilon_{33}+d_{31}^2 Y_p}{(1+\nu)} & d_{31} \\ d_{31} & d_{31} & \frac{(\nu-1)}{Y_p} \end{bmatrix} \begin{Bmatrix} \epsilon_x \\ \epsilon_y \\ D_z \end{Bmatrix} \quad (11)$$

### 1.2 Direct Piezoelectric Effect

Equations (11) describe the working of a piezoelectric as an actuator and a sensor. In particular, the equation describing the direct piezoelectric effect can be derived from the last row:

$$E_z = \frac{Y_p}{\epsilon_{33}(\nu-1)+2Y_p d_{31}^2} \left[ d_{31}(\epsilon_x + \epsilon_y) + \frac{(\nu-1)}{Y_p} D_z \right] \quad (12)$$

Holding the assumption 3,  $E_z = V_z/t_p$ . If the piezoelectric element is a sensor, open circuit condition may be assumed, yielding  $D_z = 0$ , [19]. Equation (12) is then written as:

$$V_z = \frac{Y_p t_p d_{31}}{\epsilon_{33}(\nu-1)+2Y_p d_{31}^2} (\epsilon_x + \epsilon_y) = \frac{Y_p t_p d_{31} \epsilon_s}{\epsilon_{33}(\nu-1)+2Y_p d_{31}^2} \quad (13)$$

Let classical plate theory be referred to. The action of normal loads and bending moments is taken into account; small displacement are considered. Axial deformation is neglected and curvature terms are disregarded as well. Only bending is then taken into account, so that the in-plane deformation may be expressed as follows:

$$\begin{aligned} \epsilon_x &= -z \frac{\partial^2 w}{\partial x^2} \\ \epsilon_y &= -z \frac{\partial^2 w}{\partial y^2} \end{aligned} \quad (14)$$

These relations may be numerically expressed by the finite differences approach, as (homogeneous mesh):

$$\epsilon_s|_{i,j} = -z \left[ \frac{w_{i-1,j} - 2w_{i,j} + w_{i+1,j}}{\Delta x^2} + \frac{w_{i,j-1} - 2w_{i,j} + w_{i,j+1}}{\Delta y^2} \right] \quad (15)$$

In other words, the output voltage of the PZT sensor is a function of the normal displacements at certain nodes of the region where it is placed such as illustrated in Figure 1.

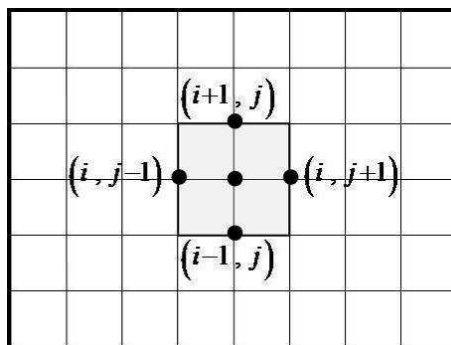


Figure 1 – Contact region between piezoelectric and structure; typical grid and node sequence.

If  $p$  PZT are added to the model, the direct coupling matrix  $G$  is a  $p \times n$  matrix the rows of which allow computing the piezoelectric voltage output.

### 1.3 Converse Piezoelectric Effect

The expression of the moment,  $M_{PZT}$ , generated by the embedded PZT element is recalled, according to the classical formulation by Crawley and de Luis, [16]. The piezoelectric patch works then as a structural actuator. Recall the basic hypotheses:

- Linear stress/strain relations;
- Linear strain along the structure and the piezoelectric ceramic thickness;
- Bonding layer quality is perfect.

This latter hypothesis yields for typical actuator-structure configuration, [16]. Whichever theory is considered, the expression for the transmitted strain at the interface between PZT actuator and the structure may be expressed as:

$$\varepsilon_{\text{int}} = \alpha \cdot \Lambda \quad (16)$$

Where  $\alpha$  is the generic transmission coefficient, a number in the interval [0;1]. Its value depends on the geometric and physical characteristics of the materials considered. The parameter  $\Lambda$  is the PZT “free” strain, or the strain that would be generated on a non-constrained piezoelectric patch, excited by an electrical tension,  $V$ :

$$\Lambda = \frac{d_{31}}{t_p} V \quad (17)$$

The classical theory, [16], reports the following value for the transmitted strain due to a couple of embedded actuators, symmetrically placed with respect to the neutral axis:

$$\varepsilon_{\text{int}} = \frac{24\theta_z}{24\theta_z^2 + \psi\theta_s^2\bar{I} + 2t_p} \frac{z}{t_p} \Lambda \quad (18)$$

If a Bernoulli-type stress-strain diagram is considered, the transmitted moment per unit of length is:

$$M_{PZT} = \frac{24\theta_z\theta_s\bar{I}Y_s t_s^2}{24\theta_z^2 + \psi\theta_s^2\bar{I} + 2} \Lambda \quad (19)$$

The parameters  $\theta_s$  and  $\theta_z$  are the ratios  $t_s/t_p$  and  $z_M/t_p$ , respectively, following the nomenclature introduced in [16]. In detail,  $z_M$  is the distance of the mean PZT line from the neutral axis. Other non-dimensional parameters are:

$$\bar{I} = \frac{12I_{EQ}}{bt_s^3} \quad (20)$$

$I_{EQ}$  being the moment of inertia of the structure, including the presence of the piezoelectric actuators, and:

$$\psi = \frac{Y_s t_s}{Y_p t_p} \quad (21)$$

the ratio among the 1D effective stiffness of the two bodies. The transmitted strain may be reported as a function of the relative thicknesses for a certain value of the Young moduli ratio. In the case considered here and represented in Figure 2,  $Y_s/Y_p = 0.7$  (fibreglass vs. piezoelectric ceramic). Really, it is not possible to refer to a non-dimensional thickness parameter, because of the formula structure. The relation looks strongly dependent on the piezoelectric thickness, as it becomes larger and larger. For small values of PZT thickness (up to 1 mm),

and for reasonable values of  $z_M$ , the functions stay near and some general remarks may be drawn. Transmitted strain attains its maximum for a relative thickness value in the range [3;6].

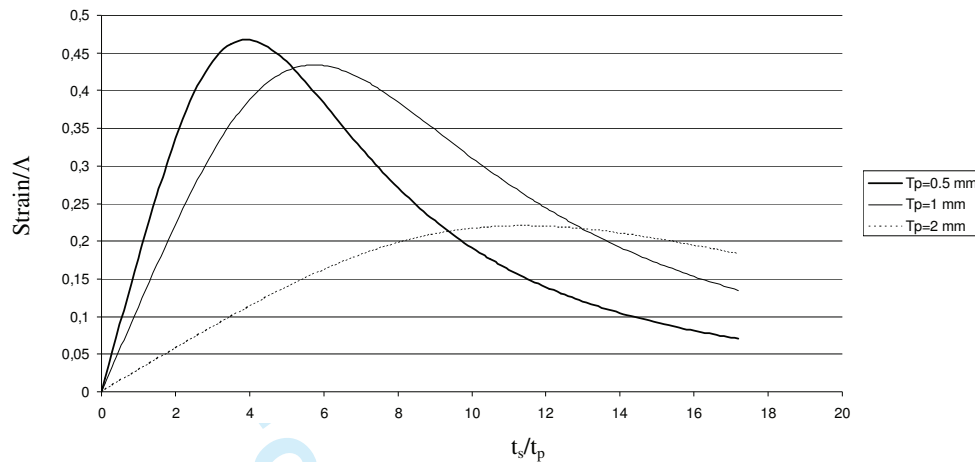


Figure 2 – Normalised strain as a function of the relative thickness for Young ratio of 0.7 (embedded PZT actuators)

The expression (19) refers to 1D, but can be easily extended to 2D configurations. It can be used as a basic reference when evaluating transmitted moments through numerical analysis. FE strategies are in fact necessary to represent complex, generally shaped structures (stiffened, tapered, etc.), when analytical solutions are not available. A solid model, HEXA8-based, was built to evaluate the strain actuation performed by PZT couples, embedded within the fibreglass structure analysed here. The piezoelectric effect is simulated by applying a unit thermal load to a temperature-dependent material, whose expansion coefficient is:

$$\alpha_{eq} = d_{31} / t_p \quad (22)$$

Results of this comparison are reported in Table 1 (moments per unit of length).

[kg mm/ sec <sup>2</sup> ]	$M_{PZT,x}$	$M_{PZT,y}$
Analytical, [16]	108,6	109,8
Numerical	82,9	83,6

Table 1 – PZT transmitted actions

The total transmitted moments may be distributed along the domain boundaries. A simple technique is to divide them into equal parts for each of the edges except for the corner nodes where it is assigned with half that value (uniform mesh). A representation of this kind of distribution is shown in Figure 3. The converse coupling matrix, referring to  $p$  actuators, acting on an  $n$ -DOF structure, is an  $n \times p$  matrix whose columns define the single piezoelectric excitation at the  $i$ -th structural node.

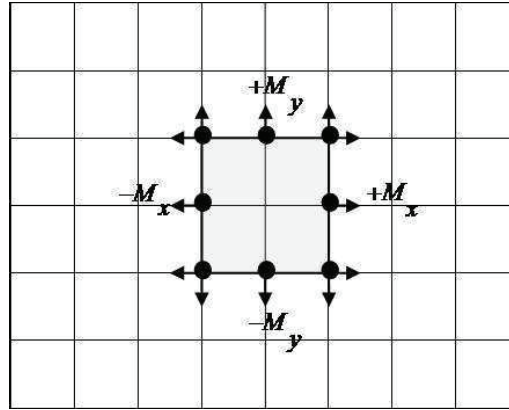


Figure 3 – Schematic of the PZT-generated moments distribution, along the contact boundaries.

## 2 Switching Shunt Control Working Principle

The basic principles of the adopted switching shunt control device are now described. The PZT element, is connected to a circuit, switching between an open and a closed (shunt) state; the latter is usually the shorter period. Previous results, [3], confirmed by successive independent studies, [14], verified that better performance levels are obtained when the switching period is set to 1/10 of the highest frequency to be controlled and is independent on the structural dynamics. When the circuit is closed, a voltage inversion on the PZT electrodes takes place. In Figure 4, examples of time signals representing the PZT voltage in the SSC system is plotted.

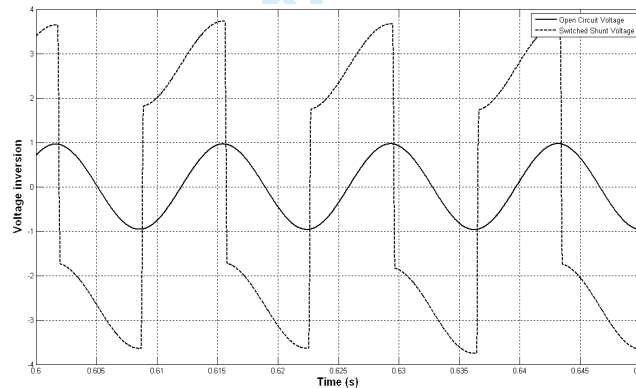


Figure 4 – Example of time evolution of the PZT voltage during a sine excitation.

The switching produces in change in local strain actuation, opposite to the structural-borne strain. The circuit pulsation  $\omega_{el}$  is simply related to  $C_p$  and  $L$  through the relation:

$$\omega_{el} = 10\omega_{mech,max} = \frac{1}{\sqrt{C_p L}} \quad (23)$$

The SSC is therefore characterized by fast state variations, following the circuit quick commutation times. The global system will then suffer a continuous transient regime. Classical frequency analysis is then replaced by time domain representations. Computation is performed using a direct implicit numerical scheme of the Newmark-Beta family algorithm. Two different equations are referred to, considering the short and open circuit state, respectively. The numerical integration method flowchart is reported in Figure 5. Through a standard sine signal inversion procedure after time integration, strain maxima are identified and the system switch to the closed state. After 1/10 of the prescribed period, the system switches back.

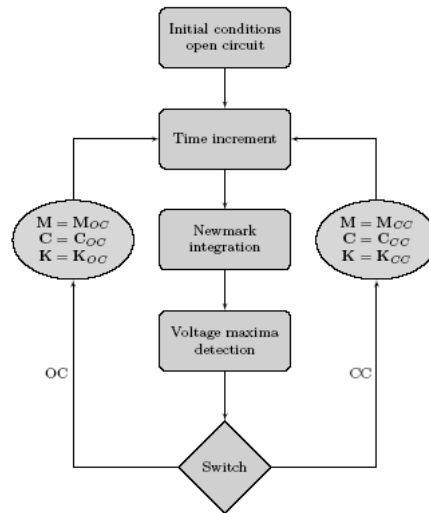


Figure 5. SSC-Newmark integration method flow chart

### 3.Modal reduction of the system equation

PZT-generated forces,  $M_{PZT}$ , and sensed voltage,  $V_{PZT}$ , may be expressed as:

$$\{M_{PZT}\} = [D]\{q\} \quad (24)$$

$$\{V_{PZT}\} = [G]\{x\} \quad (25)$$

The coupling matrices,  $D$  and  $G$ , relate the charge and displacement field to the actions, produced by the PZT actuator, or the signals, generated by the incipient strain field, acting over the PZT sensor. The equation that describes the electrical circuit dynamics is:

$$[L]\{\ddot{q}\} + [R]\{\dot{q}\} + [C_p^{-1}]\{q\} = \{V_{PZT}\} \quad (26)$$

$L$  and  $R$  are the inductance and the resistance of the adopted shunt circuit while  $C_p$  is the PZT *blocked* capacitance.

Assuming that standard equation regulates the structural dynamics, the coupled system is described by:

$$\begin{bmatrix} \underline{M_s} & 0 \\ 0 & \underline{L} \end{bmatrix} \begin{Bmatrix} \ddot{x} \\ \ddot{q} \end{Bmatrix} + \begin{bmatrix} \underline{C_s} & 0 \\ 0 & \underline{R} \end{bmatrix} \begin{Bmatrix} \dot{x} \\ \dot{q} \end{Bmatrix} + \begin{bmatrix} \underline{K_s} & \underline{D} \\ \underline{G} & 1/C_p \end{bmatrix} \begin{Bmatrix} x \\ q \end{Bmatrix} = \begin{Bmatrix} F_{ext} \\ 0 \end{Bmatrix} \quad (27)$$

Proportional damping is assumed, [20], [21]. The structural eigenvectors matrix is extracted by MSC/Nastran, the structural mass and stiffness matrixes as well. The electrical DOF,  $q$ , is invariant after this reference change. The global transformation base is, then:

$$\underline{\xi} = \begin{bmatrix} x_r \\ q \end{bmatrix} = \begin{bmatrix} \underline{\varphi} & 0 \\ 0 & I \end{bmatrix} \begin{bmatrix} x \\ q \end{bmatrix} = \underline{\Phi} \begin{bmatrix} x \\ q \end{bmatrix} \quad (28)$$

By substituting the expression (28) into (27) and pre-multiplying by  $\underline{\Phi}^T$ , the following relation is obtained:

$$[M_r]\{\ddot{\xi}\} + [C_r]\{\dot{\xi}\} + [K_r]\{\xi\} = [F_r] \quad (29)$$

In the above equation, the matrices  $M_r$ ,  $C_r$ ,  $K_r$  (system) and  $F_r$  (external forces), are:

$$\begin{aligned}
 \underline{M}_r &= \begin{bmatrix} \underline{\varphi^T M_s \varphi} & \underline{0} \\ \underline{0} & \underline{L} \end{bmatrix}; \\
 \underline{C}_r &= \begin{bmatrix} \underline{\varphi^T C_s \varphi} & \underline{0} \\ \underline{0} & \underline{R} \end{bmatrix}; \\
 \underline{K}_r &= \begin{bmatrix} \underline{\varphi^T K_s \varphi} & \underline{\varphi^T D} \\ \underline{G \varphi} & \underline{1/C_p} \end{bmatrix}; \\
 \underline{F}_r &= \begin{bmatrix} \underline{\varphi^T F_{ext}} \\ \underline{0} \end{bmatrix}.
 \end{aligned} \tag{30}$$

Time integration of the equation (29) provides the *reduced* dynamic response of the system, in the two states. Inverse transformation provides the physical time history.

#### 4. Test specimen modelling.

The technique describe above was applied to a fibreglass panel. Free boundary conditions are assumed. Materials features, properties and number of nodes are reported in Table 2. The panel's main features are then summarised in Table 3. Piezoelectric in-plane dimensions and mechanical characteristics are summarised in Table 4.

<b>Material</b>	<b>Plate</b>	Fibreglass laminate
	<b>PZT</b>	Ceramic
<b>Property</b>	<b>Plate</b>	Balanced, symmetric laminate
	<b>PZT</b>	Transversal Isotropic
<b>Nodes</b>	<b>Plate</b>	1203
	<b>PZT</b>	35 (single patch)

Table 2 – FE model features.

<b>Dimensions (mm)</b>	220 x 280 x 7
<b>Layers N</b>	10 plies
<b>Composite components</b>	7781 Fabric – 5245C Epoxy
<b>Young modulus (GPa)</b>	45
<b>Poisson modulus</b>	0.27
<b>Density (kg/m<sup>3</sup>)</b>	2700
<b>Stack sequence</b>	[0] <sub>s</sub>
<b>Constraints</b>	4-edge free

Table 3 – Structure main properties.

<b>Dimensions (mm)</b>	61 x 35 x 0.5
<b>Young modulus (GPa)</b>	62
<b>Poisson modulus</b>	0.32
<b>Density (kg/m<sup>3</sup>)</b>	7800
<b>D<sub>31</sub> (m/V)</b>	350e-12
<b>G<sub>31</sub> (Vm/N)</b>	11.3e-3
<b>Installation</b>	Embedded (Control device) – Bonded (Disturbance)

Table 4 – PZT main properties

The PZT thickness and locations were chosen to maximise strain actuation and, then, the effect over the structure. The original FE model was updated after a correlation between numerical and experimental data. In particular, a genetic algorithm-based fitting process was carried out to determine the mesh, the plate thickness

distribution and local curvature, able to minimise the differences between the modal frequencies. The resulting geometry is sketched in Figure 6. A PZT element working as external exciter is bonded on the top surface.

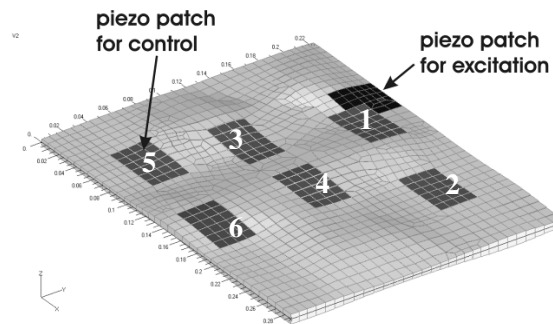


Figure 6 – Optimised FE model – Scheme (thickness distribution is exaggerated for representation purposes) PZT control element are embedded. PZT exciter is externally bonded.

In Table 5 numerical resonance frequencies are summarised.

Mode Id	Frequency [Hz]	Mode Id	Frequency [Hz]
1	156.1	5	607.5
2	227.6	6	720.6
3	391.2	7	766.2
4	452.6	8	952.6

Table 5 – Numerical structural frequencies.

Normal mode analysis on the revised model provided the results shown in Figure 7 for the first 8 mode shapes. Maximum strain is attained where the curvature is higher. Therefore, those points are held as the optimal in-plane location for the better electro-mechanical energy transmission, [12].

## 5. Experimental Characterisation

### 5.1 SS Circuit Manufacture

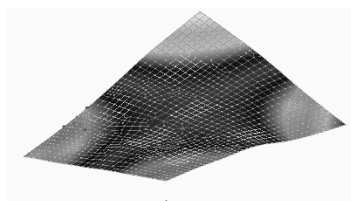
The SSC control system was designed, manufactured and tested during the activities described in [15]. Its main component blocks are:

- Derivative & LPF (Low Pass Filter) Unit, [22];
- Tachometer, [23];
- CMOS Switch (ADG452), [24].

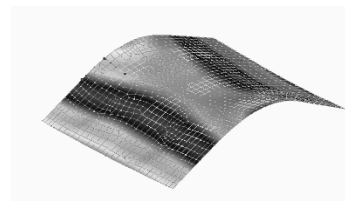
The ADG452 main features are summarized in Table 6..

Logic power supply (V)	5
Analogical signal range (V)	+/- 15
Max switching frequency (kHz)	20
Fast switching time, (nsec)	70 (t <sub>on</sub> )
	60 (t <sub>off</sub> )

Table 6 – ADG452 main features



a. 1<sup>st</sup> mode



b. 2<sup>nd</sup> mode

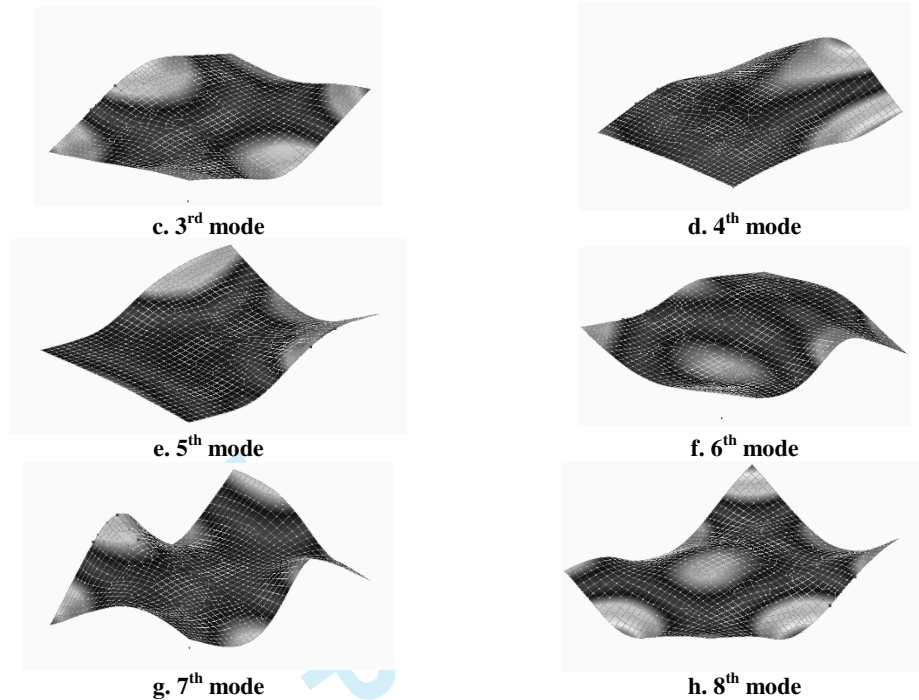


Figure 7 – First 8 plate mode shapes.

Here a 4-channel SSC system was realised using the same procedures described in reference [15], taking advantage of the peculiar characteristics of the selected CMOS. A photo of the implemented electronics is reported in Figure 8. The SSC COMS is *user-friendly* and follows a *plug-and-play* philosophy. The band of interest may be modified by simply changing some electrical components. The four channels may be independently activated or activated altogether. Synthetic inductors were not used. Experiments showed that better performance is achieved when using higher current absorption inductors: 20 mA were measured for a 28 mH inductor.

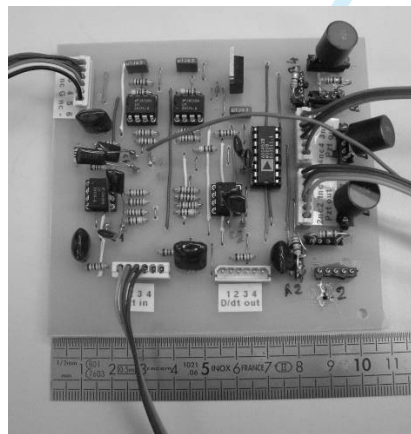


Figure 8 – The SSC electric board.

## 5.2 Specimen Manufacture

The test specimen was a 10-ply fibreglass plate, 287 x 221 mm. The 6-PZT network was embedded at the 2<sup>nd</sup> and 9<sup>th</sup> ply (symmetrical configuration). One layer worked as a sensor, the other as an actuator network. The 6 channels were completely independent. After epoxy resin infusion, the panel was then put under compression for 24 hours, cured and finally shaped into the final form pictured in Figure 9.

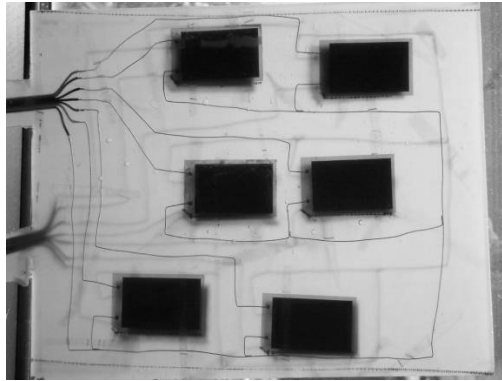


Figure 9 – FG laminate plate, with embedded PZT network.

### 5.3 Piezoelectric Ceramic Component

PIC 155 (PI, Physik Instrumente) material was used, which is a piezoelectric ceramic with high Curie temperature, high permittivity, high coupling factor and charge constants. The material is optimised for dynamic applications. High coupling factor (a measure of the efficiency in transforming electric into mechanical energy), low mechanical quality factor (internal dissipation) and low temperature coefficient (small variation of the characteristic coefficients with temperature), make this material particularly suitable for structural applications. In the form of bender actuators, they allow high deflections (up to 0.8 mm), with high force and high precision. They are also applied as structural broadband sensors (for structural health monitoring purposes, for instance) or for energy harvesting. A PI product based on the PIC 155 material is the P876 DuraAct, a ceramic patch embedded into protective films, [25]. The laminated design includes external protection and provides mechanical preload and electric insulation. In the kHz band, for usual deformations and device dimensions, generated electrical power is in the order of mW.

Operating Voltage, (V)	-100 to +400
Holding Force (N)	265
Length (mm)	61
Width (mm)	35
Thickness (mm)	0.5
Bending radius (mm)	20
Layer thickness ( $\mu\text{m}$ )	200
Electrical capacitance (nF)	90
Oper Temp Range ( $^{\circ}\text{C}$ )	-20 to +150
Mass (g)	3.5

Table 7 – P-876, Technical Data.

### 5.4 Set-up

Laboratory set-up block diagram is shown in Figure 10. In detail, the following instrumentation was used:

- Oscilloscope – Lecroy 9304AD 200MHz;
- Signal generator – Hp 33120A;
- Dual power supply – EL 302 D;
- Logic power supply – Lascar;
- Fibre vibrometer laser – Polytec OFV-552;
- Vibrometer controller – Polytec OFV-5000;
- LMS Test Lab analysis SW;
- LMS SCADAS III acquisition system.

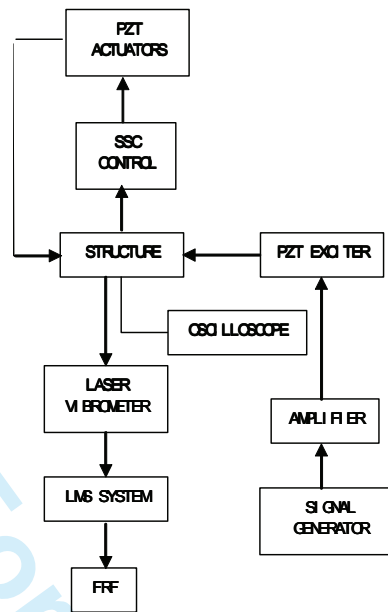


Figure 10 – Set-up flow chart

## 6 Results

### 6.1 Set-Up and Experimental Modal Analysis

The structure was excited by a piezoelectric ceramic patch bonded on its upper surface, driven by a 15 sec, 400 mV (peak-to-peak) sweep signal. 50-1000 Hz frequency band was investigated, including the first 8 structural resonance frequencies. Vertical point velocity was detected through a laser vibrometer (Figure 11). The data was collected and processed using an LMS acquisition system through the Testlab Time MDOF tool.

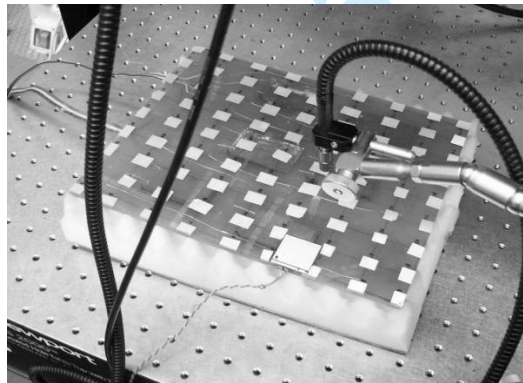


Figure 11 – Experimental modal analysis: acquisition grid (81 points).

Mode Id	Exp Freq (Hz)	Num. Dev. (%)	Mode Id	Exp Freq (Hz)	Num. Dev. (%)
1	-	-	5	627.1	3.1
2	228.6	0.4	6	725.3	0.6
3	371.8	5.2	7	750.2	2.1
4	455.6	0.6	8	953.8	0.1

Table 8 – First 8 plate eigenfrequencies; deviation from the numerical results.

Measurements at the 1<sup>st</sup> numerical resonance, 156 Hz, were affected by a considerable background noise, probably due to non-ideal boundary conditions and the small deformation field, associated to the corresponding

modal shape. Low energy could then be inserted by the action of the piezoelectric actuator. An 81-node measurement grid was used. Experimental modal shapes are reported in Figure 12.

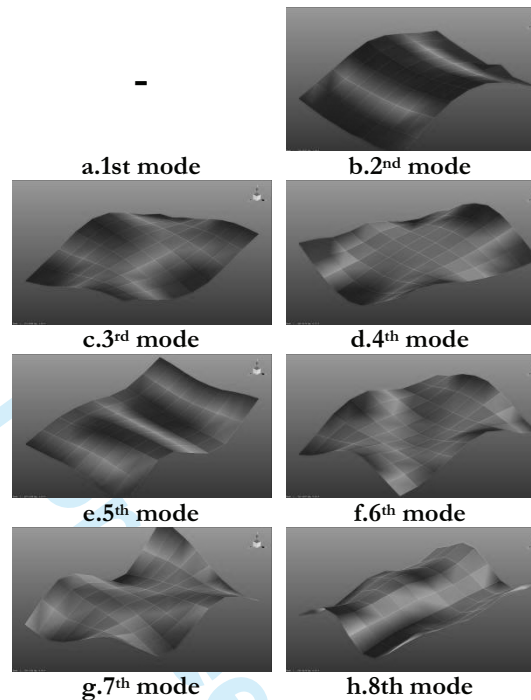


Figure 12 - Experimental plate mode shapes.

Test results showed some critical aspects when compared to the model. The numerical deviations from the experimental results were small and mainly due the specimen manufacture itself, resulting in a non-regular thickness distribution and a variation of the optimal actuator placement regions.

## 6.2 Control Implementation

The action of the SSC control system occurs through the activation of each of the 6-PZT network actuators, as each receives the signal from the respective collocated sensors. A single SSC system per channel was connected. The different actuator – sensor couples were tested alone and then combined with the others, according to various combinations. Electrical parameters, assumed in the numerical simulations, are summarised in Table 9-10.

Quantity	Value
$f_{mec}$ (Hz)	see Table 5
$C_{off}$ (F)	90.E-9
$R_{off}$ ( $\Omega$ )	1.E10
$L_{off}$ (H)	Ad-hoc value, to guarantee matrix inversion

Table 9 – Switch-off circuit numerical parameters.

Quantity	Value
$f_{el}$ (Hz)	$10 \cdot f_{mec}$
$C_{on}$ (F)	90.E-9
$R_{on}$ ( $\Omega$ )	100.
$L_{on}$ (mH)	$1 / ((2 \cdot \pi \cdot f_{el})^2 \cdot C_{on})$

Table 10 – Switch-on circuit numerical parameters.

The nodal velocities were measured at the 81 grid points used in the experimental modal analysis. Results are expressed in terms of the measured mean plate kinetic energy and evaluated in dB. In order to compare the numerical and experimental results, certain frequencies were first selected, coherently with the following procedure:

- An experimental characterisation of the panel, with and without control, is performed;
- The mean kinetic energy FRF is plotted;
- Peaks of interest are selected; the choice is supported by point information;
- A comparison with the numerical data occurs.

Numerical velocity maps of the controlled and non-controlled system are reported for two modes of interest in Figures 13-16. The selected PZT (active) control systems used are the couples 1-2-3 identified in Figure 6. Tests show a certain capability of the SSC in controlling a wide range of frequencies. For instance, the response levels at the 6<sup>th</sup> and 7<sup>th</sup> mode are clearly affected. In Table 11, numerical and experimental kinetic energy reductions (dB) are compared for the different modes. In Figures 17-19 the effect of different combinations of SSC control systems is reported.

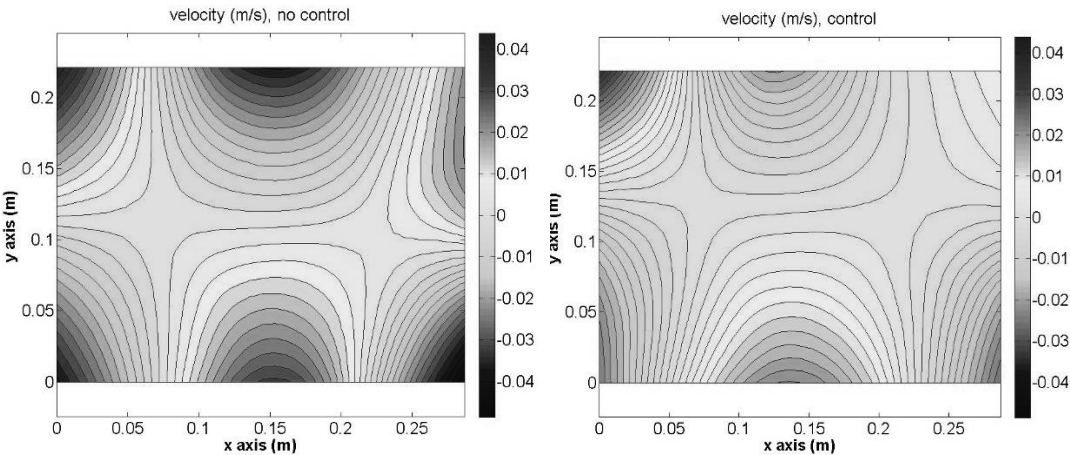


Figure 13/14 – 3<sup>rd</sup> modal frequency; numerical velocity map; uncontrolled (left) vs. controlled (right)

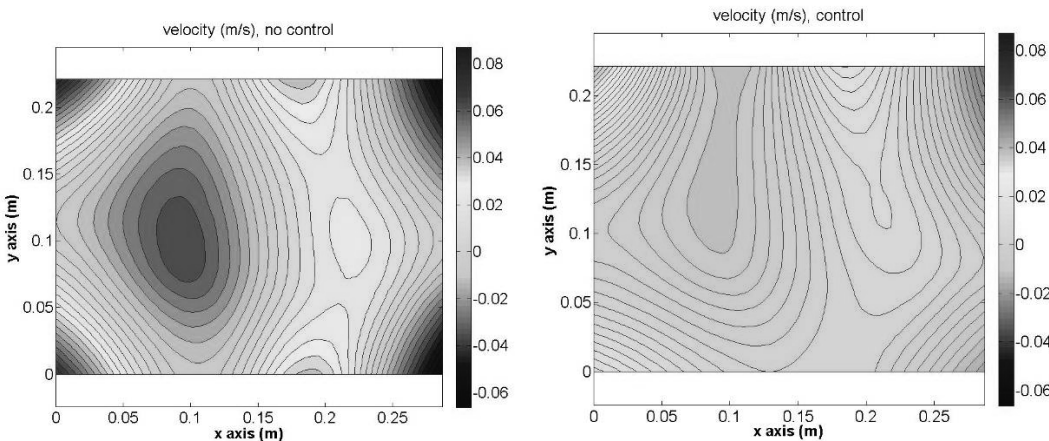


Figure 15/16 – 6<sup>th</sup> modal frequency; numerical velocity map; uncontrolled (left) vs. controlled (right)

MODE	KE (dB) – Num.	KE (dB) – Exp.	MODE	KE (dB) – Num.	KE (dB) – Exp.
1 <sup>st</sup>	-	-	5 <sup>th</sup>	7	6
2 <sup>nd</sup>	7	8	6 <sup>th</sup>	17	16
3 <sup>rd</sup>	8	6	7 <sup>th</sup>	11	9

4 <sup>th</sup>	<1	-	8 <sup>th</sup>	2	4
-----------------	----	---	-----------------	---	---

Table 11 – Kinetic energy reduction, dB; PZT 1, 2, 3.

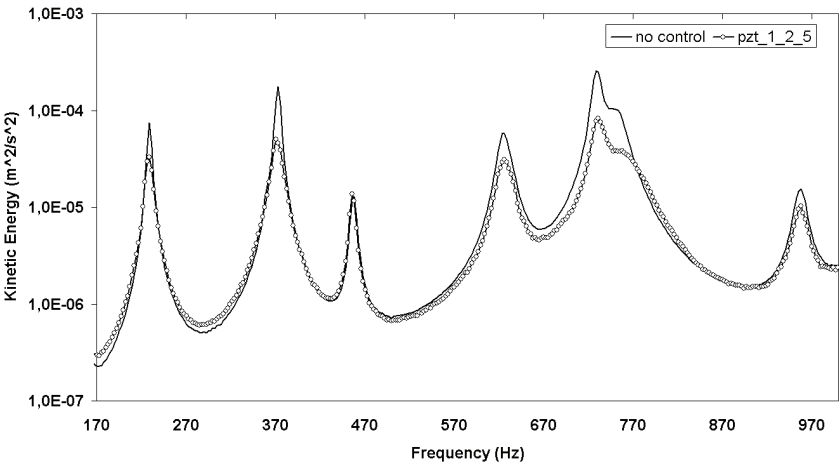


Figure 17 – Experimental results (active systems 1, 2, 5); controlled vs uncontrolled FRF.

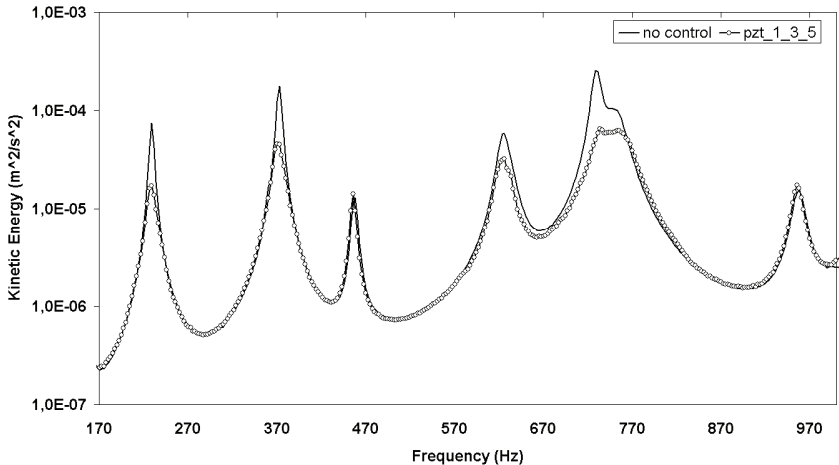


Figure 18 – Experimental results (active systems 1, 3, 5); controlled vs uncontrolled FRF.

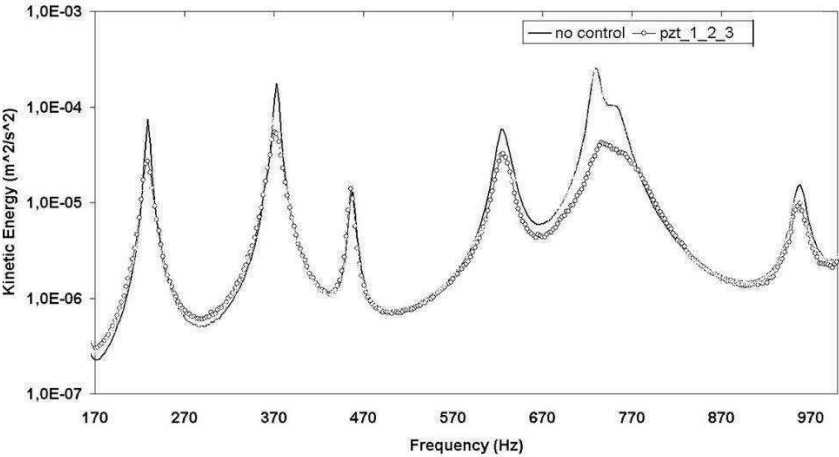


Figure 19 – Experimental results (active systems 1, 2, 3); controlled vs uncontrolled FRF.

## 7. Conclusions and future work

A semi-active Switching Shunt Control (SSC) system was tested to verify its experimental performance on a two-dimensional structure, over a broadband frequency range. The selected test specimen was a 220 x 280 mm, 7 mm thick, 10-ply fibreglass laminate plate. The SSC system was made of several actuator/sensor piezoelectric ceramic pairs linked to a 4-channel control circuit and working as independent SISO devices. Active elements were embedded into the structure, at different locations, to produce effects over a large number of modes. The placement resulted from an optimisation study performed to maximise their action over a frequency bandwidth of interest.

The equivalent induced damping was estimated, for seven out of the eight bending modes present in the investigated interval. Amplitude reductions up to 16 dB were attained. Experimental results were found to be in good accordance with the numerical predictions. The numerical model was derived and implemented in a Matlab environment, taking advantage of structural matrices, computed by a standard commercial FE code (MSC / Nastran). This choice allows the application of the method to more complex structural systems applications.

Coupling matrices, expressing the action of the actuators to the structure and the information taken by the sensors from the structure were built according to the classical strain actuation theory and piezoelectric equations, respectively. A modal reduction strategy was adopted to simplify the input and to reduce the computational costs. Modal reduction did not result in perfect diagonal matrices. Electrical degrees of freedom, one for each control device pair, represented the electrical charge.

The tests were carried out using different groups of 3 PZTs acting together over the structure. Generally, remarkable attenuations were experienced overall throughout the frequency range of interest. Concerning the switch control signal processing unit, a significant improvement is expected by adopting a noise filtering and a voltage threshold fail-safe control device in order to detect the unwanted peak detection and of course to avoid a voltage peaks that would damage the circuitry.

The results obtained here, while excellent, could be further improved if a 6-channel control system were implemented. Architectures using a single active device, switching itself between actuator and sensor behaviour, should be investigated, to migrate towards simplest hardware architectures, by paying a limited penalty in terms of algorithm complexity. Also, out-of-resonance frequencies should be addressed in further steps, in order to further extend the capabilities of the implemented system. Random excitation should also be investigated, to evaluate the capability of the system to handle non-sinusoidal strain response. Finally, the potential of the system in producing noise reduction in acoustic cavities shall be investigated.

## References

- [1] Clark, W. State switched piezoelectric systems for vibration control. *Structure, Structural Dynamics and Materials AIAA Journal* **1533** (1999), 2623-2629.
- [2] Clark, W. Vibration Control with State-Switched Piezoelectric Materials. *Journal of Intelligent Material Systems and Structures* **11** (2000), 263-273.
- [3] Richard, C., Guyomar, D., Audigier, D., and Bassaler, H. Enhanced semi-passive damping using continuous switching and Isolation, *SPIE* (2000), vol. 3989, pp.288-299.
- [4] Richard, C., Guyomar, D., Audigier, D., and Ching, G. Semi-passive damping using continuous switching of a piezoelectric device. In *Society of Photo-Optical Instrumentation Engineering (SPIE) Conference Series* (1999), vol. 3672, pp.104-111.
- [5] Lefeuvre, E., Badel, A., Petit, L., Richard, C., and Guyomar, D. Semi-passive Piezoelectric Structural Damping by Synchronized Switching on Voltage Source. *Journal of Intelligent Material Systems and Structures* **17** (2006), 653-660.
- [6] Lallart, M., Badel, A., Guyomar, D., and Lebrun, L. Non-linear semi-passive damping using constant or adaptive voltage source: a stability analysis. In *ICAST 2005 – Sixteenth International Conference on Adaptive Structures and Technologies* (2005), pp.158-165.
- [7] Corr, L., Clark, W. Energy Dissipation of Piezoelectric Semi-Active Vibration Control. *Journal of Intelligent Material Systems and Structures* **12** (2001), 729-736.
- [8] Corr, L., Clark, W. Comparison of low-frequency piezoelectric switching shunt technique for structural damping. *Smart materials and Structures* **11** (2002), 370-376.

- [9] Corr, L.R. *Investigation of real-time switching of piezoceramic shunts for structural vibration control*. PhD thesis, School of Engineering, University of Pittsburg, 2001.
- [10] Corr, L., Clark, W. A novel semi-active multimodal vibration control law for a piezoceramic actuator. *Journal of Vibration and Acoustics* **125** (2003), 214-222.
- [11] Lefeuvre E., Badel A., Richard C., Petit L., Guyomar D., *A comparison between several vibration-powered generators for standalone systems*, Sensors & Actuators A Physical, 2006, vol. 126, no2, pp. 405-416.
- [12] Petit, L., Lefeuvre, E., Richard, C., and Guyomar, D., A broadband semi passive piezoelectric technique for structural damping. In *Proc. of SPIE* (2004), vol. 5386, pp. 414-425.
- [13] Guyomar, D., and Badel, A. Nonlinear semi-passive multimodal vibration damping: an efficient probabilistic approach. *Journal of Sound and Vibration* **294** (2006), 249-268.
- [14] Ciminello M., Ameduri S., Concilio A., "FE Modelling of an Innovative Vibration Control Shunt Technique", The Smart Structures Laboratory – The Italian Aerospace Research Center, CIRA. *Journal of Intelligent Material Systems and Structures* JIMSS Vol.19, N°8, August 2008 pp.875-887.
- [15] Ciminello M., Calabrò A., Ameduri S., Concilio A., "Synchronized Switched Shunt Control Technique Applied on a Cantilevered Beam: Experimental Investigations", *Journal of Intelligent Material Systems and Structures* JIMSS Vol.19, N°9, September 2008 pp.1089-1100.
- [16] Crawley, E.F. and J. de Luis, "Use of piezoelectric actuators as elements of intelligent structures", *AIAA Journal*, 25(10), pp. 1373-1385, 1987.
- [17] Crawley, E. F. and Anderson, E. H. (1990). Detailed Models of Piezoceramic Actuation of Beams. *J.of Intell. Mater. Syst. and Struct.* 1, January, 4-25.
- [18] Dimitriadis E K, Fuller C R and Rogers C A.: "Piezoelectric actuators for distributed vibration excitation of thin plates." *ASME J. Vib. Acoust.* **113** 100–7, 1991.
- [19] Concilio A., "Teoria ed applicazioni dei materiali e delle strutture intelligenti" (Lectures on Smart Materials & Structures, in Italian), <http://www.dpa.unina.it/corsi/>.
- [20] M. Imregun, D.J. Ewins, Complex modes—origin and limits, in: Proceedings of the 13th International Modal Analysis Conference (IMAC), Nashville, TN, 1995, pp. 496–506.
- [21] Adhikari S., Damping modelling using generalized proportional damping . *Journal of Sound and Vibration* **293** (2006) 156–170.
- [22] Anonymous, National Semiconductor Corporation, LM324 Low Power Quad Operational Amplifiers, August 2000.
- [23] Anonymous, National Semiconductor Application Note 162, LM2907 Tachometer/Speed Switch Building Block Applications, June 1976.
- [24] Anonymous, Analog Device, LC2MOS 5W Ron SPST Switches, ADG452, 2004. Datasheets downloading from ChipDocs.
- [25] Anonymous, P-876 DuraAct™ Piezoelectric Patch Transducers. Datasheet from www.pi.ws



## REVIEW

**Author(s):** Salvatore Ameduri, M. Ciminello

**Title:** *Fourier expansion solution for a switched shunt control applied to a duct*

	Yes	No
1. Is the subject matter of the paper consistent with areas covered by JTAM?	<input checked="" type="checkbox"/>	<input type="checkbox"/>
2. Do the authors clearly present their results? Do they specify the relation between their results and the established knowledge?	<input checked="" type="checkbox"/>	<input type="checkbox"/>
3. Does the paper contain new results?	<input checked="" type="checkbox"/>	<input type="checkbox"/>
4. Does the paper describe new methods?	<input checked="" type="checkbox"/>	<input type="checkbox"/>
5. Are the terminology and the nomenclature correct?	<input checked="" type="checkbox"/>	<input type="checkbox"/>
6. Is the choice of references appropriate and exhaustive?	<input checked="" type="checkbox"/>	<input type="checkbox"/>
7. Is the paper written in style conforming to the accepted standards of academic writing?	<input checked="" type="checkbox"/>	<input type="checkbox"/>
<hr/>		
1. <b>The paper is appropriate for publication:</b>		
- in the presented form	<input checked="" type="checkbox"/> *	
- in the revised form	<input type="checkbox"/>	
- with essential improvements and after another reviewing	<input type="checkbox"/>	
2. <b>Evaluation of the work:</b> very good <input checked="" type="checkbox"/> good <input type="checkbox"/> poor <input type="checkbox"/>		
3. <b>The paper is not acceptable for publication</b>	<input type="checkbox"/>	

**Detailed remarks:**

\*with small corrections

Page 4 – suggestion – replace “The equipe” by “The team” or “The group”

Page 9 - Eq (5) instead eq (5), “where” instead “Being” (similary on the next pages)

Page 10 – “BCs. read”, “ICs. read”

Page 13 – “table” instead “tab.”

Page 14 – “in Figure 14”

Page 21 – “A min” - “A minimum”

Page 22 – “to maximum” instead “max”

Page 23 – “possible” instead “eventual”, “etc” instead “...”

.....  
(referee)



# Fourier Expansion Solution for a Switched Shunt Control Applied to a Duct

S. Ameduri<sup>a</sup>, M. Ciminello<sup>b</sup>

<sup>a</sup>The Italian Aerospace Research Centre – Capua - Italy

<sup>b</sup>Aerospace Engineering Dept. – “Federico II” University of Naples - Italy

## Abstract

Among the different strategies oriented to the noise and vibration control, due to their promising properties in terms of limited required power supply, broad band and no tuneable nature, semi-active switched shunt architectures have well done for themselves. The idea of using piezo transducers to convert mechanical into electrical energy and elaborating related signal within an external time variant electrical circuit, represents the inspiring principle of this type of control.

A wide amount of efforts has been spent on the semi-active switched shunt control with specific interest in the “synchronised” one; theoretical, numerical, experimental investigations, proved in different ways pros and cons of applications generally confined to the vibration field, in the low frequency band. Also the idea of extending this control to acoustics has been taken into account: problems like the structure-borne sound have been dealt with, implementing switch logic onto piezo networks mounted on structural components. An interesting industrial application in the field of aeronautics and automotive in general, is the interior sound level reduction: in this case a distribution of piezoelectric transducers suitably collocated may lead to remarkable effects, without excessive power consumption.

In the present work, a semi analytic approach aimed at estimating the effects on the reduction of pressure sound level by synchronised switched shunt logic, is described. The displacement field within a 1D longitudinal air column through a Fourier series expansion has been formalised by assigning a sinusoidal perturbation and fluid–structure interface condition on the left and right boundaries, respectively. At first, a validation procedure has been implemented: both the convergence of the series coefficients and the satisfaction of boundary and initial conditions have been verified. To simulate the no control operative condition, the solution has been computed for the entire time domain, keeping invariant all circuitry properties; then for the switch working modality, solution has been computed by splitting the entire time domain into partitions, each one delimited by the instants at which the circuit is switched on (i.e., by maxima and minima of the displacement on the right boundary domain); for any partition, specific circuitry properties (e.g. piezo voltage, electrical field...) have been selected. Based on displacement information, related sound pressure level has been compared for no controlled and controlled operative conditions, with and without signal amplification.

## Keywords:

Synchronised Switched Shunt Control, Piezoelectric, Pressure Sound Level

## Nomenclature

$BC$	boundary condition
$IC$	initial condition

$T_{el}$	electrical circuit period
$T_{mech}$	mechanical period
$T_{tot}$	total simulation time
$t_0$	initial instant
$x$	axis, fluid column length
$y$	axis, fluid column depth
$z$	axis, fluid column height
$U_0$	excitation amplitude
$u_0(t)$	displacement at $x=0$
$p(x,t)$	pressure
$\omega$	excitation angular frequency
$c$	sound speed
$\xi$	fluid decay rate
$L$	fluid column length
$M_p$	piezo transmitted moment
$d$	half beam span
$b$	depth of the column and of the beam
$\zeta$	piezo extension along the beam span, $\in [0,1]$
$D$	bending stiffness
$\rho$	fluid density
$E_0$	B.C. constant term
$\beta_1$	B.C. coefficient, proportional to the first derivative of the displacement
$\beta_2$	B.C. coefficient, proportional to the displacement
$f(x)$	initial displacement law
$g(x)$	initial velocity law
$v(x,t)$	function used for B.Cs homogenisation
$u(x,t)$	semi-analytic solution, displacement distribution
$P(x,t)$	differential equation right hand term of the B.Cs homogeneous problem
$Q(x,t)$	displacement I.C. right hand term of the B.Cs homogeneous problem
$R(x,t)$	velocity I.C. right hand term of the B.Cs homogeneous problem
$X(x)$	space depending factor of the solution
$T(t)$	time depending factor of the solution
$\lambda_n$	$n^{\text{th}}$ problem eigen value
$\varphi_n(x)$	$n^{\text{th}}$ orthogonal space dependent function used for Fourier series expansion
$b_n(t)$	$n^{\text{th}}$ time dependent function used for Fourier series expansion
$p_n(t)$	$n^{\text{th}}$ coefficient of Fourier series expansion of $P(x,t)$
$q_n(t)$	$n^{\text{th}}$ coefficient of Fourier series expansion of $Q(x,t)$
$D_{1n}, D_{2n}$	$n^{\text{th}}$ general integral constants
$A_n, B_n$	$n^{\text{th}}$ particular integral constants
$\mu_n$	$n^{\text{th}}$ coefficient of Fourier series expansion of $f(x)$
$\nu_n$	$n^{\text{th}}$ coefficient of Fourier series expansion of $g(x)$
$r_n(t)$	$n^{\text{th}}$ coefficient of Fourier series expansion of $R(x,t)$
$\hat{p}$	pressure squared value, averaged with respect time and space
$d_{31}$	piezoelectric charge constant
$g_{31}$	piezoelectric voltage constant
$Y_p$	piezoelectric Young modulus
$Y_s$	structure Young modulus
$\nu_p$	piezoelectric Poisson modulus
$\nu_s$	structure Poisson modulus

## Introduction

Sound and vibration control can be considered a real technological challenge because of the large amount of related problems and peculiar complexity. As a consequence, many efforts have been spent on defining, realising and characterising different typologies of control techniques, tailored on the specific problem.

Among the different strategies, due to their promising properties in terms of lightness, simple design and low cost, a wide amount of interest has been focused on the shunt circuits. Through the shunt control architectures, structural vibrations are reduced by using time variant electric circuits integrated with electromechanical PZT suitably positioned on structural elements.

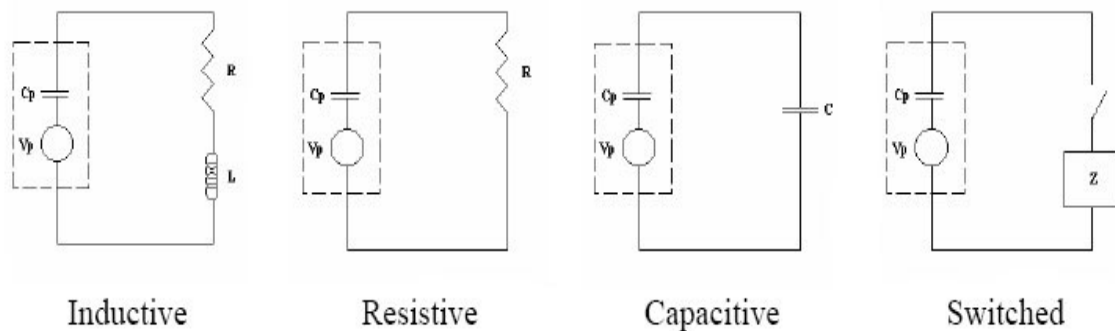


**Figure 1: Configuration of the four different shunted circuits.**

The first three schemes illustrated on the left in Fig.1 represent the most common passive shunt circuits. A lot of works in literature [1-4] have shown how the resistive shunt dissipates energy through Joule effect, the capacitive shunt changes the local stiffness of the structure, while shunting with inductive introduces an electrical resonance, which can be optimally tuned to the one of the system, analogously with a mechanical vibration absorber.

It is well known that passive techniques are among the most commonly adopted because they never provide the structure with artificial energy and their functionality is essentially based on time invariant (fixed) modifications of the structural mass, damping and stiffness matrices. However despite of their easy implementation and low cost, their performance is generally inadequate to face all the necessities, particularly concerning with optimal strategies of smart structures solutions. In this case in fact, the control system characteristics have to satisfy some important requirements, among all, its parameters adaptability.

This is the reason why in recent years, there has been a growing interest in the semi-active control. A semi-active device can be broadly defined as a passive device in which the properties (stiffness, damping, etc.) can be varied in real time with a low power input. Although they behave in a strongly nonlinear way, semi-active devices are inherently passive and cannot destabilize the system. They are also less vulnerable to power failure and have good thermal stability, particularly useful in aerospace applications [5,6]. These reasons, jointly with the good performance exhibited within the low frequency range, justified the large amount of theoretical, numerical and experimental investigations. Among the shunt schemes sketched in Fig.1, the last on the right represents a switch architecture. The principle of the shunt using a switching is to store an electric charge and use its effect in opposition to the structural movement within a very short time constant.

One of the first concept of commutation shunted circuit was proposed in [7, 8], where the author studied a case of a resistive shunt with comparable open and closed circuit periods (this is the reason why it is referred as “state switching”). This kind of system can be assimilated to a variable stiffness mechanical system.

In [9, 10] the authors proposed to close the circuit for a very short period and to add an inductor to augment the charge on the PZT device. This technique is called “Synchronized Switch Damping”, that can be specialised according to the following shunt architecture:

- Synchronized Switch Damping on Short, where the shunt is purely resistive;
- Synchronized Switch Damping on Inductance, with an inductive component;
- Synchronized Switch Damping on Voltage source, where the shunt includes a voltage source [11] (which place the system in the class of the active control, needing an external power supply) and involves a risk of instability. This problem can be mitigated with a slow variation of the voltage following the average amplitude of the vibrations, as proposed in [12].

In the cited works dealing with this technique, the damping was estimated with a simple 1D model. The development and implementation of mdof models have also been faced. The team of W. Clark [13, 14, 15] compared the state switching and the synchronized switching showing that the last one is more effective. Further improvements were presented in [16] where the authors developed a switching synchronization technique based on different modal filters. The technique required complex filters and power supply, but the performance were good. This kind of work is at the moment object of another American staff [17].

The team of Daniel Guyomar, refined the inductive switched shunt and proposed an autonomous circuit [18, 19]. They showed that the detection of a local maximum is not optimal for the case of multimodal control. The authors proposed a probabilistic criteria (detection of the maxima significantly exceeding the average level) giving a good result [20].

The necessity of extending benefits due to this technique to more realistic applications has led to numeric solving schemes, prevalently based on a FE approach. Some test cases have been carried out, including this time some example also on elasto-acoustic systems.

In their works Ameduri, Ciminello et al. [21-23] studied the finite element formulation of a synchronized switched shunt applied on both isotropic and anisotropic structure with collocated PZT patches. The multimodal control was optimized by a genetic algorithm. Finally an original circuit based on a tachometer component was presented.

However, due to the complexity of real applications, despite the efficient reduction techniques employed, numerical computations result heavy and, consequently, time consuming. On the contrary, a semi-analytical solution would allow eliminating the time consuming due to the integration.

In his work Ameduri et al. [24] faced with the implementation of a semi-analytic solution of a however complex structural system suitably reduced. Then, the analytic solution of related differential equations system, for a sinusoidal and constant excitation, is found out; finally, theoretic solution is fitted to the specific problem, i.e. the switch shunt control implementation.

In [25] a multi degree-of-freedom (dof) electromechanical model of a structure with piezoelectric elements coupled to state switching and synchronous switching electric circuits have been derived. By restricting the analysis to one mechanical dof only, the system free response has been analytically obtained. A similar analysis has been conducted to obtain the forced response of the structure subjected to a harmonic forcing of any frequency, except that no analytical expressions are available. As a general

conclusion, it has been proved that the only parameter that influences the performances of the synchronous switching devices is the coupling coefficient, that has to be maximized in order to enhance the vibration attenuation.

The interest in extending switched shunt control benefits also to acoustic applications is confirmed by the amount of numerical and experimental investigations carried out as regards [18, 20, 25]. These works deal with the problem of controlling the sound transmission properties of structural elements, used to insulate an internal noise source from the external environment. Another problem is the sound pressure level attenuation within enclosures. The fundamental idea is to implement a control acting on a PZT network, suitably distributed on the boundary of an enclosure [23]. The effects originated by this solution can be appreciated by predicting and / or measuring the sound pressure level at different points of the air volume taken into consideration.

In the work at hand attention is paid to this last problem: pressure sound level attenuation through a switched shunt architecture implemented on a metallic plate, acting on a finite length air column. A semi-analytic approach, consisting in solving the telegraph equation through a Fourier expansion series strategy, has been adopted to find out the time dependent displacement field along a 1D horizontal air column. Related boundary conditions have been assigned by imposing a sinusoidal perturbation on the left frontier and by formalising the fluid–structure interaction on the right side; here, a couple of PZT patches bonded on the two faces of a aluminium plate and connected to an external switched shunt circuit, provides the control action on the air column.

Before computing the solution, a preliminary validation process has been carried out, by verifying the satisfaction of the assigned conditions and proving its convergence by estimating the series coefficients.

Then the simulation of the displacement field within the fluid domain, in presence and absence of control, at different amplification levels, has been performed. For no control condition, the solution has been computed within the considered time interval; on the other hand, due to the non linearity of the switch architecture, the controlled solution has been estimated at different time interval: any partition is limited by the instants in which the circuit is switched on and electrical properties (i.e. voltage, electrical field, charge on the leads) undergo to a variation.

Results have been expressed in terms of displacement and sound pressure level computed on different points of the spatial domain; finally, the global attenuation achieved has been evaluated by squared average values of the sound pressure level over spatial and time domains.

## The Switched Shunt Control System

The adopted electrical network is an RLC resonant circuit having the PZT as capacitor. In Fig. 2 the circuit is sketched.

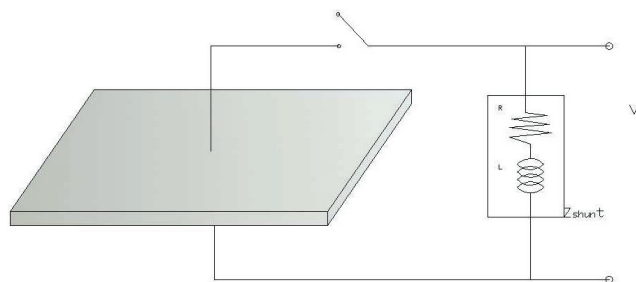


**Figure 2: Synchronised Switched Shunt Circuit**

A couple of collocated PZT patches are bonded on the structure. The idea is to generate a control force that opposes itself to the motion with the max amplitude and without tuning requirement. To this end, the “on” state (switch closed) is synchronized with the maxima signal detected by the sensors. This produces the max flowing charge into the inductor which sends it, reversed to the actuator. This means that the control force is in phase opposition respect to the local displacement of the structure.

Finally the switching time, i.e. the period the circuit is switched on, is generally assumed 10 to 50 times lower than the mechanical period to control. The inductive element of the circuit is thus chosen according to Eq.1, relating such element to the piezo capacitance and the electric angular frequency [1,2, 7-10, 13-16, 21,22].

$$L = \frac{1}{\omega^2 C} \quad (1)$$

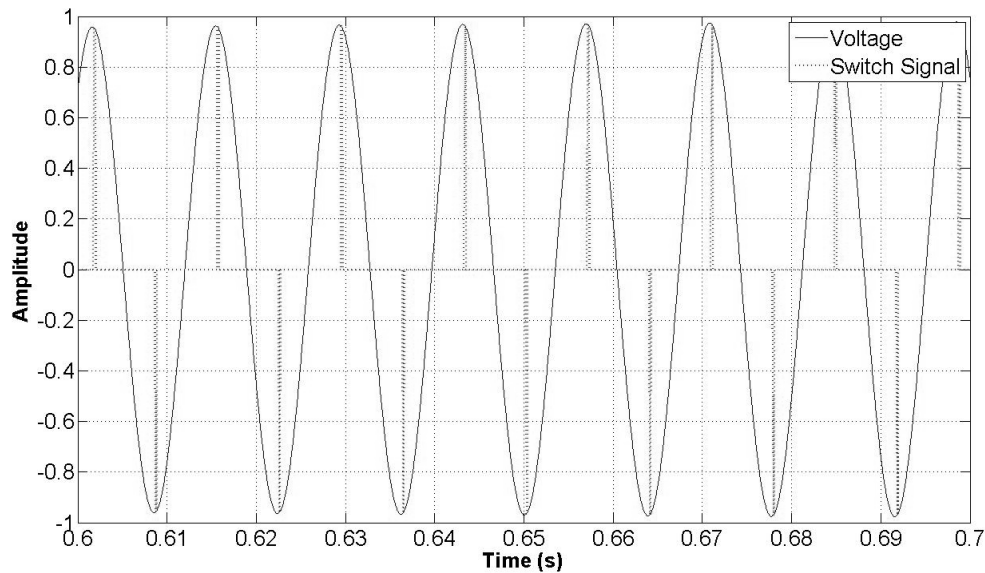


**Figure 3: Switch Signal Simulation**

Moreover if the switch mechanism is set according to the highest frequency of interest, the natural band range of the control system is naturally defined. To summarise circuit working modalities:

**Open Circuit State:** in absence of any shunted configuration, that is to say, no connection to a passive electrical network, no current flows and the voltage is a function of the displacement.

**Shunted Circuit State:** Every time the piezo voltage reaches a maximum, the switch is closed. The connection of the PZT electrodes to the external circuit is realised. The voltage is given by two contributions: the open circuit signal (proportional to the deformations) added to an offset signal (proportional to the electrical charge).

The switching mechanism produce a naturally amplified voltage (Fig. 4) and the charge behaviour of Figure 5.

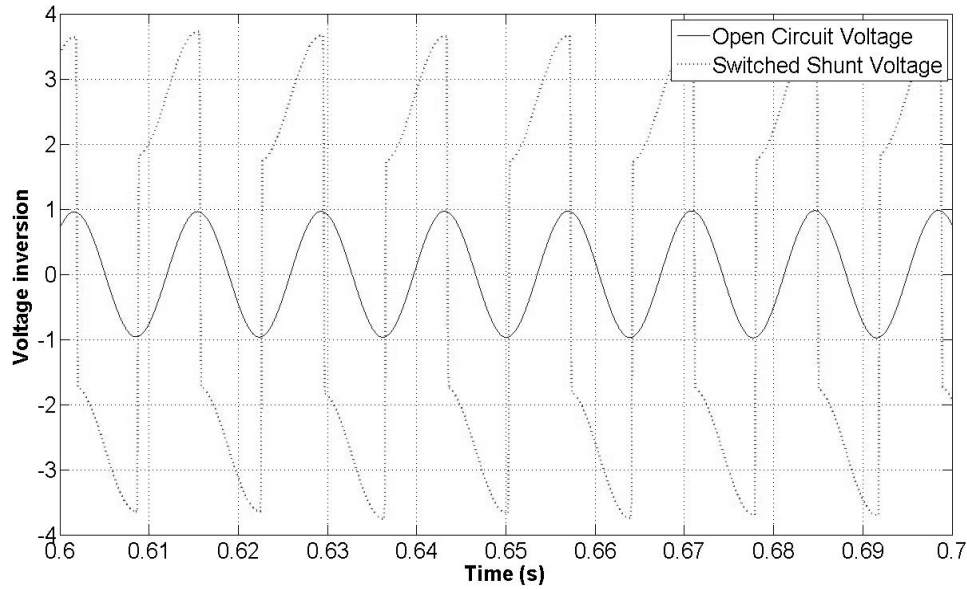


**Figure 4: Voltage Signal Simulation**

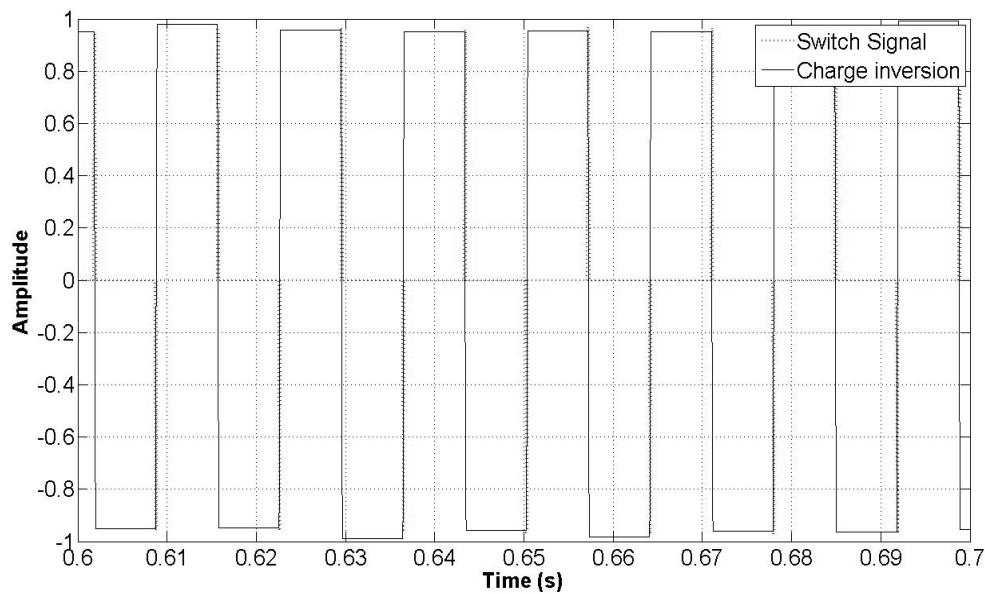


**Figure 5: Charge Signal Simulation**

The collocated configuration of the sensor-actuator and the absence of an external power supply, that means no energy injected into the system, guarantee an unconditional stability of the control.

Some drawbacks can be found in the inner behaviour of the control. The effect of this kind of control is in fact to reduce amplitude of the vibration not by damping but subtracting a fraction of the mechanical energy of the system at resonance and giving it back, transferring energy to the high frequencies.

### Problem formulation and solving strategy

The considered physical problem, is sketched in Fig. 6: a 1D air column excited on the left boundary ( $x=0$ ) by a signal  $u_0(t)$

$$u_0(t) = U_0 \sin(\omega t), \forall t \quad (2)$$

and controlled on the right by two PZT patches bonded on a aluminium alloy plate (see detail on the bottom of Fig.6).

The displacement field  $u(x,t)$  within the air column is described by the telegraph equation:

$$\frac{\partial^2 u}{\partial t^2} - c^2 \frac{\partial^2 u}{\partial x^2} + \xi \frac{\partial u}{\partial t} = 0 \quad (3)$$

resulting from the application of the mass equation and the balance of inertial (time 2<sup>nd</sup> derivative), elastic (spatial 2<sup>nd</sup> derivative) and dissipative (time 1<sup>st</sup> derivative) forces, acting on a fluid element.

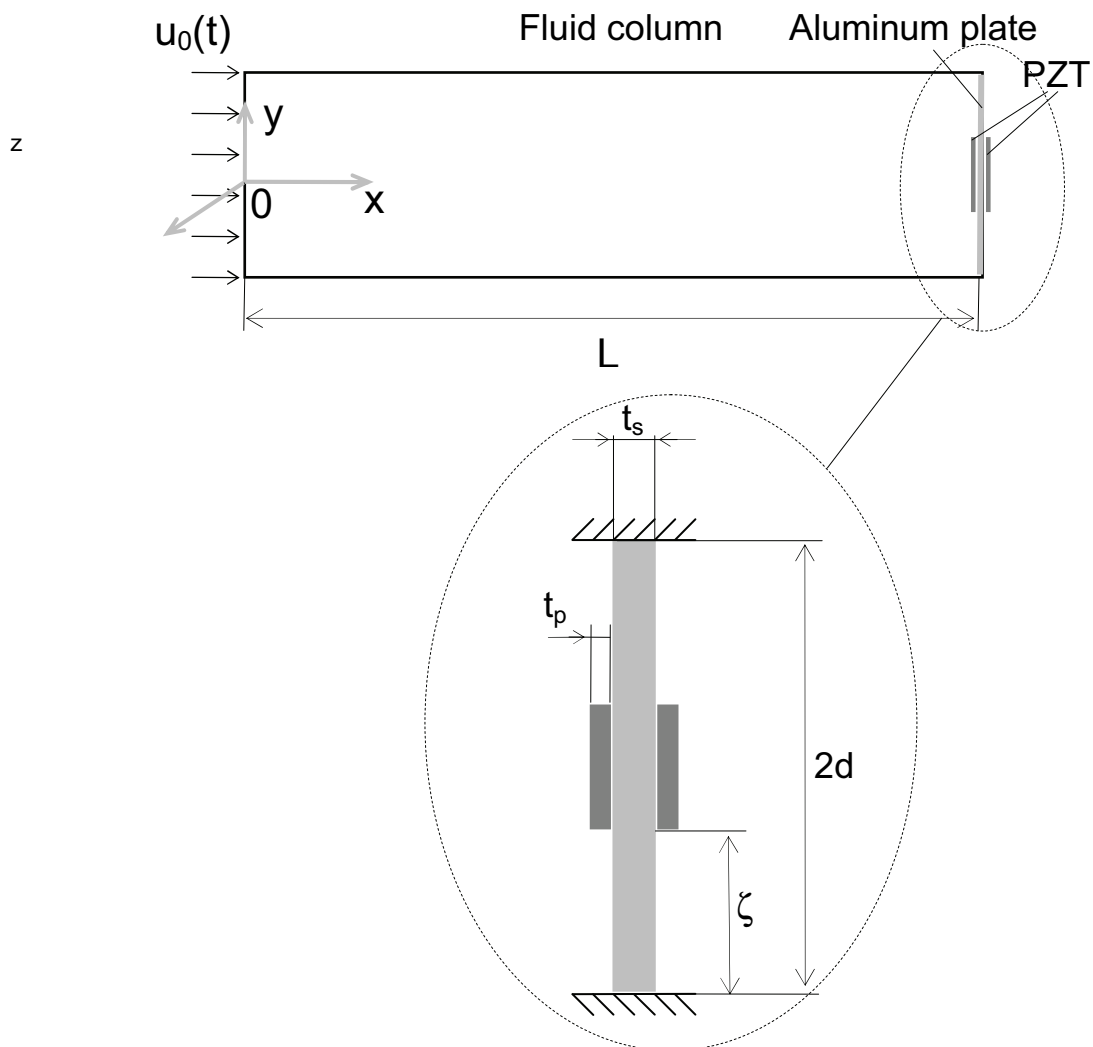


**Figure 6: Scheme of the problem**

The boundary condition on the left side of the domain, coherently with (2), is given

$$u(0,t) = u_0(t) = U_0 \sin(\omega t), \forall t \quad (4)$$

The other boundary condition on the right side of the domain ( $x=L$ ) results from the formalisation of the fluid/structure interaction at the interface and from the semi-active nature of the switched shunt control. The structure, a plate very long onto  $z$  direction, behaves according to Timoshenko “long rectangular plate” theory [26].

The acoustic pressure at the interface,  $p(L, t)$ , jointly with the piezo action (a moment,  $M_p(t)$ ), produces the displacement of the middle of the plate,  $u_p(y=0)$ , described by the classical elastic beam theory

$$u_p(t) = \frac{3}{8} \frac{p(L, t)b}{D} d^4 - \frac{M_p(t)}{D} \zeta \left( \zeta - \frac{3}{2} \right) d^2 \quad (5)$$

The same theory provides also the deformation within the piezo,  $\varepsilon_p$ . Then, by considering piezoelectric constitutive law [5], open circuit voltage,  $V$ , can be computed:

$$V = g_{31} \frac{E_p t_p}{1 - \nu_p} \varepsilon_p \quad (6)$$

being  $b$  and  $D$  the plate depth and bending stiffness.

This voltage, used by the logic to detect the instant in which the circuit must be switched on, is modified according to what explained in the previous paragraph (ref. to Figure 4, comparing open state and circuit generated voltages).

By exploiting Crawley and De Luis transmission model [30], that proposes a linear relation between transmitted actions and applied voltage, the moment  $M_p(t)$  can be computed.

Since fluid and plate displacements are the same at the interface,

$$u(L, t) = u_p(t) \quad \forall t \quad (7)$$

and recalling that

$$p(x, t) = -\rho c^2 \frac{\partial u}{\partial x} \quad (8)$$

Eq (5) can be finally rewritten to formalise required boundary condition:

$$\beta_1 \frac{\partial u}{\partial x} \Big|_L + \beta_2 u(L, t) = E_0, \quad \forall t \quad (9)$$

where

$$\begin{aligned} \beta_1 &= 1, \quad \beta_2 = \frac{8}{3} \frac{D}{\rho c^2 b d^4}, \\ E_0 &= -\frac{8}{3} \frac{M_p(t)}{\rho c^2 b d^2} \zeta \left( \zeta - \frac{3}{2} \right) \end{aligned} \quad (10)$$

For sake of simplicity, no inertial and damping terms have been taken into account in condition (9); this, as already mentioned, restricts the validity of the model to

frequencies far from the structural resonance. Such an assumption is however coherent with the low band range of interest for the switched shunt control.

The initial conditions are represented by the displacement and the velocity at time  $t_0$ , described by assigned functions  $f(x)$  and  $g(x)$ :

$$u(x, t) = f(x), \quad \forall x \quad (11)$$

$$\left. \frac{\partial u}{\partial t} \right|_{t_0} = g(x), \quad \forall x \quad (12)$$

To compute a semi-analytic solution, through a Fourier series expansion, boundary conditions (4) and (9) have to become homogeneous [27]; it is possible to demonstrate that this can be achieved by assuming the function

$$v(x, t) = u(x, t) + \left[ \frac{\beta_2 x}{\beta_1 + \beta_2 L} - 1 \right] U_0 \sin(\omega t) - \frac{E_0 x}{\beta_1 + \beta_2 L} \quad (13)$$

After introducing relation (13) into eq. (3) and related BCs, (4) and (8), and ICs, (11) and (12), a new problem is found:

$$\frac{\partial^2 v}{\partial t^2} - c^2 \frac{\partial^2 v}{\partial x^2} + \xi \frac{\partial v}{\partial t} = P(x, t) \quad (14)$$

BCs. read

$$v(0, t) = 0, \quad \forall t \quad (15)$$

$$\beta_1 \left. \frac{\partial v}{\partial x} \right|_L + \beta_2 v(L, t) = 0, \quad \forall t \quad (16)$$

ICs. read

$$v(x, t_0) = f(x) + Q(x, t_0), \quad \forall x \quad (17)$$

$$\left. \frac{\partial v}{\partial t} \right|_{t_0} = g(x) + R(x, t_0), \quad \forall x \quad (18)$$

where

$$P(x, t) = U_0 \omega \left[ \frac{\beta_2 x}{\beta_1 + \beta_2 L} - 1 \right] \cdot [\xi \cos(\omega t) - \omega \sin(\omega t)] \quad (19)$$

$$Q(x, t) = \left[ \frac{\beta_2 x}{\beta_1 + \beta_2 L} - 1 \right] U_0 \sin(\omega t) - \frac{E_0 x}{\beta_1 + \beta_2 L} \quad (20)$$

$$R(x, t) = U_0 \omega \left[ \frac{\beta_2 x}{\beta_1 + \beta_2 L} - 1 \right] \cos(\omega t) \quad (21)$$

Eq. (14) may be solved by separating space and time variables, i.e. assuming the solution  $v(x, t)$  as product of two unknown functions,  $X$  and  $T$ , the former depending on  $x$ , the latter on  $t$ :

$$v(x, t) = X(x) \cdot T(t) \quad (22)$$

As a result, eq (14) is split into two separated problems:

$$\frac{d^2 X}{dx^2} + \lambda^2 X(x) = 0 \quad (23)$$

and

$$\frac{d^2 T}{dt^2} + \xi \frac{dT}{dt} + c^2 \lambda^2 T(t) = 0 \quad (24)$$

The solution of (23) can be expressed as sum of infinite orthogonal functions,  $\varphi_n(x)$ , satisfying conditions (15) and (16):

$$\varphi_n(x) = \sin(\lambda_n x) \quad (25)$$

being  $\lambda_n$  the  $n^{\text{th}}$  root of the transcendent eq. [29]

$$\beta_1 \lambda_n + \beta_2 \tan(\lambda_n L) = 0 \quad (26)$$

By expressing the solution  $v(x, t)$  as a sum of the products of these functions with the corresponding time dependent ones,  $b_n(t)$

$$v(x, t) = \sum_{n=1}^{\infty} \varphi_n(x) \cdot b_n(t), \quad (27)$$

eq (12) can be written into a new formalism:

$$\sum_{n=1}^{\infty} \varphi_n(x) \cdot \left[ \frac{d^2 b_n}{dt^2} + \xi \frac{db_n}{dt} + c^2 \lambda_n^2 b_n(t) \right] = P(x, t) \quad (28)$$

This relation, by introducing the Fourier expansion of  $P(x, t)$

$$P(x, t) = \sum_{n=1}^{\infty} \varphi_n(x) \cdot p_n(t) \quad (29)$$

with

$$p_n(t) = \frac{\int_0^L P(x, t) \varphi_n(x) dx}{\int_0^L \varphi_n^2(x) dx} = \frac{2U_0 \omega [\xi \cos(\omega t) - \omega \sin(\omega t)]}{[\cos(\lambda_n L) \sin(\lambda_n L) - \lambda_n L]} \quad (30)$$

reduces itself to a time dependent equation:

$$\frac{d^2 b_n}{dt^2} + \xi \frac{db_n}{dt} + c^2 \lambda_n^2 b_n(t) = p_n(t) \quad (31)$$

Equation (31) admits a solution in the form

$$b_n(t) = \underbrace{[D_{1n} \sin(\omega_n t) + D_{2n} \cos(\omega_n t)] e^{-\frac{1}{2} \xi t}}_{\text{general integral}} + \underbrace{A_n \sin(\omega t) + B_n \cos(\omega t)}_{\text{particular integral}} \quad (32)$$

with

$$\omega_n = \sqrt{c^2 \lambda_n^2 - \frac{\xi^2}{4}} \quad (33)$$

Constants  $A_n$  and  $B_n$ , can be determined substituting the particular integral within eq. (31):

$$A_n = 2U_0 \omega^2 \frac{[\xi^2 - (c^2 \lambda_n^2 - \omega^2)]}{[\xi^2 \omega^2 + (c^2 \lambda_n^2 - \omega^2)^2] [\cos(\lambda_n L) \sin(\lambda_n L) - \lambda_n L]} \quad (34)$$

$$B_n = 2U_0 \omega \xi \frac{c^2 \lambda_n^2}{[\xi^2 \omega^2 + (c^2 \lambda_n^2 - \omega^2)^2] [\cos(\lambda_n L) \sin(\lambda_n L) - \lambda_n L]} \quad (35)$$

Remaining constants,  $D_{1n}$  and  $D_{2n}$ , can be computed by imposing that  $v(x, t)$ , formalised as in (27) and including (32), satisfies initial conditions (17) and (18)

$$D_{1n} \sin(\omega_n t_0) + D_{2n} \cos(\omega_n t_0) = [-A_n \sin(\omega t_0) - B_n \cos(\omega t_0) + \mu_n + q_n(t_0)] e^{\frac{\xi}{2} t_0} \quad (36)$$

*1<sup>st</sup> initial condition*

$$D_{1n} \left[ \omega_n \cos(\omega_n t_0) - \frac{\xi}{2} \sin(\omega_n t_0) \right] - D_{2n} \left[ \omega_n \sin(\omega_n t_0) + \frac{\xi}{2} \cos(\omega_n t_0) \right] = [-A_n \omega \cos(\omega t_0) + B_n \omega \sin(\omega t_0) + v_n + r_n(t_0)] e^{\frac{\xi}{2} t_0} \quad (37)$$

*2<sup>nd</sup> initial condition*

being  $\mu_n$ ,  $v_n$ ,  $q_n$ , and  $r_n$  the terms of the Fourier series expansion of  $f(x)$ ,  $g(x)$ ,  $Q(x, t)$  and  $R(x, t)$ :

$$\mu_n = \frac{\int_0^L f(x) \varphi_n(x) dx}{\int_0^L \varphi_n^2(x) dx} \quad (37)$$

$$v_n = \frac{\int_0^L g(x) \varphi_n(x) dx}{\int_0^L \varphi_n^2(x) dx} \quad (38)$$

$$q_n(t) = \frac{\int_0^L Q(x,t)\varphi_n(x)dx}{\int_0^L \varphi_n^2(x)dx} = \frac{2E_0}{\lambda_n(\beta_1 + \beta_2 L)} - \frac{2U_0 \sin(\omega t)}{[\lambda_n L - \sin(\lambda_n L) \cos(\lambda_n L)]} \quad (39)$$

$$r_n(t) = \frac{\int_0^L R(x,t)\varphi_n(x)dx}{\int_0^L \varphi_n^2(x)dx} = -\frac{2U_0 \cos(\omega t)}{[\lambda_n L - \sin(\lambda_n L) \cos(\lambda_n L)]} \quad (40)$$

Finally, by assembling (13), (25), (27) and (32), required solution for problem (3) can be written:

$$u(x,t) = \sum_{n=1}^{\infty} \sin(\lambda_n x) \left\{ [D_{1n} \sin(\omega_n t) + D_{2n} \cos(\omega_n t)] e^{-\frac{\xi}{2}t} + \right. \\ \left. + A_n \sin(\omega t) + B_n \cos(\omega t) \right\} - \left( \frac{\beta_2 x}{\beta_1 + \beta_2 L} - 1 \right) U_0 \sin(\omega t) + \frac{E_0 x}{\beta_1 + \beta_2 L} \quad (41)$$

The corresponding pressure field,  $p(x,t)$ , may be obtained by deriving with respect to  $x$  above solution and multiplying by  $-\rho c^2$ :

$$p(x,t) = -\frac{1}{\rho c^2} \sum_{n=1}^{\infty} \lambda_n \cos(\lambda_n x) \left\{ [D_{1n} \sin(\omega_n t) + D_{2n} \cos(\omega_n t)] e^{-\frac{\xi}{2}t} + \right. \\ \left. + A_n \sin(\omega t) + B_n \cos(\omega t) \right\} - \frac{\beta_2 U_0 \sin(\omega t) + E_0}{\beta_1 + \beta_2 L} \quad (42)$$

Corresponding pressure squared value averaged with respect space and time has been computed:

$$\hat{p} = \frac{1}{T_{tot}} \int_{t_0}^{t_0+T_{tot}} \frac{1}{L} \int_0^L p^2(x,t) dx \cdot dt \quad (43)$$

For the no control case simulation relations (41) and (42) can be exploited to compute displacement and pressure field within the entire considered time interval. On the other hand, for the switched control simulation, due to the discontinuity of circuitry parameters, like voltage, charge and hence  $E_0$ , the use of (41) and (42) is restricted to the time intervals in which circuit parameters keep constant, that is during the switch on and off stationary states. In practice, the solution at any time interval, is computed by assuming as initial conditions the configuration (in terms of displacement and velocity) computed at the last instant of the previous time interval.

## Numerical Results

The results herein presented have been obtained considering the parameters summarised in the following table:

Main simulation parameters	
Time interval	
1 <sup>st</sup> resonance frequency (hz)	170
2 <sup>nd</sup> resonance frequency (hz)	340
Frequency considered for out of resonance simulations (hz)	50
Fluid column properties	
Length (m), $L$	1
Depth (m), $b$	50e-2
Height (m), $2d$	6e-2
Density (kg/m <sup>3</sup> ), $\rho$	1.19
Sound speed (m/s), $c$	340
Decay rate (dB/s), $\xi$ [28]	200
Beam properties	
In-plane (y-z) dimensions (m)	6e-2 x 50e-2
Thickness (m), $t_s$	0.5e-3
Young modulus (GPa), $Y_s$	72
Poisson ratio, $\nu_s$	0.33
Density (kg/m <sup>3</sup> ), $\rho_s$	2700
1 <sup>st</sup> resonance frequency (hz), $f_s$	737
Piezo properties	
In-plane (y-z) dimensions (m)	3e-2 x 50e-2
Thickness (m), $t_p$	0.5e-3
Young modulus (GPa), $Y_p$	59
Poisson ratio, $\nu_p$	0.32
$d_{31}$ (m/V)	-350e-12
$g_{31}$ (V m/N)	8e-3

**Tab. 1. Simulation parameters**

Before computing displacement field (in Figure 14) and corresponding pressure distribution, a preliminary validation process has been carried out on solution (41).

At first, the validation of boundary conditions (4) and (8) has been proved, just expressing relation (36) at  $x=0$  and  $x=L$ . Then, the convergence of coefficients  $A_n$ ,  $B_n$ ,  $D_{1n}$ ,  $D_{2n}$  has been verified by exciting the system far and at the fluid resonance. In Fig. 7 - 9, mentioned coefficients vs. harmonic order,  $n$ , have been plotted at 50 hz and for the first two normal modes.

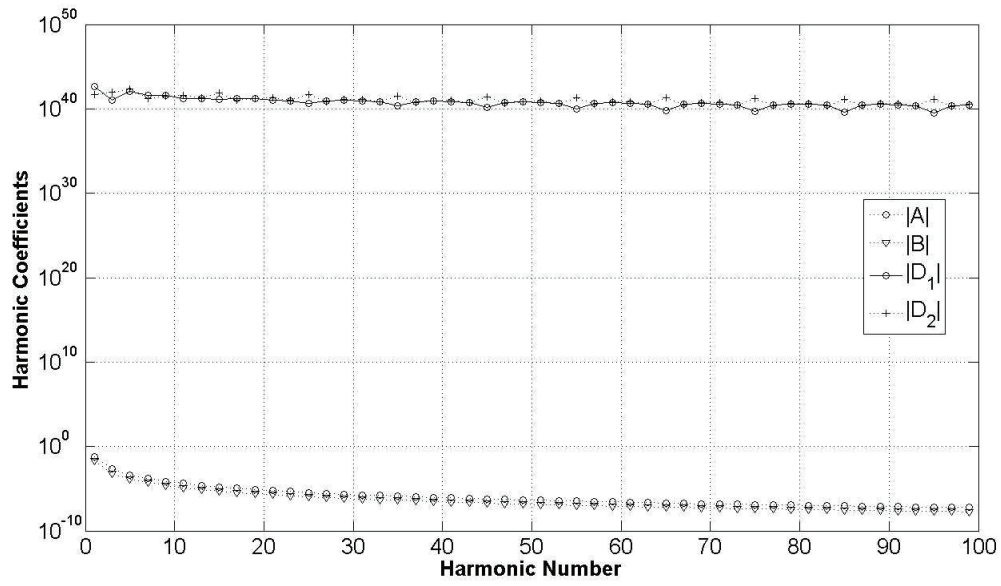


**Figure 7: Fourier series coefficients vs. harmonic order, at an excitation frequency of 50 hz.**

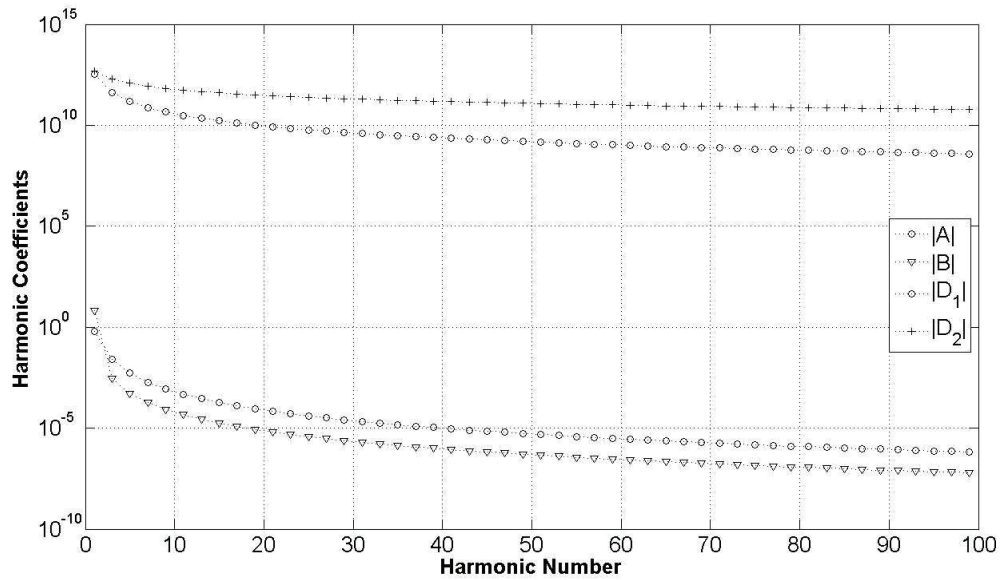


**Figure 8: Fourier series coefficients vs. harmonic order, at the 1<sup>st</sup> resonance frequency.**

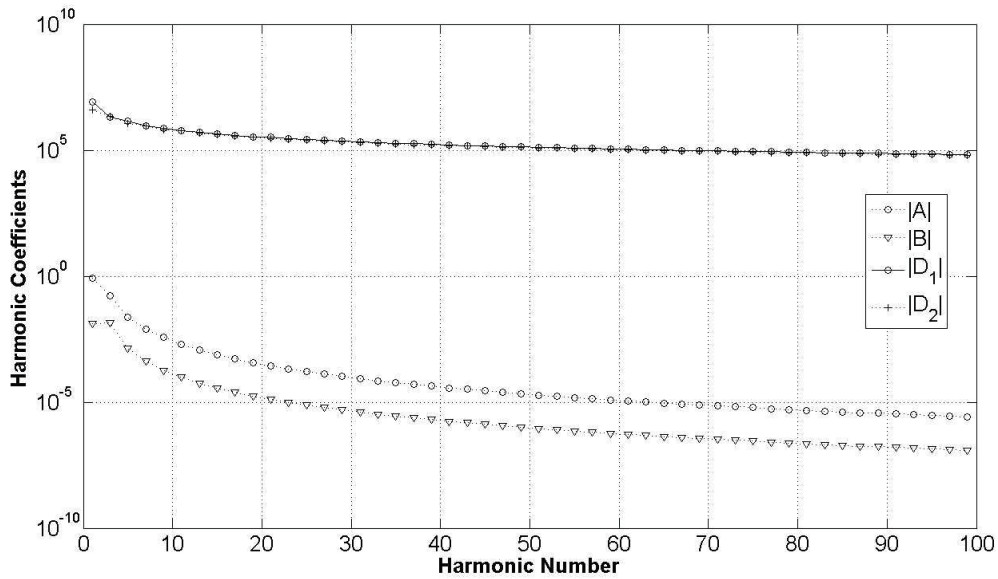


**Figure 9: Fourier series coefficients vs. harmonic order, at the 2<sup>nd</sup> resonance frequency.**

An evident convergence allows for considering a small order for a good solution accuracy.

After this preliminary validation, the results in terms of displacement and sound pressure level have been computed in time domain. At first, the lowest resonance frequency of the structure has been estimated and assumed as upper threshold, coherently with the assumption B.C. (8) is based on: absence of structural inertial and damping actions.

Normalised displacement vs. time vs. column axis, at 50 hz and for the first two resonance frequencies without control, has been plotted in Fig. 10 – 12.

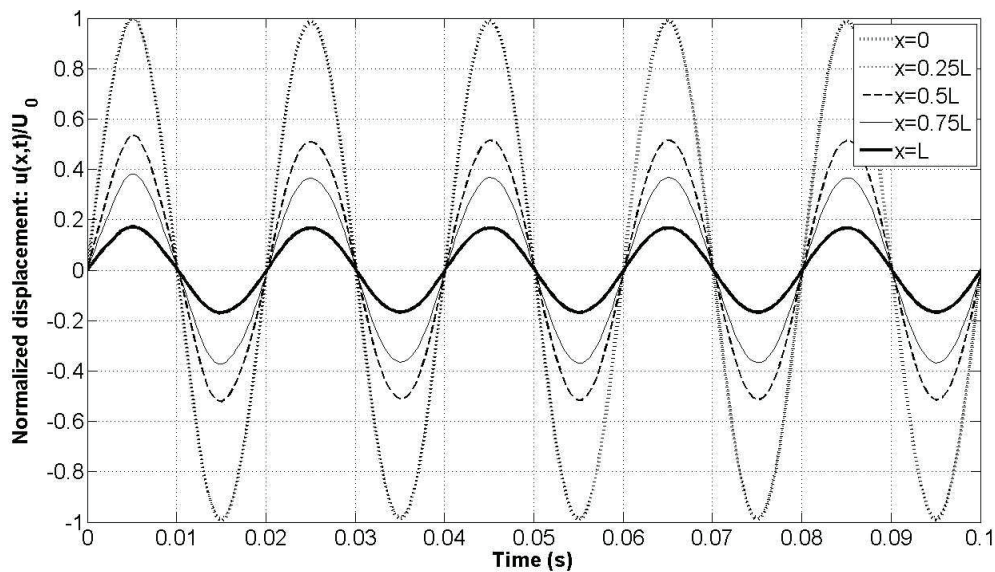


**Figure 10: Normalised displacement vs. time, for  $x/L = 0, 0.25, 0.50, 0.75, 1$ , at 50 hz.**

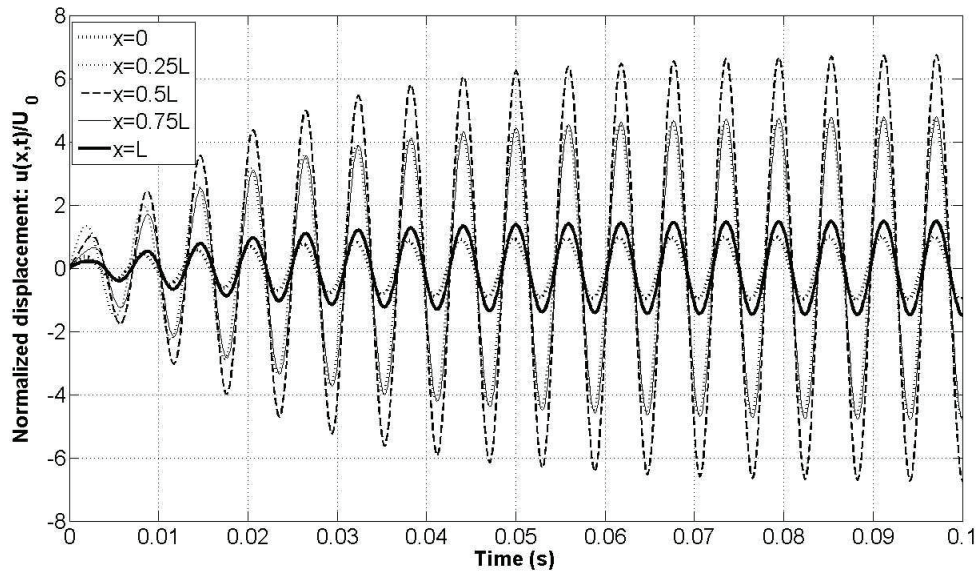


**Figure 11: Normalised displacement vs. time, for  $x/L = 0, 0.25, 0.50, 0.75, 1$ , at 1<sup>st</sup> resonance frequency.**

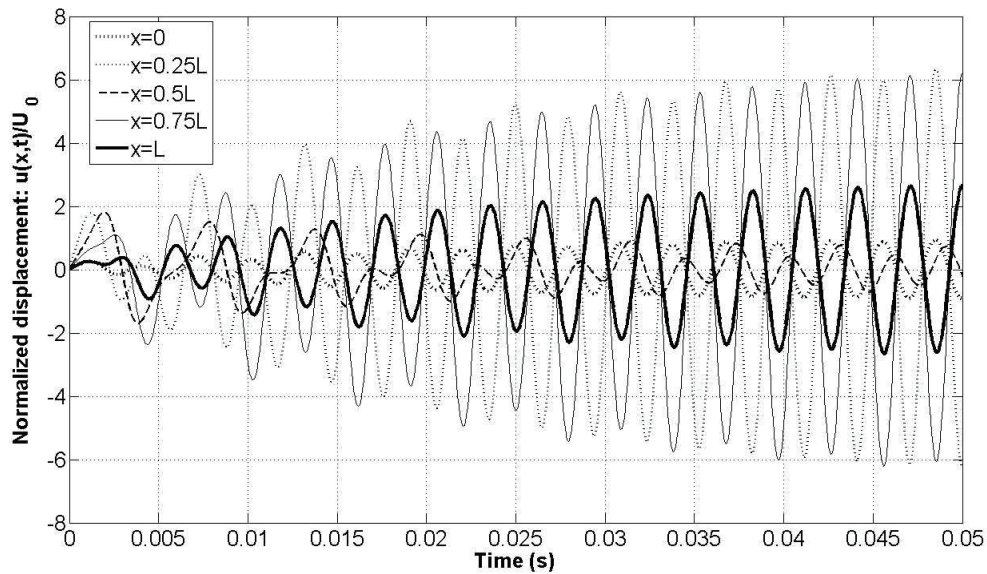


**Figure 12: Normalised displacement vs. time, for  $x/L = 0, 0.25, 0.50, 0.75, 1$ , at 2<sup>nd</sup> resonance frequency.**

Corresponding modal shapes of the fluid column has been extracted at a fixed time in steady state regime, from these last two figures. (see Fig. 13).

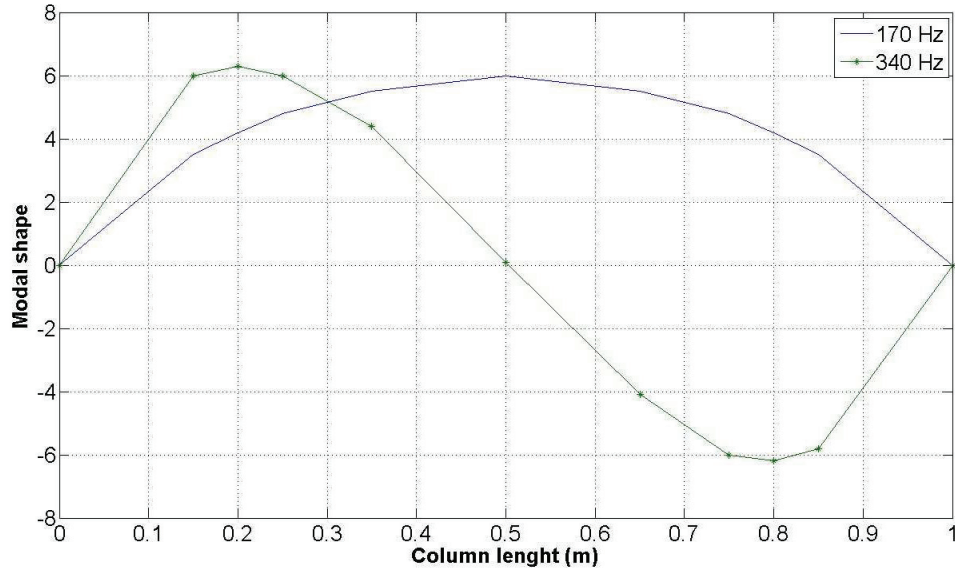


**Figure 13: 1<sup>st</sup> and 2<sup>nd</sup> modal shapes.**

The normalised displacement at  $x=L$  vs. time, for the first two resonance frequencies and for gain amplification of 1 and 10 have been compared with no controlled response in Fig. 14 -15.

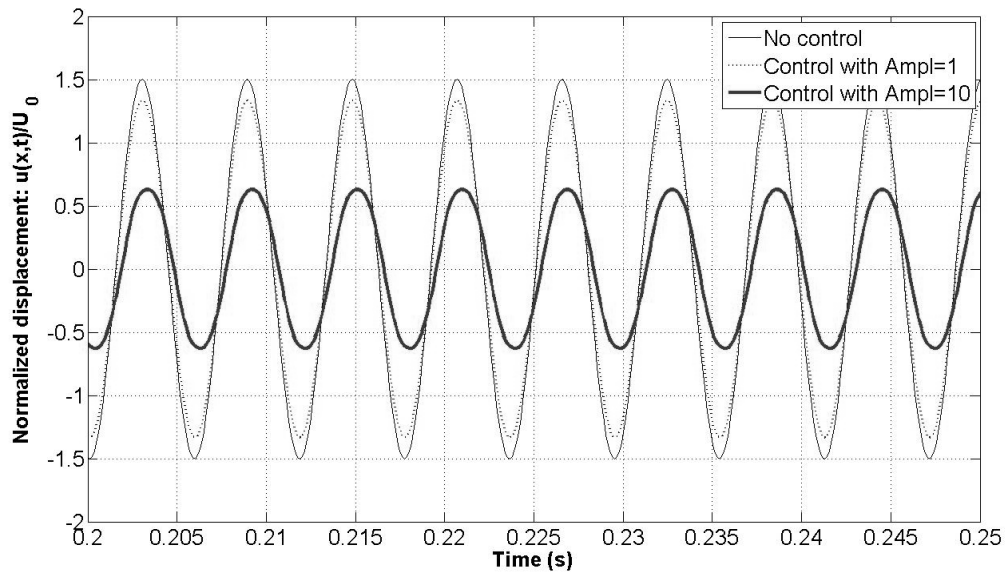


**Figure 14: Normalised displacement vs. time vs. amplification level at  $x=L$ , for the first resonance.**

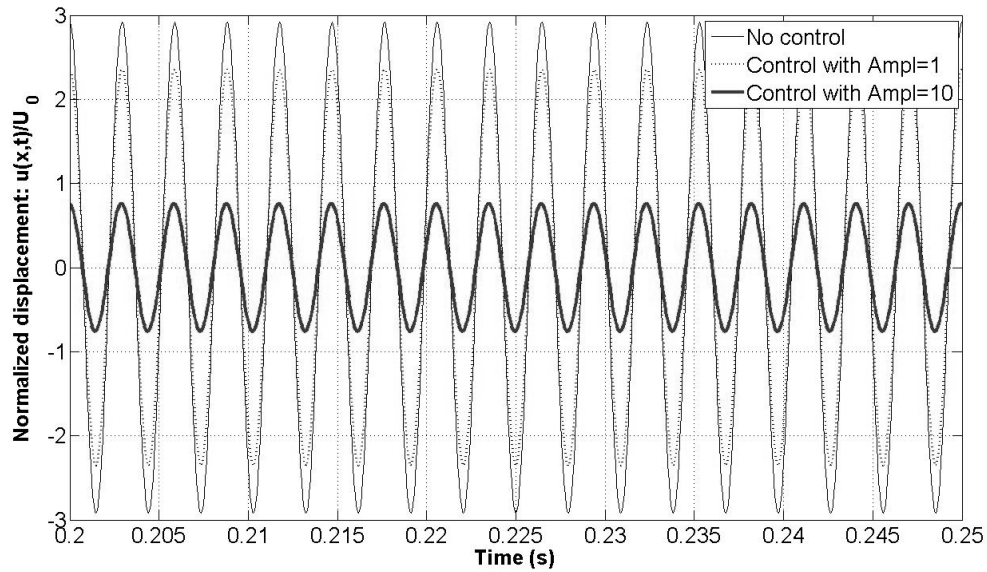


**Figure 15: Normalised displacement vs. time vs. amplification level at  $x=L$ , for the second resonance.**

In the Figure 14, it is evident circuit ability of inducing also a phase shift [9, 10, 18, 19]. Finally, in Figures 16 and 17, the normalised displacement field and the difference between no controlled and controlled (amplification = 1) case vs. time vs. column axis, has been plotted

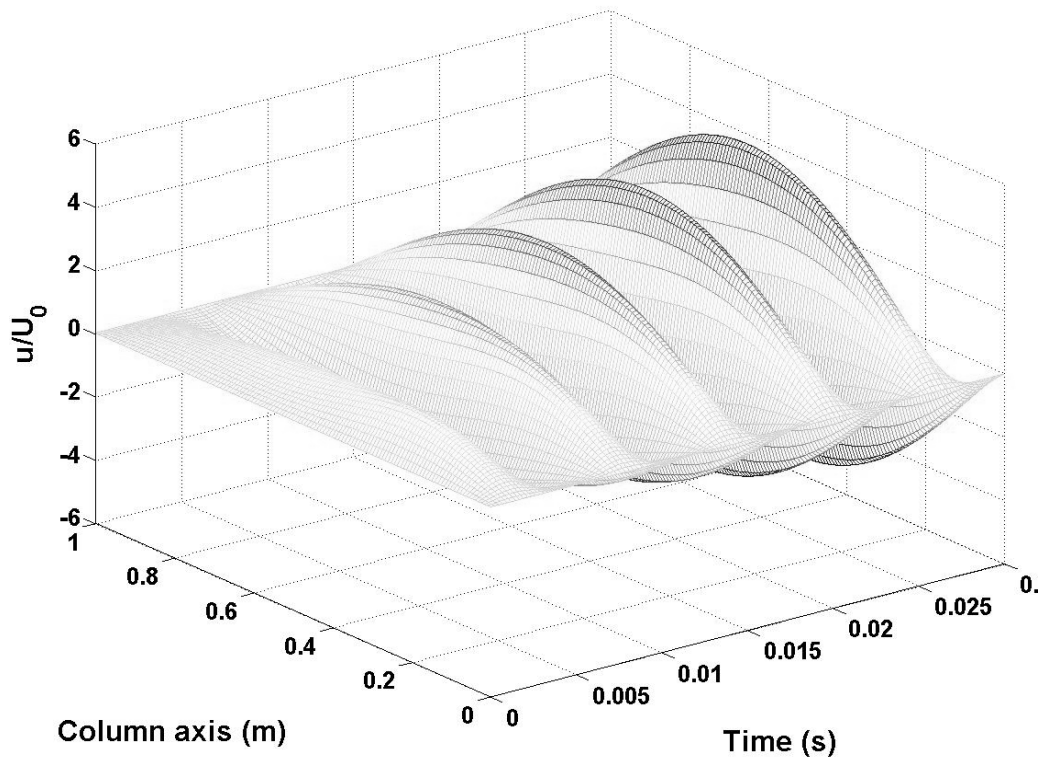


**Figure 16: Normalised displacement vs. time vs. column axis, for the first resonance.**

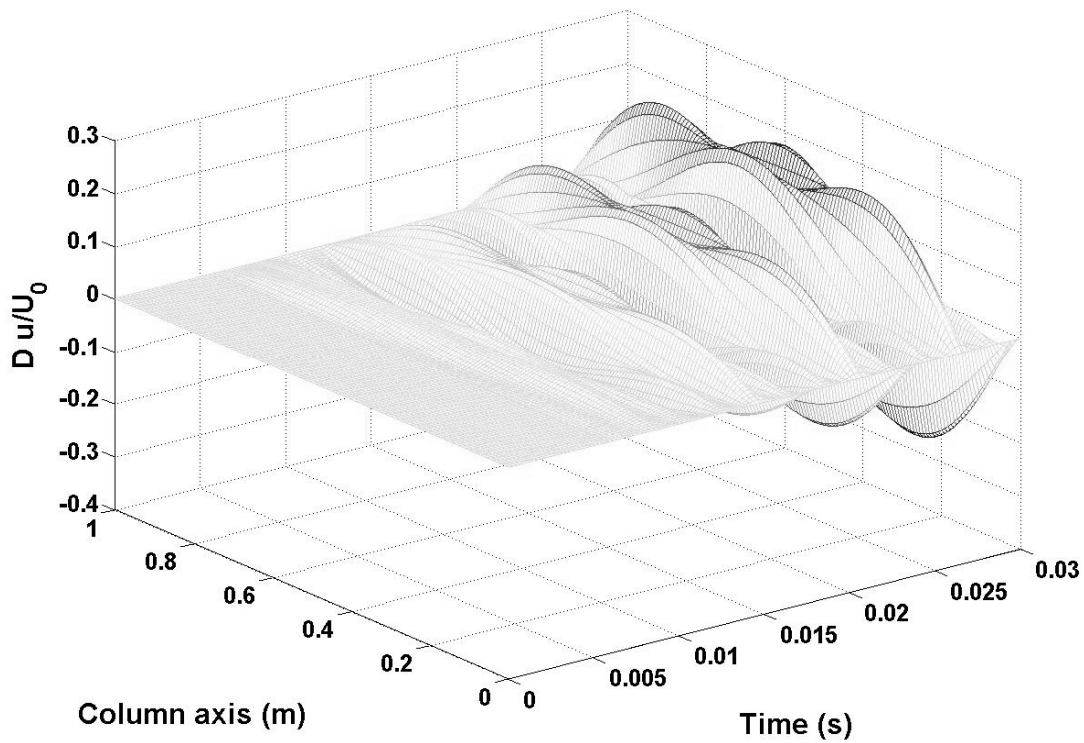


**Figure 17: No controlled - controlled normalised displacement difference vs. time vs. column axis, for the first resonance.**

An attenuation of 1.5 and 2.3 dB without amplification has been estimated at fluid-structure interface, for the first and second resonance frequencies. A max reduction (7.9, 11.2 dB at 170 and 340 Hz, respectively) has been observed for the maximum amplification considered. To have an idea of the energy attenuation, the squared value of the pressure has been computed and reported for fixed locations along the column. Corresponding squared mean energy, SME, estimated through (43), has been reported on the last column.

		170 hz				
x/L Gain	0	0.25	0.50	0.75	1.00	SME
	Sound res. Atten (dB)					
1	2.1	1.9	0	1.8	1.5	1.7
5	5.7	5.1	0	5.1	5.4	9.7
10	12	10	0	9.8	9.5	17.3
		340 hz				
x/L Gain	0	0.25	0.50	0.75	1.00	SME
	Sound res. Atten (dB)					
1	2.8	0	2.3	0	2.1	3.8
5	8.5	0	8.3	0	8.2	15.2
10	13	0	14	0	14	24.6

**Tab2. Sound pressure reduction vs. spatial domain vs. amplification**

Benefits are evident for different locations along the fluid column, even though zero attenuation values have been detected on the modal shape nodes.

Generally, the control proved to be more effective for the 2<sup>nd</sup> frequency, by achieving a mean reduction of 24.6 dB, 6.5 times higher the not amplified reference case. A minimum averaged attenuation (1.7 dB) has been detected for the 1<sup>st</sup> resonance, without amplification.

Finally to have an idea of control authority for the entire frequency range [0-500 Hz], the mean pressure level estimated with and without control (for Gain = 1) by exciting the system through a stepped sine signal have been compared in Figure 18.

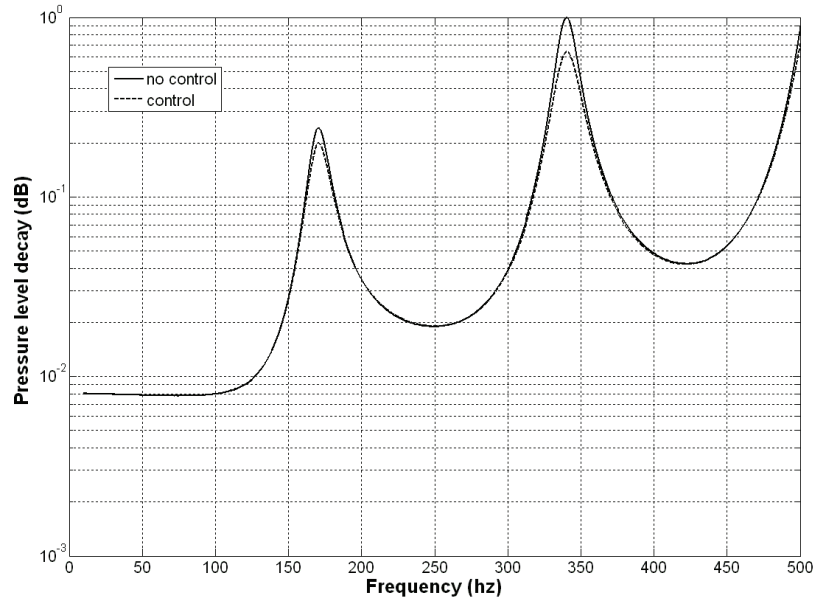


**Figure 18: No controlled - controlled mean pressure level vs. frequency.**

Related attenuation, as shown in Figure 19, has proved to mainly interest peaks zones.

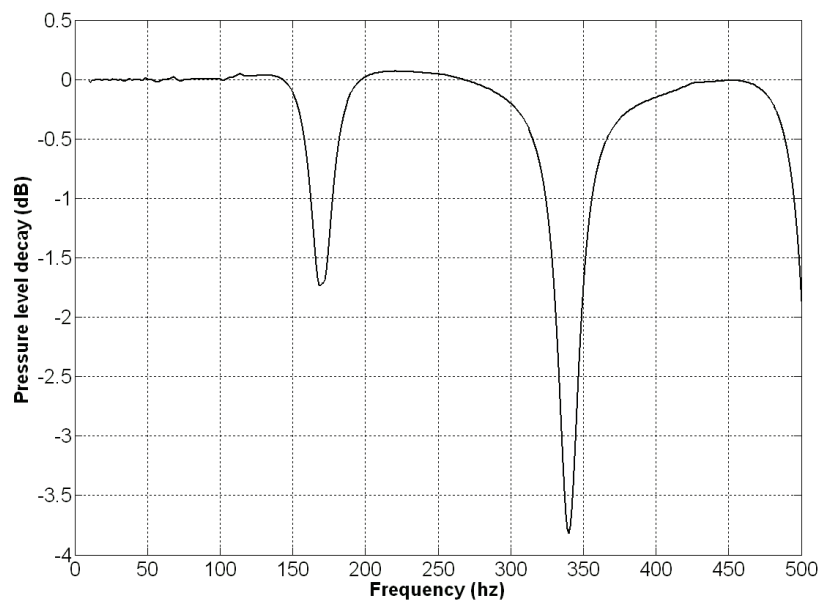


**Figure 19: No controlled - controlled dB mean pressure level reduction vs. frequency.**

## Conclusions and further steps.

In the present work the possibility of exploiting the switched shunt control architecture to the sound pressure attenuation within enclosures has been dealt with. Many applications have been published, concerning with the vibration attenuation through piezo network controlled by this mentioned logic; related benefits within low frequency band led to develop numerical tools aimed at predicting related benefits, and to address experimental campaigns to verify effectiveness and point out eventual drawbacks.

Also applications focused on acoustic problems have been carried out, generally oriented to interior noise radiation and sound pressure level within enclosures.

The main advantage of the switch logic are fully described in referred literature and summarized in the dedicated paragraph of the present paper. The idea is to generate a control force opportunely synchronized to maximum amplitude and shortly temporized with the sensor output signal. These operating conditions guarantee a pulse kind actuation force in phase opposition with respect to the local structural displacement and the independence from the structural response in a wide band range.

Moreover being the resistor negligible, the switched shunt performs more thermal stability.

The absence of external power supply injecting energy into the system guarantees an unconditional stability of the control.

The paper at hand has concerned with the formalisation of a semi-analytic solution describing the displacement and the pressure field within an air column subjected to a switch control, implemented on a piezo actuator. This approach ensures a quick estimate of the efficiency of the control, acting within an enclosure, exploitable as preliminary design reference for further, more complex, numerical modelling.

Acoustic field is described by the telegraph equation, whose solution has been expressed as Fourier expansion; disturbance (a sinusoidal excitation) and control action (given by a long plate actuated by a piezo) have been supposed localised on the two boundaries of the 1D domain.

At first, a preliminary validation of the solution has been addressed, tracking series coeffs. vs. harmonic order behaviour. Secondly, modal shapes have been plotted for the first two resonances without control. Then the control authority has been investigated, computing displacement vs. time, vs. amplification gain at fixed locations along the column axis. Related information has been expressed in terms of punctual and averaged sound pressure level. Larger authority has been observed for the 2<sup>nd</sup> normal frequency: 24.6 dB of attenuation, with a 10 times amplification. Even without any amplification, coherently with the semi-passive nature of this control, a reduction of 3.8 dB has been estimated.

In order to assess model validity and point out possible limits, a tailored experimental prototype; more in detail, a duct instrumented with microphones along the generatrix, with a loudspeaker and a pzt controlled panel mounted on the bases, will be manufactured.

Above mentioned model can be further enriched, introducing impedance contribution, for damping layer applications. Moreover, solution validity can be extended in frequency band, even though paying in terms of complexity, introducing the effects of structural inertial and damping actions.

Finally, different, more complex geometries, of major interest for real applications (axial-symmetric, tapered, etc), could be investigated, by formalising the problem through tailored BCs.

## References

- [1] Lesieutre G.A., “Vibration Damping and Control Using Shunted Piezoelectric Materials”, *The Shock and Vibration Digest*, **30 (3)**, 187-195, (1998).
- [2] Hagood N.W. and Von Flotow A., “Damping of structural vibrations with piezoelectric materials and passive electrical networks”, *MIT Journal of Sound and Vibration* (1991) **146(2)**, pp. 243-268.
- [3] Park G., Inman D.J. “A Uniform Model for Series RL and Parallel RL Shunt Circuits and Power Consumption”, *SPIE Conference Proceedings on Smart Structure and Integrated Systems*, (1999) Newport Beach, CA, **3668**, 797-804.
- [4] Erturk A., Inman D.J. “Piezoelectric shunt damping for chatter suppression in machining processes”, *Proceedings of ISMA2008*, (2008) Leuven, Belgium, isma2008-0296.
- [5] Preumont, A., 1997, *Vibration Control of Active Structures: An Introduction*, Kluwer Academic Publishers.
- [6] De Marneffe B., Horodinca M., Preumont A. “Vibration isolation via shunted electromagnetic transducer”, *Proceedings of ISMA2008*, (2008) Leuven, Belgium, isma2008-0499.
- [7] Clark, W. State switched piezoelectric systems for vibration control. *Structure, Structural Dynamics and Materials AIAA Journal* **1533** (1999), 2623-2629.
- [8] Clark, W. Vibration Control with State-Switched Piezoelectric Materials. *Journal of Intelligent Material Systems and Structures* **11** (2000), 263-273.
- [9] Richard, C., Guyomar, D., Audigier, D., and Bassaler, H. Enhanced semi-passive damping using continuous switching and Isolation, *SPIE* (2000), vol. 3989, pp.288-299.
- [10] Richard, C., Guyomar, D., Audigier, D., and Ching, G. Semi-passive damping using continuous switching of a piezoelectric device. In *Society of Photo-Optical Instrumentation Engineering (SPIE) Conference Series* (1999), vol. 3672, pp.104-111.
- [11] Lefeuvre, E., Badel, A., Petit, L., Richard, C., and Guyomar, D. Semi-passive Piezoelectric Structural Damping by Synchronized Switching on Voltage Source. *Journal of Intelligent Material Systems and Structures* **17** (2006), 653-660.
- [12] Lallart, M., Badel, A., Guyomar, D., and Lebrun, L. Non-linear semi-passive damping using constant or adaptive voltage source: a stability analysis. In *ICAST 2005 – 16<sup>th</sup> International Conference on Adaptive Structures and Technologies* (2005), pp.158-165.
- [13] Corr, L., Clark, W. Energy Dissipation of Piezoelectric Semi-Active Vibration Control. *Journal of Intelligent Material Systems and Structures* **12** (2001), 729-736.
- [14] Corr, L., Clark, W. Comparison of low-frequency piezoelectric switching shunt technique for structural damping. *Smart materials and Structures* **11** (2002), 370-376.
- [15] Corr, L.R. *Investigation of real-time switching of piezoceramic shunts for structural vibration control*. PhD thesis, School of Engineering, University of Pittsburg, 2001.
- [16] Corr, L., Clark, W. A novel semi-active multimodal vibration control law for a piezoceramic actuator. *Journal of Vibration and Acoustics* **125** (2003), 214-222.

- [17] Collinger, J.C., and Wickert, J.A. Adaptive piezoelectric Vibration Control with Synchronized Switching. In *Proceeding of ASME International Mechanical Engineering Congress and Exposition, IMECE 2007-41427* (Seattle, Washington, USA, Nov. 2007).
- [18] Petit, L., Guyomar, D., and Richard, C. Piezoelectric damping: a comparison between passive and semipassive switching techniques. In *Proc. Of 4<sup>th</sup> JFSIMS (Japan-France Seminar on Intelligent materials and Structures)* (Lyon, July 2002).
- [19] Petit, L., Lefeuvre, E., Richard, C., and Guyomar, D., A broadband semi passive piezoelectric technique for structural damping. In *Proc. of SPIE* (2004), vol. 5386, pp. 414-425.
- [20] Guyomar, D., and Badel, A. Nonlinear semi-passive multimodal vibration damping: an efficient probabilistic approach. *Journal of Sound and Vibration* **294** (2006), 249-268.
- [21] Ciminello, M., Ameduri, S., Calabrò, A., and Concilio, A. Synchronised Switched Shunt Control Technique Applied on a Cantilevered Beam: Numerical and Experimental Investigations. *JIMSS Vol.19, N°9*, September 2008 pp.1089-1100.
- [22] Ciminello, M., Iecce, L., Ameduri, S., Calabrò, A., and Concilio, A. Switched Shunt Control implemented through a PZT network embedded within a composite panel: design, manufacture and test. *Submitted to – JIMSS-08-452*.
- [23] Ciminello, M., Deu, J.-F., Ohayon, R., and Ameduri, S. Vibration reduction of structural-acoustic systems using synchronized switch damping techniques. *Proceeding of 2008 ASME International Conference on Smart Materials, Adaptive Structures & Intelligent Systems*, October 28-30, 2008, Ellicott City, MD, USA. Paper - SMASIS08-320
- [24] Ameduri, S., Ciminello, M., and Concilio, A. Semi-analytical Solution of a Structural System Controlled by a Switched Shunt Architecture. *Proceeding of the 36th International Congress and Exhibition on Noise Control Engineering - Session ANVC "Active Noise and Vibration Control*, August 28 – 31, 2007 Istanbul - Turchia. Paper N° IN07-032
- [25] Ducarne, J., Thomas, O. and Deu, J.-F. Structural vibration reduction optimization by switch shunting of piezoelectric elements. In *Proceeding of ASME International Mechanical Engineering Congress and Exposition, IMECE 2007-41427* (Seattle, Washington, USA, Nov. 2007).
- [26] Timoshenko, S. P., Woinowsky-Krieger, S, “Theory of Plates and Shells”, Mc Graw-Hill International Editions, second edition, pp. 4-6.
- [27] Haberman, R., “Elementary Applied Partial Differential Equations with Series and Boundary Value Problems”, Prentice Hall Inc., second edition, pp. 257-261.
- [28] Everest, F. A., “The Master Handbook of Acoustics”, Mc Graw-Hill International Editions, fourth edition, pp. 142-147.
- [29] Boyce, W. E., DiPrima, R. C., “Elementary Differential Equations and Boundary Value Problems”, John Wiley & Sons Inc, seventh edition, pp. 621-655.
- [30] Crawley, E. F., de Luis, J., “Use of Piezoelectric Actuators as Elements of Intelligent Structures”, *AIAA Journal*, vol. 25, no. 10, pp. 1373-1385, october 1987.

# Submitted to International Peer Reviewed Journals

*W. Larbi, J.-F. Deu, M. Ciminello, R. Ohayon, “**Structural-acoustic vibration reduction using switched shunt piezoelectric patches. A finite element analysis**”. Submitted revised version to the - Journal of Vibration and Acoustics VIB-09-1143.*

*A multi-dofs electro-mechanical coupled system has been numerically modelled by means of a finite element formulation. A finite element tool integrating Nastran features with Matlab routines has been Finite element modelling concerning the dynamic response reduction of structural-acoustic systems, attained by using a synchronized switch control technique, are also investigated. The considered coupled system is an elastic plate with a surface-mounted piezoelectric patches, coupled with an acoustic cavity filled with an inviscid, compressible and barotropic fluid, gravity effect being neglected. A full home-made finite element procedure, according to the local equation describing the fully coupled system has been implemented in Matlab environment. The effect of a passive inductive shunt and the semi-passive switched shunt have been compared in order to highlight the broad band features of the second technique.*

---

*M. Ciminello, L. Lecce, A. Concilio, “**Structure borne sound for acoustic cavity through pzt patch in switched shunt configuration: a non standard finite element analysis**”. Submitted to: Aerotecnica missili e spazio.*

*In order to validate the mentioned original general-purpose procedure simulating the SSC also for electro-elasto-acoustic systems, the results obtained from the standard finite element code discussed in the previous paper, have been compared with the not standard procedure integrating Nastran/Matlab routines. The matrices are extracted from Nastran and reassembled in Matlab where the electromechanical coupling terms have been added. Moreover taking advantage of the eigenvectors that Nastran can easily compute even for complex systems, a modal reduction has been approached. Correlations in the results demonstrate the coherence of the not standard method.*



# Structural-acoustic vibration reduction using switched shunt piezoelectric patches. A finite element analysis

W. Larbi<sup>a</sup>, J.-F. Deü<sup>a</sup>, M. Ciminello<sup>a,b</sup>, R. Ohayon<sup>a</sup>

<sup>a</sup> *Conservatoire National des Arts et Métiers (Cnam),  
Structural Mechanics and Coupled Systems Laboratory,  
Chair of Mechanics, case 353,  
2 rue Conté, 75003 Paris, France*

<sup>b</sup> *Aerospace Engineering Departement,  
Federico II University of Naples, Italy*

---

## Abstract

In this paper, we present a finite element formulation for vibration reduction of structural-acoustic systems using passive or semi-passive shunt techniques. The coupled system consists of an elastic structure (with surface-mounted piezoelectric patches) filled with an inviscid linear acoustic fluid. An appropriate finite element formulation is derived. Numerical results for an elastic plate coupled to a parallelepipedic air-filled interior acoustic cavity are presented showing the performances of both the inductive shunt and synchronized switch shunts techniques.

*Key words:* Vibration reduction, Structural-acoustic, Piezoelectric patches, Switch, Shunt, Finite element method.

---

## 1 INTRODUCTION

A considerably amount of researches is actually devoted to the study and design of new noise reduction strategies to improve acoustic comfort. Noise reduction can be practically achieved using passive sound absorbing materials such as foams or fibrous materials [1]. These materials generally provide adequate absorption at medium and high frequencies but bulky in mass and volume in the low frequencies range where the absorption increases with the thickness of the absorber. For these reasons and despite a complexity of the design and the external power required, a new trend is to use active techniques

to reduce noise and vibrations particularly in applications in which the lightness of the structure is a necessity. In this context, many researches focused on control systems with piezoelectric patches, bonded or embedded in structural elements, and shunted in a specific electric circuit [2].

A finite element model to study the response of a piezoelectric smart structure for a cabin noise problem is presented in [3]. The active control system implemented was a negative feedback. Lefèvre and Gabbert [4] presented the theoretical background of a new finite element software tool for solving 3D electro-mechanical-acoustical field problems. Numerical investigations were performed using a modal reduction technique based on the uncoupled modes of the system. Another approach to the sound and vibration control is to combine active and passive devices. Some works have dealt with this subject. Ro and Baz [5] for instance, presented a paper in which the sound radiation from a vibrating flat plate coupled with an acoustic cavity is controlled using a single piezoelectric patch with an active control and passive constrained layer damping treatments. Finite element model is developed to study the fundamental phenomena governing the coupling between the dynamics of treated plates and acoustic cavity. The model is used to compute the frequencies, mode shapes and sound radiation for different control gains. Close agreements are obtained between theoretical predictions and the experimental measurements. An attempt to control noise in a cabin is presented in the work of Gopinathan et al. [6]. Here the authors have presented a finite element/boundary element formulation for modeling and analysis of active-passive noise control system. The method considered for the numerical applications is a cubic cavity in which one of the walls is assumed to be flexible panel, which radiates sound into the cavity. The piezoelectric patches are attached to the panel at a predetermined location. The sensor patches generate a voltage then amplified and put in feedback into the actuator using an optimal feedback controller. The interior of the flexible vibrating panel is covered with a sound absorber. A formulation to calculate the coupled response of composite shells with embedded piezoelectric layers and an enclosed acoustic fluid is presented in the paper of Kaljevic and Saravanos [7]. The methodology consists of three parts: the formulation for the electro-mechanical response of the piezo shell, the formulation of the 3D acoustic response of the enclosed fluid, and finally the combination of the previous formulation to calculate the coupled smart structure acoustic fluid response. They adopted a mixed field laminate theory with a layer-wise approximation for the electric potential. A boundary element formulation is developed to calculate the acoustic response of the enclosed fluid. A different approach to the noise reduction of sound radiating into a cavity is presented by Guyomar et al [8]. The work deals with the semi passive approach in which the synchronized switch technique is implemented. The piezoceramics are continuously switched from the open circuit state to a specific electric network synchronously with the strain. The authors describe the experimental results with the analytical prediction. The experiment consists in exciting the plate

via the loudspeaker and detects the noise level of the sound wave transmitted in the external environment. The measurement is made and compared in three cases: without control, with an inductive switched shunt and with a voltage driving inductive switched shunt. Theoretical and experimental results are in good concordance, anyway some discrepancies are observed in particular for the first mode. An attenuation of 15 dB on the transmitted wave pressure is obtained with the efforts of an amplification voltage driving source. Alternative active control procedure has been also derived [9] and experimental assessment of smart damping materials may be found in [10].

The present paper concerns a finite element formulation for vibration reduction of structural-acoustic systems using passive or semi-passive shunt techniques. The coupled system consists of an elastic structure (with surface-mounted piezoelectric patch) filled with an inviscid, compressible and barotropic fluid, gravity effect being neglected. Let us first recall that the general three-dimensional piezoelectric structure completely filled with acoustic fluid has been already discussed in [11]. On the other hand, an original procedure adapted to the vibrations of an elastic structure with shunted piezoelectric patches has been derived in [12]. The originality of the present paper is to extend the previous one to the structural acoustic case. Numerical results (in the low frequency domain) are analyzed showing the performance of both the inductive shunt and the synchronized switch shunts techniques.

## 2 Finite element formulation of the structural acoustic problem with piezoelectric patches

Firstly, we briefly recall the variational formulation of a fluid/piezoelectric-structure interaction problem in terms of structural mechanical displacement  $u_i$ , electric potential in the structure  $\psi$  and fluid pressure  $p$  of the inviscid acoustic fluid (for more details, we refer the reader to [11]). Secondly, this coupled formulation is adapted to the general case of an elastic structure equipped with  $P$  piezoelectric patches (see Figure 1) as done for structural vibrations in [12]. This modified formulation allows taking into account realistic electrical boundary conditions such as equipotentiality on patches electrodes and prescribed global charges. Finally, the resulting finite element formulation is applied to a structural acoustic problem with one piezoelectric patch connected to a  $RL$  series shunt circuit.

It should be noted that standard indicial notations are adopted throughout the paper: subscripts  $i, j, k, l$  denote the three-dimensional vectors and tensor components and repeated subscripts imply summation. In addition, a comma indicates a partial derivative.

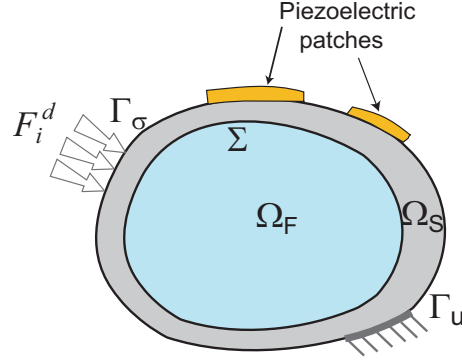


Fig. 1. Fluid/piezoelectric-structure coupled system.

### 2.1 Variational formulation of the fluid/structure/piezoelectric-patches coupled system

We consider a piezoelectric structure occupying the domain  $\Omega_S$  filled with an inviscid linear acoustic fluid occupying the domain  $\Omega_F$ . We denote by  $\Sigma$  the fluid-structure interface and by  $n_i^S$  and  $n_i^F$  the unit normals external to  $\Omega_S$  and  $\Omega_F$ , respectively.

The structure is clamped on a part  $\Gamma_u$  and subjected (i) to a given surface force density  $F_i^d$  on the complementary part  $\Gamma_\sigma$  of its external boundary and (ii) to a pressure field  $p$  due to the presence of the fluid on its internal boundary  $\Sigma$ . The electric boundary conditions are defined by a prescribed electric potential  $\psi^d$  on  $\Gamma_\psi$  and a surface density of electric charge  $q^d$  on the remaining part  $\Gamma_D$ . Thus, the total structure boundary, denoted  $\partial\Omega_S$ , is such that  $\partial\Omega_S = \Gamma_u \cup \Gamma_\sigma \cup \Sigma = \Gamma_D \cup \Gamma_\psi$  with  $\Gamma_u \cap \Gamma_\sigma \cap \Sigma = \Gamma_\psi \cap \Gamma_D = \emptyset$ .

The linearized deformation tensor is  $\varepsilon_{ij} = \frac{1}{2}(u_{i,j} + u_{j,i})$  and the stress tensor is denoted by  $\sigma_{ij}$ . Concerning the electric field variables,  $D_i$  is the electric displacement verifying the electric charge equation for a dielectric medium  $D_{i,i} = 0$  in  $\Omega_S$  and the electric boundary conditions  $D_i n_i^S = -q^d$  on  $\Gamma_D$ ;  $E_i$  denotes the electric field vector such that  $E_i = -\psi_{,i}$ .

The linear piezoelectric constitutive equations write:

$$\sigma_{ij}(u, \psi) = c_{ijkl}\varepsilon_{kl}(u) - e_{kij}E_k(\psi) \quad (1)$$

$$D_i(u, \psi) = e_{ikl}\varepsilon_{kl}(u) + \epsilon_{ik}E_k(\psi) \quad (2)$$

where  $c_{ijkl}$  denotes the elastic moduli at constant electric field,  $e_{kij}$  the piezoelectric constants and  $\epsilon_{ik}$  the dielectric permittivities at constant strain. Moreover, we denote by  $\rho_S$  the mass density of the structure.

Let us introduce the admissible spaces  $C_u$  and  $C_\psi$  of regular functions  $u_i$  and  $\psi$  defined in  $\Omega_S$ . We then consider the following subspaces  $C_u^* = \{u_i \in C_u \mid u_i = 0 \text{ on } \Gamma_u\}$ ,

$$C_\psi^d = \{\psi \in C_\psi \mid \psi = \psi^d \text{ on } \Gamma_\psi\} \text{ and } C_\psi^* = \{\psi \in C_\psi \mid \psi = 0 \text{ on } \Gamma_\psi\}.$$

The variational formulation, corresponding to the response of the piezoelectric structure subjected to the prescribed boundary conditions and to the pressure field  $p$  on the interface  $\Sigma$  writes:

Find  $u_i \in C_u^*$  and  $\psi \in C_\psi^d$  such that:

$$\int_{\Omega_S} c_{ijkl} \varepsilon_{kl} \delta \varepsilon_{ij} dv - \int_{\Omega_S} e_{kij} E_k \delta \varepsilon_{ij} dv + \rho_S \int_{\Omega_S} \frac{\partial^2 u_i}{\partial t^2} \delta u_i dv = \int_{\Gamma_\sigma} F_i^d \delta u_i ds + \int_{\Sigma} p n_i^F \delta u_i ds \quad \forall \delta u_i \in C_u^* \quad (3)$$

where  $\delta \varepsilon_{ij} = \frac{1}{2}(\delta u_{i,j} + \delta u_{j,i})$ ,  $\varepsilon_{kl}$  and  $E_k$  being functions of  $u_i$  and  $\psi$ , and

$$\int_{\Omega_S} e_{ikl} \varepsilon_{kl} \delta E_i dv + \int_{\Omega_S} \epsilon_{ik} E_k \delta E_i dv = \int_{\Gamma_D} q^d \delta \psi ds \quad \forall \delta \psi \in C_\psi^* \quad (4)$$

where  $\delta E_i = -\delta \psi_{,i}$ ,  $\varepsilon_{kl}$  and  $E_k$  being functions of  $u_i$  and  $\psi$ .

This formulation must be completed by appropriate initial conditions.

We consider now the special case of an elastic structure (domain  $\Omega_E$ ) equipped with  $P$  piezoelectric patches and completely filled with an internal fluid (domain  $\Omega_F$ ). Each piezoelectric patch has the shape of a plate with its upper and lower surfaces covered with a very thin layer of conducting material to obtain electrodes. The  $p$ th patch,  $p \in \{1, \dots, P\}$ , occupies a domain  $\Omega^{(p)}$  such that  $(\Omega_E, \Omega^{(1)}, \dots, \Omega^{(P)})$  is a partition of the all structure domain  $\Omega_S$ .

A set of hypotheses, that apply to a wide spectrum of practical applications, are now formulated:

- The piezoelectric patches are thin, with a constant thickness, denoted  $h^{(p)}$  for the  $p$ th patch;
- The thickness of the electrodes is much smaller than  $h^{(p)}$  and is thus neglected;
- The piezoelectric patches are polarized in their transverse direction (i.e. the direction normal to the electrodes).
- The electric field vector, of components  $E_k$ , is normal to the electrodes and uniform in the piezoelectric patch, so that for all  $p \in \{1, \dots, P\}$ :

$$E_k = -\frac{V^{(p)}}{h^{(p)}} n_k \quad \text{in } \Omega^{(p)} \quad (5)$$

where  $V^{(p)} = \psi_+^{(p)} - \psi_-^{(p)}$  is the potential difference between the upper and the lower electrode surfaces of the  $p$ th patch which is constant over  $\Omega^{(p)}$

and  $n_k$  is the  $k$ th component of the normal unit vector to the surface of the electrodes.

Under those assumptions and by considering successively each of the  $P + 2$  subdomains  $(\Omega_F, \Omega_E, \Omega^{(1)}, \dots, \Omega^{(P)})$ , the variational formulation of the fluid/structure/piezoelectric-patches coupled system can be written in terms of the structural mechanical displacement  $u_i$ , the electric potential difference  $V^{(p)}$  constant in each piezoelectric patch, and the fluid pressure  $p$ :

- Mechanical equation

$$\int_{\Omega_S} c_{ijkl} \varepsilon_{kl} \delta \varepsilon_{ij} dv + \sum_{p=1}^P \frac{V^{(p)}}{h^{(p)}} \int_{\Omega^{(p)}} e_{kij} n_k \delta \varepsilon_{ij} d\Omega + \rho_S \int_{\Omega_S} \frac{\partial^2 u_i}{\partial t^2} \delta u_i dv - \int_{\Sigma} p n_i^F \delta u_i ds = \int_{\Gamma_\sigma} F_i^d \delta u_i ds \quad \forall \delta u_i \in C_u^* \quad (6)$$

- Electrical equation

$$\sum_{p=1}^P \delta V^{(p)} C^{(p)} V^{(p)} - \sum_{p=1}^P \frac{\delta V^{(p)}}{h^{(p)}} \int_{\Omega^{(p)}} e_{ikl} \varepsilon_{kl} n_i d\Omega = \sum_{p=1}^P \delta V^{(p)} Q^{(p)} \quad \forall \delta V^{(p)} \in \mathbb{R} \quad (7)$$

where  $C^{(p)} = \epsilon_{33} S^{(p)} / h^{(p)}$  defines the capacitance of the  $p$ th piezoelectric patch ( $S^{(p)}$  being the area of the patch and  $\epsilon_{33} = \epsilon_{ik} n_i n_k$  the piezoelectric material permittivity in the direction normal to the electrodes) and  $Q^{(p)}$  is the global charge in one of the electrodes (see [12]).

- Acoustic equation

$$\frac{1}{\rho_F} \int_{\Omega_F} p_{,i} \delta p_{,i} dv + \frac{1}{\rho_F c_F^2} \int_{\Omega_F} \frac{\partial^2 p}{\partial t^2} \delta p dv + \int_{\Sigma} \frac{\partial^2 u_i}{\partial t^2} n_i^F \delta p ds = 0 \quad \forall \delta p \in C_p \quad (8)$$

The first two equations are directly derived from Equations (3) and (4) using the procedure described in [12]. The last equation corresponds to the variational formulation of the Helmholtz equation in the acoustic cavity  $p_{,ii} = \frac{1}{c_F^2} \frac{\partial^2 p}{\partial t^2}$  in  $\Omega_F$  together with the boundary condition  $p_{,i} n_i^F = -\rho_F \frac{\partial^2 u_i}{\partial t^2} n_i^F$  on  $\Sigma$ . This last relation expresses the continuity of the normal displacements of the inviscid fluid and the structure on  $\Sigma$ .  $c_F$  is the constant speed of sound in the fluid and  $\rho_F$  the mass density of the fluid.  $C_p$  is the admissible space of regular functions  $p$  defined in  $\Omega_F$ .

Thus, the variational formulation of the fluid/structure/piezoelectric-patches coupled problem writes as follows: given  $(F^d, \psi^d, q^d)$ , find  $(u_i \in C_u^*, \psi \in C_\psi^d, p \in C_p)$  such that Equations (6) to (8) are satisfied. The formulation must be completed by appropriate initial conditions.

*Remarks:*

- This formulation, with only a couple of electric variables per patches, is well adapted to practical applications since (i) realistic electrical boundary conditions such that equipotentiality on the electrodes and prescribed global charges naturally appear, (ii) the global charge/voltage variables are intrinsically adapted to include any external electrical circuit into the electromechanical problem and to simulate shunted piezoelectric patches.
- We will not discuss in this paper the various symmetrization of the formulation using additional fluid variable such as fluid displacement potential, neither the regularisation of the formulation for the limit static case which necessitates the following constraint  $\int_{\Omega_F} p \, dv + \rho_F c_F^2 \int_{\partial\Omega_F} u_i n_i^F \, ds = 0$ . This relation will be useful for the construction of reduced order model of dynamic substructuring type. We refer to [13], [14] and [11] for more details.
- Note that  $\delta u_i$ ,  $\delta\psi$  and  $\delta p$  are time independant and consequently  $t$  is a parameter for the corresponding admissible spaces.

## 2.2 *Finite element formulation of the fluid/structure/piezoelectric-patches coupled system*

Let us introduce  $\mathbf{U}$  and  $\mathbf{P}$  corresponding to the vectors of nodal values of  $u_i$  and  $p$  respectively, and  $\mathbf{Q} = (Q^{(1)} \, Q^{(2)} \, \dots \, Q^{(P)})^T$  and  $\mathbf{V} = (V^{(1)} \, V^{(2)} \, \dots \, V^{(P)})^T$  the column vectors of electric charges and potential differences. The submatrices corresponding to the various linear and bilinear forms involved in Equa-

tions (6) to (8) are defined by

$$\int_{\Omega_S} c_{ijkl} \varepsilon_{kl} \delta \varepsilon_{ij} dv \Rightarrow \delta \mathbf{U}^T \mathbf{K}_u \mathbf{U} \quad (9a)$$

$$\int_{\Omega_S} \rho_S u_i \delta u_i dv \Rightarrow \delta \mathbf{U}^T \mathbf{M}_u \mathbf{U} \quad (9b)$$

$$\sum_{p=1}^P \frac{V^{(p)}}{h^{(p)}} \int_{\Omega^{(p)}} e_{kij} n_k \delta \varepsilon_{ij} d\Omega \Rightarrow \delta \mathbf{U}^T \mathbf{C}_{uV} \mathbf{V} \quad (9c)$$

$$\sum_{p=1}^P \frac{\delta V^{(p)}}{h^{(p)}} \int_{\Omega^{(p)}} e_{ikl} \varepsilon_{kl} n_i d\Omega \Rightarrow \delta \mathbf{V}^T \mathbf{C}_{uV}^T \mathbf{U} \quad (9d)$$

$$\int_{\Sigma} p n_i^F \delta u_i ds \Rightarrow \delta \mathbf{U}^T \mathbf{C}_{up} \mathbf{P} \quad (9e)$$

$$\int_{\Sigma} u_i n_i^F \delta p ds \Rightarrow \delta \mathbf{P}^T \mathbf{C}_{up}^T \mathbf{U} \quad (9f)$$

$$\frac{1}{\rho_F} \int_{\Omega_F} p_{,i} \delta p_{,i} dv \Rightarrow \delta \mathbf{P}^T \mathbf{K}_p \mathbf{P} \quad (9g)$$

$$\frac{1}{\rho_F c_F^2} \int_{\Omega_F} p \delta p dv \Rightarrow \delta \mathbf{P}^T \mathbf{M}_p \mathbf{P} \quad (9h)$$

$$\sum_{p=1}^P \delta V^{(p)} C^{(p)} V^{(p)} \Rightarrow \delta \mathbf{V}^T \mathbf{K}_V \mathbf{V} \quad (9i)$$

$$\int_{\Gamma_\sigma} F_i^d \delta u_i ds \Rightarrow \delta \mathbf{U}^T \mathbf{F} \quad (9j)$$

$$\sum_{p=1}^P \delta V^{(p)} Q^{(p)} \Rightarrow \delta \mathbf{V}^T \mathbf{Q} \quad (9k)$$

where  $\mathbf{M}_u$  and  $\mathbf{K}_u$  are the mass and stiffness matrices of the structure;  $\mathbf{C}_{uV}$  is the electric mechanical coupled stiffness matrix;  $\mathbf{K}_V = \text{diag} (C^{(1)} C^{(2)} \dots C^{(P)})$  is a diagonal matrix filled with the  $P$  capacitances of the piezoelectric patches;  $\mathbf{M}_p$  and  $\mathbf{K}_p$  are the mass and stiffness matrices of the fluid;  $\mathbf{C}_{up}$  is the fluid-structure coupled matrix;  $\mathbf{F}$  is the applied mechanical force vector.

Thus, the variational equations (6) to (8) for the fluid/structure/piezoelectric-patches coupled problem can be written, in discretized form, as the following unsymmetric matrix system:

$$\begin{bmatrix} \mathbf{M}_u & \mathbf{0} & \mathbf{0} \\ \mathbf{0} & \mathbf{0} & \mathbf{0} \\ \mathbf{C}_{up}^T & \mathbf{0} & \mathbf{M}_p \end{bmatrix} \begin{bmatrix} \ddot{\mathbf{U}} \\ \ddot{\mathbf{V}} \\ \ddot{\mathbf{P}} \end{bmatrix} + \begin{bmatrix} \mathbf{K}_u & \mathbf{C}_{uV} & -\mathbf{C}_{up} \\ -\mathbf{C}_{uV}^T & \mathbf{K}_V & \mathbf{0} \\ \mathbf{0} & \mathbf{0} & \mathbf{K}_p \end{bmatrix} \begin{bmatrix} \mathbf{U} \\ \mathbf{V} \\ \mathbf{P} \end{bmatrix} = \begin{bmatrix} \mathbf{F} \\ \mathbf{Q} \\ \mathbf{0} \end{bmatrix} \quad (10)$$

with appropriate initial conditions.

*Remarks:*

- Open circuit case:  $\mathbf{Q}=\mathbf{0}$

Using the second row of Equation (10), the degrees-of-freedom associated with the electric potential difference can be expressed in terms of structure displacements as

$$\mathbf{V} = \mathbf{K}_V^{-1} \mathbf{C}_{uV}^T \mathbf{U} \quad (11)$$

Thus, after substitution of  $\mathbf{V}$  into Equation (10), we get the following problem in terms of  $\mathbf{U}$  and  $\mathbf{P}$

$$\begin{bmatrix} \mathbf{M}_u & \mathbf{0} \\ \mathbf{C}_{up}^T & \mathbf{M}_p \end{bmatrix} \begin{bmatrix} \ddot{\mathbf{U}} \\ \ddot{\mathbf{P}} \end{bmatrix} + \begin{bmatrix} \mathbf{K}_u + \mathbf{K}_A & -\mathbf{C}_{up} \\ \mathbf{0} & \mathbf{K}_p \end{bmatrix} \begin{bmatrix} \mathbf{U} \\ \mathbf{P} \end{bmatrix} = \begin{bmatrix} \mathbf{F} \\ \mathbf{0} \end{bmatrix} \quad (12)$$

where the "added-stiffness matrix"  $\mathbf{K}_A$ , which is due to the electromechanical coupling [15], is given by

$$\mathbf{K}_A = \mathbf{C}_{uV} \mathbf{K}_V^{-1} \mathbf{C}_{uV}^T \quad (13)$$

Note that  $\mathbf{K}_V$  being a diagonal matrix,  $\mathbf{K}_V^{-1}$  is easily computed.

- Short circuit case:  $\mathbf{V}=\mathbf{0}$

This case is obtained when the piezoelectric coupling constants are set to zero, i.e.  $\mathbf{K}_A = \mathbf{0}$  and leads to the classical  $(u_i, p)$  fluid-structure system:

$$\begin{bmatrix} \mathbf{M}_u & \mathbf{0} \\ \mathbf{C}_{up}^T & \mathbf{M}_p \end{bmatrix} \begin{bmatrix} \ddot{\mathbf{U}} \\ \ddot{\mathbf{P}} \end{bmatrix} + \begin{bmatrix} \mathbf{K}_u & -\mathbf{C}_{up} \\ \mathbf{0} & \mathbf{K}_p \end{bmatrix} \begin{bmatrix} \mathbf{U} \\ \mathbf{P} \end{bmatrix} = \begin{bmatrix} \mathbf{F} \\ \mathbf{0} \end{bmatrix} \quad (14)$$

- Electromechanical modal coupling factor

The open circuit and short circuit normal modes are harmonic solutions of Equations (12) and (14), respectively, with  $\mathbf{F} = \mathbf{0}$ . These natural frequencies are used to calculate the generalized electromechanical modal coupling factor, for the system  $n$ th mode, defined by [16,17]:

$$k_n = \sqrt{\frac{(\omega_n^{\text{OC}})^2 - (\omega_n^{\text{SC}})^2}{(\omega_n^{\text{SC}})^2}} \quad (15)$$

where  $\omega_n^{\text{OC}}$  and  $\omega_n^{\text{SC}}$  are respectively the open-circuit and short-circuit  $n$ th system natural frequencies (i.e. with all piezoelectric patches short-circuited or open-circuited). This parameter characterizes the energy exchanges between the mechanical structure and the piezoelectric patches.

### 2.3 Structural acoustic problem with one piezoelectric patch connected to RL series shunt circuit

The above discretized formulation (Equation (10)) can be used for a wide range of applications of mechanicals structure coupled with acoustic domain

and associated with piezoelectric patches. It is particularly adapted to the case where the piezoelectric patches are "shunted", that is to say connected to a passive electrical network [18]. In this case, neither  $\mathbf{V}$  nor  $\mathbf{Q}$  are prescribed by the electrical network but the latter imposes only a relation between them. In the case of a resonant shunt connected to one patch and composed of a resistance  $R$  and an inductance  $L$  in series (figure 2), we have this additional relation between electrical potential difference  $V$  and the electric charge  $Q$ :

$$L\ddot{Q} + R\dot{Q} + V = 0 \quad (16)$$

Due to the direct piezoelectric effect, the piezoelectric patch converts a fraction of the mechanical energy of the vibrating structure into electrical energy which can be dissipated through the resistive components of the  $RL$  circuit. It is well known that the damping effect due to this circuit is maximum when the resonance circular frequency  $1/\sqrt{LC}$  of the shunt circuit is tuned on the circular frequency of the structural-acoustic eigenmode to be controlled. The resistance  $R$  and the inductance  $L$  can be adjusted and properly chosen so as to maximize the damping effect (see subsection 3.2).

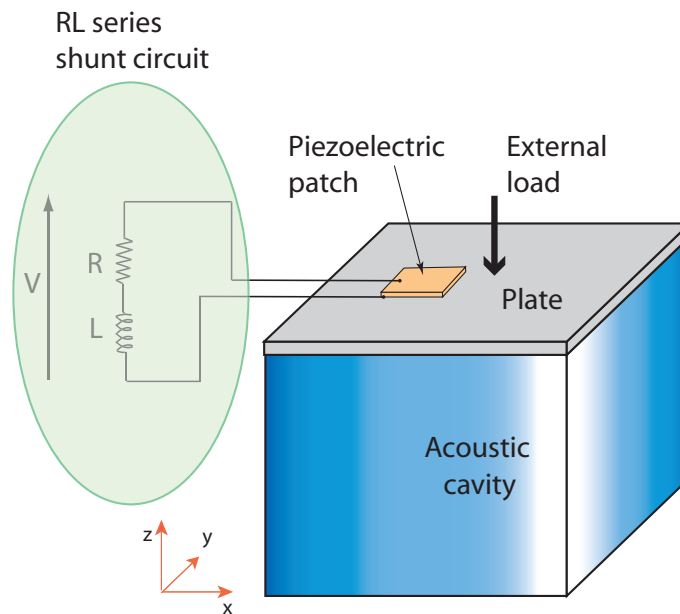


Fig. 2. Fluid/piezoelectric-structure coupled system.

Using the second row of Equation (10) and noting that in the case of a single piezoelectric patch  $\mathbf{K}_V = C$ , the degrees-of-freedom associated with the electrical potential difference  $V$  can be expressed in terms of structural displacements  $\mathbf{U}$  and electric charge  $Q$  as

$$V = \frac{1}{C} \mathbf{C}_{uv}^T \mathbf{U} + \frac{Q}{C} \quad (17)$$

Thus, after substitution of  $V$  into Equation (16) and using Equation (10), we

get the following electro-mechanical-acoustic system:

$$\begin{bmatrix} \mathbf{M}_u & \mathbf{0} & \mathbf{0} \\ \mathbf{0} & L & \mathbf{0} \\ \mathbf{C}_{up}^T & \mathbf{0} & \mathbf{M}_p \end{bmatrix} \begin{bmatrix} \ddot{\mathbf{U}} \\ \ddot{Q} \\ \ddot{\mathbf{P}} \end{bmatrix} + \begin{bmatrix} \mathbf{0} & \mathbf{0} & \mathbf{0} \\ \mathbf{0} & R & \mathbf{0} \\ \mathbf{0} & \mathbf{0} & \mathbf{0} \end{bmatrix} \begin{bmatrix} \dot{\mathbf{U}} \\ \dot{Q} \\ \dot{\mathbf{P}} \end{bmatrix} + \begin{bmatrix} \mathbf{K}_u & \frac{1}{C}\mathbf{C}_{uV} & -\mathbf{C}_{up} \\ \frac{1}{C}\mathbf{C}_{uV}^T & \frac{1}{C} & \mathbf{0} \\ \mathbf{0} & \mathbf{0} & \mathbf{K}_p \end{bmatrix} \begin{bmatrix} \mathbf{U} \\ Q \\ \mathbf{P} \end{bmatrix} = \begin{bmatrix} \mathbf{F} \\ 0 \\ \mathbf{0} \end{bmatrix} \quad (18)$$

with appropriate initial conditions. Note that this  $(\mathbf{U}, Q, \mathbf{P})$  formulation is well suited for switch shunting applications.

#### 2.4 Application to shunt synchronized switch damping on inductance

The synchronized switch damping on indicator (SSDI) technique is a semi-passive approach that was developed to address the problem of structural vibration damping [17,19–21]. This particular nonlinear technique consists of adding a switching device in parallel with the piezoelectric patch. This device is composed of a switch, an inductance  $L$  and a resistance  $R$  connected in series. Since the internal inductance and resistance of the piezoelectric material are very low in comparison to inductance and resistance of the shunt circuit, the patch can be modeled by a capacitance  $C$ , as shown in Figure 3. The switch is nearly always open, except when a displacement extremum occurs. At this moment the switch is closed. The capacitance  $C$  of the piezoelectric patch and the inductance  $L$  thus constitute an electric oscillator. The switch is kept closed until the voltage  $V$  on the piezoelectric element has been inversed. It corresponds approximately to a time  $T = \pi\sqrt{LC}$  equal to a half pseudo-period of the electric shunt circuit. There is no particular value to which the inductance should be tuned, but it is chosen to get an inversion time  $T$  roughly between ten and fifty times lower than the mechanical vibration period of interest [17,21]. When the switch is open and if no load is connected, the

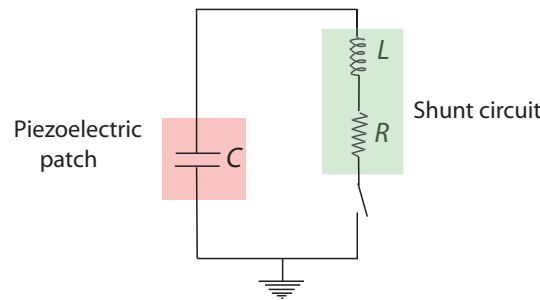


Fig. 3. PZT equivalent electrical circuit scheme within a switched shunt architecture.

outgoing piezo current is null and then the voltage and the displacement vary proportionally. In Figure 4, the typical voltage and displacement waveforms are shown with a zoom on the voltage inversion.

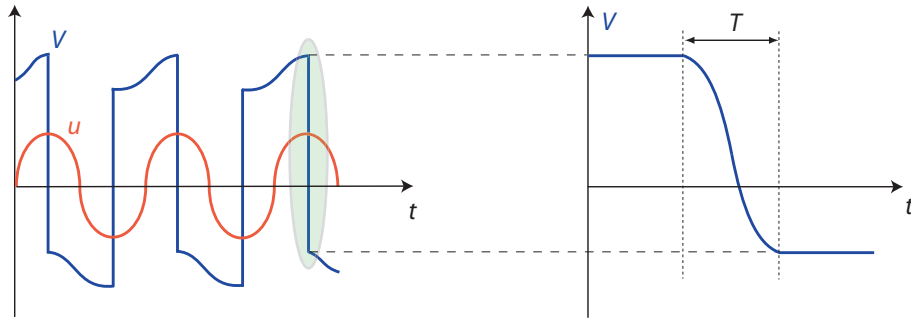


Fig. 4. Typical voltage and displacement waveforms for SSDI technique.

The synchronized switch damping technique provides more robustness if compared to the inductive shunt. The main advantages of this technique can be summarized with the following points:

- no need of large tuned inductor;
- large band pass;
- low sensitivity to environmental drifts;
- good performance in transient regime;
- no power amplifier and power supply needed;
- no complex control logic;
- simple and cheap hardware.

### 3 Numerical examples

We present in this section the analysis of an interior damped structural-acoustic systems using (i) an inductive shunt and (ii) a synchronised switch damping technique, according to the finite element formulation described in the previous section. First, the modal analysis of the electro-mechanical-acoustic problem is presented. Then, the inductive shunt and switched techniques are compared in terms of attenuation of vibration and sound pressure level.

We consider a 3D acoustic cavity of size  $A=0.5$  m;  $B=0.3$  m and  $C=0.4$  m along the directions  $x$ ,  $y$  and  $z$ , respectively. The cavity is completely filled with air (density= $1.225$  kg/m<sup>3</sup>; speed of sound= $340$  m/s). The cavity walls are rigid except the top one which is a flexible aluminium plate of thickness 1 mm clamped at its edges. The density of the plate is  $2700$  kg/m<sup>3</sup>, the Young modulus  $72$  GPa and the Poisson ratio  $0.35$ . On the top surface of the plate, a PZT patch is bonded, whose in plane dimensions are  $0.12$  m by  $0.10$  m along  $x$  and  $y$  and  $0.5$  mm thick (see Figure 5). The mechanical characteristics of the piezoelectric material (PZT-5H), related to the constitutive relations (1) and (2), are given in Table 1.

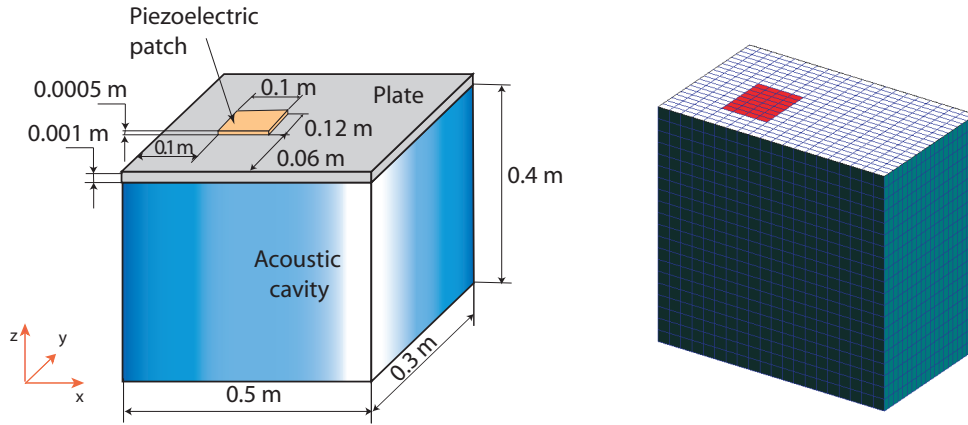


Fig. 5. Fluid/piezoelectric-structure coupled system: (a) geometrical data and (b) mesh (to scale).

Table 1

Mechanical data of piezoelectric PZT-5H material.

Material properties	
$c$ (GPa)	$c_{11} = c_{22} = 126, c_{33} = 117$ $c_{13} = c_{23} = 84.1, c_{12} = 79.5$ $c_{44} = c_{55} = 23, c_{66} = 23.3$
$e$ (C.m <sup>-2</sup> )	$e_{15} = e_{24} = 17, e_{33} = 23.3$ $e_{31} = e_{32} = -6.5$
$\epsilon$ (10 <sup>-10</sup> F.m <sup>-1</sup> )	$\epsilon_{11} = \epsilon_{22} = 150.3, \epsilon_{33} = 130$
$\rho$ (kg.m <sup>-3</sup> )	7500

Concerning the finite element discretization, we have used, for the structural part, 400 four-node membrane-shear-bending plate elements (based on the first-order shear deformation theory) with five degrees-of-freedom per node and a selective reduced integration on the transverse shear. The portion of the plate covered by the PZT patch and the patch itself has been modeled according to the first-order shear deformation laminate theory [22]. As discussed in the previous sections, only one electrical degree of freedom is used to represent the electrical charge  $Q$  in the patch. The electromechanical coupling is obtained using the submatrix  $\mathbf{C}_{uV}$  (see Equation (9c) or (9d)).

The acoustic cavity is discretized using  $20 \times 20 \times 20$  hexahedric elements with one degree-of-freedom per node corresponding to the acoustic pressure. The structural and acoustic meshes are compatible at the interface and the fluid-structure coupling is realized through the  $\mathbf{C}_{up}$  matrix (see Equation (9e) or (9f)).

It is important to note that Equation (12) (respectively (14)) has been used

to compute the fluid-structure normal modes in the open circuit case ( $Q = 0$ ) (respectively short circuit case ( $V = 0$ )) and Equation (18) for switch shunt application.

### 3.1 Modal analysis of the acoustic/structure/piezoelectric-patch coupled problem

Table 2 presents the eigenfrequencies in three following cases: (i) the 3D rigid acoustic cavity; (ii) the clamped plate with the patch short circuited; and (iii) the plate/acoustic-cavity coupled system in the short circuit case. The first nine coupled frequencies are associated with the first vibration modes of the structure (lower than 350 Hz), and the last coupled frequency corresponds to the first acoustic mode in rigid cavity. This can be confirmed by comparing the mode shapes in case (iii) with those obtained in cases (i) or (ii) which are not shown here for sake of brevity. Moreover, as expected, the natural frequencies of the coupled modes (structure dominated) are lower than those for the structure in vacuum (except for the first mode) due to the "added-mass effect" of the fluid.

Table 2

Computed frequencies (Hz) of the structural-acoustic coupled system.

Fluid in a rigid cavity	Structure without fluid	Coupled problem	Type of coupled mode*
340.35	69.27	76.77	S
425.44	100.14	99.35	S
544.82	156.25	155.86	S
567.25	182.43	181.06	S
661.52	208.42	207.32	S
682.80	232.04	230.66	S
709.06	263.81	262.86	S
804.49	333.17	332.42	S
854.00	341.05	338.96	S
887.69	352.60	341.10	F

\* S for structure mode and F for fluid mode.

For illustration purpose, Figure 6 shows the deformed plate and the pressure field for the first ten vibration modes in the coupled case. The first eight modes are clearly dominated by the structural displacement which induced the pressure level in the cavity. As shown in Table 2, the frequencies of coupled

modes 9 and 10 are close to the first frequency of the acoustic mode in rigid cavity and to the ninth mode of the structure in a vacuum. Thus, mode shapes (in terms of pressure and displacement) can be viewed as a combination of the shapes of the two associated uncoupled modes. We can also note that mode 9 is rather dominated by the structure displacement and mode 10 by the acoustic pressure.

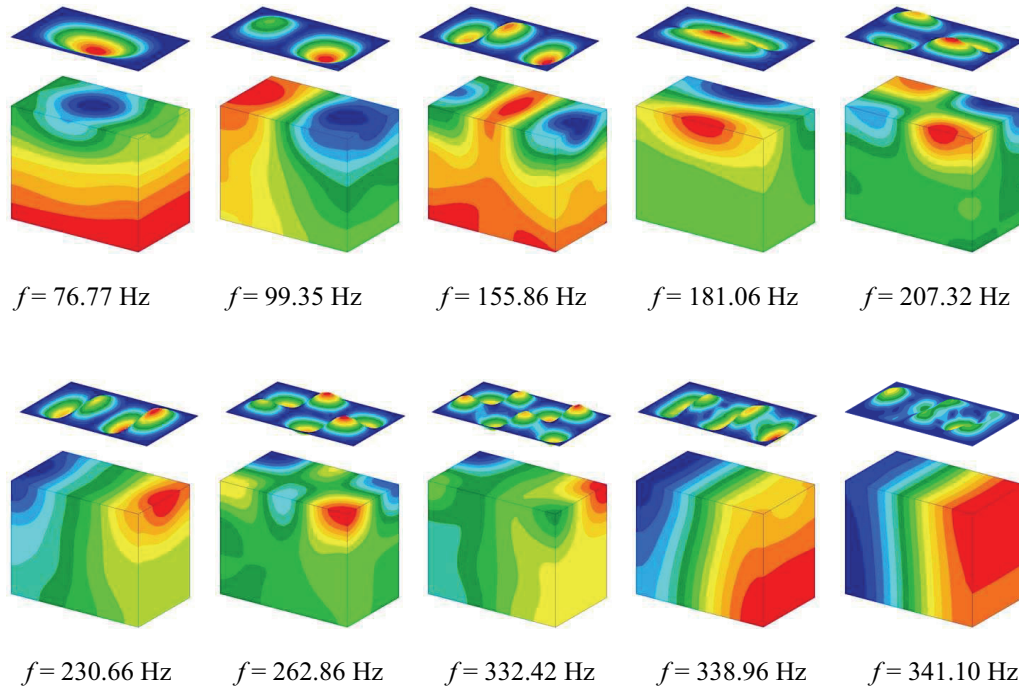


Fig. 6. Fluid-structure coupled modes : fluid pressure level and plate total displacement.

### 3.2 Transient analysis of the acoustic/structure/piezoelectric-patch coupled problem

The plate is now excited by a normal sinusoidal force applied at its center and at the considered resonance frequency. The vibration output is detected at the centre of the plate, where the displacement reaches a maximum, while the pressure is detected in the middle of the acoustic box. The responses, in the open circuit case and in the inductive and synchronized switch cases are plotted and compared in time domain.

For the resonant shunt technique, the resistor and inductor in the electrical circuit are tuned to achieve maximum energy dissipation from the mode to interest. Therefore, the optimal resistance and inductance for a series resonant

shunt can be calculated by [18,17]

$$R^{\text{opt}} = \frac{\sqrt{2k_n^2}}{C\omega_n^{\text{SC}}(1 + k_n^2)} \quad (19a)$$

$$L^{\text{opt}} = \frac{1}{C(\omega_n^{\text{SC}})^2(1 + k_n^2)} \quad (19b)$$

where  $\omega_n^{\text{SC}}$  is the short circuit natural frequency of the  $n$ th mode and  $k_n$  is the generalized electromechanical coupling coefficient given in Equation (15).

Table 3 presents the electrical parameters adopted in the numerical simulation of the inductive shunt and the switched shunt devices. In the resonant shunt case,  $R$  and  $L$  are obtained using their optimal values (Equations (19a) and (19b)) associated to the first mode and with the electromechanical coupling coefficient  $k_1 = 0.072$  ( $\omega_1^{\text{SC}} = 2\pi \times 76.77 \text{ rad.s}^{-1}$  and  $\omega_1^{\text{OC}} = 2\pi \times 76.97 \text{ rad.s}^{-1}$ ). In the switched shunt case, the chosen inductance is  $L = L^{\text{opt}}/100$ , corresponding to a switching period  $T$  twenty times lower than the mechanical period of the first mode. Moreover, in accordance with the advantages of this technique, the resistance value is chosen more than four times lower than the optimal resistance of the passive shunt case.

Table 3

Electrical parameters of the simulations.

	Inductive Shunt	Switched Shunt
$C$ (Farad)	$956 \times 10^{-9}$	$956 \times 10^{-9}$
$L$ (Henry)	4.5	$4.5 \times 10^{-2}$
$R$ (Ohm)	220	50

Since the working principle of the switched shunt system is characterized by fast state variations, due to the electric circuit quick commutation times, the system behaviour will suffer a continuous transient regime. Thus, a direct transient response analysis is needed. Computation in the time domain is performed using a direct implicit numerical scheme of the Newmark family algorithm. The output is computed assuming that the electrical circuit is closed or open (see Figure 7).

In Figures 8 to 11 the mechanical transverse displacement at the center of the plate and the sound pressure level in the middle of the acoustic cavity are plotted in three cases: (i) open circuit condition, (ii) inductive shunt, and (iii) switched shunt control. These time plots are obtained for two frequencies of the external sinusoidal excitation corresponding respectively to the frequency of the first and fourth mode of the open-circuited coupled system.

Even if the steady state is not reached in the open circuit case, due to the fact that no mechanical damping has been introduced in the model, we can

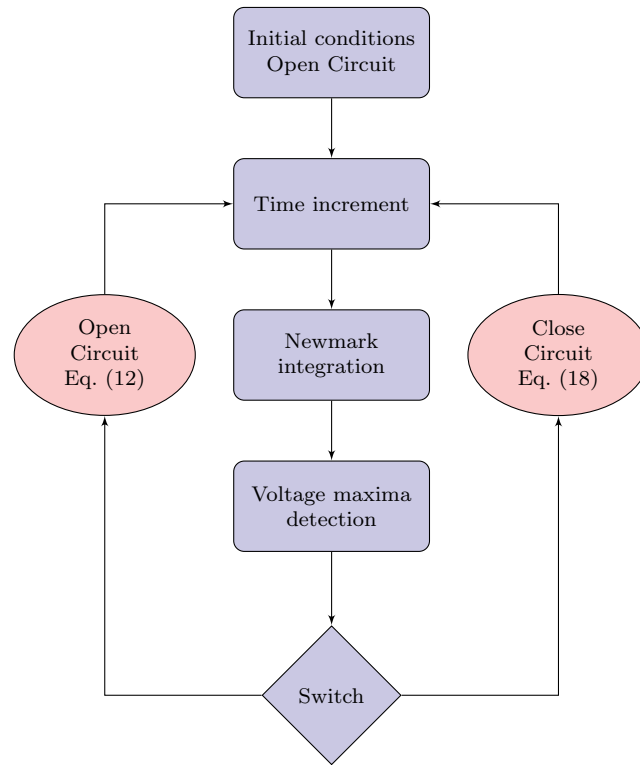


Fig. 7. Flowchart for the integration method used for the switch shunt system.

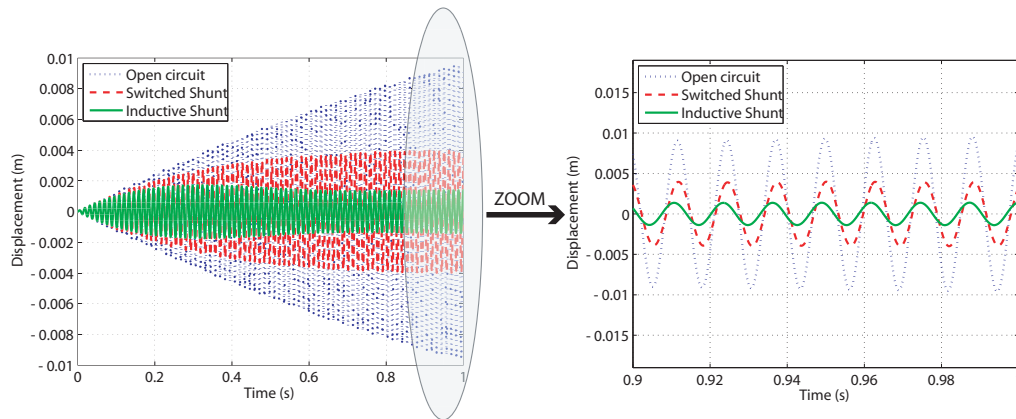


Fig. 8. Mechanical transverse displacement at the center of the plate under first mode excitation frequency.

observe from these first results the effect of the attenuation performed by the two electrical systems.

The effects of the inductive shunt are evident just for the first mode (Figures 8 and 10). The reason is due to the fact that the inductive shunt is tuned on the resonance frequency to be controlled, in the same way as the dynamic vibration absorber (or tuned-mass damper). So the electrical parameters should be changed according to the frequency of interest.

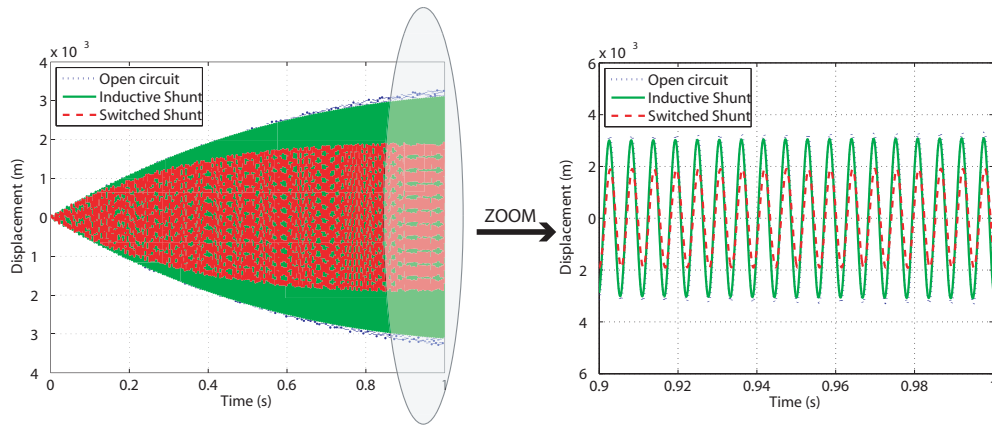


Fig. 9. Mechanical transverse displacement at the center of the plate under fourth mode excitation frequency.

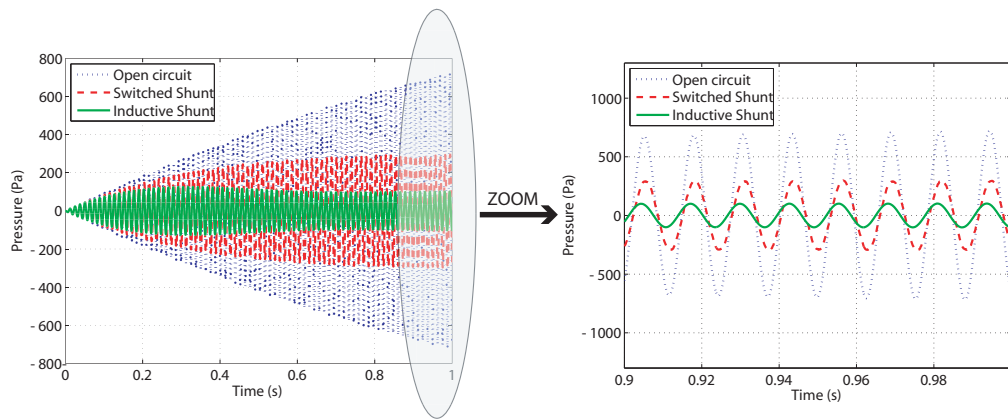


Fig. 10. Pressure level in the middle of the acoustic cavity under first mode excitation frequency.

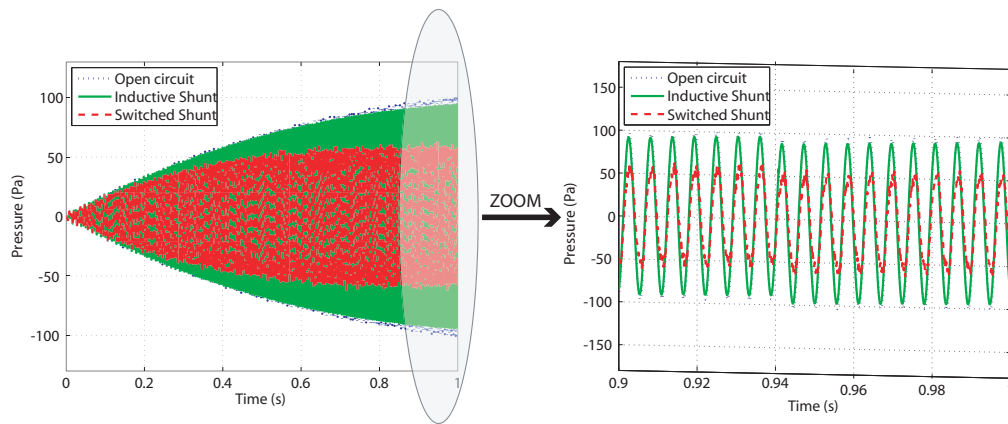


Fig. 11. Pressure level in the middle of the acoustic cavity under fourth mode excitation frequency.

On the other hand, the switched shunt damping system shows wide band performances since the amplitude of both modes have been successfully reduced. Moreover it is important to highlight that these results have been obtained

with a very low inductor and a low resistor that gives to the control system a higher thermal stability, very useful in aerospace applications. Finally no external power supply has to be added to the system.

## 4 Conclusion

We have presented in this paper a finite element formulation of structural-acoustic problems with shunted piezoelectric patches. Two different kind of vibration reduction techniques have been tested on an acoustic cavity coupled with elastic plate and with a surface-mounted piezoelectric patch: the passive inductive shunt and the semi-passive switched shunt. The numerical results show reduction of amplitudes achieved in low frequency range with the switch control using only one piezoelectric patch and without any signal amplification. Moreover, attenuations are obtained, in the present example, without optimization process to determine the best position of the patch. The results show the versatility of the proposed approach. Among future possible investigations, let us cite the problem of the experimental validation of the presented results, the analysis of more complex systems using appropriate reduced order models, and the optimization of the size and location of the piezoelectric patches in order to achieve high performances.

## 5 Acknowledgements

This research is partially supported by the European Community through the Marie Curie Research Training Network "A Computer Aided Engineering Approach to Smart Structures Design" under contract number MRTN-CT-2006-035559. The third author, Marie Curie Early Stage Researcher at CNAM/LMSSC during 2008/2009, is carrying a PhD between University of Naples and CNAM.

## References

- [1] W. Larbi, J.-F. Deü, and R. Ohayon. A new finite element formulation for internal acoustic problems with dissipative walls. *International Journal for Numerical Methods in Engineering*, 68(3):381–399, 2006.
- [2] G. A. Lesieutre. Vibration damping and control using shunted piezoelectric materials. *The Shock and vibration digest*, 30(3):187–195, 2008.

- [3] J. Kim, B. Ko, J. K. Lee, and C. Cheong. Finite element modelling of a piezoelectric smart structure for the cabin noise problem. *Smart Materials and Structures*, 8(3):380–389, 1999.
- [4] J. Lefèvre and U. Gabbert. Finite element modeling of vibro-acoustic systems for active noise reduction. *Technische Mechanik*, 25(3-4):241–247, 2005.
- [5] J. Ro and A. Baz. Control of sound radiation from a plate into an acoustic cavity using active constrained layer damping. *Smart Material and Structures*, 8(3):292–300, 1999.
- [6] S. Gopinathan, V. Varadan, and V.K. Varadan. Finite element/boundary element simulation of interior noise control using active-passive control technique. In *Mathematics and control in smart structures, SPIE proceedings, Vol. 3984*, pages 22–32, 2000.
- [7] I. Kaljevic and D.A. Saravanos. Steady state response of acoustic cavities bounded by piezoelectric composite shell structures. *Journal of Sound and Vibration*, 204(3):459–476, 1997.
- [8] D. Guyomar, T. Richard, and C. Richard. Sound wave transmission reduction through a plate using a piezoelectric synchronized switch damping technique. *Journal of Intelligent Material Systems and Structures*, 19(7):791–803, 2008.
- [9] B. Balachandran, A. Sampath, and J. Park. Active control of interior noise in a three-dimensional enclosure. *Smart materials and structures*, 5(1):89–97, 1996.
- [10] M. Ahmadian, K.M. Jeric, and D.J. Inman. An experimental evaluation of smart damping materials for reducing structural noise and vibrations. *Journal of vibration and acoustics*, 123(4):533–536, 2001.
- [11] J.-F. Deü, W. Larbi, and R. Ohayon. Piezoelectric structural acoustic problems: Symmetric variational formulations and finite element results. *Computer Methods in Applied Mechanics and Engineering*, 197(19-20):1715–1724, 2008.
- [12] O. Thomas, J.-F. Deü, and J. Ducarne. Vibrations of an elastic structure with shunted piezoelectric patches: efficient finite element formulation and electromechanical coupling coefficients. *International Journal for Numerical Methods in Engineering*, 80(2):235–268, 2009.
- [13] H.J.-P. Morand and R. Ohayon. *Fluid-Structure Interaction*. Wiley, New York, 1995.
- [14] R. Ohayon and C. Soize. *Structural Acoustics and Vibration*. Academic Press, San Diego, 1998.
- [15] A.C. Galucio, J.-F. Deü, and R. Ohayon. A fractional derivative viscoelastic model for hybrid active-passive damping treatments in time domain - application to sandwich beams. *Journal of Intelligent Material Systems and Structures*, 16(1):33–45, 2005.
- [16] ANSI/IEEE Standard 176-1987. *IEEE Standard on Piezoelectricity*, 1988.

- [17] L.R. Corr and W.W. Clark. Comparison of low-frequency piezoelectric switching shunt techniques for structural damping. *Smart Materials and Structures*, 11(3):370–376, 2002.
- [18] N.W. Hagood and A. von Flotow. Damping of structural vibrations with piezoelectric materials and passive electrical network. *Journal of Sound and Vibration*, 146(2):243–268, 1991.
- [19] L. Petit, E. Lefeuvre, C. Richard, and D. Guyomar. A broadband semi passive piezoelectric technique for structural damping. In *Smart Structures and Materials: Damping and Isolation, SPIE proceedings, Vol. 5386*, pages 414–425, 2004.
- [20] A. Badel, G. Sebald, D. Guyomar, M. Lallart, E. Lefeuvre, C. Richard, and J. Qui. Piezoelectric vibration control by synchronized switching on adaptive voltage sources : Towards wideband semi-active damping. *The Journal of the Acoustical Society of America*, 119(5):2815–2825, 2006.
- [21] A. Badel, M. Lagache, D. Guyomar, E. Lefeuvre, and C. Richard. Finite element and simple lumped modeling for flexural nonlinear semi-passive damping. *Journal of Intelligent Material Systems and Structures*, 18(7):727–742, 2007.
- [22] J.N. Reddy. *Mechanics of laminated composite plates and shells: theory and analysis*. CRC Press, Boca Raton, Florida, 2004.



# STRUCTURE BORNE SOUND CONTROL THROUGH PZT PATCH IN SWITCHED SHUNT CONFIGURATION: A NON STANDARD FINITE ELEMENT ANALYSIS

M. Ciminello<sup>a</sup>, L. Lecce<sup>a</sup>, A. Concilio<sup>b</sup>

<sup>a</sup> Aerospace Engineering Dept. DIAS - University of Naples "Federico II", Via Claudio 24 – 80125 Napoli.

<sup>b</sup> Italian Aerospace Research Centre – CIRA, Via Maiorise - 81043 Capua (CE)

In this work, a Natan/Matlab approach aimed at controlling a structural-acoustic system through a semi-active device, based on switched shunted piezoelectric elements, is presented. In order to develop a general-purpose procedure to model the coupled system (composed by the fluid, the structure and the piezoelectric-based device), a standard finite element code, according to the local equations describing the physics of the fully coupled system, has been developed in Matlab. After, the same test case is processed by means of a not standard general-purpose procedure. The simulation using commercial code such as Nastran/Matlab, is presented and validated. The considered coupled system consists of a classical elastic plate with a surface-mounted piezoelectric patch, coupled to a simple acoustic cavity, filled with an inviscid, compressible and barotropic fluid, gravity effect being neglected. Matrices are extracted and reassembled in Matlab where the electro-mechanical coupling matrices are suitably built using a proper strain actuation analytical model, in order to take into account the structural action of the piezoelectric laminate (concentrated moments at domain boundaries). Finally, taking advantage of Nastran modal-base computation, a reduced electro-mechanical fluid-structure system is obtained and solved in time domain. Numerical results are presented showing the performance of two numerical approaches on the sound pressure level and structural displacement reduction for the first bending mode and after validation, the not standard approach is adopted to compute the energy level reduction of the cavity for more multimode reduction.

**Keywords:** numerical modelling, noise reduction, switched shunt control, fluid-structure interaction

## 1.Introduction

In acoustic wave and in the vibration control field, the trend is to develop active techniques that can be an efficient strategy to reduce the broadband noise levels. The penalty to be paid is a higher complexity in the design and an external power supply required. Aiming at noise reduction, an approach is to reduce structural vibration, as a main source of acoustic radiation. A considerable number of works deals with the numerical and experimental development of techniques based on piezoelectric devices bonded or embedded in structural elements.

Kim and Ko [1] for instance worked on a FE model implementing piezoelectric elements. Optimisation procedure showed the structural regions presenting the maximum strain as the best actuators and sensors locations. In that case, the implemented active control system was a negative feedback. To take into account the acoustic pressure in the cavity but preserving a suitable size of the referred model, a classical modal reduction was accomplished. The principal advantage of this approach is the reduced size of the numerical problem. Active and passive devices may be combined. Ro and Baz [2] presented a similar work where the sound radiation from a vibrating flat plate, coupled with an acoustic cavity was controlled. A single patch of active constrained layer damping and active control treatments were used. Coupled finite element models were developed to investigate the fundamental phenomena governing the acoustic-structural interaction under the effects of control systems. Models allowed computing frequencies, mode shapes and sound radiation for different control gains. Experimental results indicated amplitude attenuation of 27, 54, and 75%, for controlling gains ranging in a magnitude, for the first resonance frequency. A different approach to noise radiation reduction into a cavity was introduced by Guyomar et al. [3]. A semi-active approach implementing a switch damping technique, synchronised with the recorded strain values was therein dealt with. The authors describe the results coming from exciting the plate via a loudspeaker and detecting the noise level of the sound waves generated to the outside. Plate vibrations speed was monitored in three cases: without control, with an inductive switched shunt on and with a voltage-driven inductive switched shunt. Acoustic pressure was measured at different locations, recording a max attenuation of 15 dB. In the present paper a FE modelling procedure is presented, directed to simulate a noise and vibration control system, implementing a switched shunt piezoelectric-based device. The specimen, referring to experimental test presented in [4], is a rigid box, 0.6 x 0.5 x 0.4

m with five rigid walls and a flexible 0.6 x 0.5 m plate, 6 mm thick. A single piezoceramic patch was eccentrically bonded on the plate, in order to detect a large number of modes. The patch was used both as a sensor and an actuator device, that would correspond to a collocated configuration in a SISO feedback control system. The plate was then excited by means of a transversal sinusoidal force. The structural vibration at the central node of the plate and the pressure level at 25 cm from the plate surface, within the cavity, were recorded and plotted as reference measures. Since the mean quadratic pressure level inside the cavity is the target parameter, it is also reported. In the first section of the paper, a variational formulation of the fluid-structure coupled problem is recalled from [5; 9] and the corresponding matrix equations are derived, following a finite element approach. In the second section, a Nastran-Matlab integrated tool is used. The fluid-structure matrices are extracted from Nastran and reassembled in Matlab, where equations are completed with the electro-mechanical matrices of the piezo. The system eigenvectors have been imported from Nastran as well and used to the modal reduction formulation of the fully coupled system. The comparison of the two approaches on the displacement and sound pressure level reduction has been presented. Finally the not standard approach is used to predict the energy level reduction of the cavity. An algorithm based on the well-established Beta-Newmark is used.

## 2. The electro-elasto-acoustic problem

Several formulations have been proposed. Non-symmetric formulations are usually obtained (“displacement-pressure” formulations) while symmetric equations can be derived through an appropriate choice of fluid field variables. The fluid is described through the substitution of  $p$  with the velocity potential [6]. It must be noted that the velocity potential formulation has the disadvantage that it leads to a symmetric but fictitious “damping” matrix requiring the use of complex eigenvalue methods. A classical finite element formulation will be used, following the content of [5], [9].

Assuming standard equation for elastic media, the fluid and the fluid structure interaction describing mathematics is derived. The local conservative equation of the fluid structure coupled system in the time domain is presented, as a function of the structural displacement  $u$ , and the fluid pressure  $p$  [9].

The fluid structure equations are then assembled with the piezoelectric device electro mechanical matrices [5]. Finally, the electrical contributions of the shunt circuit are included [9].

### 2.1. Variational formulation of the fully coupled system

The test function method is considered [6]. The following equations are derived:

$$\int_{\Omega_s} tr[\sigma(u)\varepsilon(\delta u)]dv + \rho_s \int_{\Omega_s} \frac{\partial^2 u}{\partial t^2} \cdot \delta u dv - \int_{\Sigma} p n \cdot \delta u ds = \int_{\Gamma_i} F_{ext} \cdot \delta u ds \quad (1)$$

Eq. (1) is a variational formulation of the problem and expresses the time response of the structure under the action of the fluid pressure:

$$\frac{1}{\rho_F} \int_{\Omega_F} \nabla p \cdot \nabla \delta p dv + \frac{1}{\rho_F c_F^2} \int_{\Omega_F} \frac{\partial^2 p}{\partial t^2} \cdot \delta p dv + \int_{\Sigma} \frac{\partial^2 u}{\partial t^2} \cdot n \delta p ds = 0 \quad (2)$$

Eq. (2) may be read as a variational formulation of the problem describing the pressure time response of a fluid under a structural action. Finally (1) and (2) must be completed adding the electro-mechanical equation following again, the procedure well described in [5]:

$$\sum_{p=1}^P \delta V_{CV} - \sum_{p=1}^P \frac{\delta V}{h} \int_{\Omega_p} e_{ikt} \varepsilon_{kl} n_i d\Omega = \sum_{p=1}^P \delta V_Q \quad (3)$$

### 2.2. “Standard” finite element formulation of the fully coupled system

The variational expressions (1-3) can be written in a more compact form as:

$$\int_{\Omega_s} tr[\sigma(u)\varepsilon(\delta u)]dv \Rightarrow \delta U^T K_u U$$

$$\rho_s \int_{\Omega_s} \frac{\partial^2 u}{\partial t^2} \cdot \delta u dv \Rightarrow \delta U^T M_u U$$

(4)

$$\int_{\Sigma} p n \cdot \delta u ds \Rightarrow \delta U^T C_{up} P$$

$$\int_{\Gamma_i} F_{ext} \cdot \delta u ds \Rightarrow \delta U^T F$$

$$\frac{1}{\rho_F} \int_{\Omega_F} \nabla p \cdot \nabla \delta p dv \Rightarrow \delta P^T K_P P$$

$$\frac{1}{\rho_F c_F^2} \int_{\Omega_F} \frac{\partial^2 p}{\partial t^2} \cdot \delta p dv \Rightarrow \delta P^T M_P P$$

$$\int_{\Sigma} \frac{\partial^2 u}{\partial t^2} \cdot n \delta p ds \Rightarrow \delta P^T C_{up}^T U$$

(5)

and

$$\sum_{p=1}^P \frac{V}{h} \int_{\Omega_p} e_{kij} n_k \delta \varepsilon_{ij} d\Omega \Rightarrow \delta U^T K_{uV} V$$

$$\sum_{p=1}^P \frac{\delta V}{h} \int_{\Omega_p} e_{ikl} \varepsilon_{kl} n_i d\Omega \Rightarrow \delta V^T K_{uV}^T U$$

$$\sum_{p=1}^P \delta V C V \Rightarrow \delta V^T K_{uV} V$$

$$\int_{\Gamma_\sigma} F \delta u ds \Rightarrow \delta U^T F$$

$$\sum_{p=1}^P \delta V Q \Rightarrow \delta V^T Q$$

(6)

The finite element equation can be finally assembled in the classical form where the voltage has been replaced by the electrical charge more suitable for piezoceramics in shunt circuits (7):

$$\begin{bmatrix} M_u & 0 & 0 \\ C_{up}^T & M_p & 0 \\ 0 & 0 & L \end{bmatrix} \begin{Bmatrix} \ddot{u} \\ \ddot{p} \\ \ddot{q} \end{Bmatrix} + \begin{bmatrix} 0 & 0 & 0 \\ 0 & 0 & 0 \\ 0 & 0 & R \end{bmatrix} \begin{Bmatrix} \dot{u} \\ \dot{p} \\ \dot{q} \end{Bmatrix} + \begin{bmatrix} K_u & -C_{up} & K_{uq} \\ 0 & K_p & 0 \\ K_{uq}^T & 0 & 1/C_0 \end{bmatrix} \begin{Bmatrix} u \\ p \\ q \end{Bmatrix} = \begin{Bmatrix} F \\ 0 \\ 0 \end{Bmatrix} \quad (7)$$

Equation (7) is first solved by a dedicated finite element code describing the full coupled system [4]. After, for the same test case, the matrices will be extracted and reduced by means of a suited modal base from Nastran and used in an original general-purpose integrated Nastran/Matlab tool, as described in what follows.

### 3. Not standard finite element formulation of the electro-mechanical piezo effect

An elementary rectangular PZT plate is taken into account to derive the relative FE model. Since a piezo bonded on the plate transfers both bending and in-plane actions to the structure, each node of the 2D element shall have three translational and three rotational DOF's, for a total of six [10].

### 3.1 Converse coupling matrix

To estimate the bending actions, transmitted by the PZT elements (moments) to the structure, it is necessary to establish a relation between the voltage supply and the actuator authority. This is known in literature as the inverse coupling matrix. Moment related to the voltage  $V$  may be computed according to the following eq. (8):

$$M_{x,y} = l E_s \int_{-\frac{t_s}{2}}^{+\frac{t_s}{2}} \varepsilon_{x,y}(l, z) z dz \quad (8)$$

In the equation, any strain actuation model may be taken into account. In the specific case of this work, the 2D model of Lecce-Concilio was considered [11]. According to it, the following expressions are found, in the hypothesis of perfect bonding:

$$\begin{aligned} \varepsilon(z) &= \varepsilon_i \frac{2z}{t_s}, \quad \text{being} \\ \varepsilon_i &= 6\Lambda \frac{\bar{t}^2 + \bar{t}}{\varphi \bar{t}^3 + 6\bar{t}^2 + 12\bar{t} + 8} \\ \bar{t} &= \frac{t_s}{t_p} \\ \varphi &= \frac{E_s}{E_p} \frac{1 - \nu_p}{1 - \nu_s} \end{aligned} \quad (9)$$

The free strain,  $\Lambda = V d_{31}/t_p$ , is defined as the strain occurring under a given voltage,  $V$ , when the piezoelectric element is completely unconstrained. A numerical procedure may be assessed to evaluate the PZT transmitted moments in a numerical code like the MSC/Nastran, in order to face also different and more complicated geometries. A thermal load is applied, while the device is given an equivalent thermal coefficient in order to replicate the voltage effect. MSC/Nastran is in fact not able to directly simulate a piezoelectric material. PZT strain are then retrieved and used to compute the moments, following equation (8). Standing on this assumption, a 3D FE model of the piezoelectric patch, bonded onto the structure is realized and assigned with the suitable thermal coefficient:

$$\alpha_{eq} = \frac{d_{31}}{t_p} \quad (10)$$

Operatively, a HEXA8 FE model is realised, simulating a piezoceramic – aluminium laminate . The elements are assumed to be perfectly bonded each other. Because the problem symmetry a quarter model is built, properly constrained (symmetry conditions applied). In Table 1, FEM characteristics are summarised, with reference to the isolated PZT element.

PZT FEM	
Finite element type	HEXA8
Mesh discretization	200×200×6
N° mech dof per node	6
Thermal coefficient ( $d_{31}/t_p$ )	1.7e-7

Table 1. PZT-wafer finite element parameters

Moment (Nm)	Theoretical	Numerical
$\alpha_x$	1.2e-3	1.3e-3
$\alpha_y$	1.5e-3	1.6e-3

Table 2. PZT transmitted moments for unit voltage

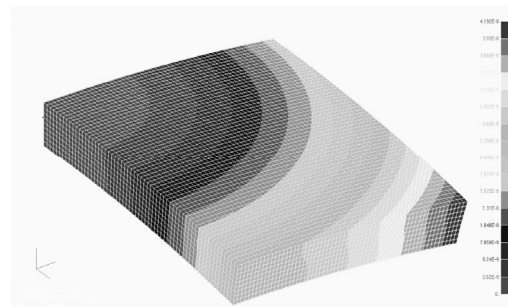


Figure 1. PZT displacement field, static analysis

A static analysis in Figure 1 for the free PZT is performed to estimate the strain. The moments transmitted by the piezo around x and y axes, indicated as  $\alpha_x$  and  $\alpha_y$  respectively, are computed and the comparison between numerical and theoretical ones, are reported in Table 2.

In a 9-node grid (Figure 2), 6-DOF node, the PZT FE representation (its print over the structure) presents 54 DOF.

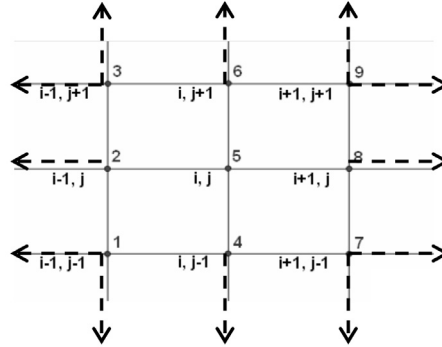


Figure 2. PZT grid

If a symmetrical couple of piezo is considered, axial forces may be neglected and the only transmitted load is a moments system. If, for the sake of simplicity, the grid nodes of the piezo are considered consecutive:

$$D_{uq} = \frac{1}{C_p} [0., \dots 0., \alpha_x, \alpha_y, 0., \dots 0.]_{1 \times 54}^T \quad (11)$$

### 3.2 Direct coupling matrix

The coupling matrix, linking piezo deformation to the voltage induced by the circuit, may be estimated by computing the normal displacement  $w$  second derivative along the in-plane directions, according to the definition of the PZT direct effect [10]. The voltage  $V$  induced by the structural strains occurring in both the in-plane directions may be estimated as:

$$V = g_{31} \frac{E_p t_p}{(1 - \nu_p)} \cdot \bar{\epsilon} \quad (12)$$

If the same discretization applied for the actuator is hold for sensing, according to the reference dotted line of Figure 4, the “global” deformation sensed by the piezo may be estimated as follows:

$$\bar{\epsilon} = \left( \frac{t_p + t_s}{2} \right) \left[ \frac{w_{i-1,j} - 2w_{i,j} + w_{i+1,j}}{\Delta x^2} + \frac{w_{i,j-1} - 2w_{i,j} + w_{i,j+1}}{\Delta y^2} \right] \quad (13)$$

Matrix  $G_{qu}$  is obtained by arranging the expressions above, eq. (12) and (13), in the following way:

$$\underline{G}_{uq} = g_{31} \frac{E_p t_p}{C_p (1 - \nu_p)} \left( \frac{t_s + t_p}{2} \right) \cdot \left[ 0, \dots, \frac{1}{\Delta x^2}, 0, \dots, 0, \frac{1}{\Delta y^2}, -2 \left( \frac{1}{\Delta x^2} + \frac{1}{\Delta y^2} \right), \frac{1}{\Delta y^2}, 0, \dots, 0, \frac{1}{\Delta x^2}, \dots, 0 \right]_{1 \times 54} \quad (14)$$

## 4. Modal reduction

For very large problems, modal reduction may significantly reduce the computational times. Being  $\Phi_{up}$  the eigenvector matrix (extracted with Nastran) of the non-dissipative system, the orthogonal transformation reduces the system matrices to:

$$\{\Phi_{up}\}^T [M] \{\Phi_{up}\} \ddot{\xi} + \{\Phi_{up}\}^T [C] \{\Phi_{up}\} \dot{\xi} + \{\Phi_{up}\}^T [K] \{\Phi_{up}\} \xi = \{\Phi_{up}\}^T \{F(t)\} \quad (15)$$

Matrix  $C$  in eq. (15) is not a damping matrix as previously mentioned, so it does not indicate any energy dissipation occurring in the system. In order to introduce some dispersion, a classical proportional damping (Rayleigh damping) may be addressed. Damping proportionality is preserved in the reduced system described in [13].

In order to specify suitable values for damping, the classical relation between the critical damping ratio and the Rayleigh damping parameters is used:

$$\zeta_i = \frac{(\alpha_R / \omega_i + \beta_R \omega_i)}{2} \quad (16)$$

The parameters  $\alpha_R$  and  $\beta_R$  may be computed at each frequency in the range of interest. Usually, a mean value is then extracted or, a best-fit spline iterative procedure [14], may be carried out.

Finally, the inductor, resistor, and blocked capacitor constant values are added to the model.

The complete assembled equation is the following (the adopted notation means the reduced matrices):

$$\begin{bmatrix} m_u & 0 & 0 \\ c_{up}^T & m_p & 0 \\ 0 & 0 & L \end{bmatrix} \begin{Bmatrix} \ddot{u} \\ \ddot{p} \\ \ddot{q} \end{Bmatrix} + \begin{bmatrix} c_u & 0 & 0 \\ 0 & 0 & 0 \\ 0 & 0 & R \end{bmatrix} \begin{Bmatrix} \dot{u} \\ \dot{p} \\ \dot{q} \end{Bmatrix} + \begin{bmatrix} k_u & -c_{up} & d_{uq} \\ 0 & k_p & 0 \\ g_{uq} & 0 & 1/C_0 \end{bmatrix} \begin{Bmatrix} u \\ p \\ q \end{Bmatrix} = \begin{Bmatrix} f \\ 0 \\ 0 \end{Bmatrix} \quad (17)$$

## 5. Time integration

In Figure 3, the switched shunt circuit is sketched.

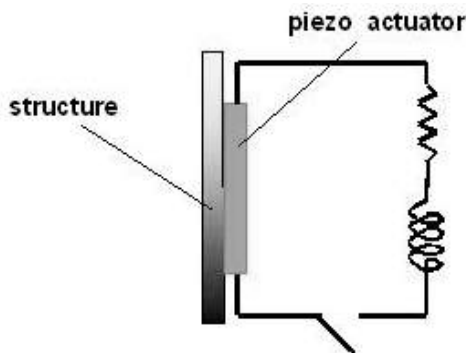


Figure 3. Synchronised Switch Circuit

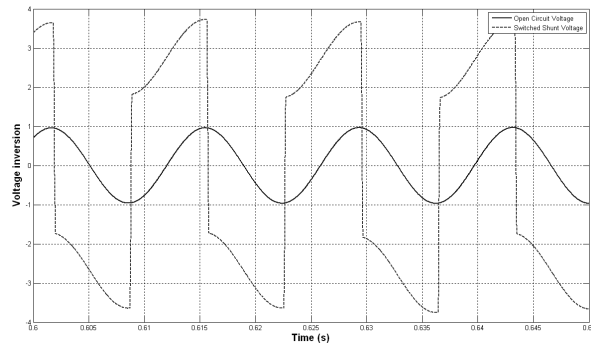


Figure 4. Open circuit vs. SSC V (straight/dotted line)

Switch is generally *off* (open). While vibrations occur, as strains attain the maxima values, switch is *on* (close) for a fraction of the excitation period. A current in the inductance is introduced, resulting in a charge inversion on the PZT electrodes. Previous results, [3], showed the system exhibit good performance for a switch period of 1/10 the excitation one. The *on-off* dynamics produce a naturally amplified voltage (Figure 4).

By the way, since the working principle of the switched shunt circuit is characterized by fast state variations, because of the quick commutation times, the system behaviour will be permanently in a transient regime. The FRF may not be implemented and the system shall be studied in time domain. A direct implicit Beta-Newmark type algorithm is adopted. The standard three-point method which is used to perform a step-by-step calculation is briefly presented starting from the linear motion equation:

$$[M] \{\ddot{u}(t)\} + [C] \{\dot{u}(t)\} + [K] \{u(t)\} = \{F(t)\} \quad (18)$$

A discrete time interval  $\Delta t$  is set as integration step. Displacement, velocity, acceleration and load,  $F$ , at three consecutive discrete steps are expressed as:

$$\begin{aligned} u &= \beta u_{n+1} + (1-2\beta)u_n + \beta u_{n-1} \\ \dot{u} &= \{u_{n+1} - u_{n-1}\} / 2h \\ \ddot{u} &= (u_{n+1} - 2u_n + u_{n-1}) / h^2 \\ F &= \beta F_{n+1} + (1-2\beta)F_n + \beta F_{n-1} \end{aligned} \quad (19)$$

By using the expressions defined in eq. (19), eq. (18) becomes:

$$[A_1](u_{n+1}) = [A_2] + [A_3](u_n) + [A_4](u_{n-1}) \quad (20)$$

Particularising the Beta-Newmark method at  $\beta=1$  (it is intrinsically stable if  $\beta>0.25$ ):

$$\begin{aligned} [A_1] &= \left[ \frac{M}{\Delta t^2} + \frac{C}{2\Delta t} + \frac{K}{3} \right] \\ [A_2] &= \frac{1}{3}(F_{n+1} + F_n + F_{n-1}) \\ [A_3] &= \left[ \frac{2M}{\Delta t^2} - \frac{K}{3} \right] \\ [A_4] &= \left[ -\frac{M}{\Delta t^2} + \frac{C}{2\Delta t} - \frac{K}{3} \right] \end{aligned} \quad (21)$$

The transient structural output is computed using a set of coupled equations describing the system *on-off* states [5]. Maxima are detected through a sine signal inversion procedure. In Table 3, the electrical parameters adopted in the numerical simulation of the control are summarized:

SSC State	<i>off</i>	<i>on</i>
Frequency: $f_{mech}$	Tab.9	-
Frequency: $f_{el}$	-	$10 \cdot f_{mech}$
Resistance: $R (\Omega)$	$1e10$	50
Inductance: $L (H)$	-	$1 / ((2 \cdot \pi \cdot f_{el})^2 \cdot C)$
PZT capacitance: $C (F)$	$265e-9$	$265e-9$

Table 3. The on-off circuit parameters

## 6. The test campaign: description and results

The system consists of an air-filled regular box. A single wall is flexible, while the others are rigid. The flexible plate is clamped at the edges. A PZT patch is eccentrically bonded on its surface. An eccentrically point force excites the system. Geometric and mechanic characteristics of the test specimen are reported in Tables 4-6:

PLATE	
Material	Steel
In-plane dimensions (m)	0.60×0.50
Thickness (m)	0.006
Young modulus (GPa)	144
Poisson ratio	0.35
Density (Kg/m <sup>3</sup> )	7700

Table 4. Mechanic and geometric plate parameters

PZT	
Material	PPK-11
N° of PZT	1
In-plane dimensions (m)	0.12×0.10
Thickness (m)	0.002
Young modulus (GPa)	59
Poisson ratio	0.34
Density (Kg/m <sup>3</sup> )	8100
$g_{31}$ (Vm/N)	$8.0e-3$
$d_{31}$ (C/N)	$3.5e-10$

Table 6. Mechanic and geometric PZT parameters

<b>FLUID</b>	
<b>Material</b>	Air
<b>In-plane dimensions (m)</b>	0.60×0.50
<b>Thickness (m)</b>	0.40
<b>Sound velocity (m/s)</b>	340
<b>Density (Kg/m<sup>3</sup>)</b>	1225

**Table 5. Physic and geometric fluid parameters**

### 6.1 Modal analysis

In order to validate the FE implementation of the proposed model, a modal analysis was preliminarily carried out. Herein the numerical computation of the eigenvalues of the plate, the cavity and the coupled system is respectively presented, according to the main FE model characteristics, reported in the following Tables 7-9:

<b>PLATE</b>	
<b>Finite element type</b>	QUAD4
<b>Mesh discretization</b>	10×10
<b>N° nodes</b>	121
<b>N° constrained nodes</b>	40
<b>N° mech dof per node</b>	6
<b>Total dof</b>	486
<b>Constrained type</b>	Four clamped edges

**Table 7. FE parameters of the plate model**

<b>FLUID</b>	
<b>Finite element type</b>	HEXA8
<b>Mesh discretization</b>	10×10×10
<b>N° nodes</b>	1331
<b>N° mech dof per node</b>	1
<b>Total dof</b>	1331

**Table 8. FE parameters of the fluid model**

Table 9 presents the first eight eigenfrequencies for the considered isolated systems (elastic plate and fluid, contained in a rigid box). The columns corresponds, respectively, to the FE modelling and the theoretical values as computed in [15]. In the next Table 10, the values of the coupled system eigenfrequencies are reported, comparing the Nastran results with what obtained in [4].

<b>Eigenfrequencies (Hz)</b>			
<b>PLATE</b>		<b>FLUID</b>	
<b>Nastran</b>	<b>Ref. [15]</b>	<b>Nastran</b>	<b>Ref. [15]</b>
153.2	152.2	284.4	283.3
274.1	273.3	341.3	340.0
344.2	342.8	426.7	425.0
443.2	440.0	444.4	442.6
472.6	474.3	512.8	512.0
617.4	615.2	546.5	545.7
638.4	635.9	576.0	576.5

**Table 9. Isolated plate and fluid eigenfrequencies**

<b>Coupled System Eigenfrequencies(Hz)</b>	
<b>Nastran</b>	<b>Ref. [4]</b>
153.1	160.6
272.5	280.9
286.2	294.4
338.2	338.0
347.3	375.8
426.7	422.9
439.8	441.9

**Table 10. Eigenfrequencies of the coupled system**

In Figure 5, a scheme of the FE model of the rigid cavity is reported, evidencing the PZT location. First 7 fluid-structure eigenmodes are presented in Figure 6. Structural and fluid dominant modes are evident.

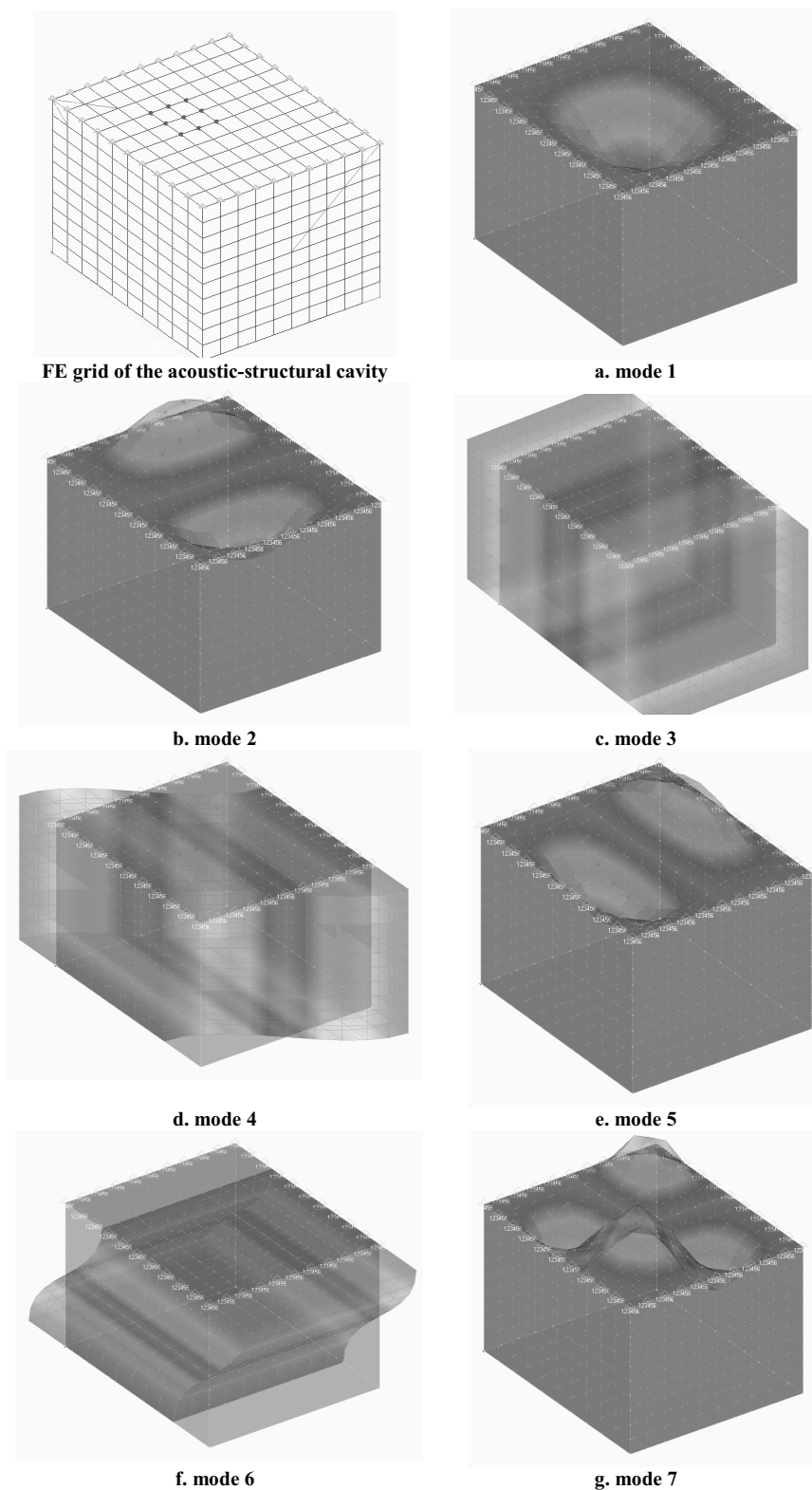


**Figure 5. Coupled system eigenmodes**

### 6.2. SSControl in time domain

The plate is excited by a sinusoidal wave, tuned on a single resonance frequency of the structure. Since we are interested in the structure borne sound, the SSC has been applied to the structural modes of interest. The full Matlab approach is now exploited. The effect of the SSC is evaluated for the first bending mode. The displacement and the pressure amplitude reductions are plotted in both time and frequency domain in Figures 6 and 7 respectively.

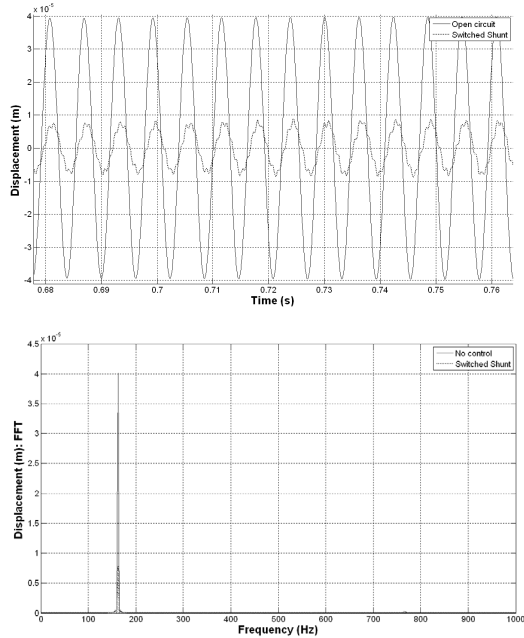


**Figure 6. Full Matlab control on the displacement level reduction for the first bending mode. Time domain (up); frequency domain (down).**

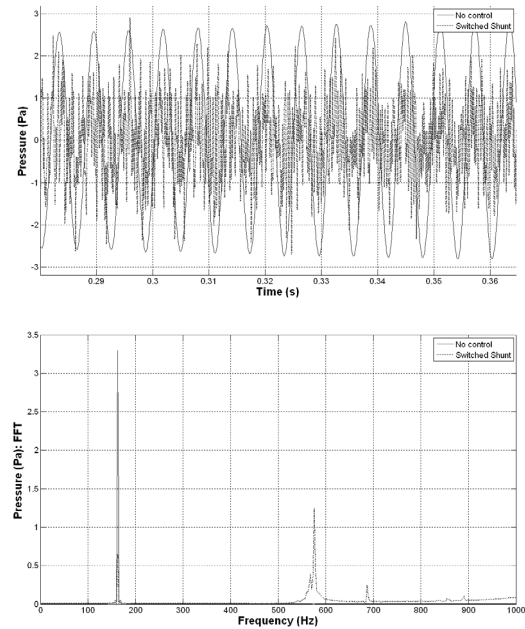


**Figure 7. Full Matlab control on the pressure level reduction for the first bending mode. Time domain (up); frequency domain (down).**

The integrated Nastran/Matlab reduced approach is now exploited. The effect of the SSC is again evaluated for the same bending mode. The displacement and the pressure amplitude reductions are plotted in both time and frequency domain in Figures 8 and 9 respectively.

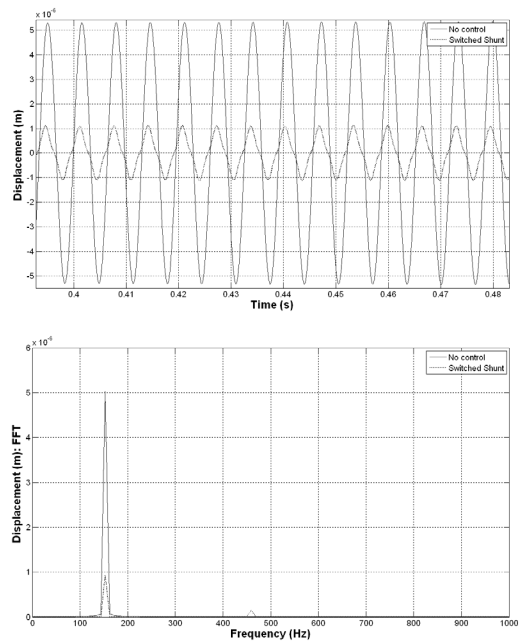


**Figure 8. Integrated Nastran/Matlab control on the displacement level reduction for the first bending mode. Time domain (up); frequency domain (down).**

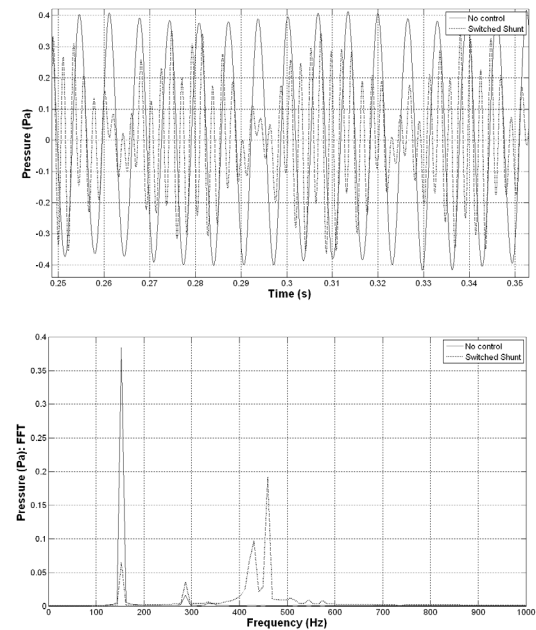


**Figure 9. Integrated Nastran/Matlab control on the pressure level reduction for the first bending mode. Time domain (up); frequency domain (down).**

In Table 11, structural and acoustic damping in dB are compared for modes 1:

Mode	Matlab model		Nastran/Matlab reduced model	
	Disp(dB)	Pres(dB)	Disp(dB)	Pres(dB)
1	13.7	14.8	14.6	15.8

**Table 11. Estimated structural and acoustic damping for the first bending mode**

In Table 12, structural and acoustic damping in dB are reported also for modes 2, 5 and 7, having adopted the reduced Nastran/Matlab approach:

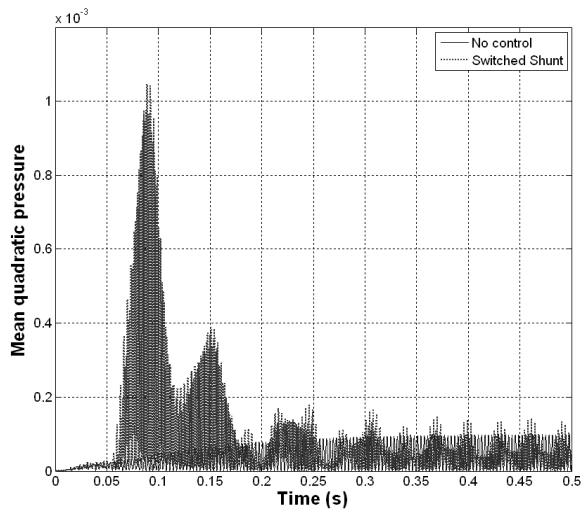
Mode	Frequency (Hz)	Damping (dB)	
		Structural	Acoustic
2	272.5	10.7	12.1
5	347.3	5.5	2.6
7	439.8	1.2	1.4

**Table 12. Estimated structural and acoustic damping for other structural modes.**

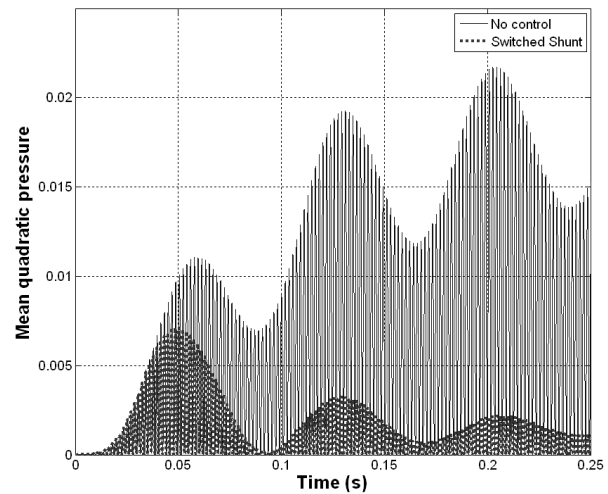
Being interested in the reduction of the acoustic pressure level of the whole cavity, for the investigated modes (Fig. 10), the mean quadratic pressure in the closure is employed as the indicator for this evaluation:

$$\langle p^2 \rangle = \frac{1}{2N_a} \sum_{i=1}^{dof} p_i^2 \quad (22)$$

where  $N_a$  is the nodes number in the acoustic domain FE grid and  $p_i$  is the pressure in node  $i$ .



**Time evolution of the mean energy pressure level (1<sup>st</sup> coupled mode)**



**Time evolution of the mean energy pressure level (2<sup>nd</sup> coupled mode)**

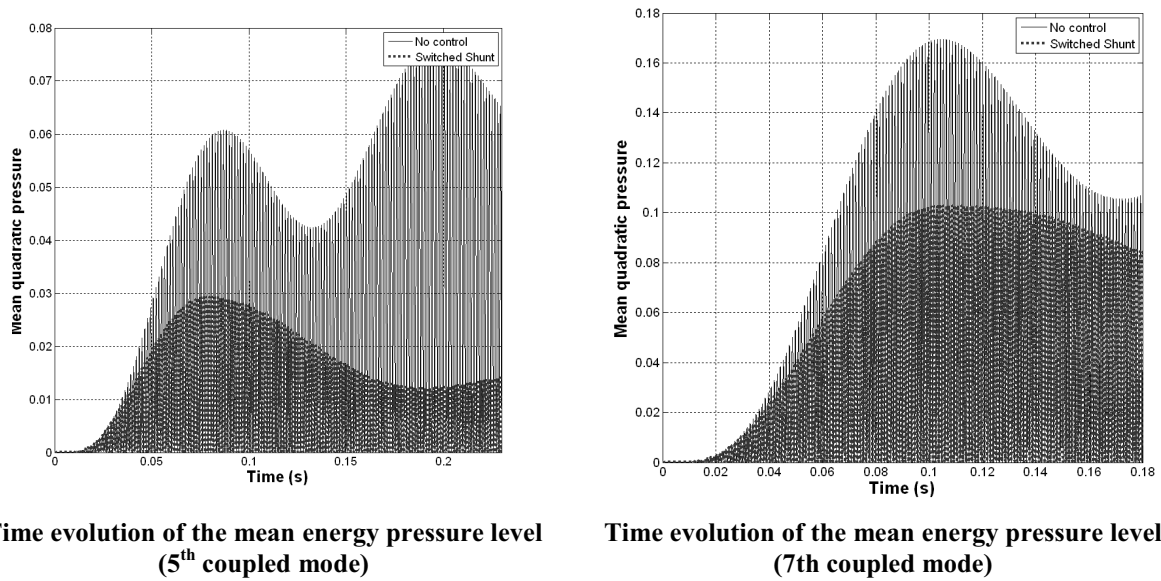


**Figure 10. Estimated mean quadratic pressure in the closure**

The associated pressure level, expressed in decibel (dB), is defined as:

$$SPL(dB) = 10 \log_{10} \frac{\langle p^2 \rangle}{4.10e^{-10}} \quad (23)$$

The acoustic energy level loss in dB, for the modes that were taken into account, are summarised in Table 12, according to the equation above.

Mode	Frequency (Hz)	Energy (dB)
1	153.1	-
2	272.5	8.21
5	347.3	3.95
7	439.8	1.10

**Table 12. SPL for the elasto-acoustic system**

## 7. Conclusions

A finite element code in Matlab environment has been developed to describe a fully electro-elasto-acoustic coupled system according to the local equation of the problem. A second “simplified” numerical approach has been implemented using the potentialities of Nastran to solve more general purpose configurations. The two approaches have been compared on the same test case. The numerical test showed a good correlation among this methods. Moreover a reduction of the vibration and pressure levels at the corresponding bending modes, have been plotted for the band range of interest of 500 Hz.

Significant performances were achieved in some cases. Results are remarkable if it is considered that no optimisation process was carried out to define the best position of the active element, as a function of the dynamic response of the plate.

Apart the possibility of referring to a large number of control system devices for multi-tone control, it should be taken into account also the capability of attenuation of one single piezo device without tuning.

The most important improvement factor of this work may be then identified as the following, planned to be object of further steps:

- Piezoelectric location, number and shapes on the structural element;
- The switch mechanism introduces high frequency noise, that can be reduced by low-pass filters;
- Cavity-dominated modes may be hardly controlled if the related structural energy is low, i.e. if the coupling is weak.

This last point is usual in vibration-oriented control system, oriented to acoustic suppression.

Damping showed to be a synthetic index well dealing with the effective system energy reduction and will be still considered in the next activities. The authors plan to set an experimental campaign in order to validate their models and evaluate all these additional aspects.

### Acknowledgments

The authors are pleased to thank Prof. Roger Ohayon at CNAM, with whom they had precious discussions over the Fluid-Structure Interaction subject.

This study is part of the PhD work of Monica Ciminello at the University of Naples, Department of Aerospace Engineering, Italy.

It has been partially funded by the European Union through the Marie Curie Research Training Network “A Computer Aided Engineering Approach to Smart Structures Design” under contract number MRTN-CT-2006-035559.

### References

1. Kim J. and Ko B., “Optimal design of a piezoelectric smart structure for noise control”, *Smart Material and Structures*, 7, pp. 801-808, 1998.
2. Ro J. and Baz A., “Control of sound radiation from a plate into an acoustic cavity using active constrained layer damping”, *Smart Material and Structures*, 8, pp. 292-300, 1999.
3. Guyomar D., Richard T. and Richard C., “Sound wave transmission reduction through a plate using a piezoelectric synchronized switch damping technique”, *Journal of Intelligent Material Systems and Structures*, published online, 2008.
4. Larbi W., Deü J.-F., Ohayon R., “Vibroacoustic finite element formulation for active-passive reduction of sound and vibration”, III ECCOMAS, Gdansk, Poland, July 9-11, 2007.
5. J.-F. Deü, W. Larbi, and R. Ohayon, “Piezoelectric structural acoustic problems: Symmetric variational formulations and finite element results”, *Computer Methods in Applied Mechanics and Engineering*, 197(19-20):1715–1724, 2008.
6. Morand H. J.-P., Ohayon R., *Fluid-structure interaction*, Wiley, 1995.
7. Fernholz C. M., Robinson J. H., “Fully-coupled fluid-structure vibration analysis using MSC-Nastran”, NASA internal report, December 1990.
8. Chargin M., Gartmeier O., “A Finite Element Procedure for Calculating Fluid-Structure Interaction Using MSC/NASTRAN”, NASA Technical Memorandum 102857.
9. Ciminello M., Deü J.-F., Ohayon R., Ameduri S., “Vibration reduction of structural-acoustic systems using synchronized switch damping techniques”, *Proceeding of 2008 ASME International Conference on Smart Materials, Adaptive Structures & Intelligent Systems*, October 28-30, 2008, Ellicott City, MD, USA. Paper - SMASIS08-320.
10. Ciminello M., Ameduri S., Concilio A., “FE Modelling of an Innovative Vibration Control Shunt Technique”, published on-line on the *Journal of Intelligent Materials Systems and Structures* Vol.19, N°8, August 2008 pp.875-887.
11. Concilio A., “Controllo attivo del rumore in cabina mediante attuatori piezoelettrici distribuiti sulla struttura”, PhD Thesis in Aerospace Engineering, University of Naples “Federico II” (in Italian).
12. Crawley E.F. and de Luis J., “Use of piezoelectric actuators as elements of intelligent structures”, *AIAA Journal*, 25(10), pp. 1373-1385, 1987.
13. Gladwell G.M.L. and Zimmermann G., “On Energy and Complementary Energy Formulations of Acoustic and Structural Vibration Problems. *J. of Sound and Vibration*, vol. 3, no. 3, 1966, pp. 233-241.
14. Wilson E. L. and Penzien J., “Evaluation of orthogonal damping matrix”, *Int. J. of Num Meth. in Engineering*, 4, 1972, 5-10.
15. Blevins R.D., “Formulas for natural frequency and mode shape”, Krieger Publishing C., Malabar, Florida, USA.



# International Conferences Abstract Proceedings

Monica Ciminello, Salvatore Ameduri, Antonio Concilio, **Simulation of a Combined Switched and Inductive Shunt Control Acting on a 2D Structure** – The 14th International Congress on Sound and Vibration, 9 – 12 July 2007, Cairns, Australia. Proceedings of the ICSV, Vol. 5952, pp. 314-323, 2007.

*The possibility of jointly implementing both a switched and an inductive shunt architectures may guarantee a more efficient multi mode control. As a matter of fact, it is possible to simultaneously control a low and a high frequency mode through a switch and an inductive architecture.*

---

Monica Ciminello, Salvatore Ameduri, Antonio Concilio, **Semi-analitical Solution of a Structural System Controlled by a Switched Shunt Architecture** – Proceeding of the 36th International Congress and Exhibition on Noise Control Engineering - Session ANVC "Active Noise and Vibration Control, Paper N° IN07-032. August 28 – 31, 2007 Istanbul - Turkey.

*The necessity of extending benefits due to this technique to more realistic applications has led to numeric solving schemes, prevalently based on a FE approach. However, due to the complexity of real applications, despite the efficient reduction techniques employed, numerical computations result heavy and, consequently, time consuming. On the contrary, a semi-analytical solution would allow eliminating the time consuming due to the integration.*

---

Monica Ciminello, Salvatore Ameduri, Antonio Concilio, Leonardo Lecce, **Flow-chart design of a pzt network based on a Switched Shunt Control** - Proceeding of the International Conference and Exhibition on new Actuators and Drive Systems (Actuator 2008), Session "Aerospace applications" P143. June 9 –11, Bremen, Germany.

*The simulation control scheme focusing attention on the FE model integration within the logic of control is fully described.*

---

Monica Ciminello, Jean-François Deü, Roger Ohayon, Salvatore Ameduri, **Vibration reduction of structural-acoustic systems using synchronized switch damping techniques** - Proceeding of 2008 ASME International Conference on Smart Materials, Adaptive Structures & Intelligent Systems, Paper - SMASIS08-320. October 28-30, 2008, Ellicott City, MD, USA.

*Numerical results concerning vibration reduction of structural-acoustic systems using the synchronized switch control technique has also taken into consideration. In order to develop a general procedure to model the coupled system (composed by the fluid domain, the structure and the piezoelectric elements), the idea is to use the performances of a standard commercial code such as Nastran.*

---

*Daniele Ghiglione, Wim Desmet, Monica Ciminello, Salvatore Ameduri, Antonio Concilio, **Noise Reduction in coupled vibro-acoustic systems using synchronized switch control** - Proceeding of AC2009 Adaptronic Congress, Paper AC2009-pp. 159-167. May 19-20, 2009, Berlin - Germany.*

*The wide band performances of the switched shunt control in the low frequency domain (low modal density) and the low inductor and resistor values needed were the main peculiarities of this approach. The tested system showed a good independence on environmental drifts and a high thermal stability.*

---

*Monica Ciminello, Leonardo Lecce, **Experiences on Switched Shunt Control on Radiating Elastic Plate Structures** - Proceeding of ICSV16 The sixteenth International Congress on Sound and Vibration, paper ICSV16-476-S09. July 5-9 2009, Kraków, Poland.*

*An attempt to critically summarise the most remarkable points of the author's work in the last period, corresponding to her PhD studies is finally presented.*

**ICSV14**  
Cairns • Australia  
9-12 July, 2007



## **SIMULATION OF A COMBINED SWITCHED AND INDUCTIVE SHUNT CONTROL ACTING ON A 2D STRUCTURE**

Salvatore Ameduri<sup>1</sup>, Monica Ciminello<sup>2</sup> and Antonio Concilio<sup>1</sup>

<sup>1</sup>Laboratory of Smart Structures, The Italian Aerospace Research Centre C.I.R.A. scpa  
Capua, Via Maiorise, Italy

<sup>2</sup>Department of Aeronautical Engineering, "Federico II" University  
Naples, Via Claudio, Italy  
[s.ameduri@cira.it](mailto:s.ameduri@cira.it)

### **Abstract**

Several control techniques have been developed to improve the reduction of sensitivity of structural elements dynamic response to both parameter variations and disturbances attenuations within the control system bandwidth.

The research activity has shown how passive and active control strategies may be complementary for facing many of the structural dynamic problems. As a matter of fact, while the passive ones demonstrate efficiency for the highest frequencies band, the active systems demonstrate efficiency in a wider broad band domain, despite of the large required power supply and the high cost hardware.

Semi-active controls assure advantages of both passive and active control techniques. In detail, the absence of an external power supply, the reduced vulnerability to power failure, the self-powered architecture, make the semi-active controls simple to be managed and cheaper.

The possibility of jointly implementing both a switched and an inductive shunt architecture may guarantee a more efficient multi mode control. As a matter of fact, it is possible to simultaneously control a low and a high frequency mode through a switch and an inductive architecture. To achieve this result, the RLC parameters of the switch circuit (synchronised on the lower mode) have to be chosen so that its normal frequency is coincident with the higher structural mode to be controlled.

### **1. INTRODUCTION**

Numerical and experimental investigations have proved the ability of piezoceramics in passive shunt configuration to control structural vibrations. Different type of shunt circuits have been taken into account but the inductive one is the most widely adopted [1], [2]. By absorbing mechanical vibrations if suitably tuned on specific structural mode, the inductive circuit behaves like a dynamic vibration absorber (DVA), control system, with the incontrovertible truth that it is lightest and more easy to be managed than the mechanical





# INTER-NOISE 2007

28-31 AUGUST 2007

ISTANBUL, TURKEY

## **Semi-analytical solution of a structural system controlled by a switched shunt architecture.**

Salvatore Ameduri<sup>a</sup>, Monica Ciminello<sup>b</sup> and Antonio Concilio<sup>c</sup>

The Italian Aerospace Research Centre, CIRA

Smart Structures and Materials Laboratory

Via Maiorise, 81043 Capua (CE)

ITALY

### **ABSTRACT**

Many theoretical investigations describe the behavior of structural systems controlled through piezo actuators in switched shunt architecture. The main advantages of this control technique are represented by the low power supply required and by the scarce dependence of its efficiency by the environmental changes. These reasons, jointly with the good performance exhibited within the low frequency range, justified the large amount of theoretical, numerical and experimental investigations. Available theoretic models describe the behavior of very simple structural systems, characterized by a limited number of dofs; the main utility of these models is the possibility of identifying parameters that influence control performance. The necessity of extending benefits due to this technique to more realistic applications has led to numeric solving schemes, prevalently based on a FE approach. However, due to the complexity of real applications, despite the efficient reduction techniques employed, numerical computations result heavy and, consequently, time consuming. On the contrary, a semi-analytical solution would allow eliminating the time consuming due to the integration. In the present paper, a strategy adopted to find out a differential eq. semi-analytic solution, the validation with a numeric computation (MSC/Nastran) and related ability of describing system behavior have been illustrated.

### **1 INTRODUCTION**

Through the switched shunt control architecture structural vibrations are reduced by using time variant electric circuits integrated with electromechanical piezos suitably positioned on the structural element. A peculiarity of this control architecture is represented by a switch component that can be closed in some instant of time in such a way to reduce the control system dependence from the structural frequency.

The most remarkable contributions in this field have to be addressed to Corr and Clark [1] who defined, for a sdof clamped-clamped aluminium beam, a switched shunt architecture with a shutting time period of 1/10th to 1/50th of the exciting signal period to be controlled. Then Richard and Guyomar [2], for cantilevered aluminium and epoxy beams, have suggested the maxima structural deformations as the optimal instant of time the switch should be shut.

Anyway, the necessity of extending those theoretical and experimental results to more realistic applications justified the arising interest towards the development and implementation of mdof models.

---

<sup>a</sup> Email address: s.ameduri@cira.it

<sup>b</sup> Email address: monicacimm@libero.it

<sup>c</sup> Email address: a.concilio@cira.it



## Flow chart design of a PZT network based on Switched Shunt Control

**S. Ameduri, A. Concilio**

Centro Italiano di Ricerche Aerospaziali (CIRA), Capua (CE), ITALY  
Laboratorio di Smart Structures



**M. Ciminello, L. Lecce**

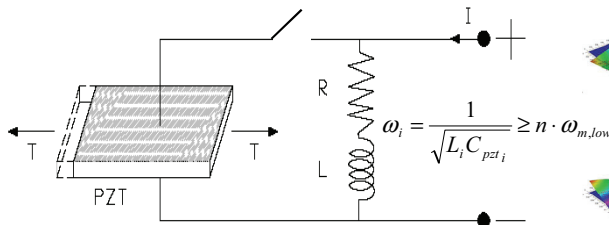
Università degli Studi di Napoli "Federico II", Napoli, ITALY  
Dipartimento di Ingegneria Aerospaziale



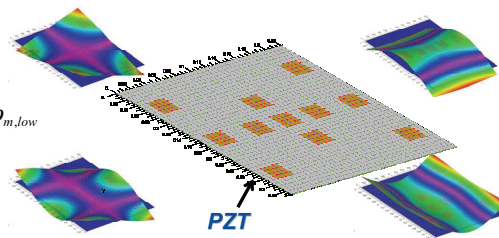
### INTRODUCTION

In this work, the flow chart design of a Switched Shunt Control, SSC, is illustrated, by using as an example an isotropic plate controlled by 11 PZT patches. Firstly, the plate FE modelling and the PZTs disposition criterion are illustrated; then, the simulation control scheme focusing attention on the FE model integration within the logic of control is described. Finally, effects due to the SSC system are presented in terms of amplitudes reduction in the time domain.

### SSC WORKING PRINCIPLE

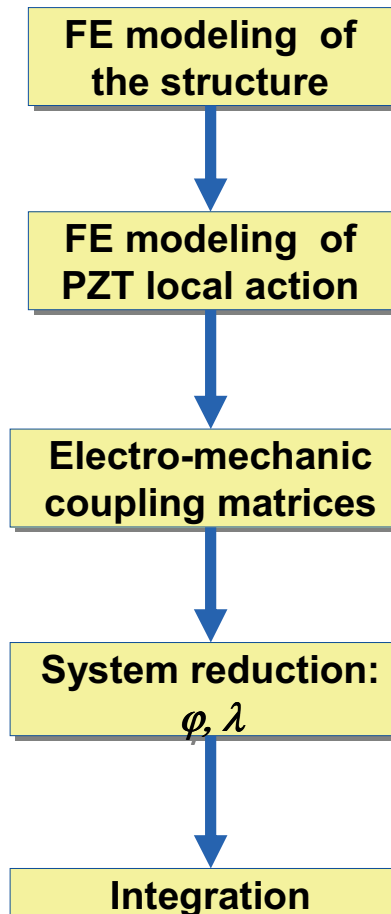


### NUMERICAL SPECIMEN



Constraint conditions	free
Plate dimensions	330 x 220 x 2 mm
Plate material	Al 7075 T6
Plate Young mod	70 GPa
Plate Poisson mod.	0.32
Piezo number	11
Piezo dimensions	33 x 22 x 1 mm
Piezo Young mod	59 GPa
Plate Poisson mod.	0.30
Dielectric const. d <sub>31</sub>	350e-12 (C/N)
Total nodes	1681
Total elements	1600
Node per piezo	5 x 5 x 1 mm

### SIMULATION FLOW CHART



**mass matr.** **damping matr.** **stiffness matr.** **coupling matr.** **structural DOF**

$$\begin{bmatrix} \underline{M} & \underline{0} \\ \underline{0} & \underline{L} \end{bmatrix} \begin{bmatrix} \ddot{\underline{x}} \\ \ddot{\underline{q}}_e \end{bmatrix} + \begin{bmatrix} \underline{B} & \underline{0} \\ \underline{0} & \underline{R} \end{bmatrix} \begin{bmatrix} \dot{\underline{x}} \\ \dot{\underline{q}}_e \end{bmatrix} + \begin{bmatrix} \underline{K} & \underline{D} \\ \underline{G} & \underline{K}_e \end{bmatrix} \begin{bmatrix} \underline{x} \\ \underline{q}_e \end{bmatrix} = \begin{bmatrix} \underline{F} \\ \underline{0} \end{bmatrix}$$

**inductance matr.** **resistance matr.** **capacitance matr.** **electric DOF** **excitation**

**eq. thermal coeff.** **perfect bonding hp.** **PZT<sub>ip</sub>** **structure** **displ./strain estimate** **estimate of transmitted moments**

$$\alpha_{eq} = \frac{d_{31}}{t_p}$$

$$M_{l/y,x/y} = l_{x/y} E_s \int_{-\frac{l_y}{2}}^{+\frac{l_y}{2}} \epsilon_{x/y}(l_{y/x}, z) z dz$$

$$\underline{G}_p = g_{31,p} \frac{E_{p,p} t_{p,p}}{C_{p,p} (1 - \nu_{p,p})} \left( \frac{t_s + t_{p,p}}{2} \right) \cdot \begin{bmatrix} 0, & \dots, & \frac{1}{\Delta x^2}, & 0, & \dots, & 0, & \frac{1}{\Delta y^2}, & \dots, & 0 \end{bmatrix}$$

$$-2 \left( \frac{1}{\Delta x^2} + \frac{1}{\Delta y^2} \right), \frac{1}{\Delta y^2}, 0, \dots, 0, \frac{1}{\Delta x^2}, \dots, 0$$

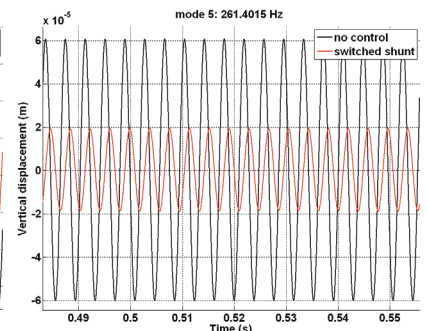
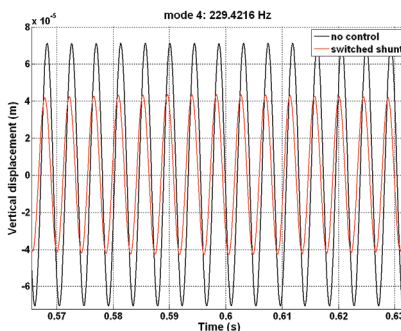
**G: charge induced in the circuit per unit strain**

$$\underline{D}_{ip} = \frac{1}{C_{p,p}} \begin{bmatrix} 0, & \dots, & \dots, & \dots, & 0, & \dots, & \dots, & \dots, & 0 \end{bmatrix}$$

$$M_{1v,x}, M_{1v,y}, 0, \dots, 0]^T$$

**D: force transmitted per unit charge**

$$\begin{bmatrix} (\phi^T \underline{M} \phi) & \underline{0} \\ \underline{0} & \underline{L} \end{bmatrix} \begin{bmatrix} \ddot{\underline{q}} \\ \ddot{\underline{q}}_e \end{bmatrix} + \begin{bmatrix} (\phi^T \underline{B} \phi) & \underline{0} \\ \underline{0} & \underline{R} \end{bmatrix} \begin{bmatrix} \dot{\underline{q}} \\ \dot{\underline{q}}_e \end{bmatrix} + \begin{bmatrix} (\phi^T \underline{K} \phi) & \phi^T \underline{D} \\ \underline{G} \phi & \underline{K}_e \end{bmatrix} \begin{bmatrix} \underline{q} \\ \underline{q}_e \end{bmatrix} = \begin{bmatrix} \phi^T \underline{F} \\ \underline{0} \end{bmatrix}$$



### Contacts

Name	Tel	E-mail
Salvatore Ameduri, Ph. D.	+39 0823 62 3556	s.ameduri@cira.it
Antonio Concilio, Ph. D.	+39 0823 62 3342	a.concilio@cira.it
Monica Ciminello, Ph. D. student	+39 081 726 5216	monicacimmi@libero.it
Leonardo Lecce, Full Prof.	+39 081 768 3327	leonardo@unina.it



Proceedings of SMASIS 2008  
2008 ASME International Conference on Smart Materials, Adaptive Structures & Intelligent Systems  
October 28-30, 2008, Ellicott City, MD, USA

**SMASIS08-320**

## **VIBRATION REDUCTION OF STRUCTURAL-ACOUSTIC SYSTEMS USING SYNCHRONIZED SWITCH DAMPING TECHNIQUES**

**Monica Ciminello**

**Jean-François Deü**

**Roger Ohayon**

**Conservatoire National des Arts et Métiers (CNAM)  
Structural Mechanics and Coupled Systems Laboratory, Chair of Mechanics  
2 rue Conté, 75003 Paris, France  
email: [monicacimm@libero.it](mailto:monicacimm@libero.it) ; [deu@cnam.fr](mailto:deu@cnam.fr) ; [ohayon@cnam.fr](mailto:ohayon@cnam.fr)**

**Salvatore Ameduri**

**Italian Aerospace Research Centre (CIRA)  
Smart Structures Laboratory, Via Maiorise, Capua, Italy  
email: [s.ameduri@cira.it](mailto:s.ameduri@cira.it)**

### **ABSTRACT**

In this paper we present numerical results concerning vibration reduction of structural-acoustic systems using the synchronized switch control technique. In order to develop a general procedure to model the coupled system (composed by the fluid domain, the structure and the piezoelectric elements), the idea is to use the performances of a standard commercial code such as Nastran. A symmetric reduced order model is derived from a general finite element description through the extraction of appropriate system matrices. For sake of brevity, we just recall that depending upon the choice of fluid field variables, non symmetric formulations are usually obtained (so-called displacement-pressure formulations), the symmetrization can be derived through appropriate choice of fluid field variables [1,2]. A simple fluid-structure system for which an analytic solution exists will be used to verify the finite element results and to demonstrate the capabilities of the control procedure. Referring to experimental tests [3], the system consists of a straight air-filled tube with a square cross section. The tube is a rigid cavity with an elastic plate at one end and a piezoelectric patch bonded in its centre. Firstly, the conservative structural-acoustic problem is presented. The symmetric variational and finite element formulations are then described. The model is constructed using Nastran software and the finite element matrices are then extracted and assembled in Matlab. In a second step, the electro-mechanical coupling matrices are built using three-dimensional finite elements in order to take into account local moments of the piezoelectric wafers

according to the equivalent thermal coefficient theory [4,5]. Finally, the reduced electro-mechanical fluid-structure system, obtained through a modal projection, is integrated in time using a Newmark type algorithm. Numerical results are then presented showing the performance of the synchronized switch damping for vibro-acoustic applications in the low frequency domain (low modal density).

### **INTRODUCTION**

In acoustic wave control field, as well as in the vibration control field, the trend is to use active technique that seems to be one of the most efficient strategies to reduce the noise level, at a wide broadband range, despite a complexity of the design and an external power supply required. Actually, for the purpose of noise reduction, the approach is to reduce acoustic radiation field through the vibration reduction of the structure, since the structure itself may be a noise source. A considerable amount of works deals with the numerical or experimental development of techniques of noise reduction using piezoelectric devices bonded or embedded in structural elements.

Kim and Ko [6] worked on finite element modeling for piezoelectric structures. The optimization procedure shows the best location of the actuators and sensors are close to those regions where the strain is maximal. The active control system implemented is a negative feedback. To take into account the acoustic pressure in the cavity the modal approach is used invoking the orthogonality of the modes shapes. The principal





**Adaptronic Congress 2008, 20-21 May 2008**  
**Lower Saxony Representation in Berlin (Germany)**

## **Noise reduction in coupled vibro-acoustic systems using switched shunt control**

### ***Authors:***

***Daniele Ghiglione, KU Leuven, Dept. Of Mechanical Engineering, Belgium***

***Monica Ciminello, Aerospace Engineering Dept. Univeristy of Naples "Federico II", Italy***

***Salvatore Ameduri, Italian Aerospace Research Centre, Capua, Italy***

***Antonio Concilio, Italian Aerospace Research Centre, Capua, Italy***

***Wim Desmet, KU Leuven, Dept. Of Mechanical Engineering, Belgium***

### **ABSTRACT**

This paper reports on the control of structure-borne noise by switched shunt architecture based on resistor-inductor electric components, and focuses on aspects of numerical modelling of the structure and its controller.

The working principle is based on synchronized commutations according to the piezo voltage picks from an open circuit to a closed circuit state.

The wide band performances of the switched shunt control in the low frequency domain (low modal density) and the low inductor and resistor values needed were the main peculiarities of this approach. The tested system showed a good independence on environmental drifts and a high thermal stability, so assuring certain promises for application in the aeronautics and the aerospace field.

### **1. INTRODUCTION**

Noise reduction using smart materials is an emerging field of research in vibro-acoustics. Due to their nature, these materials are used in active and semi-active [<sup>1-4</sup>] control devices and act locally on the structure to attain a global noise reduction in the target fluid volume.

The goal of this paper is the numerical evaluation of performance of a smart control device (the synchronized switch damping) to reduce the noise generated within an acoustic cavity by a vibrating panel on its boundary [<sup>5-8</sup>].





# The Sixteenth International Congress on Sound and Vibration

## Kraków, 5-9 July 2009

### EXPERIENCES ON SWITCHED SHUNT CONTROL ON RADIATING ELASTIC PLATE STRUCTURES

Monica Ciminello and Leonardo Lecce

*Aerospace Engineering Dept. University of Naples "Federico II" - Via Claudio 23 , 80125 Naples, Italy.*

*e-mail: [monica.ciminello@gmail.com](mailto:monica.ciminello@gmail.com); [leonardo@unina.it](mailto:leonardo@unina.it);*

An overview of the author's research experiences, carried out in the last years on switched shunt vibration control on plate structures is herein presented. The activity results were object of former journal publications and conference proceedings: this paper is an attempt to critically summarise the most remarkable points of the author's work in the last period, corresponding to her PhD studies.

## 1. Introduction

The Synchronized Switch techniques, has been introduced by Guyomar et al. [1] and Clark et al. [2]. In their work they compare the state switching technique and the synchronized switching. They showed that the last one is more efficient. The authors are basically involved in the multimode control. The improvement of a technique of switching based on the different modal filters have been developed. The technique requires complex filters and power supply, but it is shown to have good performances.

Important results can be also reported by the research activities carried by Daniel Guyomar of the Laboratoire de Génie Electrique et Ferroélectricité (LGEF) in Lyon. They refined the Synchronized Switch techniques and proposed an autosupply circuit. The authors showed that the method consisting in the detection of the local maximum, is not optimal for the multimodal control, so a new probabilistic criteria has been developed. This method has been proposed for the case of study of a 1D model [3, 4].

The goal of this article is to built a collection of numerical and experimental results for vibration level reduction on both isotropic and anisotropic plate structures object of former journal publications and conference proceedings of the author [5-7]. The author has been working on a finite element formulation for the case of both isotropic and anisotropic plate in the case of a vibration control by means of the Synchronized Switch techniques. An original circuit, based on the tachometer device has been realized in the Smart Structures Lab of the Italian Aerospace Research Centre (CIRA). One of the facilities of this circuit board is the multi channel design which allow to drive more piezoelectric element in one time.

So in what follows a brief description about the Finite Element Model implemented is reported and the description of the SSC circuit is presented and modelled by an additional equation added to take into account the electric dof.

The main results about the reduction of the structural vibration of beam and plate are shown.



# **Appendix:**

## **Complementary Ongoing Activities**



# Sound Power Radiation in Elasto-Acoustic System

Demonstration of the viability of active noise control and active structural-acoustic control in cavity noise applications have been described by several authors. The demand for improvement in sound quality and noise reduction, has led to include investigations on the effectiveness of other kind of approaches as the semi-passive technique, for automotive interior noise reduction as encountered, for instance, in aircraft cabins and vehicle interiors is typical example.

A dedicated experimental campaign has been carried out in order to evaluate both the capability and the relevant restrictions of the switching shunt architecture to provide enough authority to control the vibrations and acoustic energy level reduction of an elastic radiating plate.

The aim of the experimental campaign, partially described in the paragraph, is to reduce the structural-acoustic radiation of a flexible mechanism considering in the objective function the vibration energy and the control system energy. The benefits of this methodology are intended to be demonstrated on a vibro-acoustic cabin mock-up in the following described.

## The specimen

The specimen, a 1.2 mm thick, 60x20 cm aluminium alloy plate, instrumented with a couple of 2x2 PPK 11 piezo clusters, is depicted in Figure 1. Piezo location on one side was chosen to control the largest number of modes in the range of interest (80–270 hz), while their thickness, 0.75mm, was defined according to the classical strain actuation prescriptions [Crawley and de Luis]. On the other panel side, two PPK 23 piezo patches, used as sensors, were bonded in collocated configuration; main piezo features are reported in Table 1.

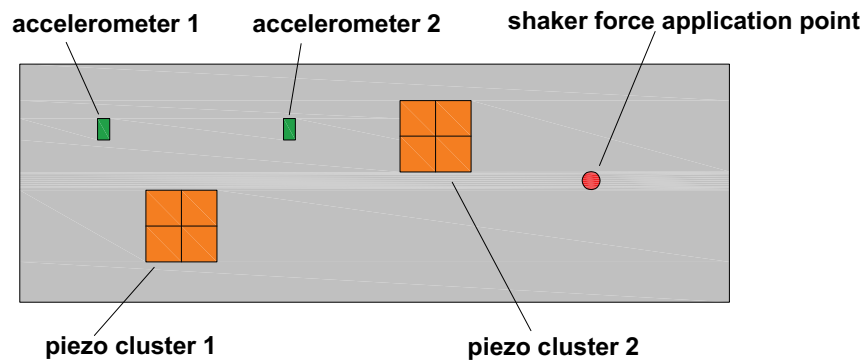


**Figure 1. Instrumented plate sketch.**

Microphones	
Model	BRUEL 4958, 1/4 "
Sensitivity	12.5 mV/Pa
Accelerometers	
Model	PCB-Piezotronics Model 352A71
Sensitivity	10mV/g

Piezo actuators	
Model	PPK11
In-plane dimensions	30 x 30 mm
Thickness	0.75 mm
$d_{31}$	350e-12 C/N
$g_{31}$	8e-3 Vm/N
Young modulus	59.0GPa
Piezo sensors	
Model	PPK23
In-plane dimensions	20 x 30 mm
Thickness	0.50 mm
$d_{31}$	130e-12 C/N
$g_{31}$	20e-3 Vm/N
Young modulus	59.0GPa

**Table 1. Setup components main characteristics.**

The plate constitutes a partial window of a cubic (8 m<sup>3</sup>) room (shown in Figure 2), internally instrumented with six microphones (see Table 1), dislocated at different distances. The acoustic room is intended to represent a simplified car cavity with concrete walls to provide well-defined acoustic boundary conditions. A simply support condition was assumed as constraint for panel edges.



**Figure 2. Plate windowed acoustic room.**

The signal provided by any sensor is derived and given as input to a tachometer, in charge of producing a zero crossing synchronised logical signal, drawing a switch component (CMOS). For further details refer to [Ciminello et al.].

A chirp signal (swept sine) has been used to excite the structure. The swept sine used to impose a broadband excitation signal with the same intensity at all frequencies. The experimental investigation has been carried out in the frequency range 0-300 Hz. The voltage amplitude of each piezoceramic sensor has been monitored and used to drive the relative actuator on the base of the switched shunt control architecture. Two accelerometers (PCB Piezotronics model 352A71, Sensitivity 10mV/g ) were bonded on the reference panel. The acoustic field of the monitored

enclosure has been measured by 6 microphones BRUEL 4958 size  $\frac{1}{4}$  ", sensitivity 12.5 mV/Pa), as described in Figure 3. The LMS acquisition system has been employed to acquire, analyze and display the signal waveforms.

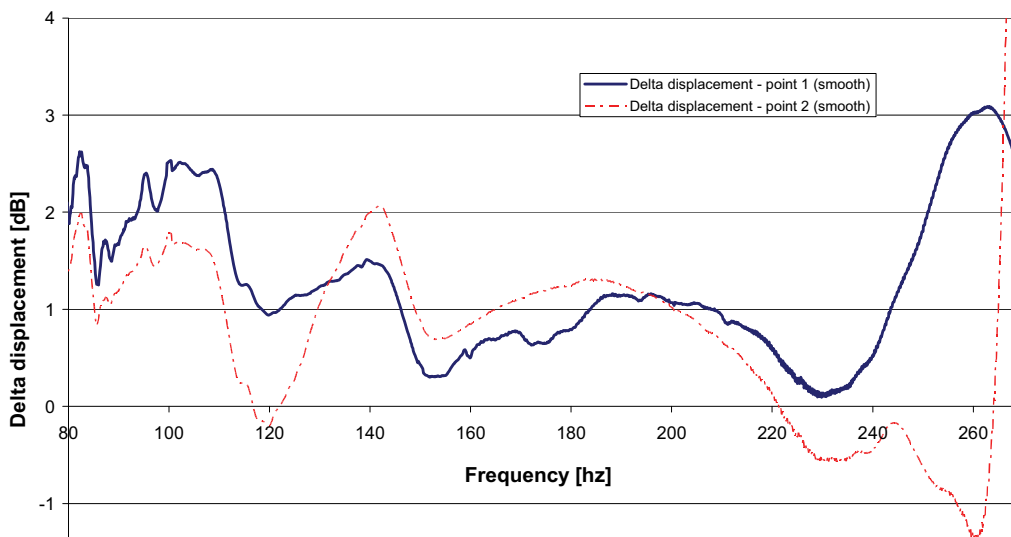


**Figure 3. Experimental displacement vs. frequency on accelerometer locations.**

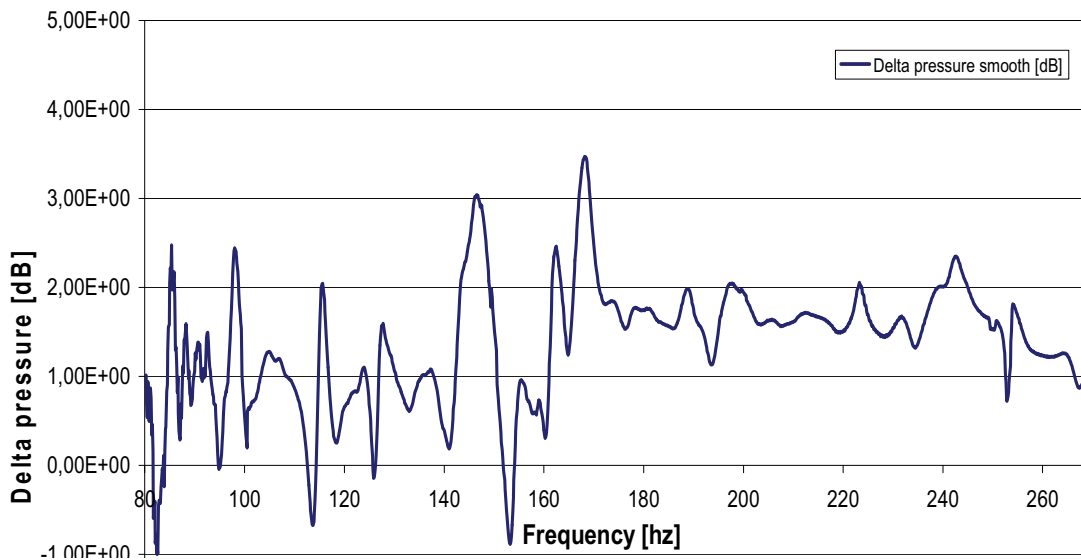


**Figure 4. Experimental mean sound power radiated vs. frequency.**

### The numerical tool

A finite element model has been produced (Figure 5) in order to evaluate the eigenfrequencies (Figure 6) of the test specimen with the experimental resonances detected from the accelerometer sensors (Figure 3).

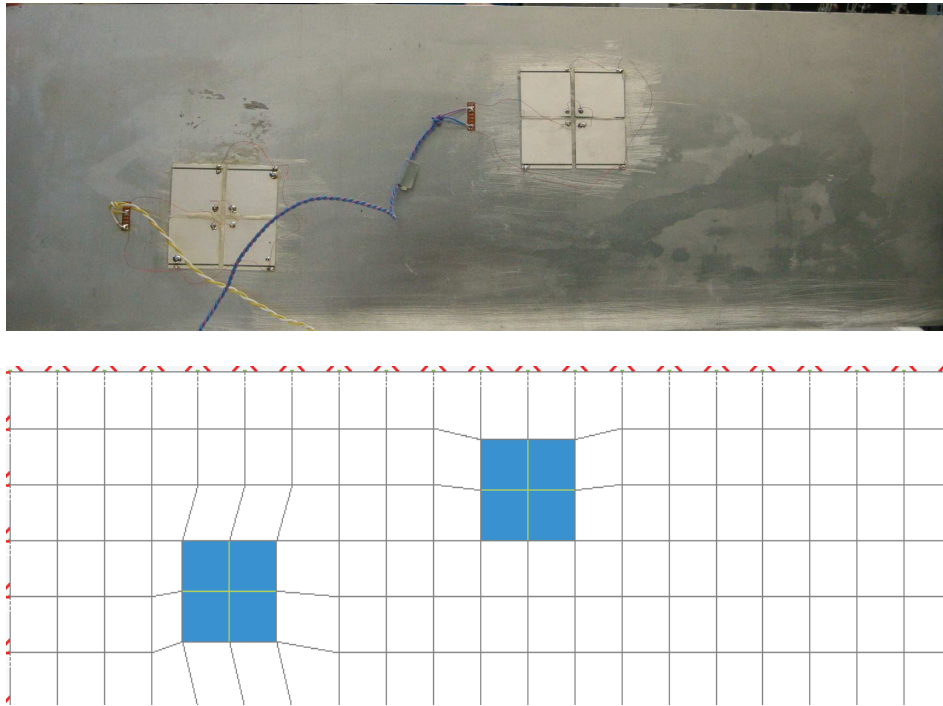


**Figure 5. Plate Finite element model.**

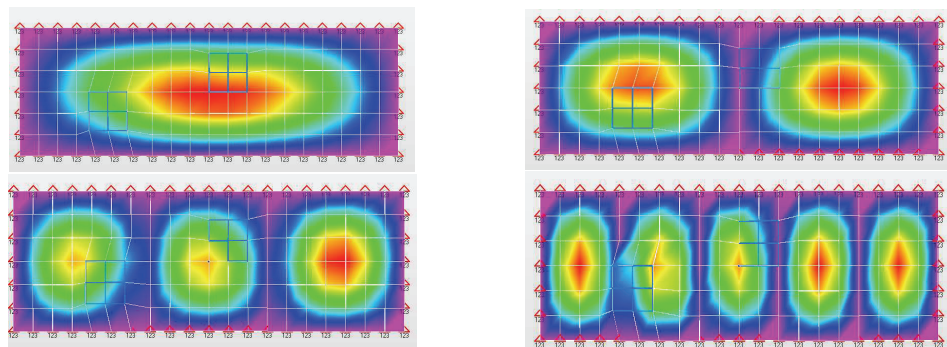


**Figure 6. Plate Finite element model.**

Numerical and experimental resonances within the band range of interest are sketched in Table 2

N° Mode	Exp Frequency (Hz)	Num Frequency (Hz)
1	95	82
2	110	105
3	147	142
5	280	270

**Table 2. Setup components main characteristics**

The radiated sound pressure will be computed by means of the impedance matrix,  $Z$ , which provides radiated power,  $W$ , as a function of the panel source points, suitably weighted by the area matrix  $A$ :

$$Z = \frac{\omega \rho_0 k}{2\pi} \begin{bmatrix} 1 & \frac{\sin(kr_{12})}{kr_{12}} & \dots & \frac{\sin(kr_{1n})}{kr_{1n}} \\ \frac{\sin(kr_{21})}{kr_{21}} & 1 & \dots & \frac{\sin(kr_{2n})}{kr_{2n}} \\ \frac{\sin(kr_{n1})}{kr_{n1}} & \frac{\sin(kr_{n2})}{kr_{n2}} & \dots & 1 \end{bmatrix} [A] \quad (1)$$

being  $k$ ,  $\rho_0$ ,  $\omega$ ,  $r$ , the wave number, the fluid density, the angular frequency and the distance from two points. In this work the power radiated just on the panel will be computed, considering the each other panel point distances.



# Computational Modal Analysis for FSI Problems

Nastran software doesn't implement fluid structure interactions model well suited for specific acoustic situation where an added mass operator is needed, i.e. as incompressible fluid. In order to use Nastran, the standard processing tool for aerospace industry, to implement some direct and reduction procedures for more general fluid-structure interactions problems, a specific formulation in terms of  $(u, p, \phi)$  has been implemented by means of DMIG code. The symmetric and regularized model is well suited for the case of heavy fluids or even huge volume of gas interactions. The preliminary investigations have been conducted without any passive or active treatment and it has been the occasion to interact with researchers of ONERA. This formulation has been derived from the standard one without introducing a pseudo (gyroscopic) damping matrix and in this way the computation of complex modes has been avoided. Moreover, the modal reduction applied to this method gives a very performing reduced model thanks to the presence of the acoustic added mass, which is generally negligible for light fluids, but which must be mandatory considered for heavy fluid, to keep a good convergence rate to this approach (Figure 7).

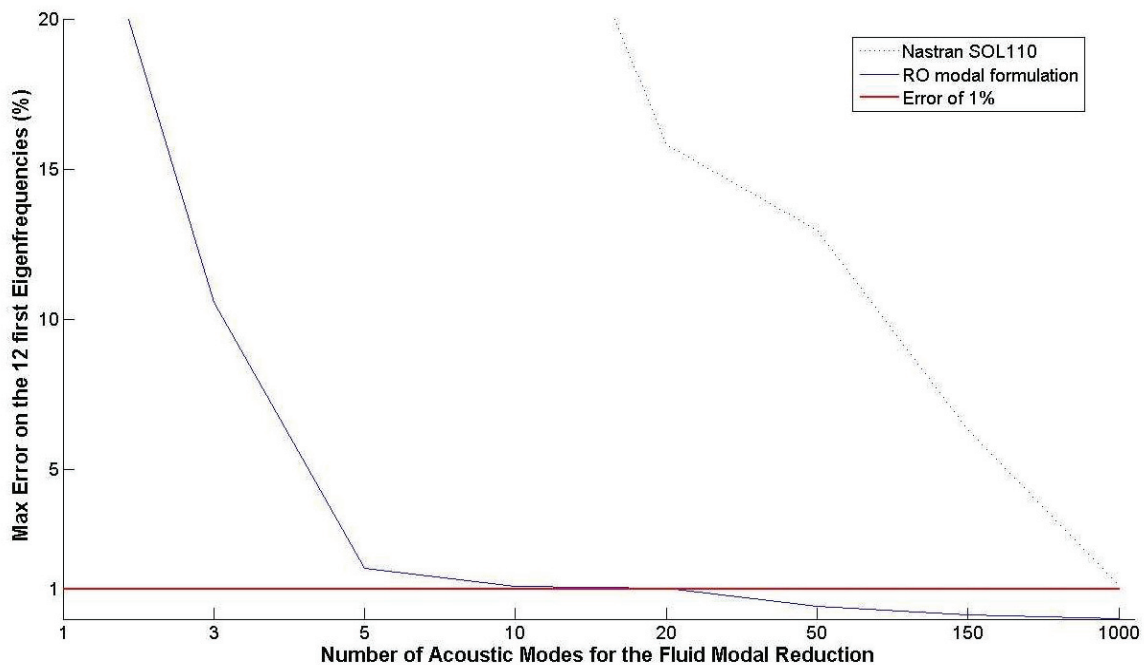


**Figure 7. RO modal formulation Vs. Nastran SOL110: Convergence Rate .**



# Conclusions and Prospects

The thesis shows how the approach based on the semi-passive technique can solve some of the classical drawbacks belonging to active and passive vibration control systems. The semi-passive synchronised switch shunt architecture is modelled and investigated. The idea of using piezo transducers to convert mechanical into electrical energy and elaborating related signal within an external time variant electrical circuit, represents the inspiring principle of this type of control. Connecting a resonant circuit to a piezoelectric transducer with a temporized switch device, a simple and low cost technique for vibrations reduction is realized in such a way to fulfil the demands for smart damping systems, such as:

- External power source not required for operation
- Device does not need to be tuned to a specific frequency
- Device operation is not affected by changes in modal frequency
- Device suppresses vibration over a number of modes, i.e. it is broadband
- Weight and size of the device should be minimized
- Device is to be a self-contained unit

The state of art addressed to this kind of control refers to: finite element formulation based on local equations of the fully coupled system; numerical and experimental validation for sdof models; analytical and experimental validation of the vibrations reduction efficiency based on the electromechanical coupling coefficient for isotropic structures.

Finally different type of “autonomous” circuits basically based on transistors and synthetic inductors have been proposed.

In the published and submitted papers, included in this thesis, the following summarised original aspects, have been considered.

A multi-dofs fully coupled system has been described by means of a finite element formulation. A full home-made finite element procedure, according to local equation describing the fully coupled system has been implemented in Matlab environment. Moreover the abovementioned finite element modelling has been compared with a “non standard” FE approach including Nastran/Matlab integrated routines in order to built a general purpose numerical tool oriented to more real test specimen. The matrices are extracted from Nastran and reassembled in Matlab where the electro-mechanical coupling terms have been added. Piezo strain actuation has been modelled using the analogy between thermal and piezoelectric strain. The effects exerted on the structure have been applied as concentrated moments at the piezo nodes interface. The piezo moments have been compared and validated using well-established strain actuation analytical model. The sensing has instead been modelled with a 2D piezoelectric constitutive equation and experimentally validated. The piezo sensor-actuator collocated couples have been used in both bonded and embedded configurations.

Moreover an original circuit, based on a tachometer and CMOS devices (needing a very weak supply), has been realised to implement the synchronized shunt control. The tachometer device can generate a pulse train signal activating the CMOS perfectly synchronized with the zero crossing of the input. Moreover the amplitude of the logical signal can be opportunely set according to a voltage threshold fail-safe criterion. A 4-independent channel electric card of 10×10cm in-plane dimensions and 80gr in weight with a plug and play philosophy have been built up, in order to friendly manage a set of piezo transducers network for multimode control

test. The control system has been tested to compare experimental and numerical results for aluminium and laminated beam and plate structures.

At first, a cantilevered beam has been taken into consideration for simplicity. The damping ability of the techniques has been estimated for the first bending mode; a max reduction of the displacements of 16.2 has been found. The experienced test campaign showed to be in good accordance, confirming the goodness of the adopted numerical model.

A second test article has been a 10 ply fibreglass laminate plate, 220 x 280 mm in-plane dimensions, 7 mm thick. In this case a multi-tone strategy has been tested. Referring to the dedicated 4-channel board, a network of collocated embedded piezo sensor/actuator have been fully integrated into a laminated plate. The 3D FE model of the embedded PZT system has been set-up within MSC/Nastran. The equivalent induced damping has been estimated, for seven bending modes. A maximum reduction of 16 dB has been found. Test campaign showed a good accordance with the numerical predictions.

Further numerical tests have been planned to extend the ability of the SSC to evaluate noise reduction in acoustic cavities in fluid-structure interaction problems. The numerical results have shown reduction of amplitudes achieved in low frequency range at various peaks.

The effect of a passive inductive shunt and the semi-passive switched shunt have been compared in order to highlight the broad band features of the second technique.

Moreover the finite element tool integrating Nastran features with Matlab routines has been also used on the same test case. Results have been tested just for the first bending mode showing good correlation and validating the “non standard” methodology.

An attempt to face with a semi analytic solution exclusively for a simple 1D test case of a fluid duct, has also been taken into account.

A complementary ongoing activities are going to be concluded. A numerical and experimental validation has been planned to compare the sound power radiation of an elastic plate partly windowing an acoustic room with the mean acoustic energy level. The plate excited by a tonal, sweep and random signals.

Moreover in order to implement some direct and reduction procedures for more general fluid-structure interactions problems, a specific formulation in terms of  $(u, p, \varphi)$  has been implemented by means of DMIG code and tested in Nastran environment. The preliminary investigations have been conducted without any passive or active treatment and it has been the occasion to interact with researchers of ONERA.

In conclusion the main advantage of the switch logic have been described and summarized. Different from the classical shunt resonator techniques, the SSC does not require any tuning between the circuit resonance and the specific structural mode to be controlled: generally speaking it is a broadband control system. No high inductive elements are necessary to control low frequencies modes; moreover, a higher stability degree with respect to environmental changes may be achieved. Moreover being the resistor negligible, the switched shunt performs more thermal stability. The absence of external power supply injecting energy into the system guarantees an unconditional stability. Some drawbacks can be highlighted in the excitation of the high frequency modes due to the switching mechanism. Moreover interesting but even being still open problem, is the optimal switching control law for multimodal excitations.

It has been shown that the coupling of the structure with distributed piezoelectric transducers, makes possible the control of a large multimodal frequency bands with good damping factor. For future prospects, this feature could be used in controlling the generation and transmission noise, which requires a capacity to reduce structural-acoustic coupling, even for sloshing problems.

Moreover, the same type of electro-mechanical systems lends itself to applications relating to the shape control of a given structure, of natural frequencies and modes of buckling. Actually, the shape control is obtained, using the direct piezoelectric effect, applying a field of localized strain by imposed voltage on the transducers. This kind of actuation system allows to change the values of the structural frequencies and critical load of buckling by varying the structural stiffness associated with a variation of the applied voltage.



## Riassunto (extended abstract in Italian language)

Fino ad oggi una grande quantità di ricercatori si è dedicata allo studio e alla progettazione di strategie di riduzione del rumore e delle vibrazioni. Nel campo del controllo acustico, come pure nel campo delle vibrazioni, la tendenza è quella di applicare tecniche attive che sembrano essere la strategia più efficace per ridurre il livello di rumore entro una ampia banda di frequenze, nonostante la relativa complessità di progettazione e l'energia esterna richiesta che rendono tali sistemi poco robusti e stabili. Al contrario le tecniche di controllo passive, realizzate in linea di principio, con l'uso di materiali smorzanti e dissipanti, sono molto efficienti alle alte frequenze ma ingombranti in massa e in volume alle basse, risultando a volte non applicabili dove la leggerezza e la poca invasività del sistema di controllo da imbarcare è un requisito indispensabile, come appunto nelle applicazioni aerospaziali.

Allo scopo di ridurre il rumore generato dalla vibrazione di strutture elastiche è possibile adottare un diverso approccio, rappresentato dai sistemi di controllo semi passivi. In questo lavoro tale approccio viene adottato e realizzato attraverso attuatori piezoceramici incollati alla struttura e che, sincronizzati con l'istante di tempo in cui il massimo livello di deformazione locale viene raggiunta durante la vibrazione, si chiudono in una rete elettrica che riesce a ridurre l'energia cinetica del sistema meccanico con una logica molto semplice e senza che energia esterna sia fornita alla struttura, raggiungendo quindi un buon livello di robustezza e stabilità.

Gli obiettivi di questo lavoro dunque sono, da un lato, di sviluppare uno strumento di calcolo agli elementi finiti per lo sviluppo e la simulazione di un sistema shunt di tipo sincronizzato, sfruttando le potenzialità che il software Nastran, e dall'altro di convalidare sperimentalmente il modello numerico sviluppato con un circuito originale basato su un tachimetro e su circuiti integrati CMOS (che necessitano di 12V di alimentazione). Un adattamento per l'utilizzo simultaneo di più piezoceramici è altresì proposto.

La modellizzazione agli elementi finiti ed il controllo di un elemento elastico anche accoppiato con una cavità acustica a pareti rigide viene quindi realizzata. Le matrici sono estratte dal Nastran ed assemblate in Matlab secondo la classica formulazione non simmetrica che descrive l'interazione fluido struttura. A tali matrici vengono aggiunte quelle di accoppiamento elettromeccanico del piezoceramico con l'ipotesi semplificativa che solo gli effetti sui bordi di interfaccia vengano presi in considerazione. Infine, del circuito elettrico ne viene simulato il comportamento. A causa del rapido tempo di commutazione del meccanismo, il sistema risulta non lineare e tempo variante, quindi un approccio transitorio diretto, attraverso un algoritmo di Newmark è risultato necessario per computare la risposta nel tempo del sistema.



## Résumé (extended abstract in French language)

De nombreuses recherches sont aujourd'hui consacrées à l'étude et au développement de stratégies de réduction du bruit et des vibrations. Dans le domaine de l'acoustique comme dans le domaine des vibrations, différentes approches peuvent être envisagées. Une tendance actuelle est d'appliquer des techniques actives qui sont reconnues pour être efficaces sur une large bande de fréquence, mais qui souffrent cependant d'une complexité de mise en œuvre et d'une nécessité d'un apport d'énergie extérieur qui rendent ces systèmes peu robustes et potentiellement instables. Les techniques passives, qui utilisent par exemple des matériaux isolants, sont quand à elles très efficaces pour les hautes fréquences mais plus limitées en basse fréquence pour un problème de poids et d'encombrement, ce qui peut être un inconvénient dans certaines applications aéronautiques ou aérospatiales où la légèreté est un paramètre primordial.

Afin de diminuer le bruit engendré par les vibrations des structures, il est possible d'adopter une approche différente basée sur l'utilisation de systèmes semi-passifs. Cette technique, qui sera utilisée dans ce travail, est réalisée grâce des éléments piézo-céramiques collés à la structure et connectés à un circuit électrique de type shunt résonant avec un interrupteur (switch shunt). L'interrupteur permet d'ouvrir et de fermer le circuit électrique à des moments bien précis de façon à maximiser l'atténuation des vibrations. Par rapport aux systèmes actifs, ce type d'approche est relativement simple à mettre en œuvre, robuste et stable. De plus, par rapport aux techniques piézoélectriques purement passives, il n'est pas nécessaire de fournir de l'énergie extérieur au système ni d'accorder précisément les composants électrique pour garder une efficacité sur une bande de fréquence relativement large.

L'objectif du travail est double. Il s'agit de développer un outil de calcul par éléments finis (basé sur les logiciels Matlab et Nastran) pour simuler la réponse dynamique de système couplés élasto-acoustiques amortis grâce à l'utilisation de pastilles piézoélectriques connectées à un circuit de type shunt avec interrupteur. De plus, des expérimentations sont réalisées de façon à tester un dispositif piézoélectrique original et valider certains développements numériques. Concernant l'expérimentation, une approche originale basée sur l'utilisation d'un tachymètre et de circuits intégrés CMOS (nécessitant une alimentation de 12 V) a été développée. Une adaptation est également proposée pour l'utilisation simultanée de plusieurs patches piézoélectriques.

Une modélisation éléments finis d'une structure élastique couplée à une cavité acoustique est tout d'abord réalisée. Les matrices globales des parties fluide, structure et couplage fluide-structure sont extraites du code de calcul Nastran et sont réassemblées dans Matlab selon la formulation classique non symétrique en termes de déplacement de la structure et de pression dans le fluide. Ensuite, la matrice de couplage électro-mécanique est ajoutée pour prendre en compte les effets piézoélectriques. Enfin, le comportement du circuit résonnant avec interrupteur est modélisé et simulé. Etant donné les temps de commutation très courts, une approche temporelle directe (basée sur le schéma de Newmark) a été utilisée de façon à calculer la réponse transitoire du système couplé.



# References

[AHG92] Anderson, E. H., N. W. Hagood and J. M. Goodliffe: SelfSensing Piezoelectric Actuation: Analysis and Application to Controlled Structures. In Proc. AIAA/ASME/ASCE/AHS/ASC Structures, Structural Dynamics, and Materials, pages 2141–2155, 1992.

[AHvFV93] Aldrich, J. B., N. W. Hagood, A. von Flotow and D. W. Vos: Design of Passive Piezoelectric Damping for Space Structures. Smart Structures and Intelligent Systems, 1917:692–705, 1993.

[AJI01] Ahmadian, M., K. M. Jeric and D. J. Inman: An Experimental Analysis of the Benefits of Shunted Piezoceramics for Damped and Undamped Structures. In Proc. SPIE Smart Structures and Materials - Damping and Isolation, Vol.4331, pages 281–293, Newport Beach, CA, USA, March 2001.

[BAK05] Baker J, Roundy S and Wright P 2005 Alternative geometries for increasing power density in vibration energy scavenging for wireless sensor networks Proc. 3rd Int. Energy Conversion Engineering Conf. (San Francisco, CA, Aug.) pp 959–70.

[BEN95] Bent A A, Hagood N W and Rodgers J P 1995 Anisotropic actuation with piezoelectric fiber composites J. Intell. Mater. Syst. Struct. 6 338–49.

[BH01] Bozorgi, J. and M.A. Hawwa: Piezoelectric vibration damping for disk drives. Read Rite Corp. (US) , U.S. Pat. 6,310,746, October 2001.

[BM02] Behrens, S. and S. O. R. Moheimani: Current Flowing Multiple Mode Piezoelectric Shunt Dampener. In Proc. SPIE Smart Materials and Structures, Paper No. 4697-24, pages 217–226, San Diego, CA, March 2002.

[BSP99] Bianchini, E., R. L. Spangler and T. Pandell: Use of piezoelectric dampers for improving the feel of golf clubs. In Proc. SPIE Smart Structures and Materials, Damping and Isolation, SPIE Vol.3668, pages 824–834, Newport Beach, CA, USA, March 1999.

[CC03] Corr, L.R. and W. W. Clark: A Novel Semi-Active Multi-Modal Vibration Control Law for a Piezoelectric Actuator. Journal of Vibration and Acoustics, Transactions on the ASME, 125:214–222, April 2003.

[CF02] Cross, C. J. and S. Fleeter: Shunted piezoelectrics for passive control of turbomachine blading flow-induced vibrations. Smart Materials and Structures, 11(SO964-1726(02)33249):239–248, 2002.

[CHO05a] Cho J, Anderson M, Richards R, Bahr D and Richards C 2005a Optimization of electromechanical coupling for a thin-film PZT membrane: I. modeling J. Micromech. Microeng. 15 1797–803.

[Cla00] Clark, W. W.: Vibration Control with State-Switched Piezoelectric Materials. Journal of intelligent material systems and structures., 11:263–271, April 2000.

[CON92] Concilio A., “Controllo attivo del rumore in cabina mediante attuatori piezoelettrici distribuiti sulla struttura”, PhD Thesis in Aerospace Engineering, University of Naples “Federico II”, 1992, [www.openarchives.org](http://www.openarchives.org)

- [COR05] Cornwell P J, Goethal J, Kowko J and Damianakis M 2005 Enhancing power harvesting using a tuned auxiliary structure J. Intell. Mater. Syst. Struct. 16 825–34.
- [COT04] F. Coté et al., Composite Structures 65 (2004) 471–484 Dynamic and static modelling of piezoelectric composite structures using a thermal analogy with MSC/NASTRAN.
- [CRA87] Crawley, E. F. & de Luis, J., 1987, ‘Use of piezoelectric actuators as elements of intelligent structures’, AIAA Journal, 25(10):1373–1385.
- [CRA89] Crawley, E. F. & Anderson, E. H., 1989, ‘Detailed models of piezoceramic actuation of beams’, AIAA 89-1388-CP.
- [CRA91] Crawley, E. F. & Lazarus, K. B., 1991, ‘Induced strain actuation of isotropic and anisotropic plates’, AIAA Journal, 29(6):944–951.
- [DDL01] Davis, C.L., J.J. Dosch and G.A. Lesieutre: Piezoceramic vibration control device and tuning control thereof. Penn State Res Found (US), U.S. Pat. 6,193,032, February 2001.
- [DIG92] Dosch, J. J., D. J. Inman and E. Garcia: A Self-Sensing Piezoelectric Actuator for Collocated Control. Journal of Intelligent Material Systems and Structures, 3:166–185, January 1992.
- [DIM91] Dimitriadis, E. K., Fuller, C. R. & Rogers, C. A., 1991, ‘Piezoelectric actuators for distributed vibration excitation of thin plates’, Transactions of the ASME, Journal of Vibrations and Acoustics, 113:100–107.
- [DLD97] Davis, C. L., G. A. Lesieutre and J. J. Dosch: Tunable electrically shunted piezoceramic vibration absorber. In Proc. SPIE Smart Structures and Materials, Passive Damping and Isolation, SPIE Vol.3045, pages 51–59, San Diego, CA, March 1997.
- [dMP04] dell’Isola, F., C. Maurini and M. Porfiri: Passive damping of beam vibrations through distributed electric networks and piezoelectric transducers: prototype design and experimental validation. Smart Materials and Structures, 13(2):299–308, 2004.
- [DUC09] Julien Ducarn Modélisation et optimisation de dispositifs non-linéaires d’amortissement de structures par systèmes piézoélectriques commutés Conservatoire National des Arts et Métiers Soutenue le 27 Mars 2009.
- [DUR] P-876 DuraAct™ Piezoelectric Patch Transducers. Datasheet from [www.pi.ws](http://www.pi.ws)
- [FA06] Adil Faiz, Amortissement vibratoire et anéchoïsme par traitement non-linéaire d’éléments piézoélectriques. institut national des Sciences Appliquées de Lyon, 30 mai 2006.
- [FEN96] Fuller, C. R., S. J. Elliott and P. A. Nelson: Active Control of Vibration. Academic Press, 1996.
- [FM03a] Fleming, A. J. and S. O. R. Moheimani: Adaptive Piezoelectric Shunt Damping. IOP Smart Materials and Structures, 12:36–48, January 2003.
- [FM03b] Fleming, A. J. and S. O. R. Moheimani: An Autonomous Piezoelectric Shunt Damping System. In Proc. SPIE Smart Structures and Materials - Smart Structures and Integrated Systems, Vol.5052, San Diego, CA USA, March 2003.

- [FM05] Fleming, A. J. and S. O. R. Moheimani: Control oriented synthesis of high performance piezoelectric shunt impedances for structural vibration control. *IEEE Transactions on Control Systems Technology*, 13(1):98–112, January 2005.
- [For79] Forward, R. L.: Electronic Damping of Vibrations in Optical Structures. *Applied Optics*, 18(5):690–697, March 1979.
- [HA91] Hagood, N. W. and A. Von Flotow: Damping of Structural Vibrations with Piezoelectric Materials and Passive Electrical Networks. *Journal of Sound and Vibration*, 146(2):243–268, 1991.
- [HA91] Hagood, N. W. and A. Von Flotow: Damping of Structural Vibrations with Piezoelectric Materials and Passive Electrical Networks. *Journal of Sound and Vibration*, 146(2):243–268, 1991.
- [HA92] Ha, S. K., Keilers, C. & Chang, F. K., 1992, ‘Finite element analysis of composite structures containing distributed piezoceramic sensors and actuators’, *AIAA Journal*, 30(3):772–780.
- [HO00] Ohayon, R., Meidinger, N., and Berger, H., “Symmetric variational formulation for the vibration of damped structural-acoustic systems. Aerospace applications”. In *Proceedings of 28<sup>th</sup> Structures, Structural Dynamics and Materials Conference* (Monterey, USA, April 6-18, 1987).
- [HO01] Ohayon, R., Deu, J.-F., Larbi, W., Galucio, A., Carra, S., and Schotté, J.-S., “Intelligent adaptive fluid-structure interaction systems”. In *Workshop Challenges in Computational Mechanics* (Cachan, France, May 10-12, 2006).
- [HT94] Hollkamp, J. J. and T. F. Starchville. Jr.: A Self-Tuning Piezoelectric Vibration Absorber. *Journal of Intelligent Material Systems and Structures*, 5:559–565, July 1994.
- [HW93] Hwang, W. S. & Park, H. C., 1993, ‘Finite element modeling of piezoelectric sensors and actuators’, *AIAA Journal*, 31(5):930–937.
- [IEEE] IEEE std, 1988, ‘IEEE standard on piezoelectricity’, ANSI/IEEE Std 176-1987.
- [JI05] Jiang S, Li X, Guo S, Hu Y, Yang J and Jiang Q 2005 Performance of a piezoelectric bimorph for scavenging vibration energy *Smart Mater. Struct.* 14 769–74.
- [JOH06] Johnson T J, Charnegie D, Clark W W, Buric M and Kusic G 2006 Energy harvesting from mechanical vibrations using piezoelectric cantilever beams *Proc. Smart Structures and Materials Conf.; Proc. SPIE* 6169 61690D.
- [KAN03] Kanjuro Makihara, “Energy-recycling Semi-active Vibration Suppression of Space Structures”, Ph.D. Thesis of The University of Tokyo 2003.
- [KC01] Kim, J. and J. Y. Choi: Passive piezoelectric damping tuned by using measured electrical impedance. In *Proc. SPIE Smart Structures and Materials - Damping and Isolation*, Vol.4331, Newport Beach, CA, USA, March 2001.
- [KL01] Koestinger, I. and H. Lammer: Vibration damping device for a racket. *Head Sport Aktiengesellschaft*, 6921 Kennelbach (AT), European Patent Nr. EP 1 080 746 A1, March 2001.
- [KO98] Koppe, H., Gabbert, U. & Tzou, H. S., 1998, ‘On three-dimensional layered shell elements for the simulation of adaptive structures’, in *Proceedings of the Euromech 373*

Colloquium: Modeling and Control of Adaptive Mechanical Structures - Preprint, ADAMES, University of Magdeburg.

[KPVG00] Konak, M. J., I. G. Powlesland, S. P. Van Der Velden and S. C. Galea: Analysis of a self-powered piezoelectric vibration damper. In Proc. SPIE Smart Materials, Structures, and MEMS, Smart Structures and Devices, SPIE Vol. 4235, pages 328–39, Melbourne, Australia, December 2000.

[KPVG97] Konak, M. J., I. G. Powlesland, S. P. Van Der Velden and S. C. Galea: A Self-Powered Discrete Time Piezoelectric Vibration Damper. In Proc. SPIE Smart Materials, Structures, and MEMS, Smart Structures and Integrated Systems, SPIE Vol. 3241, pages 270–279, Adelaide, Australia, December 1997.

[KPVG97] Konak, M. J., I. G. Powlesland, S. P. Van Der Velden and S. C. Galea: A Self-Powered Discrete Time Piezoelectric Vibration Damper. In Proc. SPIE Smart Materials, Structures, and MEMS, Smart Structures and Integrated Systems, SPIE Vol. 3241, pages 270–279, Adelaide, Australia, December 1997.

[KUR03] Kurdila, A.J., Clark W.W., Wang W., McDaniel D.E., 2003, “Stability of a class of real time switched piezoelectric shunts”, Journal of intelligent material system and structures. 13(4), pp.107-116.

[Lam03] Lammer, H.: Ski, Method of Stiffening the Ski and Method of Manufacturing the Ski. HEAD SPORT AG (AT). U.S. Pat. Application 20030155740, August 2003.

[Lam04] Lammer, H.: Racket for ball sports and method for manufacturing thereof. Head Technology GMBH, U.S. Patent 20040152544, August 2004.

[LE04] Lin, Q. and P. Ermanni: Semi-active damping of a clamped plate using PZT. International Journal of Solids and Structures, 41(7):1741–1752, April 2004.

[LEE02] Lee J.K., Kim J., Rhee C.J., Jo C.H. and Choi S.B., “Noise reduction of passive and active hybrid panels”. Smart materials and Structures, 2002. 11:p940-946.

[LEE04] Lee C. S., Joo J., Han S. and Koh S. K. 2004, Multifunctional transducer using poly(vinylidene fluoride) active layer and highly conducting poly(3,4-ethylenedioxythiophene) electrode: actuator and generator Appl. Phys. Lett. 85 1841–3.

[LEE05] Lee C. S., Joo J., Han S., Lee J. H. and Koh S. K. 2005, Poly(vinylidene fluoride) transducers with highly conducting poly(3,4-ethylenedioxythiophene) electrodes Proc. Int. Conf. on Science and Technology of Synthetic Metals vol 152 pp 49–52.

[LEE96] Lee, H.-J. & Saravanos, D. A., 1996, ‘Coupled layerwise analysis of thermopiezoelectric composite beams’, AIAA Journal, 34(6):1231–1237.

[LGR+01] Lazarus, K.B., D. Gilbert, F.M. Russo, J.W. Moore, C. Prestia, R. Spangler, J.C. Allen, E. Bianchini and R.N. Jacques: Golf club. Active Control Experts, Inc. (Cambridge, MA), U.S. Pat. 6,196,935, March 2001.

[LGR+01] Lazarus, K.B., D. Gilbert, F.M. Russo, J.W. Moore, C. Prestia, R. Spangler, J.C. Allen, E. Bianchini and R.N. Jacques: Golf club. Active Control Experts, Inc. (Cambridge, MA), U.S. Pat. 6,196,935, March 2001.

[Lie01] Lieven, N. A. J.: Piezo-Electric Actuation of Helicopter Rotor Blades. In Proc. SPIE Smart Structures and Materials - Damping and Isolation, Vol.4331, pages 432–442, Newport Beach, CA, USA, March 2001.

- [LLH03] Law, W.W., W.-H. Liao and J. Huang: Vibration control of structures with self-sensing piezoelectric actuators incorporating adaptive mechanisms. *Smart Materials and Structures*, 12:720–730, September 2003.
- [LMA+02] Lazarus, K.B., J.W. Moore, J.C. Allen, E. Bianchini and R.N. Jacques: Recreational snowboard. Active Control Experts, Inc. (Cambridge, MA), U.S. Pat. 6,345,834, February 2002.
- [LMJA99] Lazarus, K.B., J.W. Moore, W. Jeffrey R.N. Jacques and J.C. Allen: Adaptive sports implement. Active Control Experts, Inc. (Cambridge, MA), U.S. Pat. 5,857,694, January 1999.
- [LOH03] Lesieutre, G. A., G. K. Ottman and H. F. Hofmann: Damping as a result of piezoelectric energy harvesting. *Journal of Sound and Vibration*, 269:991–1001, 2003.
- [LOI98] Loix, N., 1998, *Amortissement Actif de Structures Flexibles*, Ph.D. thesis, Université Libre de Bruxelles, Brussels, Belgium.
- [LPP98] Loix, N., Piefort, V. & Preumont, A., 1998, ‘Modeling aspects of active structures with collocated piezoelectric actuators and sensors’, *Benelux Quarterly Journal on Automatic Control (Journal a)*, 39(1).
- [LRM+00] Lazarus, K.B., F.M. Russo, J.W. Moore, R. Spangler and R.N. Jacques: Adaptive sports implement with tuned damping. Active Control Experts, Inc. (Cambridge, MA), U.S. Pat. 6,102,426, August 2000.
- [Mat03] Mathur, G.P.: Piezoelectric damping system for reducing noise transmission through structures. Boeing Co., U.S. Pat. 6563250, May 2003.
- [MAT05] Mateu L and Moll F 2005 Optimum piezoelectric bending beam structures for energy harvesting using shoe inserts *J. Intell. Mater. Syst. Struct.* 16 835–45.
- [MATA06] Gaudiller L, Harari S., and Richard C., “New semi-active multi-modal vibration control using piezoceramic components”. *Journal of Intelligent Material Systems and Structures*. 2009. 0: 1045389X09102561v1.
- [MdV04] Maurini, C., F. dell’Isola and D. Del Vescovo: Comparison of piezoelectronic networks acting as distributed vibration absorbers. *Mechanical Systems and Signal Processing*, 18:12431271, 2004.
- [MK01] Moon, S. H. and S. J. Kim: Active and Passive Suppression of Nonlinear Panel Flutter Using Finite Element Method. *AIAA Journal*, 39(11):2042–2050, November 2001.
- [MOH03] Mohammadi F, Khan A and Cass R B 2003 Power generation from piezoelectric lead zirconate titanate fiber composites *Proc. Materials Research Symp.* p 736 .
- [Moh03] Moheimani, S. O. R.: A survey of recent innovations in vibration damping and control using shunted piezoelectric transducers. *IEEE Transactions on Control Systems Technology*, 11(4):482–494, July 2003.
- [MOS05] Mossi K, Green C, Ounaies Z and Hughes E 2005 Harvesting energy using a thin unimorph prestressed bender: geometrical effects *J. Intell. Mater. Syst. Struct.* 16 249–61.
- [MPS+99] Maly, J. R., S. C. Pendleton, J. Salmanoff, G. J. Blount and K. Mathews: Hubble Space Telescope solar array damper. In *Proc. SPIE Smart Structures and Materials, Passive Damping and Isolation*, SPIE Vol.3672, pages 186–197, Newport Beach, CA, USA, March 1999.

- [NFMM04] Niederberger, D., A. J. Fleming, S.O.R. Moheimani and M. Morari: Adaptive Multi-mode Resonant Piezoelectric Shunt Damping. *Journal of Smart Materials and Structures*, IOP Publishing, 13(4):1025–1035, October 2004.
- [NG04] Ng T H and Liao W H 2004 Feasibility study of a self-powered piezoelectric sensor *Proc. Smart Structures and Materials Conf.; Proc. SPIE* 5389 377–88.
- [NG05] Ng T H and Liao W H 2005 Sensitivity analysis and energy harvesting for a self-powered piezoelectric sensor *J. Intell. Mater. Syst. Struct.* 16 785–97.
- [NGDH93] Nye, T. W., R.A. Ghaby, G. R. Dvorsky and J. K. Honig: *The Use of Smart Structures for Spacecraft Vibration Suppression*. 44th IAF International Congress, Graz, Austria, 1993.
- [NIE05] Dominik Niederberger, “Smart Damping Materials using Shunt Control”. A dissertation submitted to the SWISS FEDERAL INSTITUTE OF TECHNOLOGY (ETH) ZURICH 2005.
- [OHL03] Ottman, G. K., H. F. Hofmann and G. A. Lesieutre: Optimized Piezoelectric Energy Harvesting Circuit using Step-Down Converter in Discontinuous Conduction Mode. *IEEE Transactions on Power Electronics*, 18(2):696–703, march 2003.
- [Par03] Park, C.-H.: Multi-mode vibration damping device and method using negative capacitance shunt circuits. University Pohang (KR), US2003209953, November 2003.
- [PAR96] Park, C. & Chopra, I., 1996, ‘Modeling piezoceramic actuation of beams in torsion’, *AIAA Journal* , 34(12):2582–2589.
- [PdFM04] Porfiri, M., F. dell’Isola and F.M. Frattale-Mascioli: Circuit analog of a beam and its application to multimodal vibration dumping, using piezoelectric transducers. *International Journal of Circuit Theory and Applications*, 32(4):167–198, 2004.
- [PF05] Pfeiffer A., Storm S., Roder A., Maier R. and Frank P., “Active Vibration Control for High Speed Train Bogies”, *Smart Materials and Structures*, 2005. 14:p.1-18.
- [PIE00] Piefort V., “Finite Element Modelling of Piezoelectric Active Structures”, Thesis submitted in candidature for the degree of Doctor in Applied Sciences Academic Year 2000-2001. Université Libre de Bruxelles.
- [PKPM99] Prajna, S., O. Kaiser, S. J. Pietrzko and M. Morari: Robust Active Control of the Vibrations of a Plate. Technical Report, Automatic Control Laboratory, Swiss Federal Institute of Technology, 1999.
- [PL05b] Platt S R, Farritor S and Haider H 2005b The use of piezoelectric ceramics for electric power generation within orthopaedic implants *IEEE/ASME Trans. Mechatronics* 10 455–61.
- [PLC+04] Park, J. S., S. C. Lim, S. B. Choi, J. H. Kim and Y. P. Park: Vibration reduction of a CD-ROM drive base using a piezoelectric shunt circuit. *Journal of Sound and Vibration*, 269:1111–1118, 2004.
- [PLRG04] Petit, L., E. Lefeuvre, C. Richard and D. Guyomar: A broadband semi passive piezoelectric technique for structural damping. In *Proc. SPIE’s 11th Annual International Symposium on Smart Structures and Materials*, San Diego, CA USA, March 2004.

- [PRE97] Preumont, A., 1997, *Vibration Control of Active Structures - An Introduction*, Kluwer Academic Publishers, Dordrecht, The Netherlands.
- [QSWH02] Qualey, D. G., D. A. Sluzewski, J. Wright and A. K. Himes: Passive damping method and circuit for data storage device actuator. U.S. Patent 2002012184, January 2002.
- [RA93] Rao, S. S. & Sunar, M., 1993, 'Analysis of distributed thermopiezoelectric sensors and actuators in advanced intelligent structures', *AIAA Journal*, 31(7):1280–1286.
- [RGAB00] Richard, C., D. Guyomar, D. Audigier and H. Bassaler: Enhanced Semi-Passive Damping Using Continuous Switching of a Piezoelectric Devices on an Inductor. In *Proc. SPIE Smart Structures and Materials, Damping and Isolation*, SPIE Vol.3989, pages 288–299, Newport Beach, CA, March 2000.
- [RIC04] Richards C D, Anderson M J, Bahr D F and Richards R F 2004 Efficiency of energy conversion for devices containing a piezoelectric component *J. Micromech. Microeng.* 14 717–21.
- [RIC07] Thibaut Richard Diminution du coefficient de transmission acoustique d'une paroi à l'aide d'amortisseurs piézoélectriques semi-passifs, *institute national des Sciences Appliquées de Lyon*, 17 décembre 2007.
- [ROU05] Roundy S 2005 On the effectiveness of vibration-based energy harvesting *J. Intell. Mater. Syst. Struct.* 16 809–23.
- [ROU05] Roundy S and Zhang Y 2005 Toward self-tuning adaptive vibration based micro-generators *Smart Materials, Nano- and Micro-Smart Systems* (Sydney, Dec.).
- [SAM96] Samanta, B., Ray, M. C. & Bhattacharyya, R., 1996, 'Finite element model for active control of intelligent structures', *AIAA Journal*, 34(9):1885–1893.
- [SAR97] Saravanos, D. A., 1997, 'Mixed laminate theory and finite element for smart piezoelectric shell structure', *AIAA Journal*, 35(8):1327–1333.
- [SC98] Sung, C. C. and C. Y. Chiu: Control Of Sound Transmission Through Thin Plate. *Journal of Sound and Vibration*, 218(4):605–618, 1998.
- [SCH06] Schonecker A J, Daue T, Bruckner B, Freytag C, Hahne L and Rodig T 2006 Overview on macro fiber composite applications *Proc. Smart Structures and Materials Conf.; Proc. SPIE* 6170 61701K.
- [SHA06a] Shahruz S M 2006a Design of mechanical bandpass filters for energy scavenging *J. Sound Vib.* 292 987–98.
- [SHA06b] Shahruz S M 2006b Limits of performance of mechanical band-pass filters used in energy scavenging *J. Sound Vib.* 293 449–61.
- [SOD04a] Sodano H A, Lloyd J and Inman D J 2004a An experimental comparison between several active composite actuators for power generation *Proc. Smart Structures and Materials Conf.; Proc. SPIE* 5390 370–8.
- [SOD04c] Sodano H A, Park G and Inman D J 2004c Estimation of electric charge output for piezoelectric energy harvesting *Strain* 40 49–58.
- [SOD05a] Sodano H A, Inman D J and Park G 2005a Comparison of piezoelectric energy harvesting devices for recharging batteries *J. Intell. Mater. Syst. Struct.* 16 799–807.

[SP01] Shenck, N. S. and J. A. Paradiso: Energy Scavenging with ShowMounted Piezoelectrics. IEEE Micro, 21(3):30–42, May-June 2001.

[STE] PPK23 Piezoelectric Patch Transducers. Datasheet from [www.stettner.de](http://www.stettner.de)

[SUL95] Suleman, A. & Venkayya, V. B., 1995, 'A simple finite element formulation for a laminated composite plate with piezoelectric layers', Journal of Intelligent Material Systems and Structures, 6:776–782.

[Tre01] Treyde, T.: Apparatus with vibration-damped component, especially a brake. U.S. Patent 2001042661, November 2001.

[TW99] Tsai, M. S. and K. W. Wang: On The Structural Damping Characteristics of Active Piezoelectric Actuators With Passive Shunt. Journal of Sound and Vibration, 221(1):1–22, 1999.

[TZ90] Tzou, H. S. & Tseng, C. I., 1990, 'Distributed piezoelectric sensor/actuator design for dynamic measurement/control of distributed parameter systems: a piezoelectric finite element approach', Journal of Sound and Vibration, 138(1):17–34.

[TZ91] Tzou, H. S. & Tseng, C. I., 1991, 'Distributed modal identification and vibration control of continua: Piezoelectric finite element formulation and analysis', Transactions of the ASME, Journal of Dynamic Systems, Measurement and Control , 113:500–505.

[TZ96] Tzou, H. S. & Ye, R., 1996, 'Analysis of piezoelastic structures with laminated piezoelectric triangle shell elements', AIAA Journal, 34(1):110–115.

[TZOU] H.S.Tzou: Piezoelectric Shells – Distributed Sensing and Control of Continua Kluwer Academic Publishers (pag 462) .

[Van98] Vandergrift, J.A.: Piezoelectric damper for a board such as a snow ski or snowboard. K2 Corp., U.S. Patent 5775715, July 1998.

[WB96] Wynn, W.D. and D.R. Browning: Vibration damping system using active negative capacitance shunt circuit with piezoelectric reaction mass actuator. AT & T Corp., EP0715092, June 1996.

[WH97] Warkentin, D. J. and N. W. Hagood: Nonlinear Piezoelectric Shunting for Structural Damping. In Proc. SPIE Smart Structures and Materials, Smart Structures and Integrated Systems, SPIE Vol.3041, San Diego, Ca, USA, March 1997.

[WIL95] Williams C B and Yates R B 1995 Analysis of a micro-electric generator for microsystems Transducers 95/Eurosensors IX vol 1 pp 369–72.

[WIT96] Witsenhausen, H.S. 1996. "A class of hybrid state continuous time dynamic system", IEEE Transactions on automatic control, 11(2), April, pp.161-176.

[Wu00] Wu, S.Y.: Broadband piezoelectric shunts for structural vibration control. Mc Donnell Douglas Corp. (US), U.S. Pat. 6,075,309, June 2000.

[Wu01] Wu, S.Y.: Broadband piezoelectric shunts for passive structural vibration control. In Proc. SPIE Smart Structure and Materials 2001: Damping and Isolation, SPIE Vol.4331, pages 251–261, Newport Beach CA, USA, March 2001.

[Wu96] Wu, S. Y.: Piezoelectric Shunts with Parallel R-L Circuit for Structural Damping and Vibration Control. In Proc. SPIE Smart Structures and Materials, Passive Damping and Isolation, SPIE Vol.2720, pages 259–269, March 1996.

[YAN05] Yang J, Zhou H, Hu Y and Jiang Q 2005 Performance of a piezoelectric harvester in thickness-stretch mode of a plate IEEE Trans. Ultrason. Ferroelectr. Freq. Control 52 1872–6.

[ZCVV01] Zhang, J. M., W. Chang, V. K. Varadan and V. V. Varadan: Passive underwater acoustic damping using shunted piezoelectric coatings. IOP Smart Materials and Structures, 10(2):414–420, April 2001.



# Career Development Plan

## Personal data

Name: CIMINELLO MONICA

Date of birth: 8/10/1973

Born at: NAPLES

Nationality: ITALIAN

## Home University

Address Via Claudio, 21 - 80125 Napoli, Italia

Link: [www.dpa.unina.it](http://www.dpa.unina.it)

## Host University

Address: 2 Rue Conté, 75003 Paris, France

Link: [www.cnam.fr/lmssc](http://www.cnam.fr/lmssc)

## Education

Master Degree of Science in Physics @ “Federico II” - Naples, Italy

Master on Smart Structures industrial research and development @ CIRA – Capua, Italy

Ph.D. in Aerospace Engineering @ “Federico II”

Ph.D. in Mechanical Engineering @ “CNAM”

## Ph.D. Training Classes

Aeroelasticity, Prof. Marulo.

Aircraft structures, Prof. Lecce.

Fluid Structure Interaction, Prof. Ohayon.

Introduction to smart structures, Dr. Concilio.

Non linear dynamics, Dr. Crescitelli.

Composite structures design, Prof. Accardo.

Elements of combinatorial optimization, Dr. Bruno.

## Ph.D. Training Conferences, Lectures, Workshops and Study Visits

Passive participation: 6th International Symposium on Hysteresis Modeling and Micromagnetics HMM-07, Naples 4-6 June 2007.

Active oral presentation: The 14th International Congress on Sound and Vibration, 9 – 12 July 2007, Cairns, Australia.

Active oral presentation: 36th International Congress and Exhibition on Noise Control Engineering - Session ANVC, Active Noise and Vibration Control, August 28 – 31, 2007 Istanbul – Turkey.

Active oral presentation: International Conference and Exhibition on new Actuators and Drive Systems- Session “Aerospace applications” Actuator 2008, Giugno 9–11, Bremen / Germany.

Passive participation: ISMA 2008 International Conference on Noise and Vibration Engineering, Leuven, Belgium 15-17 Settembre 2008.

Active oral presentation: ASME International Conference on Smart Materials, Adaptive Structures & Intelligent Systems, October 28-30, 2008, Ellicott City, MD, USA.

Active oral presentation: AC2009 Adaptronic Congress, May 19-20, 2009, Berlin – Germany.

Active oral presentation: ICSV16 The sixteenth International Congress on Sound and Vibration, 5-9 July 2009, Krakòw, Poland.

“Fracture Mechanics Problems of Aluminum Alloy Fuselages”, Seminario all’ Università Federico II di Napoli, Novembre 2007.

“Méthode des Champs Virtuels pour la caractérisation des matériaux et structures”, Journée des Séminaires Scientifique de l’Onera, 1 Avril 2008.

“Projectors and their applications in computational mechanics”, Sèminaires Cnam-Onera, Laboratoire de Mècanique des structures, 25 Juin 2008.

ISAAC19 Seminar on Advanced Techniques in Applied and Numerical Acoustics Katholieke Universiteit, Leuven-Belgium 18-19 September 2008.

ONERA/CNAM Seminar on Advanced Techniques in Applied Aeroelasticity and Structural dynamics, Paris 17 November 2008.

Passive participation : Workshop RTN 3-4 September 2008 Leuven

Active oral presentation : Workshop RTN 9-11 December 2008 Leuven

Study visit to KTH Royal Institute of Technology, Stockholm: 18-22 February 2009

Study visit to Fraunhofer Institut, Darmstadt: 24-25 February 2009

Cooperation with the French Aerospace Research Centre: ONERA

Cooperation with the Belgium Katholieke Universiteit Leuven: KUL